FAILURE OF LAYERED MODAVE SANDSTONE: EFFECT OF LAYER ORIENTATION AND MATERIAL PROPERTIES

Abbass TAVALLALI

Supervisor:
Prof. A. Vervoort

Members of the Examination Committee:
Prof. A. Bultheel, chairman
Prof. J. Carmeliet (ETH Zürich, Switzerland)
Prof. C. Schroeder (ULB)
Prof. D. Van Gemert
Prof. M. Wevers

Dissertation presented in partial fulfilment of the requirements for the degree of Doctor of Engineering

August 2010

ISBN 978-94-6018-229-7
D/2010/7515/68

Acknowledgements

First I would like to thank my spouse Pegah and my pretty daughter Tina. Without their endless support, my Ph.D. would not have been possible.

Generally research work is carried out with the support and the help of others. I wish to express my sincere thanks to my promoter, Professor André Vervoort, for the trust he put in me and for giving me the opportunity to work under his supervision. He offered me ample freedom to pursue this research. He was always ready to discuss my concerns and give expert advice. His questions, remarks and guidelines have greatly contributed to this research. I doubt that there are many supervisors who read as punctiliously through the work of their researchers as Professor André Vervoort does.

I would like to thank the other members of the advisory committee, Professor Jan Carmeliet and Professor Martine Wevers, for their suggestions and for the thorough reading of the draft of this thesis. Their suggestions were valuable in compiling the final version of the thesis. I would also like to thank the other members of the jury, Professor Christian Schroeder, Professor Dionys Van Gemert and Professor Adhemar Bultheel for spending some of their valuable time to read through this thesis.

It has been a great pleasure to work at the Civil Engineering department of K.U.Leuven during the past years. I thank all colleagues, past and present, for their camaraderie and for their contributions to this work: Annelies, Bjørn and Patrick. However, I should also mention numerous other colleagues of the Civil Engineering department.

For the experimental work, several people from the laboratory have helped me throughout the years. I also wish to thank them: Frank, Luc, Stephan, Noel and Roger.

I would like to extend my sincere thanks to Prof. Rudy Swennen from the Geology Section of K.U.Leuven for his helpful comments. I also thank his fellow researchers: Koen, Peter and An for their helpful comments in the geological part of the study. Thanks to Herman too who carefully prepared the thin sections. Also Dr. David Lagrou and Dr. Roland Dreesen from Vito (Flemish Institute for Technological Research) are thanked for permitting the use of their microscopic instruments.

I would like to thank my parents, family and friends for all their support during my academic pursuits.

This research is made possible thanks to the financial support of the Research Council of the Katholieke Universiteit Leuven (OT-project OT/03/35).

Abbass Tavallali
Leuven, 21 June 2010

Summary

Rock is a natural combination of different minerals with different characteristics; therefore, fracture behavior of rock material is complex. It becomes more complex when a dominant anisotropy is present in the rock material. In this research the focus is on transversely isotropic (layered) rock material as one specific form of anisotropy. It is a form of anisotropy that is often present in geological material. In this study layered sandstone is considered. Fracture patterns in layered sandstone are often a complex combination of fractures along layer boundaries and in other directions. For layered rock material most studies are limited to the strength variation of rock sample in different configuration of layer orientation (with respect to the load direction).

This study investigates the fracture pattern and rock strength of samples under Brazilian test conditions, not only as a function of layer orientation but also as a function of microscopical parameters. It is observed that the failure stress and fracture pattern are considerably affected by the layer orientation. The samples with low inclination angles (from horizontal) are more fractured and have higher strength. Fractures of samples with larger inclination angles mostly correspond to layer activation.
The effect of the number of layer boundaries, mineral composition and grain size is quantified on fracture behaviour of studied layered sandstone. It is observed that Brazilian tensile strength of studied layered sandstones is higher for larger observed quartz content and for larger average grain size. Also layer activation is found to be larger if more layer boundaries (e.g. per cm) are present and for larger observed weak minerals percentages.

In order to contribute to the development of a better understanding of the fracture process in brittle rock material, initiation and growth of individual fractures are observed by petrographical microscope. It is observed that growing cracks prefer to open the grain bonds rather than fracturing the minerals and also prefer to pass through a path with higher amount of weak minerals.

List of Symbols and Abbreviations

Symbols

t	thickness of disc-shape sample	[mm]
c	crack half-length	[mm]
D	diameter of disc-shape sample	[mm]
E	Young's modulus	[MPa]
F	applied load	[kN]
R	radius of disc-shape sample	[mm]
Th	threshold level	[dB]
α	surface energy per unit area of the crack surfaces	[J/mm^2]
θ	layer inclination angles from horizontal	[°]
λ	wave length	[mm]
ρ	density	[t/m^3]
σ_c	compressive stress required for fracture	[MPa]
σ_t	indirect tensile strength	[MPa]
σ_x	horizontal normal stress	[MPa]
σ_y	vertical normal stress	[MPa]

Abbreviations

AE	Acoustic Emission
APE	Applied Energy
BFF	Before Final Failure
BSE	Backscattered Electron
BTS	Brazilian Tensile Strength
C	Carbonate
CF	Central Fracture
Cl	Clay mineral

DIGS	Discontinuity Interaction and Growth Simulation
ESEM	Environmental Scanning Electron Microscopy
FEM	Finite Element Method
FF	Final Failure
IL	Inclusion Line
ISRM	International Society for Rock Mechanics
LA	Layer Activation
LB	Layer Boundary
LD	Loading Direction
LO	Layer Orientation
LVDT	Linear Variable Differential Transformer
M	Mica
MC	Micro-Crack
NCF	Non-Central Fractures
PC	Planar Contact
PFC	Particle Flow Code
Q	Quartz grain
SST	Sandstone Sub-Type
TFL	Total Fracture Length
UCS	Uniaxial Compression Strength
UCS_{50}	Uniaxial Compression Strength of cylindrical sample with D=50 mm
UDEC	Universal Distinct Element Code

Table of Contents

1 Introduction

1.1 General context

In general, rock material near the earth's surface has mechanical properties that are a function of the direction, or in other words are anisotropic. Transverse isotropy (as a form of anisotropy) is a characteristic of intact foliated metamorphic rocks (slates, gneisses, phyllites, schists) and intact laminated, stratified or bedded sedimentary rocks (shales, sandstones, siltstones, limestones, coal, etc.) (Chen et al. 1998). More and more this anisotropy is taken into account when testing the rock material, as input for design and for numerical modelling. Hence, knowledge of the anisotropic properties is required in studies of civil, mining and petroleum engineering with applications such as the stability of underground excavations, slope stability, borehole deformation and breakage of rock by mechanical tools and explosives. Despite its importance, rock anisotropy is often poorly understood.

Although in situ rock is mostly in compression, tensile stresses could be encountered on a macro-scale in the vicinity of excavations or around boreholes, and are certainly present on micro-scale. The Brazilian test has proved to be a simple, fast and relatively reliable technique for tensile strength estimation of rock (Jaeger and Cook 1969). Recently, the Brazilian test has been used to model the effect of planar discontinuities and their stiffness on the activation of the discontinuities and on the occurrence of newly induced fractures (Debecker et al. 2006).
In this study, one specific type of material is considered. The tests are conducted on stratified Modave sandstone and the Brazilian tensile method (diametrical loading of cylindrical discs) is applied. However, many other techniques are used in this study and they are introduced later.

In experimental studies on stratified rocks, the number of required specimens to be able to evaluate a property is more than that required for isotropic rock. For stratified rocks, in different orientations of stratification respect to loading axis, different failure behaviour can be achieved. This aspect that becomes very obvious during the process of the research presented here.
The failure modes of anisotropic rocks depend not only on the stress state, but also on the orientation of the specimen. Thus, the failure modes and fracture patterns of an anisotropic rock are generally much more complicated than that of an isotropic rock. This is why some studies in order to evaluate mechanical properties and failure mechanisms of anisotropic rocks, use artificially created rock specimens (Tien et al. 2006, Tien and Tsao 2000). Tien et al. 2006 believe that the use of artificially created specimens is more advantageous than the use of the natural rocks for the following reasons: (1) specimens can be made fast with uniform properties at a reasonable cost; and (2) by varying sample preparation and

composition, simulated rocks with a wide range of mechanical behaviours can be produced. But geotechnical engineering is facing natural rocks that can be very different (even for similar rocks). Therefore it is very important to know what these differences are and making efforts to quantify their effects on the behaviour.

1.2 Stress distribution around underground excavations

Rock masses in nature are stressed by gravitational, tectonic and other forces from different directions. The excavation of an underground opening results in the redistribution of the primary in situ stress field. This disturbance involves both changes in magnitude and orientation of the principal stresses. Eberhardt (2001) made a numerical model to study the three-dimensional stress rotation ahead of an advancing tunnel face. He remarked that the rotation of the principal stress axes becomes a controlling factor in the direction of fracture propagation. Eberhardt (2001) mentioned that if this orientation changes during the progressive advancement of the tunnel face, the type of damage induced in the rock mass and the resulting failure mechanisms may also vary depending on the type and degree of stress rotation. However, Eberhardt (2001) considered isotropic material properties whereby the data were based on laboratory testing of granites.

Underground excavations are also situated in more complex geological environments such as layered rock, where analysing the effect of disturbance and redistribution of the in situ stress field needs more attention. Figure 1.1 shows a constructed tunnel in a foliated rock mass, which can be approximated as a transversely isotropic rock (Tien et al. 2006). The principal stresses in the tunnel circumference have two axes of radial and tangential. It means that the orientation of principal stresses around the tunnel circumference varies, while layer orientation in the rock material does not change. Therefore, as can be seen in Figure 1.1 the angle between layer direction and e.g. tangential stress orientation changes around the circumference. In order to answer the question “how the tangential stress around such a tunnel might cause rock failure?”, it is essential to understand the modes of failure in these circumstances. The modes of failure in this case (transversely isotropic rock) are different to those for a tunnel excavated in an isotropic rock.

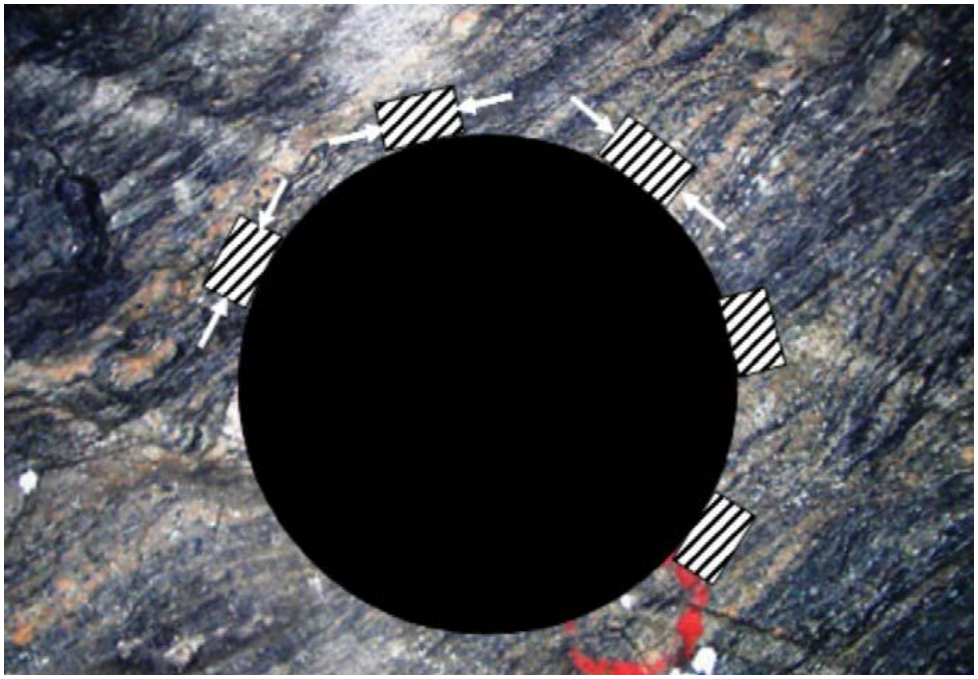

Figure 1.1 Relation between tangential stresses and orientation of foliated rock around a circular opening (after Tien et al. 2006). Orientation of principal stresses varies from parallel to perpendicular to the layer direction.

1.3 Studies in "Research Unit Mining"

In the Research Unit Mining of KULeuven, the process of brittle fracturing of rock is one of the ongoing research topics, while the emphasis is on individual fracture growth. For a better understanding of fracture initiation and growth, similar research topics are conducted from different approaches (Vervoort et al. 2008).

Van de Steen (2001) studied the behaviour of brittle rock in both a homogeneous compressive stress field and in a heterogeneous, anisotropic stress field. He also investigated how successful a micromechanical model is in simulating qualitatively the fracture growth of a rock sample subjected to the above-mentioned stress fields. He observed that fracture initiation occurs either in an area of large stress gradients (e.g. around a circular opening) or in an almost homogeneous stress field. He concluded that observed fractures can only be well explained by a model using flaws. He used for his simulations the DIGS code which stands for Discontinuity Interaction and Growth Simulation (Napier and Hildyard 1992). DIGS is a two-dimensional boundary element code. In his study most of the tests were applied on crinoidal limestone which was assumed to be isotropic and homogeneous at a centimetre scale.

Experimental and numerical studies of the Kaiser effect in cyclic Brazilian tests with disc rotation were conducted on crinoidal limestone by Lavrov (Lavrov et al. 2002). Tests were performed in which discs were loaded and unloaded in two cycles without or with rotations between successive cycles. The rotation angle varied between 0° and 90°. Lavrov et al. 2002 observed that the Kaiser effect became gradually less pronounced with small increasing rotation angles, but was undetectable for angles >10°. These experimental observations were

confirmed by numerical simulations using the DIGS code (Lavrov et al. 2002). Kaiser effect and the effect of confining stress in tri-axial tests on crinoidal limestone were also investigated (Vervoort and Govaerts 2006).

Debecker (Debecker et al. 2006) studied fracture processes in transversely isotropic rock e.g. slate and siltstone. The main focus is on how anisotropic elastic and strength parameters on micro-scale determine the fracture process in rock. His study comprehended both numerical and experimental work. In the experimental work techniques like AE-localization and image analysis were applied. The numerical simulations were performed with a discrete elements code (UDEC, Universal Distinct Element Code) and with a displacement discontinuity boundary element code (DIGS), allowing to simulate individual fracture growth. By combining the knowledge from experiments and simulations he observed that the key parameter is the degree of anisotropy on micro-scale. Debecker (2009) concluded that for small anisotropy, micro-scale strength properties (cohesion and tensile strength) vary little in different directions and therefore the strength and fracture pattern are almost independent of the inclination angle between load direction and normal to the schistosity. In the mentioned case for small anisotropy almost no fractures in the layer direction occur. Debecker (2009) observed that for higher degree of anisotropy more fractures in the layer direction occur. He also observed that for large strength anisotropy, macro fractures in non-layer directions are absent and the sample strength is predominantly dependent on the strength properties in the layer direction.

Ganne (2007) studied the influence of stress history on the process of brittle fracturing in rock materials. In his study the crinoidal limestone blocks are sawed and rectified into rectangular slabs. At one side, half a cylinder is drilled (see Figure 1.2). The specific sample geometry leads to specific macro-tensile or macro-compressive stress states in the region adjacent to the half-cylindrical hole. The loading direction determines the stress distribution. In the mentioned study samples were loaded to be in compression (or tension) configuration. Before failure samples were unloaded, turned and loaded again to be in tension (or compression) configuration. By applying the mentioned loading sequences, the stress history effect was investigated. Ganne (2007) observed that previously induced (by compressive stresses) intragranular cracks influence the occurrence and growth of the intergranular crack caused by tensile stresses. The previously induced intragranular cracks are used by the intergranular crack as an easy path to grow. Therefore less damage than the sum of damage of the individual loadings is observed. Ganne and Vervoort (2007) also observed that the previously induced (by tensile stresses) intergranular crack influences the occurrence and growth of intragranular cracks caused by compressive stresses. Ganne (2007) stated that although the conclusions cannot be extrapolated directly to other rock types, it is shown that the evolutionary sequence of the compressive and tensile stresses within a experiment is an important factor of the amount of (micro-) damage (Ganne and Vervoort 2007).

As for the doctoral research by Ganne (2007), the research of this thesis is also situated within the OT-project (OT/03/35) that has as main objective the further investigation of the effect of the stress variation around circular excavation on the behaviour of rock. Around circular excavations there is a variation of the stress state (size of the principal stress components, but also of their orientation). While the thesis of Ganne (2007) looked at isotropic material, for this study it was decided to concentrate on transversely isotropic material. In other words the preliminary objective of the present thesis was investigating the behaviour of (weak) layered rock material by using similar models as presented in Ganne (2007) (see Figure 1.2). It was decided to use weak material like schistose sandstone or slate,

in order to be able to make a comparison to the study which was done by Ganne (2007), but mainly to address problems linked to underground excavations in weak rock materials. Furthermore better understanding of transversely isotropic rock material was one of the aims.

However, in the stage of finding suitable material (weak and repetitive), some practical difficulties were encountered which finally caused modifications on the thesis objective. The mentioned problems and modifications are discussed in detail in Paragraph 1.4 (Aim of the study).

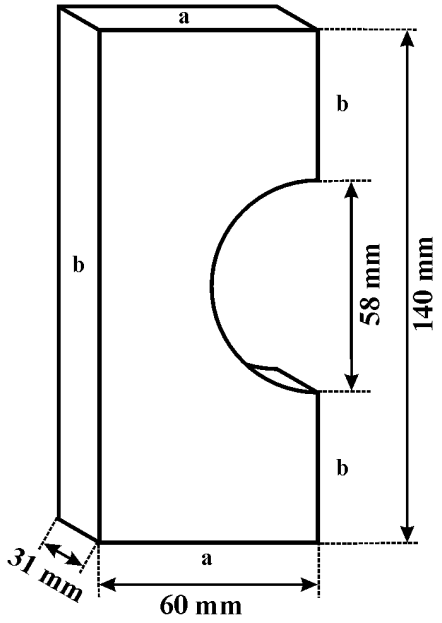

Figure 1.2 Geometry of the test samples. The letter a and b refer to the parallel planes of 31 mm × 60 mm and 31 mm × 140 mm planes respectively (Ganne 2007).

1.4 Aim of the study

1.4.1 Preliminary aim

The preliminary objective of the present thesis was aimed at fracturing caused by a sequence of stress states similar to the study of Ganne (2007), but on weak transversely isotropic rock. Several layered rock (assumed to be transversely isotropic) were selected in order to prepare similar samples as presented in Figure 1.2. Layered rock materials during sample preparation failed. Sample failure happened during different stages of preparation such as cutting, coring and rectifying. Figure 1.3 shows two samples which failed during the preparation process. Left sample in Figure 1.3 is schistose sandstone which failed during cutting. Right sample is slate and failed while rectifying, however some of the slate samples failed during coring. As it can be seen in Figure 1.3 both samples failed through their layer boundaries. It is logic that fractures make use of the layers, as it is expected that they have weaker mechanical properties. Therefore it was decided to select stronger layered rock material. This was the first change in the scope of this thesis. So, it would be possible to compare the strong transversely isotropic rock behaviour (of this research) with the behaviour of isotropic rock

material (Ganne 2007). Furthermore having several blocks with the same mechanical properties showed also to be difficult (problem of repetitious), which was the second problem encountered.

Several blocks of layered sandstone were taken from a quarry in Modave in the South of Belgium. These blocks were taken at very short distance (from 1 to 10 m) from each other. Visual inspection (hand samples) would normally lead to the conclusion that they are all similar material. These materials are expected to have enough strength to tolerate sample preparation process. Several disc-shaped samples from one single block were prepared to verify if rock can be approximated as transversely isotropic material. Brazilian tests were conducted for several samples (of mentioned block) which were positioned with a different layer orientation angle and the effect of layer orientation was quantified (see the details later in Paragraph 4.1).

Figure 1.3 Failed samples during preparation process (see Figure 1.2). Left sample (schistose sandstone) failed during cutting. Right sample (slate) failed during rectifying. Both samples failed along their layer boundaries, LO = Layer orientation.

As a good code of practice and before starting to prepare the specific sample geometry (see Figure 1.2), a few discs were drilled and cut of each block and tested to make sure that the same effect of layer orientation was also observed in the other blocks. This proved to be a good decision, as it became clear that the effect of the layer orientation of, at first sight, similar samples was different for various blocks, even taken at close ranges of 1 to 10 m (problem of repetition). Hence, for the second time, the scope of this thesis was changed.
Therefore, it was decided to concentrate on layer orientation effect of individual blocks, by using Brazilian test conditions, and to investigate in detail why these, at first sight, similar samples behave in different way.

1.4.2 Objective: modification of preliminary aim

As it is already mentioned in paragraph 1.4.1 relatively similar blocks of Modave sandstone do not behave in a similar way. Hence, applying load on samples with different layer orientations taken from different blocks of layered sandstone does not present only the layer orientation effect, but also the material effect. The results of such tests would be a combination of layer orientation effect and some other unknown parameters. To learn more about the latter became the main objective of the study e.g.:
- What are the relevant microscopic differences in relatively similar blocks of Modave sandstone that cause different failure behaviour?
- What are the effects of microscopic differences on macroscopic behaviour of layered Modave sandstone?

1.5 Overview of the work

In chapter 2, an overview is given on micromechanical studies, the theoretical approach of Brazilian tensile tests, the effect of microscopic parameters on macroscopic behaviour of rock material and also the classification of fractured samples.

In chapter 3, the layered rock material (Modave sandstone) which is used in this study is described. Special attention is paid to the microscopic parameters (which are different) in relatively similar blocks of layered sandstone. A petrographical study is done on untested samples. Also the structure of the work illustrated by a flowchart is described, as well as the applied experimental techniques.

In chapter 4, Brazilian test results are presented. Tensile strength and fracture pattern as the main macro-scale behaviour of samples are described. In this chapter, a new classification method for fractured samples is also formulated.

In chapter 5, results of petrographical analyses on layered Modave sandstone are described. In this chapter micro-scale quantification of tested samples is done and the effect of mineral composition (a microscopic parameter) on the acoustic emission results is highlighted. The microscopic quantification is conducted by optical microscopy.

In the 6th chapter, the micro-scale parameters are linked to the macro-scale behaviour. This chapter presents a correlation between chapters 4 and 5. The effect of micro-scale parameters on strength and on the fracture pattern of samples is illustrated.

In the 7th and the final chapter, the conclusions of the study are presented and some recommendations for further research are proposed.

2 Literature Survey

Brittle failure of rock materials is a broad and fundamental subject of rock mechanics that has been studied extensively. But the failure process is still not fully understood, except qualitatively (Andreev 1996). The rock brittle fracture is a fast progressive process which evolves from the initiation of micro-cracks to coalescence of them which eventually leads to failure. Rock failure is affected by microscopic parameters and also by the stress state.

In this chapter, first an overview of micromechanical studies is presented (see paragraph 2.1). Then in paragraph 2.2 the Brazilian test is described, both from a micromechanical and a theoretical perspective. And finally classification of fractured samples and also scale effect in rock strength properties are described.

2.1 Micromechanical studies

The micromechanical studies mainly consider micro-fractures. In these studies, one tries to observe and describe the micro-cracks which exist in rock materials (pre-existing cracks) and also the micro-cracks which are induced by the loading. It is important to observe how these micro-cracks develop, coalescence and finally form the macro-crack(s) that cause(s) the final failure. First, the terms used in micromechanical studies should be described.

2.1.1 Terminology

'A **micro-crack** is an opening that occurs in rocks and has one or two dimensions smaller than the third. For flat micro-cracks, one dimension is much smaller than the other two and the width to length ratio must be less than 10^{-2} and is typically 10^{-3} to 10^{-5}. The length is typically of the order of 100 μm or less' (Simmons and Richter 1976).

Generally, cracks are divided into three types: intragranular cracks, intergranular cracks and grain boundary cracks (Kranz 1983). **Intragranular cracks** that are sometimes termed as intracrystalline cracks stand totally within the grain crystal and they are relatively small (less than 1 μm in width). **Intergranular cracks** that are sometimes termed as intercrystalline cracks extend from a grain boundary crossing into one or more other grains. This type of cracks is longer and often wider than the intragranular cracks and its orientation may be deflected by the grain boundaries and by other cracks. However, intragranular cracks and intergranular cracks are morphologically similar. **Grain boundary cracks** are associated and coincident with grain boundaries.

It is useful to have some information about how the grains are in contact to each other and also the different kinds of grain contact. Different forms of grain contact depend on the compaction pressure and chemical processes which have occurred in the sediment. Tucker

(1995): "Once the grains within an uncemented sediment have assumed their densest configuration by slippage on grain surface, grain orientation and fracture of radical grains, overburden pressure is transferred through grain to grain contacts, commonly point contacts (Figure 2.1a). Progressive increase in overburden pressure increases the stress at grain to grain contacts, with resultant deformation of the crystal lattice at these contact points plus changes in the chemical potential within the immediate area of the contacts (Figure 2.1b). Continuation of stress causes dissolution of the contact area. Progressive solution compaction leads to alteration of the grain to grain contacts, from the original point contacts, through planar (or tangential) contacts to interpenetrating (concave-convex) and sutural grain to grain contacts (Figure 2.1c to e)". It seems that as the grains are more locked to each other, the occurrence of the grain boundary crack needs more energy. Tuğrul and Zarif (1999) observed that the greater degree of grain interlocking present in granitic rocks is a primary factor to have higher mean strength. Also Meng and Pan (2007) observed that sandstones with line-contact (planar contact) between grains have larger strength than those with point-contacts or no-touch.

When rock materials prior to testing are studied in the laboratory, many **pre-existing cracks** are observed. They can have occurred because of different natural mechanisms (Simmons and Richter 1976). During the ascent of the rock to the surface of the earth, grain boundary cracks may occur because of the changing stresses and thermal gradient in the earth. Also different compressibility and thermal expansion in neighbouring grains can cause the crack occurrence. When rocks appear at the surface of the earth, weathering conditions can induce all types of cracks.

Investigation on untested rock samples using micro-crack observational techniques such as scanning electron microscope and optical microscope indicates that untested rock samples contain a large number of pre-existing cracks. Numerous and different crack density data are published (Table 2.1).

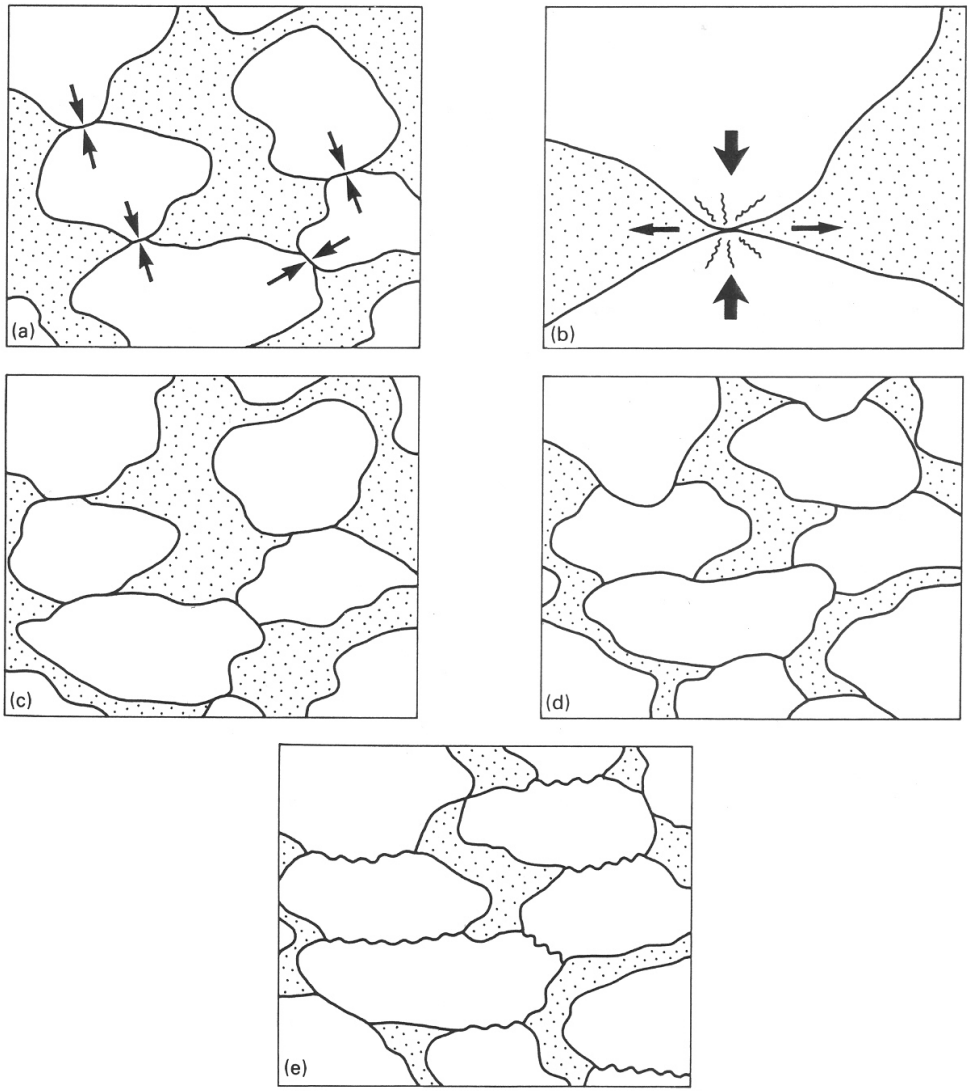

Figure 2.1 Solution compaction between individual grains (porosity is stippled throughout) (after Tucker 1995): (a) point grain to grain contacts (arrowed). (b) Stresses grain to grain contacts (thicker arrows), leading to formation of dislocations in crystal lattice and subsequent dissolution, with lateral fluid transport of solutes (thinner arrows). (c) Planar grain to grain contacts. (d) Interpenetrating grain to grain contacts. (e) Sutural grain to grain contacts.

Table 2.1 Overview of pre-existing crack densities reported in literature.

Crack density (mm/mm^2)	Rock material	Reference
0.220	Carboniferous sandstone	Kožušníková and Marečková 1999
3.560	Inada granite	Chen et al. 1999
2.460	Kurihashi granodiorite	Chen et al. 1999
0.936	Inada granite	Takemura and Oda 2004
0.425	Granodiorite	Hoxha et al. 2005
0.104 – 0.512	Granite	Nasseri et al. 2005
0.330	Crinoidal limestone	Ganne 2007

Theoretically the strength of a perfect, monocrystalline material is 10 to 1000 times higher than the strength usually observed in many materials. Rock and other brittle materials are assumed to contain numerous minute defects. Kannien and Poperlar (1985) stated that a solid body can fail due to the enlargement of a dominant crack contained in that body. Griffith (1924) assumed that a fracture is initiated from a small flaw, present in the material. In other words the initiation of micro-cracks cannot be described without the existence of flaws such as pre-existing cracks that lower the global strength by magnifying the stress locally (Van de Steen et al. 2001, Anderson 2005). Micro-crack's propagation can only be described by the local increase of the stress, caused by the micro-crack itself. The crack interaction and coalescence phase which is followed by the initiation of macro-scale failure is without doubt the least understood and the most complex phase due to its unstable and uncontrolled character.

Delannay (1994) gives the theoretical magnitude of the maximum stress at the end of a crack in a body that can be represented by an elliptical hole with a very small radius of curvature at the ends. He indicated that the stress concentration increases when the size of the crack increases and also when the radius at the ends decreases. At the limit in the case of an ideally sharp crack the magnified stress becomes infinite. The material at the crack tip cannot withstand infinite stresses and therefore must undergo plastic deformation or some form of damage. The size of the plastic zone is sufficiently small in comparison to the size of the crack and the specimen and consequently the entire body may be assumed to behave in an elastic manner (Delannay 1994).

2.1.2 Crack initiation and growth

In the micromechanical approach, cracks in rock materials are produced when the local stress exceeds the local strength (Simmons and Richter 1976). The local stresses are produced either mechanically or thermally. Mechanically induced stresses lead to a variety of crack initiation processes. Prediction of crack initiation in rock materials due to a macro-stress field is difficult, as a macro-stress field produces a very complex stress state on a microscopic scale (as a function of rock material texture). In the literature, the crack initiation is attributed to one or more of the following mechanisms (see Figure 2.2):

- Stress concentration at twins
- Activation of planes of weakness
- Elastic mismatch between components
- Point contact between grains
- Stress concentrations around pores
- Grain rotations and translations

Stress concentration at twins

Olsson and Peng (1976) identified three different types of micro-crack initiation at the edges of twin lamellae in calcite. The cracks are initiated in the grain containing the lamella, in the adjoining grain (Figure 2.2a) or along the grain boundary. The twin lamellae themselves are most probably the result of twin gliding, caused by a shear stress. When the twin lamellae form, the shear stress is relieved in the lamellae and is concentrated at the edges. The location of crack initiation depends on the relationship between the optimal crack orientation and the direction of the weak planes such as cleavage planes or grain boundaries. Twin induced micro-cracking has also been observed in plagioclase and quartz (Kranz 1983).

Activation of planes of weakness

Cleavage planes in crystals are generally those planes with the lowest bond strength and lowest surface energy (Brace and Walsh 1962). Thus in suitably oriented grains (with respect to the local principal stresses), strain energy stored in the grain as a result of applied stresses tends to be relieved on those planes first (Kranz 1983). Cleavage cracks as a subset of intragranular cracks are sufficiently important to be considered separately. They are often seen to occur in parallel sets of various lengths within the same grain (Kranz 1983).

Depending on the type of minerals in contact with each other, grain boundaries can also be planes of weakness (Sprunt and Brace 1974). Grain boundaries can start sliding under the influence of deviatoric stresses or can be wedged apart by neighbouring grains (Kranz 1983).

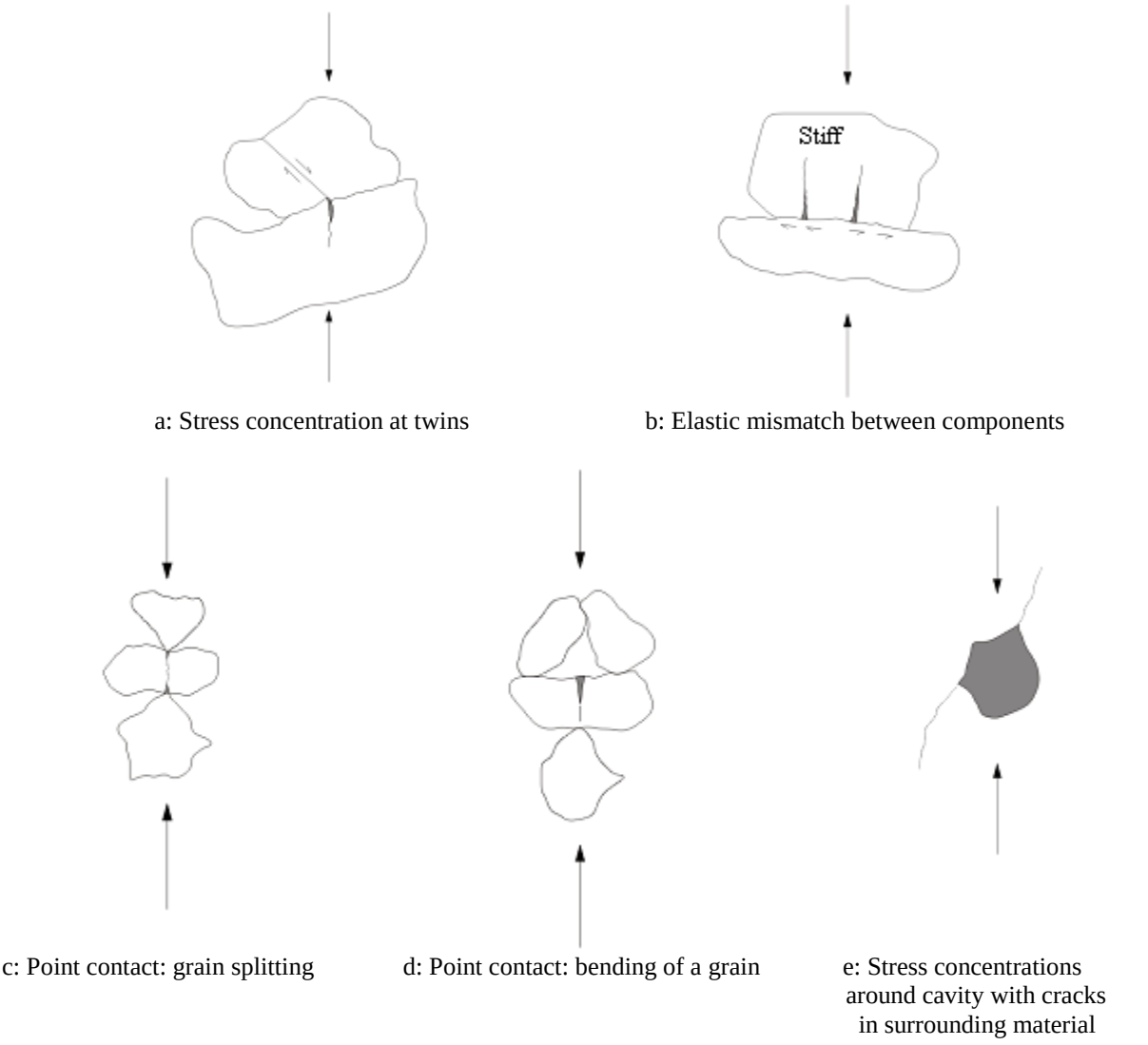

Figure 2.2 Crack initiation mechanisms. The arrows indicate the direction of the major principal stress (Van de Steen 2001).

Elastic mismatch between components
When two minerals with different elastic properties are welded together and are subjected to the same externally applied stress, the mineral with the higher Young's modulus or the lower Poisson's ratio can also be subjected to an additional boundary traction (Dey and Wang 1981). These can exceed the local tensile strength of bonds at the boundary, leading to extension cracks in a stiffer mineral perpendicular to the mutual grain boundary (Kranz 1983), as presented in Figure 2.2b. An elastic mismatch can also arise in two similar minerals due to anisotropy in the elastic properties or due to a difference in grain size (Olsson and Peng 1976).

Point contact between grains
Point and line contacts between parts of grain boundaries are sites of highly concentrated stresses. Tensile stresses exceeding local tensile strength are easily attained and micro-cracks which are initiated in these regions are almost always extensional, Mode I cracks (Kranz 1983). Gallagher et al. (1974) give some examples of micro-cracking initiated at grain boundaries caused by diametrical compression (Figure 2.2c) or bending (Figure 2.2d). Hallbauer et al. (1973) report that point loading of quartz grains by other grains is a frequent source of micro-crack initiation in quartzite.

Stress concentrations around pores
Both pre-existing intragranular cracks and pores concentrate stresses within the surrounding solid material. The sign and magnitude of these stresses depend primarily on the orientation and geometry of the micro-cavity with respect to the externally applied stress field and, secondly, on the tensor mechanical properties of the surrounding medium (Kranz 1983). The resulting micro-cracks are observed as a result of both smooth and sharp-edged intragranular voids (Figure 2.2e) (Kranz 1979, Wong 1982).

Grain rotations and translations
Under deviatoric stresses, grain boundary sliding in crystalline rock may occur, producing coincident grain boundary cracks. Cemented grains in sedimentary rock may be wedged apart and rotated by neighbouring grains, producing cracks in the cement or along the grain boundary (Kranz 1983). Savanick and Johnson (1974) report that for example the pebble-matrix interface in a conglomerate has an unconfined tensile strength of about 15 MPa, while quartz-feldspar interfaces separate under 10 MPa tensile stress. In crystalline rock, grain rotations and translations may be more difficult, because of tighter interlocking, but still can occur during cataclastic deformation (Kranz 1983).

2.1.3 Heterogeneities effect

Rock is heterogeneous because e.g. it is composed of different minerals and/or it contains pores, cracks, cleavage planes and layering. These heterogeneities are valid for the intact material, as well as for the natural discontinuities. Independent of the complexity of the behaviour being integrated into a model, one should never forget that the most typical characteristic of rock material is its heterogeneous nature. Heterogeneity is seen to significantly affect the patterns of failure (Yuan and Harrison 2005).

Van de Steen (2001) considered the importance of heterogeneities such as flaws in computer simulations. Recently Debecker et al. (2008) show that in the simulation of uniaxial compressive tests introducing some weaker elements has a much larger effect than one would expect from a weighted average. For example the introduction of about 20% of weaker

elements results in a strength value of about one third of the weighted average strength. Also the deformation and the fracturing process are different in each simulation.

2.2 Brazilian tests

In rock mechanics normally the Coulomb criterion with tension cut-off is used as the failure criterion. Triaxial tests are commonly applied to determine the cohesion and the friction angle of the rock material. For tensile strength determination, an additional test is required. For this purpose a large number of tests can be used such as: direct tensile tests, bending tests, uniaxial loading of rectangular samples containing a hole, Brazilian tests, diametrical loading of rings, hydraulic extension tests, indentation tests and point load tests (Van de Steen 2001). In the evaluation of possible configurations some factors such as complexity of sample preparation, complexity of testing procedure and also the amount of required material should be taken into consideration.

Without doubt the test most frequently conducted to determine the tensile strength of rock is the Brazilian test. This test is known as diametral compression of cylinders and also as the splitting tensile test. Brazilian test popularity is due to the simplicity of the sample preparation, execution and analysis compared to the other methods (Clatworthy et al. 1993, Chen et al. 1998). Moreover, the other advantage that especially is taken into account in this research is the limited amount of material required. For Brazilian tests rock samples can be directly obtained from a drill core.

The Brazilian test is not only used to test the tensile strength of rock in geotechnical engineering applications, but also used to determine the elastic constants of isotropic and transversely isotropic rocks (Nguyen and Derkx 1997, Chen et al. 1998) and also the tensile elastic modulus (Jianhong et al. 2009).

2.2.1 General description

In the Brazilian test, a disc of rock with a thickness approximately equal to the disc radius is positioned as in Figure 2.3a and compressed vertically until failure. Normally, the disc splits along the loaded diameter, dividing the disc in two halves (see Figure 2.3b). Generally the disc-shaped samples are loaded by the two platens (jaws) of a loading machine without any additional equipment or material between the platens and sample.

In this research the indirect tensile strength, σ_t, perpendicular to the loaded diameter corresponds to

$$\sigma_t = \frac{2F}{\pi D t}$$

where F is the applied load when the sample fails, and D and t are the diameter and thickness of the disc-shaped sample. Of course this formula is considered for the loaded diameter in the condition of a typical fracture (as in Figure 2.3 b) which is often not the case in this study (see further, chapter 4). However, it is even not straightforward to judge that the failure through inclined fracture or through a layer boundary is in tension or shear. Later in chapter 4 it is shown that failure is not always through the loaded diameter.

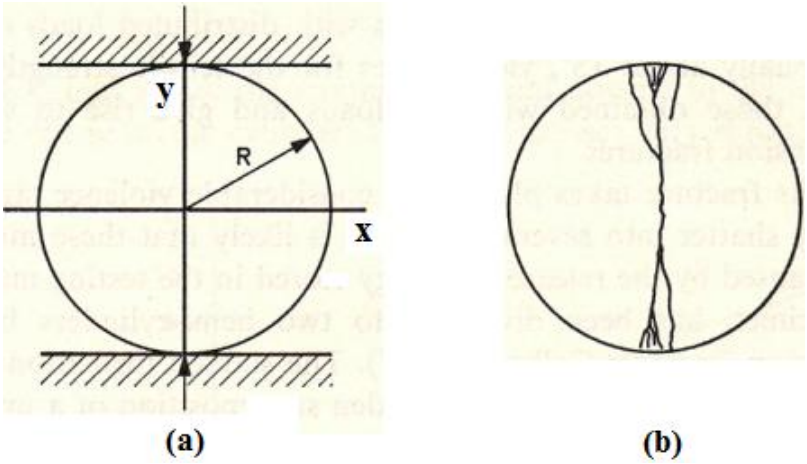

Figure 2.3 (a) A cylinder (disc) compressed between parallel surfaces generating a line load. (b) Typical fractures resulting from (a).

2.2.2 Theoretical approach

The analytical solution for the stresses in a disc-shaped sample under Brazilian tensile test conditions exists whereby the rock material is assumed to be homogeneous and isotropic and to behave in a linear elastic way. It is further assumed that the problem can be treated as a plane strain problem and consequently variables are presented in two dimensions. The boundary stresses are written as a complex Fourier series and Jaeger and Cook (1979) presented the stresses in polar co-ordinates. However by considering the applied load as a line (and not as an arc), Andreev (1995) mentioned that the stresses can be conveniently expressed in Cartesian coordinates.

The stresses in disc-shaped samples under Brazilian test conditions by considering Andreev (1995) equations for a particular case are presented in Figure 2.4. The sign convention for compressive and tensile stresses is considered as positive and negative, respectively. The particular case is a disc-shaped sample with a diameter of 50 mm and a thickness of 25 mm. From Figure 2.4 it is clear that the stress state in the Brazilian test is not uniaxial. The minor principal stress is tensile and the major principal stress is compressive. As the analytical solution is based on the plane stress assumption the intermediate principal stress is zero.

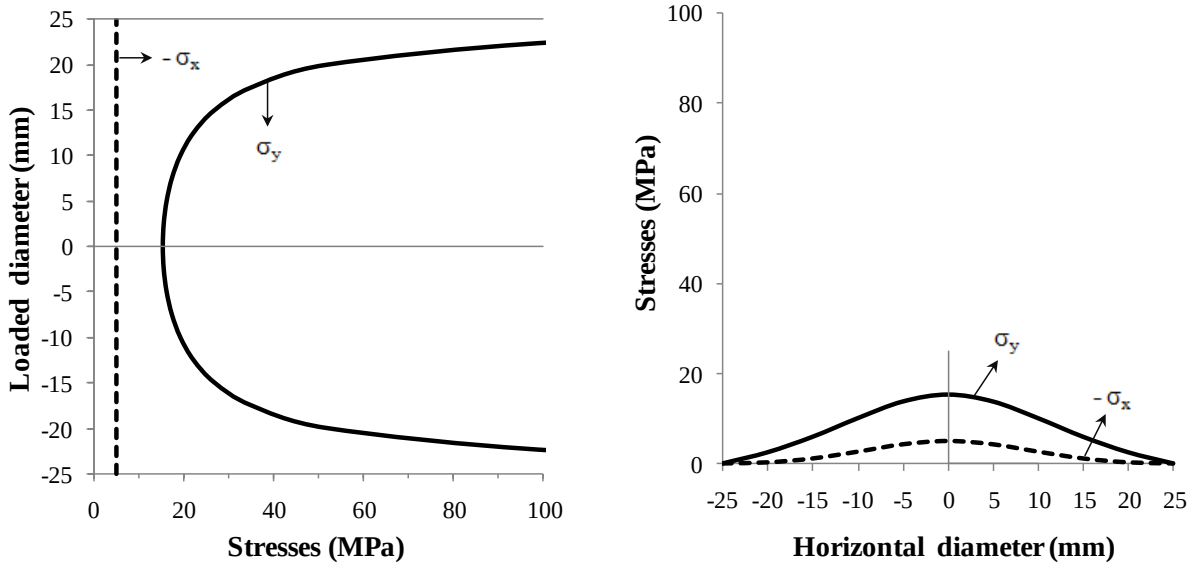

Figure 2.4 Stresses calculated along the loaded (vertical) diameter and horizontal diameter of disc-shaped sample under Brazilian test conditions (see Figure 2.3). The diameter and thickness of the rock sample are considered as 50 and 25 mm, respectively. The applied load is 10 kN.

As can be observed from Figure 2.4, the two areas near the ends of the loaded diameter are subjected to large compressive stresses. From analytical solution (Andreev 1995) the end points of the loaded diameter are singular points in the stress field. Therefore stress concentration is present in the region near these two points. If a sample fails in shear in one of these regions, the validity of Brazilian test to determine the tensile strength can be questioned. However, mentioned stress concentrations disappear at the region away from the loading point. As expected, the two areas near the ends of the horizontal diameter are free of stresses. From Figure 2.4 it can be observed that the compressive stress σ_y is about three times the absolute value of the tensile stress σ_x in the central part of the loaded diameter.

2.2.3 Micromechanical approach

The microstructure of rock is known to influence its macro-scale behaviour. This part of literature review concerns the understanding on how cracks initiate and propagate in the microstructure. Acoustic emission (AE) techniques allow us to extend our hearing to detect sounds of higher frequencies and lower intensities such as crack propagation in rock materials (Wevers 1987). AE event emissions are sound waves emitted by changes in microstructure. These changes can be micro-cracks or fractures as they are created or propagate. The sound waves propagate through the rock sample and are recorded by sensors which are connected to an acquisition system. Processing techniques are applied in order to determine the damage conditions and locations. AE hits and rates show the amount and intensity of fracturing.
The monitoring of AE waves in the laboratory, usually in the range of 200 to 2000 kHz has proven to be a powerful tool available to study the brittle failure of rocks in a controlled stress environment (Cai et al. 2004). There is generally a good correlation between AE rate and inelastic strain rate (Cai et al. 2004), therefore the AE rates can be used to quantify damage initiation and accumulation in rock samples (Ganne et al. 2007).

It is known that the stress state in the Brazilian test is not uniaxial. The minor principal stress is tensile, the intermediate principal stress is zero (plane stress assumption) and the major

principal stress is compressive (Andreev 1995, Van de Steen 2001). Yu et al. (2009) mentioned that each of the principal stresses can have some effect on rock strength. Yu et al. (2009) explained that the compressive stresses can help the vertical micro-cracks at the initiation point to open during experiment, reducing the tensile stress required to cause failure.

Colback (1966) conducted Brazilian tests on dolerite and granite and showed quite conclusively that fracture starts either in the centre of the disc or under the platens, depending on the load distribution at the platen contact. From a theoretical analysis, Fairhurst (1964) concluded that failure only occurs in tension. The evidence provided by Mellor and Hawkes (1971) suggested that the fracture originates in the centre. In some instances they were able to arrest the crack before it reached the platens. Also Yanagidania et al. (1978) by using strain gages as a crack detector in Brazilian tests found that the crack is not initiated from the loading point but from the tensile stress zone.

On the other hand the experiments of Hudson et al. (1972) indicate that failure in most of their samples initiates under the loading platens. In their finite element analysis of the Brazilian test, Clatworthy et al. (1993) use both a linear elastic model and a continuum damage model (Van de Steen 2001). Using the Griffith failure criterion in the linear elastic model, they concluded that failure is most likely to initiate at a short distance under the platen, and that failure is least likely to initiate in the centre of the disc (Van de Steen 2001). Also Yu (2005) based on 3D-finite element method (FEM) analyses, pointed out that the specimen is initially destroyed by the stress concentrations at the loading points, instead of at the centre of specimen where the tensile stress is nearly uniform (cited by Yu et al. 2009).
Lavrov et al. (2002) simulated the micro-fracturing processes in loaded Brazilian discs. They observed that cracks appear first in the vicinity of the disc-insert contact. This is in full agreement with the results of the earlier experiments by Falls et al. (1989 and 1991). Falls et al. (1989) monitored the acoustic emission during Brazilian tests. They also determined the source location and the source mechanisms. They conclude that most of the events originate in the region close to the sample-platen contact, and those shear-type mechanisms are as abundant as simple tensile micro-fracturing. They argue that both types of failure do not occur independently from each other, but are in fact the result of a mixed shear-tensile mechanism (Van de Steen 2001). The sliding of a flaw or micro-crack thus causes a tensile failure (Brace et al. 1966). From the preceding discussion, it appears that the initial failure mechanism is still not clearly understood.

2.2.4 Effect of micro-scale parameters on macro-scale behaviour

In fact, rock failure occurs for certain conditions, e.g. it is function of the petrographic characteristics and the stress state. Petrographic characteristics are e.g. mineral composition percentage and microstructures, such as average grains size of major constitutive grains, cement and contact modes between grains (Meng and Pan 2007). In this paragraph the correlations between the micro-scale parameters and macro-scale behaviour of rock materials are explained and highlighted. The variability in macro-scale behaviour (strengths and fracture patterns) seems to be closely related to the changes in the mineral composition and microstructures of rock samples.

Rock strength is one of the most important parameters in rock mechanical studies. Its variation is explained by many factors including mineral composition, density, porosity, fabric, moisture content, state of alteration or changes due to weathering, etc. (Přikryl 2001).

Also stress state, shape (Hawkes and Mellor 1970) and size (Bieniawski 1968) of test specimens and test conditions like temperature and strain rate (Paterson 1978) are important. The effect of micro-scale parameters on strength of rock materials is investigated at large, mostly for uniaxial compression strength (UCS). However, this study focuses on Brazilian tensile strength (BTS). The first question that comes to mind is if it is logic to compare the effects of micro-scale parameters on UCS-values with their effects on BTS-values. Tuğrul and Zarif (1999) mentioned that a direct linear correlation between the tensile strength and uniaxial compressive strength for the granitic rocks exists. Similar correlations between these two properties were obtained for sandstones by Shakoor and Bonelli (1991) and for basaltic rocks by Tuğrul and Gürpinar (1997). Also Tuğrul and Zarif (1999) mentioned that the tensile strength of rock is controlled by the same factors as compressive strength, which are mineral composition and texture (grain size and shape).
The knowledge of the fracture patterns in anisotropic rock material is required in studies of civil, mining and petroleum engineering with applications like e.g. stability and movement of superficial and deep foundations on stratified rocks, stability of underground excavations, slope stability and borehole deformation. Despite its importance, fracture patterns are often poorly discussed and understood. McWilliams (1966) portrayed that the defects perhaps act as surfaces of weakness to dictate the direction of failure. Willard and McWilliams (1969) reported that micro-fractures, grain boundaries, mineral cleavages and twinning planes may act as surfaces of weakness, which control the direction in which failure occurs. Although the mentioned conclusions are logical, they are expressed in an uncertain way because expressing an exact rule on the effect of micro-scale parameters on fracture pattern is really complicated.

2.2.4.1 Mineral composition effect

Mineralogical composition is one of the main properties controlling the rock strength. The experimental results in many studies show that rock strength is considerably affected by the existence of different minerals. The Nature of minerals suggests that the presence of strong elements such as quartz increases the rock strength and, on the other hand, the abundance of weak minerals such as mica and carbonate decrease the rock strength. It is widely accepted that for higher quartz content, rock strength increases. Contrary to quartz the abundance of easily cleavable minerals would result in lowering the strength values. Tuğrul and Zarif (1999) in their study on granitic rocks observed that the feldspars have a very important role in strength reduction. The presence of mineral cleavage and micro-fissures in feldspars within the intact specimen lowers the tensile strength, as it lowers the compressive strength (Onodera and Asoka Kumara 1980).

In several studies a strong positive correlation between quartz content and compressive strength is observed and for higher composition percentage of quartz, an increase of the strength of the rock is reported (Gunsallus and Kulhawy 1984, Tuğrul and Zarif 1999, Meng and Pan 2007). Meng and Pan (2007) indicated that for sandstone some granular minerals such as quartz become the main stress-bearing skeleton and are able to accumulate large quantities of elastic strain energy and that it is due to their higher strength than other flaky minerals such as mica and clay. They also mentioned that for higher percentage of detritus (or quartz) in sandstone, the rock strength and brittleness are gradually increased and the duration from peak strength to complete failure becomes shorter.

Contrary to all the mentioned studies Tuğrul and Zarif (1999) noted that any significant relationship between the quartz content and the strength of rock was not observed in the study of Bell (1978) on Fell sandstones. As the quartz content is an important factor in rock

strength, reported result (i.e. lack of a relationship between the quartz content and the strength) of Fell sandstones should be reviewed and clarified. The current study is done on stratified sandstone and it is observed that sandstone samples with higher quartz content show a higher strength (see later in paragraph 6.1.1). Consequently review of the results of Bell (1978) on Fell sandstones becomes important.

Thin section microscopic examination of the sandstones by Bell (1978) revealed that these sandstones were principally composed of quartz, with lesser amounts of feldspar and occasionally very small amounts of mica. In fact the average total quartz content was 86.5% with a standard deviation of 4.1%. The mica content was of little or no importance and in fact, it was absent in 16 of the 30 samples (Bell 1978). Its mean value was only 0.5%. According to the classification of ultimate unconfined compressive strength proposed in the report to the Geological Society of London on the Logging of Cores for Engineering Purposes (1970), Bell (1978) observed that 78.6 % of these sandstones were strong, 10.7% very strong and the other 10.7% moderately strong. It is logic to conclude that the high strength of these tested samples is linked to the high amount of quartz in them. As the percentages of quartz content in all the samples of Bell (1978) are roughly close to each other, it seems acceptable that other properties present a significant effect on strength variation. For example in the study of Meng and Pan (2007), increasing rock strength is observed for higher composition percentage of quartz; where, the range of quartz content is from 15% to 60%. In the study of Bell (1978) on Fell sandstones, although for example 87% quartz content is more than 81% quartz content, one should not always expect a higher strength for the sample with 87% quartz content as it is not the only factor that has influence on rock strength.
The samples of Bell (1978) are taken from the surface up to a depth of 96.6 m. He reported that the influence of weathering seems to have penetrated to a depth of about 18 m. In his study, density is related to strength and it is observed that the rocks which are more compact generally have a higher strength than those which are less compact. The Fell sandstones do tend to show an increase in strength with increasing density. He mentioned that, as expected, there is an inverse relationship between compressive strength and effective porosity; that is, as the porosity of the Fell sandstones increases, their strength decreases. He also observed that there is a highly significant relationship between the tensile strength of the Fell sandstones and the effective porosity, again it decreases as pore volume increases. In his research a relatively high variation of void space is recorded. The void space of Fell sandstones samples in his research is from 3.1% to 16.2% where its arithmetic mean is 6.8% with a standard deviation of 3.6%. Therefore as expected the effect of this property on rock strength is significant.
From the above explanation it can be concluded that the conflicting results about the effect of quartz content on rock strength can be attributed to the variation range in quartz content. It is important to consider the variation range in different parameters. As the variation range in one parameter is more extended than for the other parameters, a more obvious influence of that parameter is expected.

2.2.4.2 Grain size effect

The experimental results in many studies suggest that the relationship between grain size and strength is very important. Also in this research it is explained later that the most important parameter that affects the tensile strength is grain size. Přikryl (2001) suggested that the grain size of rock forming minerals seems to be the main cause of strength variation. However, the effect of grain size on the strength of materials and especially of rocks is still receiving

insignificant attention in geomechanical testing. It is important to note that the term ‘grain size’ is applied for the average grain size of the major rock-forming mineral.

Recently Meng and Pan (2007) have investigated a correlation between petrographic characteristics and some macroscopic behaviour of some sandstone types. Meng and Pan (2007) have reported that the uniaxial compressive strength of the rock increases for larger average grain size (see Figure 2.5). They observed that for larger average size of major detritus grains, from very fine-grained argillaceous sandstone, fine-grained sandstone to medium-grained sandstone, the coarse granular minerals such as quartz and feldspar increase whereas the fine flaky minerals decrease. Therefore, it is realized that due to loading, the coarser composition such as quartz becomes the main stress-bearing skeleton and is able to accumulate large quantities of elastic strain energy because of their higher strength. The range of grain size in the study of Meng and Pan (2007) is from 0.1 to 0.3 mm. This grain size range in comparison to some studies which are further mentioned (in this paragraph) is very limited.

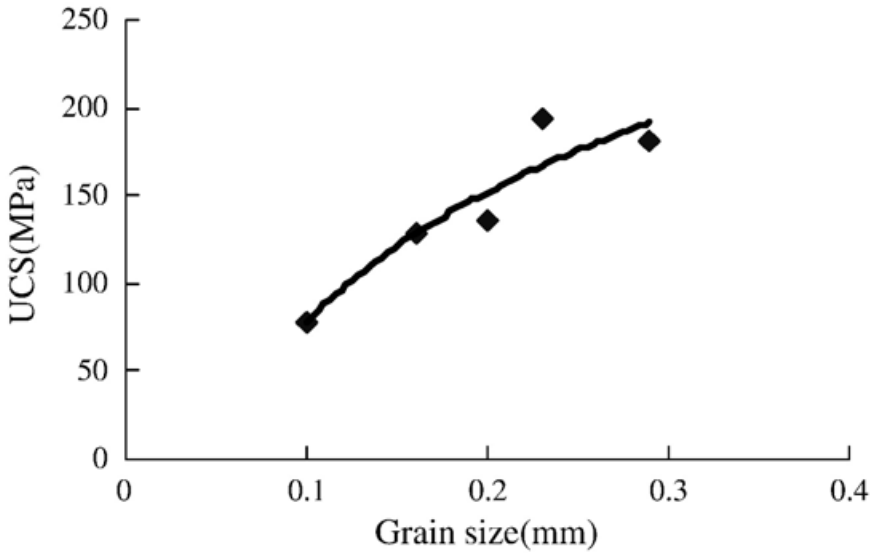

Figure 2.5 Uniaxial compressive strength as a function of grain size for selected sandstone from east of China (after Meng and Pan 2007).

However, in many studies on crystalline rocks it is mentioned that the strength of rock material decreases for larger grain size (Přikryl 2001; Tuğrul and Zarif 1999; Eberhardt et al. 1999). Most of the authors refer to the relationship between grain size and strength which was first linked to Griffith’s theory (Griffith 1920) by Brace (1961). Brace (1961) assumed a close relation between Griffith’s crack length and the maximum grain size diameter. Griffith (1920) suggested that a low tensile strength of glass was due to failure caused by stress concentration at the end of very small internal and surface flaws (Jaeger and Cook 1969). These flaws have become known as Griffith’s crack. The practical application of the Griffith’s theory primarily involves the determination of the stress threshold at which a crack initiates and begins to propagate. Griffith (1924) extended his theory for an elliptical crack loaded in compression and found that the crack extends when

$$\sigma_c \geq 8 \times \sqrt{\frac{2E\alpha}{\pi c}}$$

where: σ_c = compressive stress (required for fracture);

E = elastic or Young's modulus;
α = surface energy per unit area of the crack surfaces;
c = crack half-length.
Therefore it can be seen that the smaller the crack length, the greater the stress required for fracture initiation. Numerous studies have confirmed that the peak strength of rock decreases inversely with the square root of the grain size (Eberhardt et al. 1999 and Wong et al. 1996). In these cases, the Griffith's crack length can be taken as being roughly proportional to the grain size. Also other authors show that the decrease of rock strength for larger grain sizes has a non-linear trend (Přikryl 2001) and some studies in general suggested that the strength of rocks is greater for finer grained rocks (Tuğrul and Zarif 1999, Hatzort and Palchic 1997 and Brace 1961). However, use of Griffith's essentially microscopic theory to predict the macroscopic behaviour of rock material under a variety of boundary conditions, requires the introduction of a set of Griffith crack size, shape and their orientation distribution (Brady and Brown 1994).
The general conclusion of the mentioned studies on crystalline rocks indicates that rock strength for larger grain size decreases. Another important factor that should be considered in these studies is the grain size range of studied rock materials. Therefore the grain size range of some of these studies is presented to give an idea about the effect of grain size on rock strength in a particular grain size range.

In the study of Eberhardt et al. (1999), rock strength is found to decrease for larger grain sizes. Their results are obtained by investigating three rock materials with similar mineralogical compositions. These rock materials are granodiorite, grey granite and pegmatite. The average grain size for the first two of them is 1 and 3 mm, respectively. The grain size range for the third rock (pegmatite) is from 10 to 40 mm with an average of about 20 mm. In the mentioned study the result that rock strength decreases for larger grain size is obtained from three grain sizes i.e. 1, 3 and 20 mm. The grain sizes of 1 (or 3) and 20 mm are two extremes without looking at the grain sizes in between. So the result is valid for comparing the extremes and there is no proof to develop the conclusion for a large range of grain sizes between the extremes.

Tuğrul and Zarif (1999) have reported that the smaller grain size is a primary reason for the higher mean strength of particular studied granitic rocks (see Figure 2.6). Quartz, plagioclase and K-feldspar are the main minerals in all their studied samples. For their samples the range of average grain size of quartz, plagioclase and K-feldspar is from 0.5 to 1 mm, 0.35 to 1.6 mm and 1 to 4 mm, respectively. The grain size range of rock material in this research in comparison to Eberhardt et al. (1999) is limited.

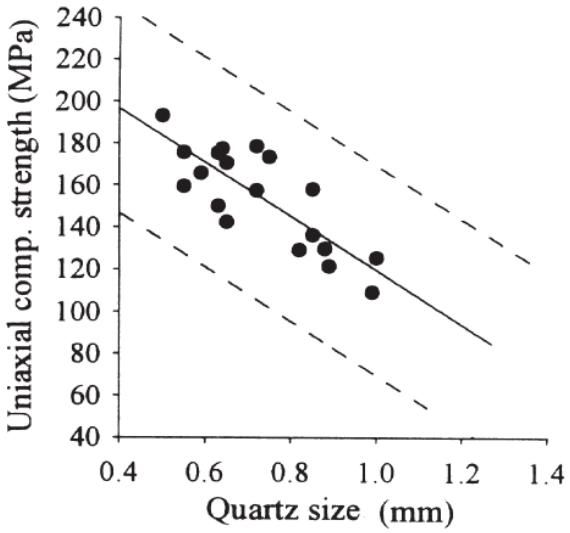

Figure 2.6 Uniaxial compressive strength as a function of quartz grain size for selected granitic rocks from Turkey (after Tuğrul and Zarif 1999).

Other research on granite which is done by Přikryl (2001) is considered. He has concluded that the uniaxial compressive strengths of low porosity (from 0.9 to 4.5%) magmatic rocks (granites) are found to be increased for smaller grain size of rock (see Figure 2.7). In the mentioned study, grain size is calculated from weighted average of all rock-forming minerals. The range of average grain size in this study is from 0.12 to 0.74 mm. In other words average grain size of samples with the coarsest grain is more than 6 times the average grain size of samples with the finest grain. The above reported studies look at the effect of grain size at a relatively wide range.

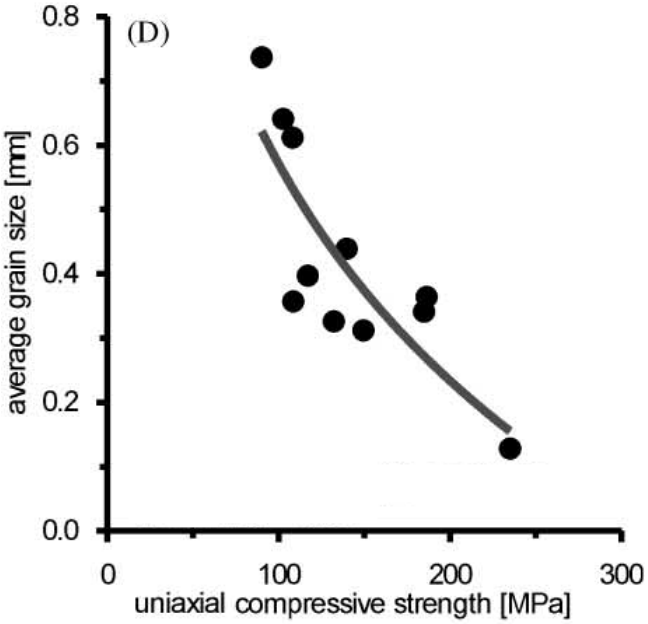

Figure 2.7 Uniaxial compressive strength as a function of grain size for selected granites from Czech Republic (after Přikryl 2001).

Some important factors in stating the correlation between the grain size and rock strength should be considered. Different rock types have different mineralogical composition and consequently they have different micro-scale fracture processes. Mineralogical composition and micro-scale fracture processes of clastic rocks (e.g. sandstone) and crystalline rocks (e.g. granite) are not the same (as briefly explained earlier). Another important factor that should be considered is the grain size range of studied rock materials. When the effect of grain size is looked at a relatively wide range, other parameters such as porosity can play a role. The porosity is an important factor in rock strength, as the voids reduce the integrity of the material. In the study of Tuğrul and Zarif (1999), as expected, inverse relationships between the uniaxial compressive strength and both the effective and total porosity have been reported. Similar results are observed by Přikryl (2001) and he noted that, although the variable grain size seems to be the main cause of strength variation, the influence of porosity can neither be underestimated. Therefore it seems that declaring the effect of grain size on rock strength without saying the grain size range cannot be done. In an investigation of the grain size effect on rock strength, mentioning the grain size range makes it more meaningful; however, the variation range of other parameters (e.g. porosity) should also be considered.

Table 2.2 summarise all the mentioned studies about grain size effect on rock strength. Also the result of current study is presented in Table 2.2 to have a comparison between this study and the reported results (results of this part of the study is explained later in detail in paragraph 6.1.1). Different correlations between strength and grain size for two different rock types (crystalline and clastic) are highlighted in Table 2.2.

In literature, the number of reports investigating the effect of grain size on the fracture pattern is limited (contrary to grain size effect on rock strength). Recently Eberhardt et al. (1999) mentioned that grain size effects were seen to have a significant influence on cracks originating along grain boundaries, but were found to be minimal with respect to sample deformation. It was reasoned that longer grain boundaries and larger intergranular cracks, due to increased grain size, provided longer and more continuous paths of weakness for growing cracks to propagate along. This is an interesting result, however one should pay attention to the fact that the study of Eberhardt et al. (1999) looked at three grain sizes, i.e. 1, 3 and 20 mm.

Table 2.2 Overview of grain size effect on the strength of crystalline rocks (items I, II, III) and clastic rocks (items IV, V).

Item	Material	Considered mineral	Grain size measurement method	Grain size range in different samples (mm)	Strength variation for larger grains	Reference
I	Granodiorite and granite [1]	All minerals [2]	Not mentioned	1, 3, 20 [1]	Decrease	Eberhardt et al. (1999)
II	Granitic rocks	Quartz	Point-counting	0.5 – 1	Decrease	Tuğrul and Zarif (1999)
		Plagioclase	Point-counting	0.35 – 1.6	Decrease	
		K-feldspar	Point-counting	1 - 4	Decrease	
III	Granite	All minerals [2]	Equivalent circle [3]	0.12 – 0.74	Decrease	Přikryl (2001)
IV	Sandstone	Detritus grain [4]	Not mentioned	0.1 – 0.3	Increase	Meng and Pan (2007)
V [5]	Sandstone	Quartz	Point-counting	0.07 – 0.11	Increase	This study

1- Grain sizes of 1, 3 and 20 mm correspond to granodiorite, grey granite and pegmatite granite, respectively. All the three materials have similar mineralogical composition.
2- Grain size is calculated from weighted average of all rock-forming minerals.
Constitutive minerals in granites of item **I** are: K-feldspar, plagioclase, quartz and biotite.
Constitutive minerals in granite of item **III** are: quartz, K-feldspar, plagioclase, muscovite and biotite.
3- Grain size is expressed as the diameter of the circle of the equivalent area as it is occupied by analysed grain.
4- In this study composition of rocks are called: detritus grain, matrix and cement. Quartz, feldspar and rock debris are considered as the detritus grain.
5- Result of this study is also presented for comparison.

2.3 Classification of fractured samples

Various modes of failure of rock samples have been observed and classified for both isotropic and anisotropic materials. Most of them considered cylindrical samples (Reinhart 1966, Paul and Gangal 1966, Fairhurst and Cook 1966, Szwedzicki and Shamu 1999, Tien et al. 2006, Szwedzicki 2007). However, failure of a disc-shaped sample in a Brazilian test is also classified (Chen et al. 1998). Some of the classifications are presented in this paragraph. By getting some ideas from following classifications, later on the classification which is formulated in this study is presented (in chapter 4).

Cylindrical rock sample under uniaxial compressive stress, due to localised stress concentrations around microscopic discontinuities, can fail in tension, in shear or in combination of tension and shear stresses (Szwedzicki 2007). Szwedzicki and Shamu (1999) suggested for hard and brittle cylindrical rock samples, five distinct modes of failure: simple extension, multiple extension, multiple fracturing, multiple shear and simple shear (see Figure 2.8). Szwedzicki (2007) explained the mentioned modes as follows:
The simple extension mode denotes a failure along a plane parallel to the loading direction. This mode does not happen frequently and such a failure mode may suggest that the sample was relatively free of microscopic discontinuities.
Multiple extension happens when two or more fractures run parallel to the loading direction.

Multiple fracturing is considered if sample disintegrates along a number of planes at various angles. When tensile failure is predominant, most of the fractures are vertical and shear failure is predominant if the sample disintegrates along inclined planes.
Multiple shear takes place along two or more planes situated obliquely to the loading direction, but not being parallel to each other.
Simple shear involves one or more parallel planes situated at an oblique angle to the loading direction.

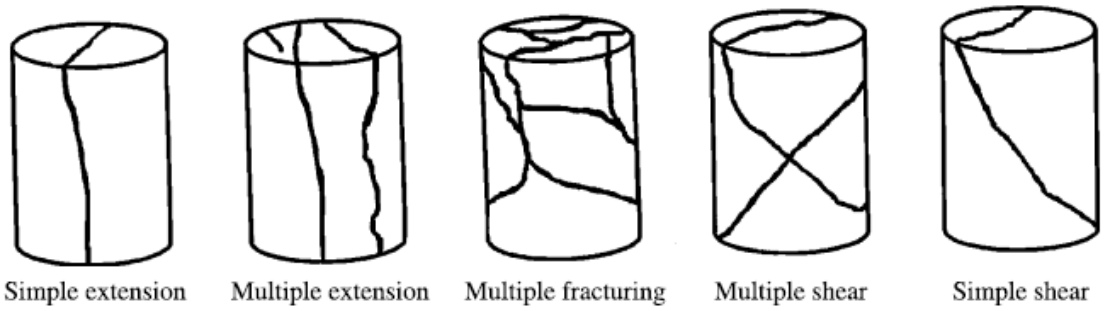

Figure 2.8 Modes of failure for cylindrical sample (Szwedzicki 2007).

Recently Tien et al. (2006) conducted an experimental investigation of failure mechanism on artificial transversely isotropic rocks. They classified failure modes of cylindrical samples from simulated transversely isotropic rocks under different confining pressure. They considered two main failure modes as sliding failure along discontinuities and non-sliding failure along discontinuities (see Table 2.3). In the first one the specimen mainly fails by sliding along the discontinuities and thus fracture orientation is parallel to the bedding plane. In non-sliding failure along discontinuities, the failure is not related directly to the discontinuity. Tensile splitting can occur along or across the discontinuities and shear fractures can occur across the discontinuities and develop in both components of the interstratified rock (see Table 2.3). These different failure modes happen by changing layer orientation and confining pressure of tested samples.

Table 2.3 Classification of failure modes for simulated transversely isotropic rocks (after Tien et al. 2006)

Main failure mode	Sub-failure mode	Label	Specimen orientation/confining condition
Sliding failure along discontinuities		Discontinuity, Fracture — SD mode	$45° \leqslant \theta \leqslant 75°$/0–35 MPa
Non-sliding failure along discontinuities	Tensile-split along discontinuities	Fracture, Discontinuity — TD mode	$\theta = 90°$/0 MPa
	Tensile fracture across discontinuities	Discontinuity, Fracture — TM mode	$0° \leqslant \theta \leqslant 30°$/0 MPa
	Sliding failure across discontinuties	Discontinuity, Fracture — SM mode	$\theta = 90°$/6–35 MPa and $0° \leqslant \theta \leqslant 30°$/6–35 MPa

θ is the angle between the direction of minor principal stress and the discontinuity.

The last classification which is presented in this paragraph is on disc-shaped samples under Brazilian test conditions. Chen et al. (1998) investigated the tensile strength of layered sandstone by conducting Brazilian tests. In their study samples are tested for different layer orientation from θ = 0° (horizontal layers) to θ = 90° (vertical layers). In the study of Chen et al. (1998) two major modes of failure are observed. They mentioned that when θ varies between 0° and 60° or θ is equal to 90°, tensile splitting along the loaded diameter is the dominant mode of failure. However, when θ varies between 60° and 90° shear failure along the sandstone layers with or without branching is dominant (Chen et al. 1998). The combination of the two mentioned failure modes (tensile splitting and shear) is also observed in certain cases as shown in Figure 2.9 for θ = 60° (Chen et al. 1998). From the explanation above it can be concluded that the failure along layer boundaries (except for θ = 90°) is considered as shear failure (by Chen et al. 1998). However, it is important to mention that it is even not straightforward to judge that the failure through inclined fracture or through a layer boundary is in tension or shear.

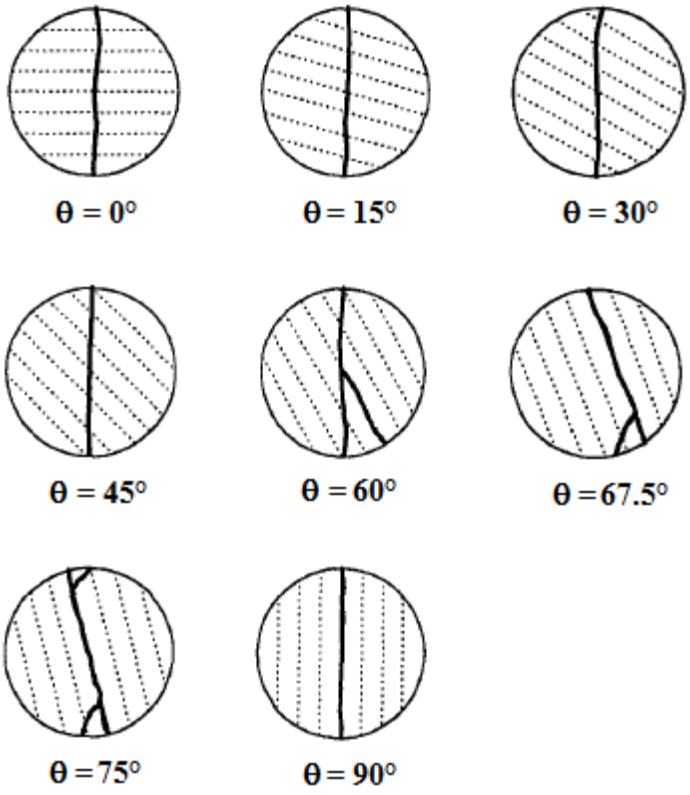

Figure 2.9 Failure modes under Brazilian test conditions for different layer orientation (after Chen et al. 1998).

In all the mentioned classifications effort has been made to link the fracture pattern to failure modes (shear or tensile). However, for some samples with complicated fracture pattern i.e. multiple fracturing in Figure 2.8 or Brazilian sample for θ = 60° in Figure 2.9, it is difficult to judge about the dominant mode of failure. Furthermore when the material is complex (anisotropy in comparison to isotropy), the precise determination of the failure mode needs more attention, a better understanding of the material and the failure mechanism. Also it is good to note that the fracture patterns in all above classifications are considered qualitatively.

Fracture pattern of a single sample can be classified differently when this is done qualitatively. To prevent different interpretation for fracture pattern of one sample, the classification method which is presented in this study (see later in chapter 4) is formulated in a quantitative way.

2.4 Scale effect in rock strength properties

Experimental methods are the most important and reliable way to study rock properties and rock failure mechanisms. The failure mechanism of rock materials due to their mineralogical texture is complex. However, experimental observations are expensive and time consuming (and sometimes infeasible) when conducting a large number of experiments with different sizes. Numerical methods have become increasingly popular in the study of rock failure processes in geotechnical engineering. However, numerical models which are simplified from real conditions must always be validated against experiments.

In rock mechanics the uniaxial (unconfined) compressive strength (UCS) test and Brazilian tensile strength (BTS) test are considered to be the most widely used methods to obtain rock strength properties. Change in rock strength properties (e.g. UCS and BTS) with sample size is referred to as scale effect. In this context the so-called scale effect is split up into two categories: size effect and shape effect (Thuro et al. 2001 and Pan et al. 2009). The size effect can be studied by comparing the rock strength values (UCS and BTS) from specimens with the same shape but different sizes (the same length/diameter ratio but with different diameters). The shape effect can be studied by comparing the rock strength values from specimens with the same diameter (or length) but a variation in length/diameter ratio (Thuro et al. 2001 and Pan et al. 2009).

Most researchers believe that scale effects exist in the failure process of rocks, although some have found that there is no scale effect of rocks under uniaxial compression (Pan et al. 2009). Traditional explanation of scale effects experienced in physical testing indicated that the larger specimens can have more weak elements to initiate failure. In other words the scale effects are caused by the heterogeneities of rock specimen, in the traditional point of view.

2.4.1 Size effect

In the behaviour of many materials two type of size effects play a role: a deterministic size effect and a statistical size effect. A deterministic size effect is caused by strain localization which cannot be appropriately scaled in laboratory tests (Tejchman and Górski 2007). A statistical size effect is due to the presence of the randomness of the local material strength caused by a number of weak links (Tejchman and Górski 2007). In this study as the focus is on laboratory tests, only the statistical size effect is considered.

Rocco et al. 1999a by conducting 110 Brazilian tests on granite and mortar specimens have observed that the specimen size is not the only variable that affects the splitting tensile strength. They observed that the specimen shape and the width of the bearing strips used to distribute the load during the test are also important variables that affect substantially the results of the Brazilian test. They also did theoretical analysis of size effect and boundary conditions in the Brazilian test (Rocco et al. 1999b). They have concluded that for widths of load-bearing strip smaller than 4% of the specimen diameter, the effect of the specimen size

is negligible and the splitting strength approaches the tensile strength for any practical specimen size.

Thuro et al. 2001 studied the size effect of limestone samples by conducting uniaxial and Brazilian tests. In their study the diameter of the cores was varied between 45 and 80 mm. Thuro et al. 2001 for uniaxial samples took a constant length/diameter ratio of 2 and calculating a mean value out of 3 to 5 samples for each diameter. For Brazilian samples they took a constant length/diameter ratio of 1 and calculating a mean value from 4 samples for each diameter. Figure 2.10 shows the variation in rock strength as a function of diameter in the mentioned study. By considering the results presented in Figure 2.10 it is concluded that there is no remarkable size effect in the tested diameter range neither for indirect tensile strength nor for unconfined compression strength (Thuro et al. 2001). These results seem to be compatible with the result of numerical simulation of scale effect in rocks under compression (Pan et al. 2009). Pan et al. 2009 observed that for rock specimens with the same degree of homogeneity, the size and the shape effects do not seem to be dominated by the heterogeneity of the rock specimens. They observed that with the same heterogeneity, if there is no friction between the sample ends and platen, no discernible size effect occurs. The same heterogeneity implies that the properties of the rock samples with different lengths correspond to the same stochastic random distribution, which means that the rock specimens contain flaws with the same probability (Pan et al. 2009).

On the other hand Figure 2.11 shows a typical example for expressing scale dependency on the compressive strength of intact rock, in which the results of laboratory tests on many rock types are compiled. In mentioned figure UCS_{50} is the uniaxial compressive strength of cylindrical sample with diameter D=50 mm, and UCS is the uniaxial compressive strength of a sample with an arbitrary diameter, D (10–200 mm). For all the tested samples, the length is two times of the diameter. Figure 2.11 effectively presents the decreasing trend of rock strength for samples with larger diameters (Yoshinaka et al. 2008).
Jackson and Lau (1990) presented a study on scale effect in hard rock that was performed on Lac du Bonnet granite sampled from a level of 240 m in an underground research laboratory (URL) in Canada (Yoshinaka et al. 2008). A total of 95 cylindrical specimens were tested. Prepared specimens had ranging diameters from 33 to 294 mm and the ratio of length to diameter was approximately 2. Figure 2.12 shows that for the specimens with diameter larger than 63 mm clearly a decrease in strength with increasing specimen diameter is observed.

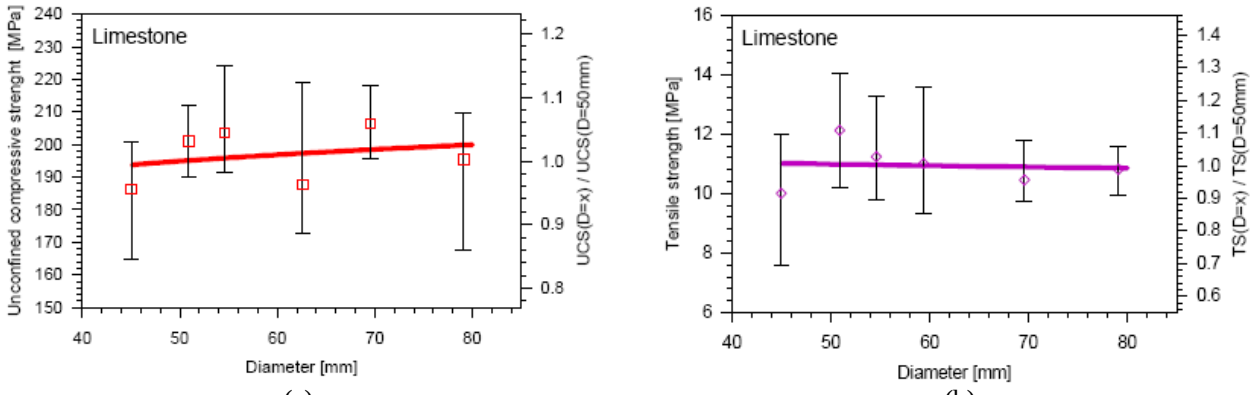

(a) (b)

Figure 2.10 Size effect of limestone samples on their strength (Thuro et al. 2001). (a) Variation in UCS-values as a function of diameter. Length/diameter ratio for all the samples is 2 and for each diameter 3 to 5 samples are tested. (b) Variation in BTS-values as a function of diameter. Length/diameter ratio for all the samples is 1 and for each diameter 4 samples are tested.

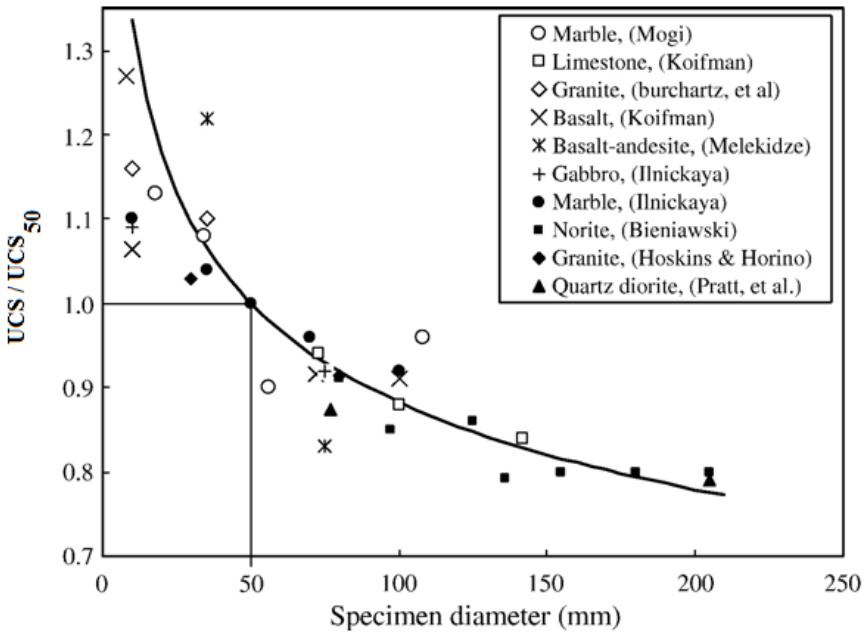

Figure 2.11 Scale effect on uniaxial compressive strength of intact rock (after Hoek and Brown 1980): Vertical axis is strength ratio normalized by strength of 50-mm-diameter specimen (after Yoshinaka et al. 2008).

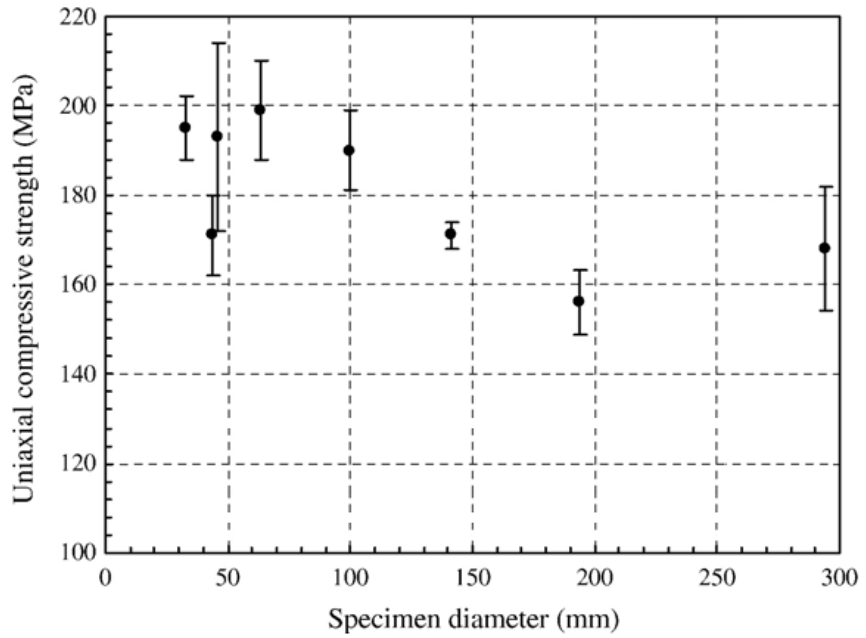

Figure 2.12 Uniaxial compressive strength of Lac du Bonnet granite and specimen diameter (after Jackson and Lau 1990): Vertical axis shows the average strength and standard deviation (after Yoshinaka et al. 2008).

The presented studies in this paragraph show that for a limited diameter range (e.g. 45-80 mm) samples have the same heterogeneity and consequently size effect cannot be observed. However, for extended diameter range (e.g. 30-300 mm) larger samples have more weak elements; therefore, they show less strength.

2.4.2 Shape effect

Thuro et al. (2001) studied the shape effect of kersantite (a type of mafic dyke) samples by conducting uniaxial tests. In their study, for uniaxial tests the diameter of 50 mm is taken, length/diameter ratio varies from 1 to 3 and a mean value is calculated from 3 to 5 samples. Thuro et al. (2001) studied also the shape effect of limestone samples by conducting Brazilian tests. For Brazilian tests in their study the diameter of 70 mm is taken, length/diameter ratio varies from 0.5 to 2 and a mean value is calculated from 3 to 4 samples. Figure 2.13 shows the variation in rock strength as a function of length/diameter ratio for the mentioned samples. Figure 2.13a shows that there is no remarkable shape effect in the UCS-values of tested samples (Thuro et al. 2001). The existence of friction leads the rock sample ends to a state of triaxial stress during the uniaxial compressive test. Therefore, rock samples with a smaller length/diameter ratio have a greater proportion of their volume in a triaxial stress state. If the length/diameter ratio is greater, especially greater than 2, the strength of rock specimen roughly becomes constant (Hudson et al. 1971, Pan et al. 2009).

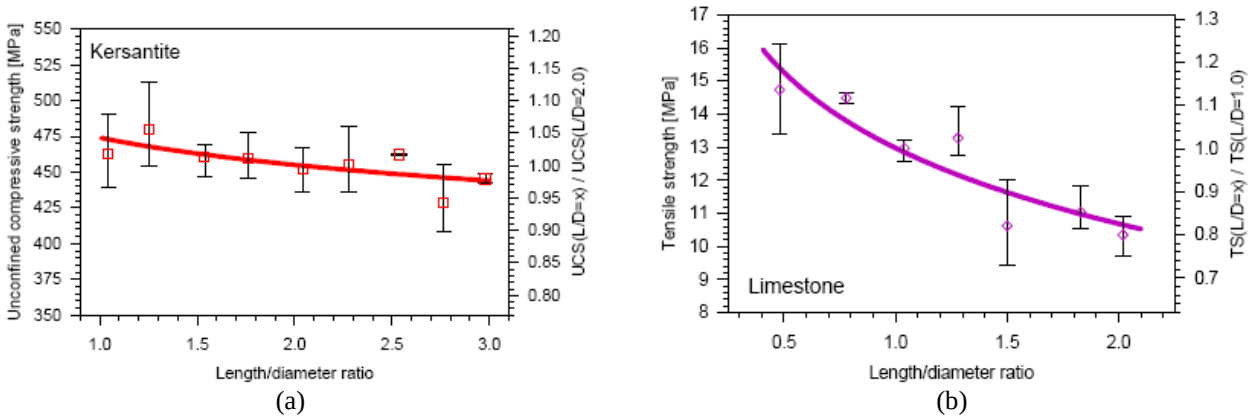

(a) (b)

Figure 2.13 Shape effect of rock samples on their strength (Thuro et al. 2001). (a) Variation in UCS-values as a function of length/diameter ratio for kersantite samples with diameter of 50 mm. Mean values are calculated from 3 to 5 tested samples. (b) Variation in BTS-values as a function of length/diameter ratio for limestone samples with diameter of 70 mm. Mean values are calculated from 3 to 4 tested samples.

Figure 2.13b shows the variation in indirect tensile strength as a function of length/diameter ratio for limestone samples. Before interpreting this figure, some important notes should be considered. In Brazilian test the minor and major principal stresses are tensile and compressive, respectively. The intermediate principal stress depends on length/diameter ratio. Lower length/diameter ratio makes the state of the rock sample (disc) closer to plane stress rather than plane strain (Lavrov et al. 2002). The intermediate principal stress for the low length/diameter ratio can be assumed zero; while, it is not the case when this ratio is increased. Therefore, it can be concluded that the stress state of samples in Figure 2.13b varies from plane stress to plane strain condition by increasing the length/diameter ratio. In other words the tensile strengths of samples presented in Figure 2.13b are not comparable to each other as they are not in the same stress state condition. The mentioned explanations are the criticism on the conclusion made by Thuro et al. (2001). They concluded that the shape effect of limestone samples on their tensile strength is quite significant, while (as explained); the stress state condition of the samples is quite different. However, if one compares the first four points in Figure 2.13b (roughly plane stress condition) with each other, a significant shape effect cannot be observed. This is also the case for the last three points in Figure 2.13b

(roughly plane strain condition). Therefore, from above discussion it can be concluded that shape effect (similar to size effect) in uniaxial and Brazilian tests for the rock samples with the same degree of homogeneity is not dominant.
In general terms it can be stated that dominant scale effect in uniaxial and Brazilian tests for the rock samples with a limited size variation is not observed, because they have the same degree of homogeneity. However, for rock samples with a large size variation, the degree of homogeneity is different and consequently scale effect is observed.

2.5 Summary

The variability of macro-scale behaviour (strengths and fracture patterns) is closely related to the differences in the mineral composition and microstructures of rock samples. It is widely accepted that for larger content of strong elements (i.e. quartz) rock strength and brittleness increases. On the other hand, the abundance of weak and easily cleavable minerals such as mica and carbonate would result in lowering the strength values. Also an inverse relationship between rock strength and porosity exists.

The experimental results in many studies show that the relationship between grain size and rock strength is very important. In this study the term ‘grain size’ is applied for the average grain size of the major rock-forming mineral. Rock type and also the grain size range are important factors that should be considered for the correlation between the grain size and rock strength. When in a series of samples great difference in their average grain size is observed, other parameters such as porosity can play a role. The porosity is an important factor in rock strength, as the voids reduce the integrity of the material. Therefore it seems that declaring the effect of grain size on rock strength with mentioning the grain size range makes it more meaningful; however, the variation range of other parameters should also be considered.
It should also be considered that all the micro-parameters have some effect on rock strength. As the variation range of one parameter is more extended than the other parameters, logically its influence is expected more obvious.
Fracture pattern in all explained classifications is linked to the failure modes (shear or tensile). For complex material, precise determination of failure mode needs more attention with a better understanding of failure mechanism. However, the fracture patterns in all mentioned classifications are considered qualitatively.
A dominant scale effect in uniaxial and Brazilian tests of rock samples with a limited size variation cannot be observed, as they have the same degree of homogeneity. However, for rock samples with a large size variation a clear scale effect is observed, as the samples have different degree of homogeneity.

3 Material, Methodology and Experimental Techniques

3.1 Material information

In this study, one specific form of anisotropy is considered. The tests are conducted on hard and brittle stratified sandstone (psammite) and the Brazilian tensile method (diametrical loading of cylindrical discs) is applied. The stratified (layered or banded) rock material is sometimes called transversely isotropic rock material (Jianhong et al. 2009), i.e. rocks with one dominant direction of planar anisotropy.
Five blocks of layered sandstone are taken from a quarry in Modave in the South of Belgium (see Figure 3.1). These blocks are taken at very short distance (from 1 to 10 m) from each other. Visual inspection (hand samples) would normally lead to the conclusion that they are all similar material. This sandstone is also known as "Psammite of Condroz" (Poty and Chevalier 2004). This sandstone is characterized by numerous thin and parallel layers (Figure 3.2). The plane of anisotropy (transverse isotropy) is assumed to be parallel to the apparent direction of rock layering.

The number of layer boundaries on hand samples from each block is counted. The number of layer boundaries over 1 cm of five blocks is not the same; therefore, the five blocks are further called the five sub-types. The number of layer boundaries over 1 cm for sandstone sub-types 1 to 5 is 8.8, 5.4, 2.6, 4.2 and 1.4, respectively. Only in sandstone sub-type 5, ripples are observed. Therefore, sandstone sub-type 5 cannot be considered as a transversely isotropic rock material. It should be noted that ripples are not considered as the layer boundary. Sandstone sub-type 1 (reference) has the maximum number of layer boundaries over 1 cm (8.8). Hence, the effect of layer orientation on conducted samples of the reference sub-type should be more pronounced.

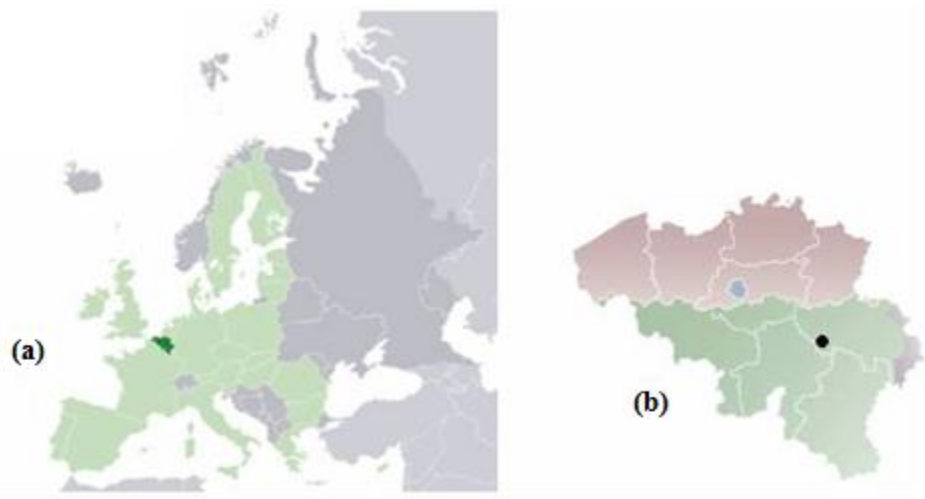

Figure 3.1 Location of studied place (Wikipedia, online website). (a) Location of Belgium in Europe. (b) Location of quarry in Belgium (indicated by black spot).

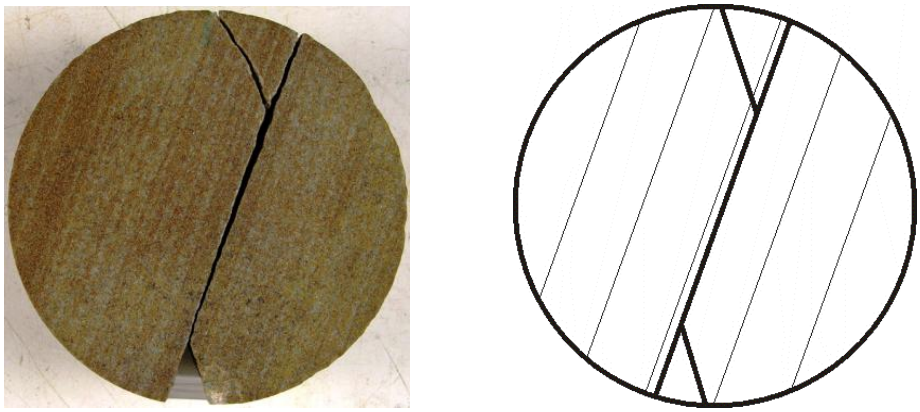

Figure 3.2 Picture (left) and schematic drawing (right) of a sandstone sample after conducting a Brazilian test. Thin lines symbolise average layer direction (bedding) while the bold lines are the observed fractures.

3.1.1 Geological description

The sandstone studied is stratified and massive, and from Famennian stage. The Famennian stage is one of the two stages in the Late Devonian epoch. It lasted from 374.5 ± 2.6 million years to 359.2 ± 2.5 million years ago (Gradstein et al. 2004). The name of Famennian stage originated in the 19th century from the Famenne region in the Southern part of Belgium. This geographical region corresponds to a shaly depression located South and East of the Meuse river, in between the Condroz area (folded sandstone-limestone succession) in the North and the limestone ridge (La Calestienne) and the succeeding Lower Paleozoic Ardennes hills in the South (Thorez et al. 2006).

The Famennian stage (Uppermost Devonian) corresponds in Belgium to a sedimentary sequence of up to 600 m of predominantly siliciclastic shelf sediments inserted in between

upper Devonian (Frasnian) and lower Carboniferous (Tournaisian) shelf carbonates (Thorez et al. 2006). Over time a lithofacies shift has occurred from predominantly pelitic sediments in the early Famennian (the Famenne Shales) to predominantly sandy sediments during the late Famennian (the Condroz Sandstones).

3.1.2 Physical properties

Physical properties investigated include dry and saturated density, effective porosity (interconnected porosity) and P-wave velocity.
The densities and effective porosity of the sandstone sub-types are determined by saturation and buoyancy techniques (see Figure 3.3). The specimens are prepared and tested generally in accordance with the procedure given in ISRM (International Society for Rock Mechanics) suggested methods (2007). The rock blocks are cored to have cylindrical specimens and then are cut to have disc-shaped samples (similar for Brazilian test). For each block (sub-type) five samples are prepared and the tests are carried out to determine each property. The density and effective porosity of samples from five sub-types of Modave sandstone are presented in Table 3.1. The dry density of five samples of reference sub-type varies from 2.60 to 2.62 gr/cm^3 and their wet density varies from 2.63 to 2.64 gr/cm^3. The variation in the effective porosity in the samples of reference sub-type is from 2.2% to 3.2% with an average value of 2.6%. The variation in effective porosity for all the samples is from 2% to 3.2%, where the variation in the average value is from 2.4% for sandstone sub-type 5 to 3.0% for sub-type 3. The variation in average dry density is from 2.57 g/cm^3 for sub-type 3 to 2.63 g/cm^3 for sub-type 2.
So, it can be concluded that the variation in physical properties of Modave sandstone sub-types is relatively small and they have similar properties. Although all Modave sandstone sub-types are massive in visual inspection and also the results show a low porosity, normally the total porosity is larger than the presented data. For the total porosity the pore volume obtained includes closed and interconnected pores while in effective porosity only interconnected pores which are obtained by water saturation are considered.

Figure 3.3 Saturation and buoyancy techniques. Left picture: vacuuming the dessicator before saturation of the samples. Right picture: a sample in the basket in the immersion bath.

Also two disc-shaped samples from each sandstone sub-type are prepared for P-wave velocity measurements. Diameter of samples from each sub-type is 80 or 100 mm. In this study a P-wave with frequency of 200 kHz is used. The wave length ($\lambda \approx 25$ mm) of the P-wave is in the same order of samples diameter as the used travel path. Therefore, an aluminium horn-like transmitter and receiver are used, which permit the P-wave to fully develop and be

guided into the rock material (Ganne 2007). By measuring the travel path (sample diameter) of the P-wave and the travel time which is given by the measuring system, the P-wave velocity is calculated.
P-wave velocity is measured between parallel to the layer direction and direction perpendicular to the layers. In different configurations, slight differences in wave velocity are recorded (Figure 3.4 a). However, minimum and maximum wave velocities are always measured perpendicular and parallel to the layers, respectively (Figure 3.4 b). The recorded data for both samples of each sub-type are compatible with each other; therefore, it would be possible to get the average of them. The variation in their average wave velocities for the sub-types 1 to 5 respectively vary from 4.7 to 5.1, 4.6 to 4.9, 4.4 to 4.5, 4.5 to 4.9 and 4.5 to 5.0 km/s. So, one can conclude that they are in a similar range.
The minimum difference of wave velocities is measured in samples of sandstone sub-type 3. In other words sub-type 3 has the lowest degree of transverse isotropy. In this sub-type average wave velocity perpendicular to the layers is 4.4 km/s while in direction parallel to the layers it is 4.5 km/s.

Table 3.2 summarise the variations and the averages of dry density, porosity and wave velocity of the five sub-types of layered sandstone.

Table 3.1 Density and effective porosity of five Modave sandstone sub-types

Sandstone		Density (g/cm^3)		Effective porosity (%)	
Type	**Sample**	**Dry**	**Sat**	**Sample**	**Average**
1	1	2.62	2.64	2.6	2.6
	2	2.61	2.63	2.6	
	3	2.61	2.63	2.5	
	4	2.61	2.64	2.2	
	5	2.60	2.63	3.2	
2	1	2.62	2.65	2.4	2.5
	2	2.62	2.65	3.0	
	3	2.62	2.65	3.0	
	4	2.63	2.65	2.0	
	5	2.63	2.65	2.0	
3	1	2.57	2.60	2.9	3.0
	2	2.58	2.60	2.8	
	3	2.57	2.60	3.0	
	4	2.57	2.60	3.1	
	5	2.57	2.60	3.2	
4	1	2.60	2.63	2.6	2.5
	2	2.61	2.64	2.3	
	3	2.58	2.61	3.1	
	4	2.61	2.64	2.2	
	5	2.61	2.63	2.3	
5	1	2.60	2.62	2.5	2.4
	2	2.60	2.63	2.4	
	3	2.58	2.61	3.0	
	4	2.61	2.63	2.1	
	5	2.61	2.63	2.1	

Method of saturation and buoyancy techniques is used. Tested samples of sandstone sub-types 2 to 5 are disc-shaped with diameter of 50 mm. Their thickness in sandstone sub-types 2 and 3 varies from 13 to 20 mm, in sub-type 4 is 25 mm and in sub-type 5 is 20 mm. Tested samples of sandstone sub-types 1 have no particular shape.

Table 3.2 Physical properties of the five sub-types of layered Modave sandstone

Sandstone sub-type	Dry density (g/cm^3)		Porosity (%)		P-wave velocity (km/s)			
	Range	Avg.	Range	Avg.	Perpendicular Range	Avg.	Parallel Range	Avg.
1	2.60-2.62	2.61	2.2-3.2	2.6	4.7-4.8	4.7	5.0-5.2	5.1
2	2.62-2.63	2.63	2.0-3.0	2.5	4.5-4.7	4.6	4.9-5.0	4.9
3	2.57-2.58	2.57	2.8-3.2	3.0	4.3-4.4	4.4	4.5-4.6	4.5
4	2.58-2.61	2.60	2.2-3.1	2.5	4.4-4.6	4.5	4.8-5.0	4.9
5	2.58-2.61	2.60	2.1-3.0	2.4	4.5-4.6	4.5	5.0	5.0

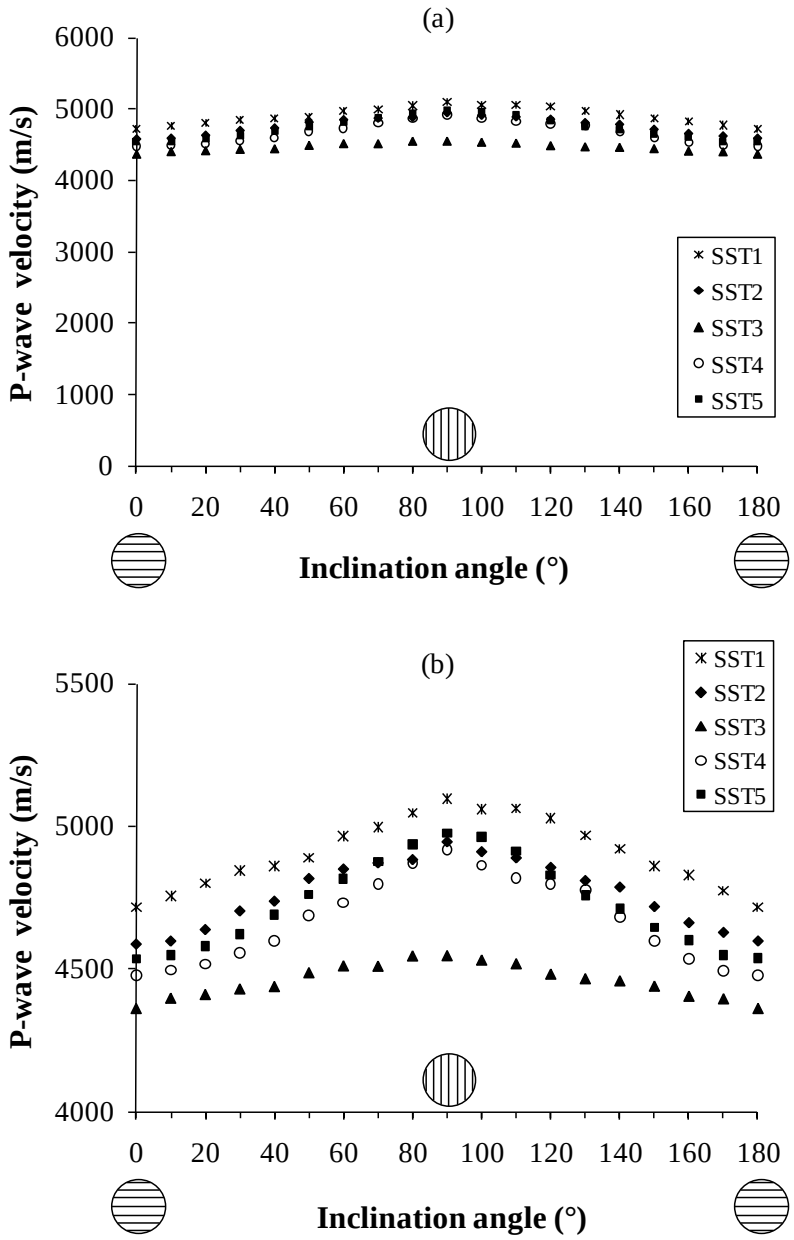

Figure 3.4 P-wave velocity of Modave sandstone sub-types (SST). P-wave velocity is measured between parallel to the layer direction and direction perpendicular to the layers. Graph b is considered for a limited range of velocity (from 4.0 to 5.5 km/s) in order to show the variation of wave velocity in different configurations.

3.1.3 Petrographical characteristics of untested samples

Rock material properties are influenced by the mineral composition, texture (grains size and shape), fabric (arrangement of minerals and voids) and weathering state (İrfan 1996). The correct interpretation of rock behaviour variation is mainly influenced by precise determination of many parameters. Although often neglected, micro-scale parameters are the most crucial factors.

For a petrographical description, thin sections from an untested sandstone sample from each sub-type are prepared and analysed. The diameter of the samples is 50 mm. As the samples

are massive, impregnation is not needed. A thin section is a planar section of rock material with a thickness of about 30 μm. As the thickness is very small, the rock material becomes transparent. Therefore the texture (grain structure, clay minerals, voids,…) can be seen under a transmitted light microscope. Figure 3.5 shows the position of the thin section in a sample. A quantitative analysis of petrographic characteristics is carried out on thin sections using a Zeiss petrographical microscope. Grain size distribution, composition and layer characteristics are studied.

Although the samples from different blocks of sandstone are relatively similar, at micro-scale they are different. The samples are different in layer thicknesses, grain size, presence of ripples, quantity and quality of weak minerals, etc. All these parameters are explained in more detail in this paragraph. In all the samples, quartz, carbonate and mica are observed but they are different in quantity. Also pores, organic material, clay minerals and feldspar are observed, although in very small quantities.

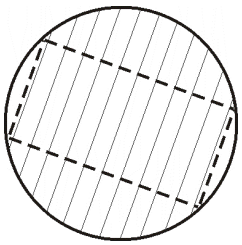

Figure 3.5 Location of thin section in an untested sample. Layer orientation is indicated (thin lines).

3.1.3.1 Number of layer boundaries

Figure 3.6 presents a part of the thin section of the reference sandstone sub-type (sub-type 1). In this sample (similar to other samples), quartz, carbonate and mica are observed. As indicated in Figure 3.6c the grains that are white, gray and dark gray are quartz. Quartz is easily distinguished in thin sections because it is generally unaltered and lacks visible twinning or cleavage (MacKenzie and Guilford 1993). It may contain fluid inclusions and if they are very small and numerous they may give the quartz a dusty appearance (MacKenzie and Guilford 1993). Carbonates have a rhombic shape and their colour is light gray. Because of the rhombohedral cleavage most crystals show at least one good cleavage (MacKenzie and Guilford 1993). Micas are very thin (20-30 μm) and long.

In the sedimentation process the order of deposited grains in water flow is from coarse to fine grain (coarse grains deposit first and position at the bottom of the layer). As water flow becomes stable, flaky minerals such as mica and very fine grains such as clay minerals deposit. Normally the orientation of micas presents the deposition direction. In the next flow the first deposited grains are coarse grains, as already mentioned. The line that separates the recent coarse grains from fine grains of previous flow is considered as the layer boundary. This line at microscopic scale (if it can be observed) is not necessarily straight and continuous. Normally layer boundaries are planes of weakness because they are the places of discontinuities in the sedimentation process. Furthermore the quantities of clay mineral and mica increase in this zone (see Figure 3.6c).
In Figure 3.6a layer boundary is indicated by a vertical arrow. The colour of clay minerals is black. In Figure 3.6b the part of layer boundary that can be visualised at micro-scale is presented. It is important to note that at the microscopic scale, visualising the layer

boundaries is very difficult and complicated. For instance, in a disc-shaped sample of 50 mm diameter (of the reference sandstone), forty-four layers were counted by visual inspection (see Figure 3.7). Among them only a small part of a layer boundary is observed under microscope (see the layer boundary in the middle of Figure 3.6a; its direction is indicated by the arrow). Location of layer boundaries can roughly be estimated by visual inspection of the thin section and also by the colour change of layers at a larger scale. The composition of minerals in different flow is not exactly the same and for example a negligible percentage of iron can considerably change the colour of deposited layer.

The best way to see the layer boundaries is visual inspection of hand samples (see Figure 3.7). In the petrographical study of layered rock one should not search the layer boundaries by microscope. The layer boundaries are not always a straight continuous detectable line at the micro-scale (see Figure 3.6a). Figure 3.7 presents one of the fractured samples of sandstone sub-type 1 (reference sub-type). In this figure, some layer boundaries are indicated by the straight lines, while the layers are indicated by the white arrows.

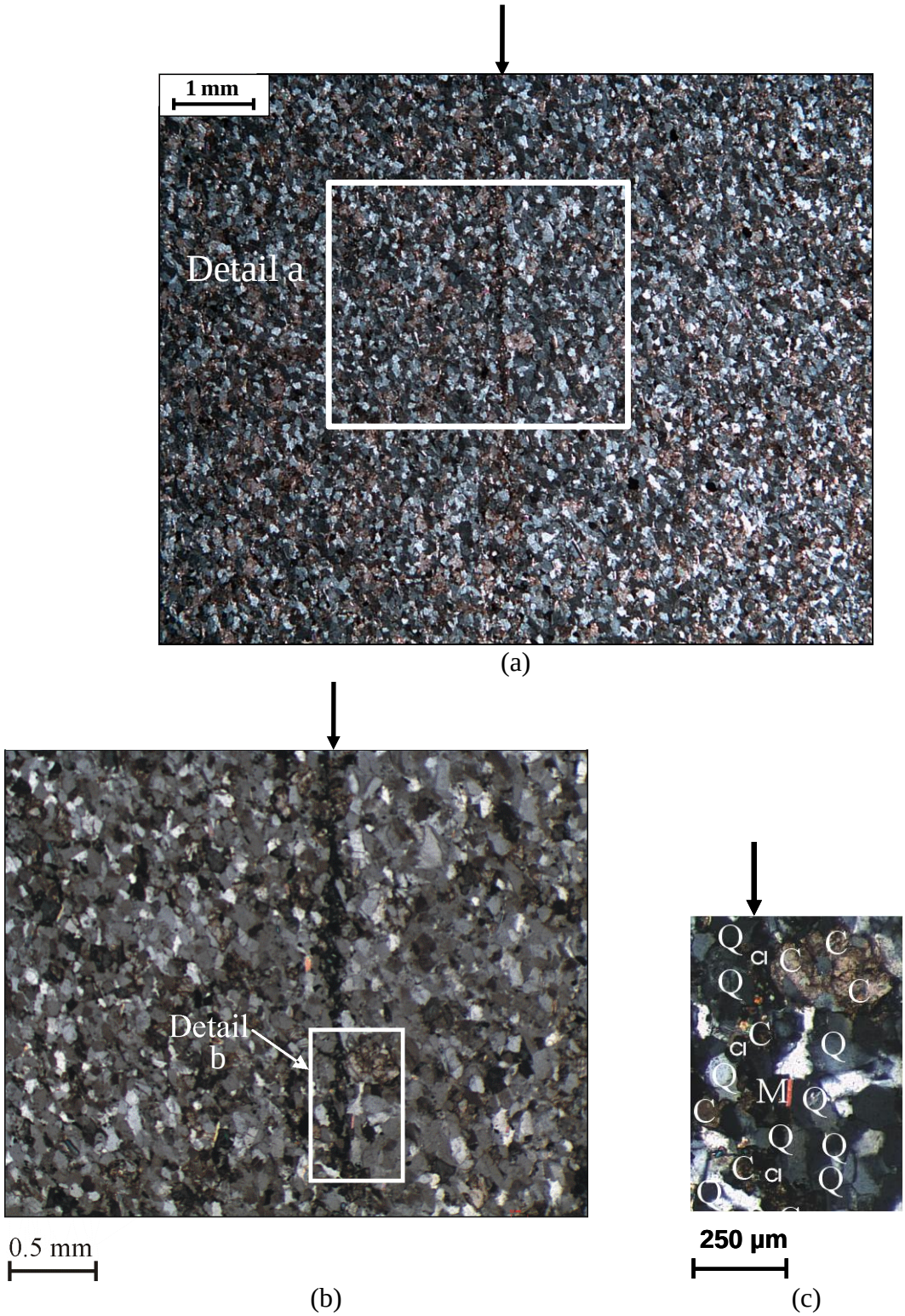

Figure 3.6 Digital pictures of a part of the thin section from studied sandstone sub-type 1 (reference). Layer boundary is indicated by the arrow. (a) General view of thin section where a small part of layer boundary can be seen (pixel resolution is 7.1 µm), (b) Magnification of detail (a) (pixel resolution is 2.7 µm), and (c) Magnified layer boundary, Q: Quartz, C: Carbonate, M: Mica, Cl: Clay mineral (pixel resolution is 1.3 µm).

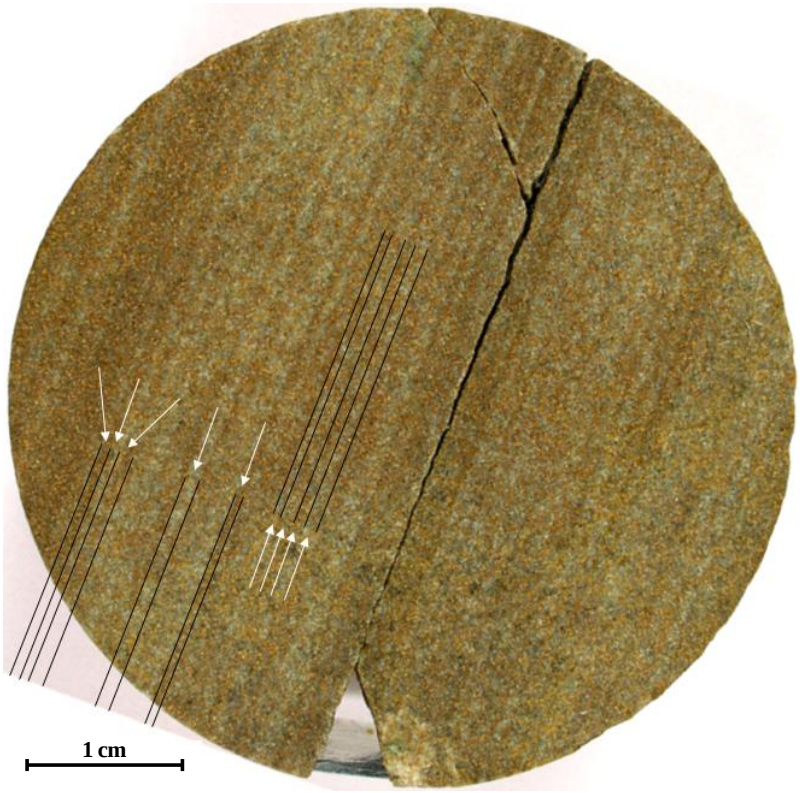

Figure 3.7 Fractured sandstone sample of reference sub-type after conducting Brazilian test. Straight lines indicate layer boundaries and white arrows indicate the layers. Inclination angle of layer direction from horizontal is 70°.

For all the samples the number of layer boundaries is counted (on hand samples). In Figure 3.8 the number of layer boundaries over 1 cm is given for the five sandstone sub-types. Graded bedding of shallow-water environments is generally composed of thin layers from a few millimetres to 1 or 2 cm, and seldom makes sequences more than 10 or 20 cm thick (Reineck and Singh 1986). From Figure 3.8 it can be concluded that all the blocks are from shallow-water environments as their layer thicknesses are from 1.1 mm for the reference sub-type to 6.4 mm for sandstone sub-type 5. As layer boundaries are planes of weakness, it is important to note that, for example in sub-type 1, the number of weak planes is more than three times this number in sub-type 3.

Also by locating the studied quarry (in Modave in the South of Belgium) on the Late Devonian palaeogeography map (Scotese and McKerrow 1990) that is presented in Figure 3.9 it can be understood that all the sandstone sub-types are from shallow-water environments. Comparison of Figure 3.9 with location of the quarry shows the movement of lands, seas and the oceans after about 367 million years time.

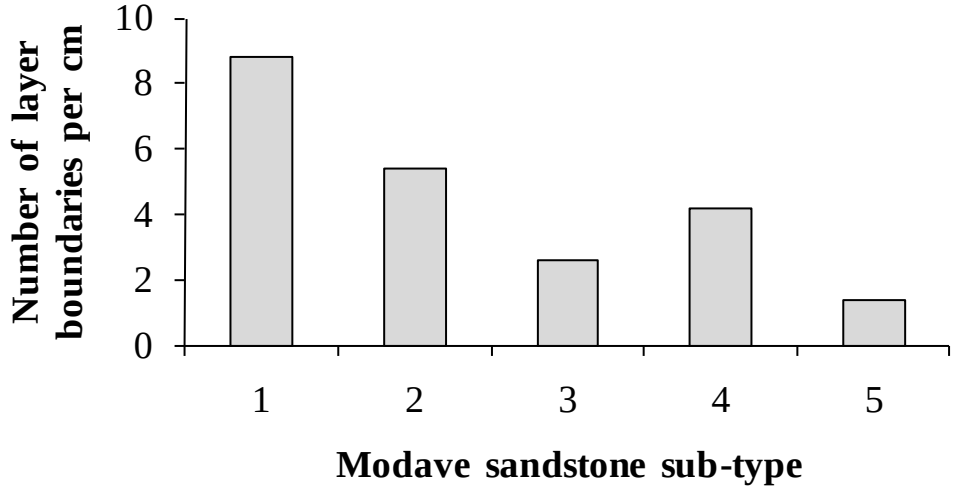

Figure 3.8 Number of layer boundaries per 1 cm in different sub-types of sandstones.

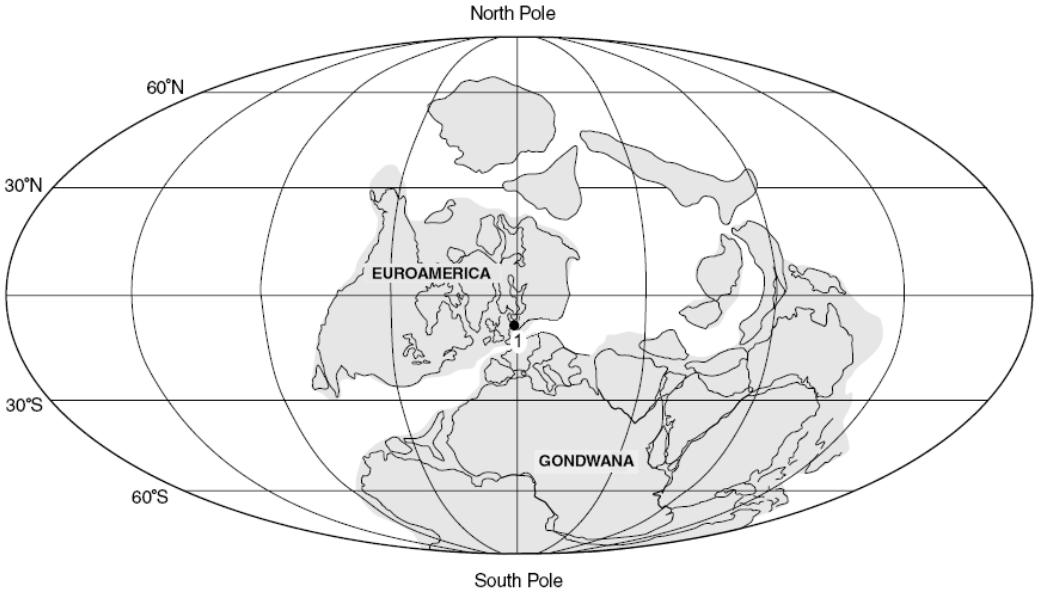

Figure 3.9 Location of the studied quarry of sandstone (Modave in the South of Belgium) on the Late Devonian palaeogeography map (after Scotese and McKerrow 1990 and Olempska 2002).

3.1.3.2 Presence of ripples

Layer orientation affects the fracture pattern (see further in chapter 4). If apart from the layer boundaries other planes of weakness exist, both types of planes can affect the fracture behaviour. Only in sandstone sub-type 5, ripples are observed as the secondary plane of weakness (see Figure 3.10). Ripples are a series of parallel or sub-parallel ridges in sand or sediment that is caused by the rhythmic or directional movement of wind or water (see Figure 3.11). The mica lines in Figure 3.10 show such ripples. Modave (studied place in the South of Belgium) on the Late Devonian palaeogeography map (see Figure 3.9) is situated on a shoreline and consequently existence of ripples is expected.

It should be noted that ripples are not considered as the layer boundary in Figure 3.8 (number of layer boundaries as a function of sandstone sub-type). The reason for it is that ripples are

not in the main direction of sedimentation and that they are dispersed between layer boundaries.

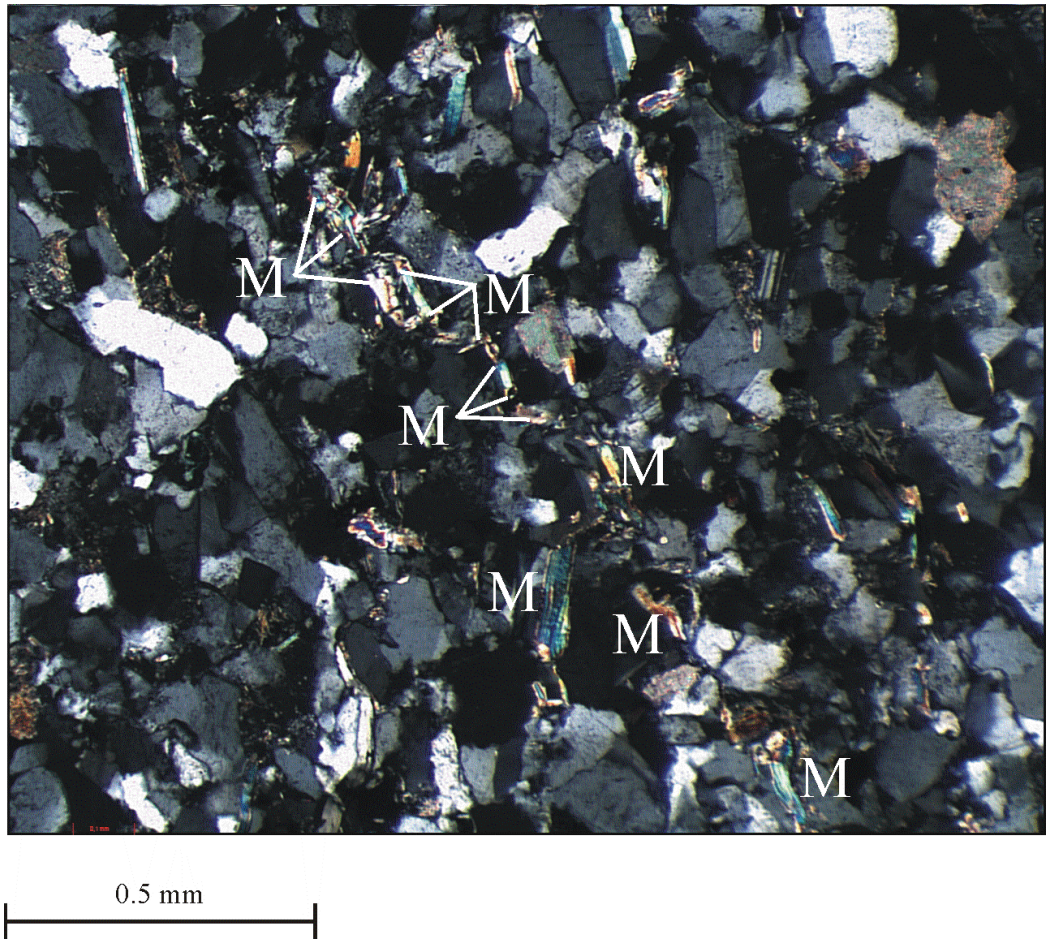

Figure 3.10 Digital picture of thin section of sandstone sub-type 5 (pixel resolution is 1.31 µm). In this picture, direction of layers is vertical, while direction of ripples is different. Direction of ripples corresponds to the mica-lines. Micas are indicated by white arrows or by M next to it.

Figure 3.11 Asymmetrical wave ripples; land toward the right (Reineck and Singh 1986).

3.1.3.3 Mineral composition

In thin sections from all sandstone sub-types weak minerals such as mica and carbonate are observed, especially in the layer boundaries themselves. Thin section observation is done by petrographical microscope with transmitted polarized light. To be able to quantify the relative amount of weak minerals, the point-counting method is applied (Přikryl 2001, Chayes 1956). The thin section is put in the point-counting apparatus which is attached to the petrographical microscope. Mentioned apparatus moves the thin section with a given interval. After each movement the mineral in the centre of the microscopic view is observed. For example if in 100 steps of movement 75 times quart grain is observed in the centre of microscopic view, it is concluded that quartz content in that rock material is 75%.
In this study 500 points in each thin section are counted in a regular pattern with a fixed interval of 400 µm between the points. The direction of counting is perpendicular to the layers and between the lines of point-counting the distance of 800 µm is taken. Figure 3.12 presents the percentage of different minerals in each sandstone sub-type. In these sub-types, the majority of the grains are quartz. The amount of weak minerals (mainly mica and carbonate) is different for the five sub-types, but it is the largest for sub-type 1 (reference). This is one of the reasons why the effect of layer orientation for sub-type 1 is much more pronounced than for the other sub-types (see further in chapter 4).
The amount of weak minerals as a function of the number of layer boundaries is also remarkable (Figure 3.13). As the grains are counted perpendicular to the layers and the number of weak elements increases in the layer boundary, sandstone with more layer boundaries should have a larger percentage of weak elements (see Figure 3.13). Apart from sub-type 5, this corresponds to a very good correlation. The presence of ripples as the second planes of weakness in sandstone sub-type 5 is probably the reason for this exception.

Clay minerals are ultra fine grained and are considered to be less than 2 microns in size (based on the British Standards, Craig 1990). Clay minerals are common weathering products. Clays are found usually mixed with microscopic crystals of carbonates, feldspars, micas and quartz. These minerals are very common in fine grain sedimentary rocks such as the five studied sub-types of sandstone. Determining precisely the clay mineral by means of an X-ray analysis and some spectroscopic methods is possible. By referring to some studies it is understood that the clay minerals in the studied sandstone sub-types is dominated by illite (Thorez et al. 1988, Han et al. 2000). Illite has a basic structure consisting of a sheet of alumina octahedrons between and combined with two sheets of silica tetrahedrons (Craig 1990).

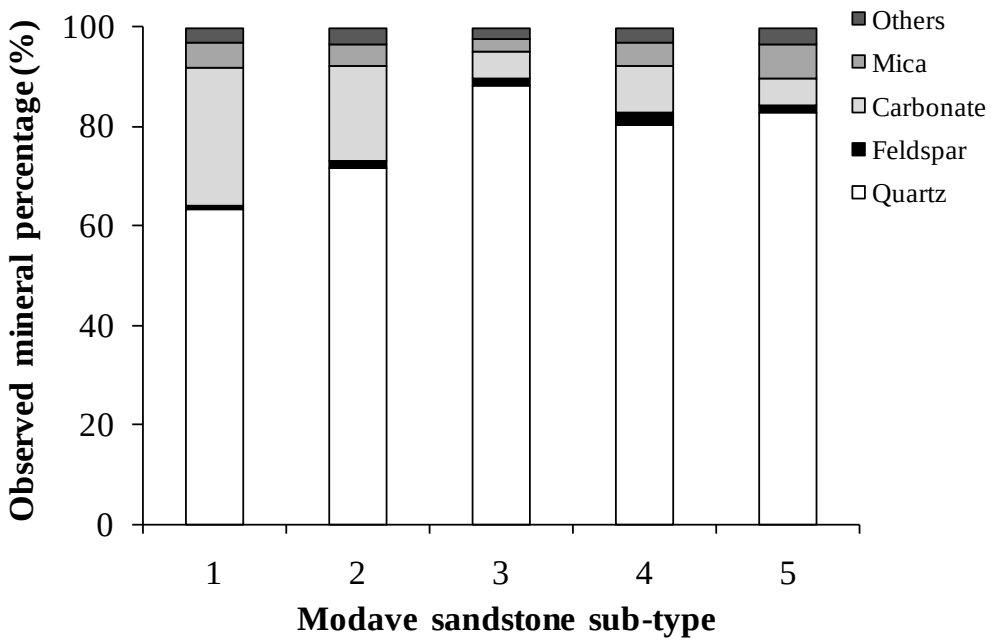

Figure 3.12 Observed mineral percentage in different sandstone sub-types by 500 counted points. Category 'Others' corresponds to pores, organic material and clay minerals.

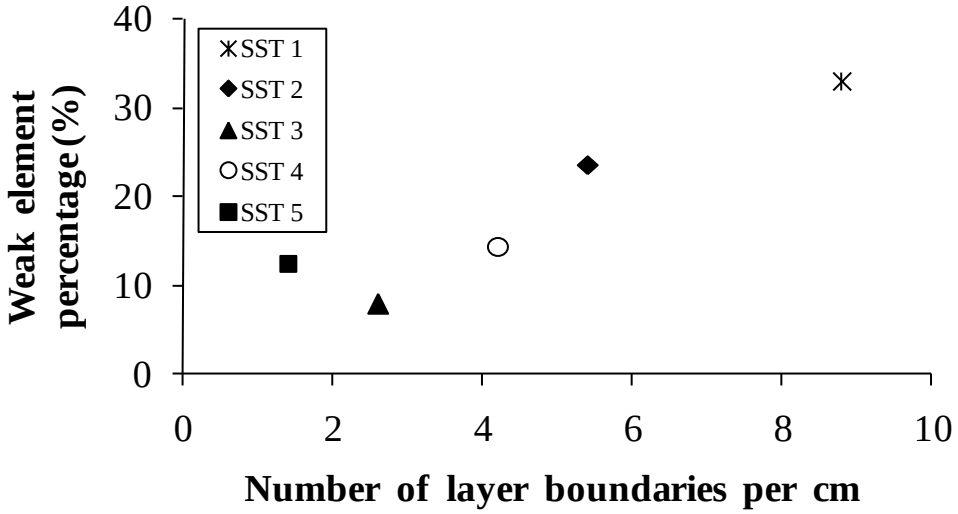

Figure 3.13 Variation in weak elements (carbonate and mica) percentage as a function of number of layer boundaries per centimetre in different sandstone sub-types (SST).

3.1.3.4 Grain size

The grain size distribution has attracted the attention of many mining engineers, civil engineers and geologists. This is due to the fundamental relationship with the geotechnical characteristics of a rock mass (Attewell & Farmer 1976, Singh et al. 2001). Grain size is the most fundamental property of sediment particles, affecting their entrainment, transport and deposition (Blott and Pye 2001). Many researchers investigated the correlation between grain size and rock strength, and have come out with some interesting viewpoints; however, the relationship between grain size and rock strength are mainly based on the investigation of marbles and granitic rocks (Meng and Pan 2007). Přikryl (2001) suggested that grain size is

the main controlling factor for strength variation in groups of granites. Eberhardt et al. (1999) presented the effects of grain size on the initiation and propagation thresholds of stress induced brittle fracturing in crystalline rocks with similar mineralogical compositions. Their results were obtained for three different grain sizes. However, the current research is also focused on the possible effect of grain size on layer activation and crack propagation, in addition to finding a correlation between grain size and Brazilian tensile strength in the different sub-types of the Modave sandstone.

In the studied sub-types of Modave sandstone the majority of the grains are quartz (see Figure 3.12) and they are the focus for the grain size determination. The quartz grain size is not the same and this is also the case for the different studied sandstone sub-types. Although the grain size of the five sub-types is not identical, the shape and roundness of the grains are the same. For roundness of sand grains, Shepard (1963) and Powers (1953) distinguish six groups (Reineck and Singh 1986). These groups are shown in Figure 3.14. All grains of these five sandstone sub-types are in the class of subangular (class C) according to Figure 3.14.

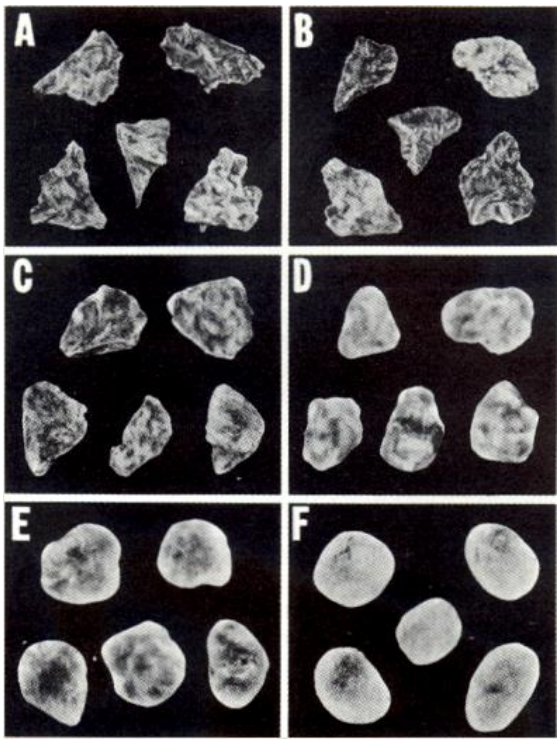

Figure 3.14 Six classes are used for roundness determination of sand grains. A = very angular; B = angular; C = subangular; D = subrounded; E = rounded; F = well rounded (Classes after Powers 1953, Shepard 1963, and Reineck & Singh 1986).

Many methods exist for grain size determination. In this study for quartz grain size measurements the point-counting method is applied. 300 points in each thin section are counted (in a regular pattern similar to the mineral composition quantification). Similar to sieving analyses the smallest dimension of the grains is considered. In addition to the grain size distribution the average and standard deviation which is a measure of how much grains are dispersed from the average are calculated by the arithmetic method.

Grain size frequency histograms for the five sub-types of Modave sandstone are presented in Figure 3.15. From this Figure it can be concluded that sandstone sub-type 3 in comparison to other sub-types is well graded, i.e. the distribution of its grains is widely spread. The average (and minimum, maximum) values in μm for the grain of sandstone sub-types 1 to 5 are 80 (26, 144), 69 (22, 141), 107 (42, 218), 87 (33, 162) and 82 (29, 146) respectively. Table 3.3 presents the information about the grain size, standard deviation and composition percentage of these sub-types of sandstone. The standard deviation of sub-type 3 is larger than the other sub-types which shows that the grain size is more dispersed (in agreement with indicated grain size range). By considering the British Standards (Craig 1990), all grains of these five sandstone sub-types are in the size range of fine sand as it can be concluded by Table 3.3.

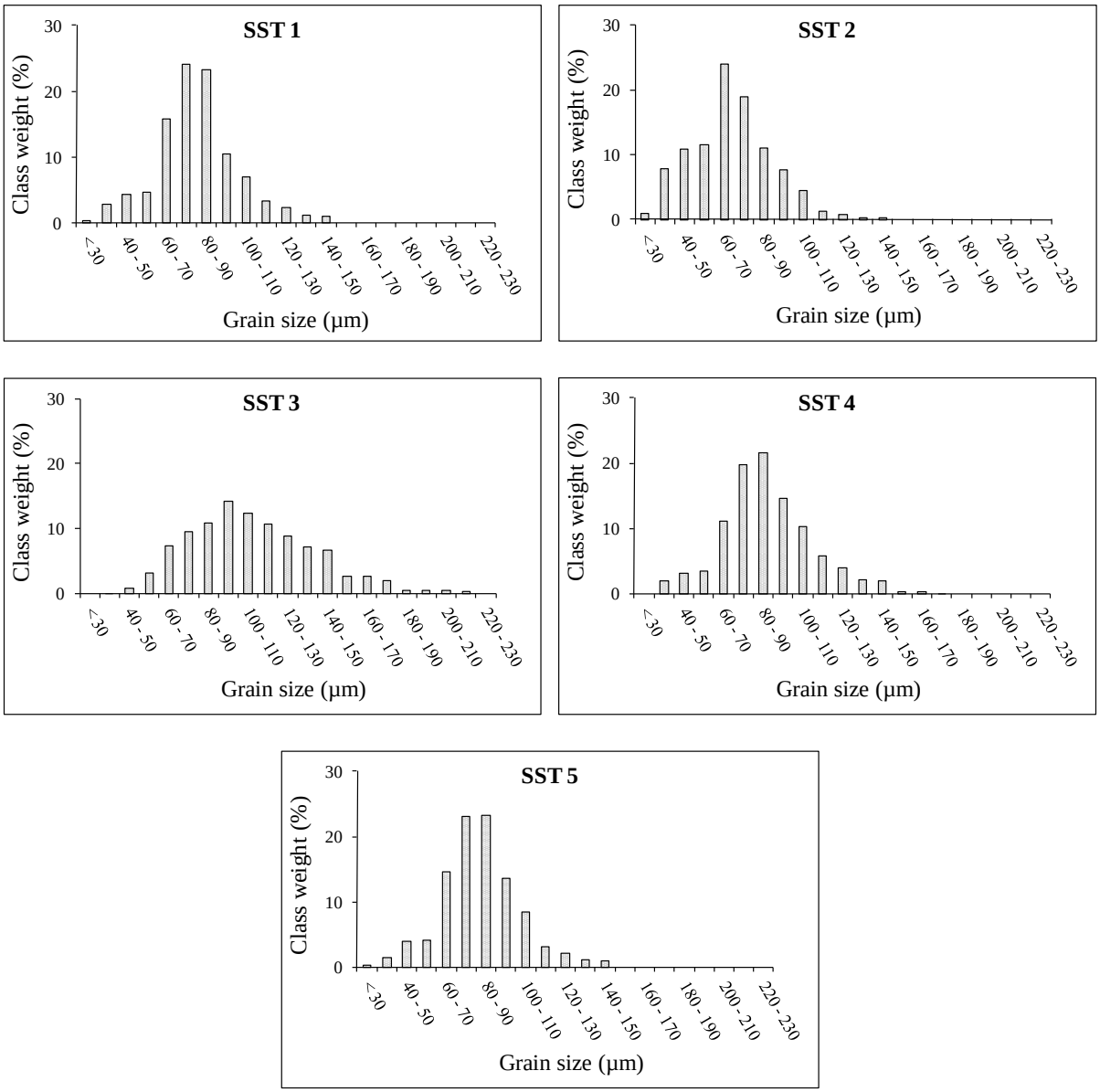

Figure 3.15 Grain size frequency histogram for the five Modave sandstone sub-types (SST).

Table 3.3 Grain size information of the five sub-types of layered Modave sandstone

Sandstone sub-type	Grain size (μm)			STDEV (μm)	Composition percentage (%)			
	Min.	Avg.	Max.		Coarse silt	Fine sand	Medium sand	Total
1	26	80	144	20	13.3	86.7	0.0	100
2	22	69	141	20	34.7	65.3	0.0	100
3	42	107	218	31	5.0	94.7	0.3	100
4	33	87	162	22	9.7	90.3	0.0	100
5	29	82	146	19	11.0	89.0	0.0	100

The grain size from 20 to 63 μm, from 63 to 210 μm and from 210 to 600 μm are respectively considered as coarse silt, fine sand and medium sand based on the British Standards (Craig 1990).

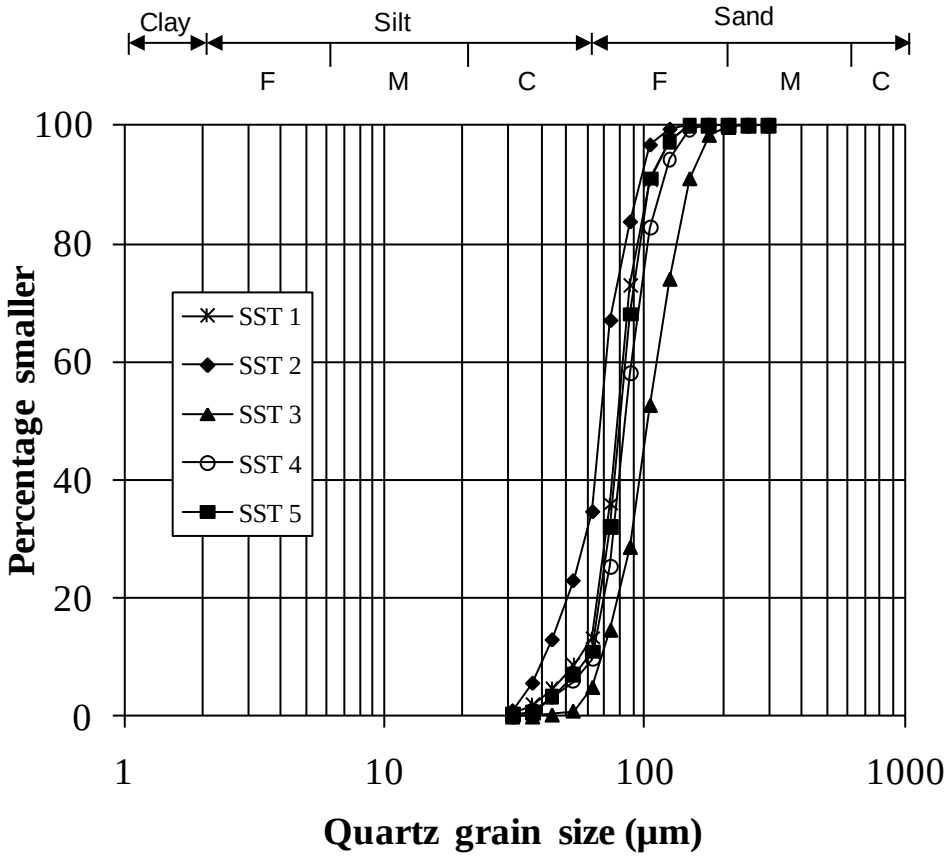

Figure 3.16 Particle size distribution curves for the Modave sandstone sub-types (SST). Classification is based on the British Standards (Craig 1990). F = Fine; M = Medium; C = Coarse.

The particle size distribution curves of the five sub-types of Modave sandstone are presented in Figure 3.16. In this figure all the curves are close to each other, which indicate the same classification for all of them. Most grains (more than 85%) are in the range of fine sand and only the second sub-type has about 35% of coarse silt. As already mentioned above, the average in μm varies from 69 to 107. These measurements are in agreement with the research of Thorez et al. (2006) on the sandstone of the same area. They mentioned that the sandstone of Famennian stage in the South of Belgium is fine grain with the average from 45 to 120 μm.

3.1.3.5 Micro-cracks in quartz grain

From each Modave sandstone sub-types 1 to 4 an untested sample is impregnated under vacuum with a fluorescent (FITC) dyed epoxy resin to enhance the contrast between the grains, the intergranular spaces and also the cracks. The sandstone sub-type 5 has the secondary plane of weakness (ripples) in addition to the layer boundaries which is the main difference with the other four sub-types. Therefore, the investigation are performed on specimens of the sandstone sub-types 1 to 4, which are more similar. Thin sections with a thickness of 30 µm are prepared from the four mentioned samples. For the untested samples the thin sections are from the central part of the samples, parallel to the layer orientation (see Figure 3.17).

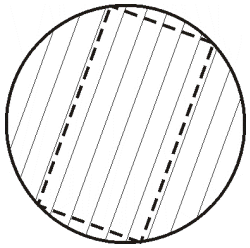

Figure 3.17 Location of thin section in an untested sample in order to detect micro-cracks in quartz grains. Layer orientation is indicated (thin lines).

In these sub-types of Modave sandstone, quartz grains as the main constitutive mineral are considered before and after the Brazilian test. In this part pre-existing intragranular cracks in quartz grain with their orientation are recorded. Later in the tested samples, micro-cracks in quartz grain (intragranular cracks) are also recorded. Therefore it is possible to monitor the changes in the micro-structure of samples due to the applied load. The detecting process of micro-cracks in quartz grains of studied sandstone samples, before and after the Brazilian tests is similar.
When a micro-crack in a quartz grain is observed, its orientation is also measured. The micro-cracks in quartz grains are searched through 12 rows in the thin sections. The method for detection of micro-cracks in a quartz grain is explained later in paragraph 3.3.3.2. The results are presented on the left side of Figure 3.18. In the mentioned graphs all the quartz grains with intergranular crack(s) are presented as a function of their crack orientations for sandstone sub-types 1 to 4. These graphs are summarized as the number of cracked quartz grains for successive intervals of 10 degrees (see Figure 3.18, right).

The inclination of the micro-cracks in quartz grains are scattered all over the range of inclination angles from 0° to 180°. The layer orientation in all the samples is 70°. Figure 3.18 shows that the number of fractured quartz grain in sandstone sub-types 1 and 2 in the bedding direction (inclination of 70°) is less frequent than for the other directions. For these sandstone sub-types, inclinations of micro-cracks in quartz grain are more perpendicular (160°) to the layer direction (70°). Pre-existing micro-cracks in rock materials can occur because of different natural mechanisms. The natural mechanisms can apply stresses mechanically or thermally to the rock materials. These stresses can produce some micro-cracks.
The crack density in the untested samples of the four sandstone sub-types is close to each other. The number of observed pre-existing micro-cracks in quartz grains of sandstone sub-types 1, 2, 3 and 4 is 24, 20, 18 and 20, respectively.

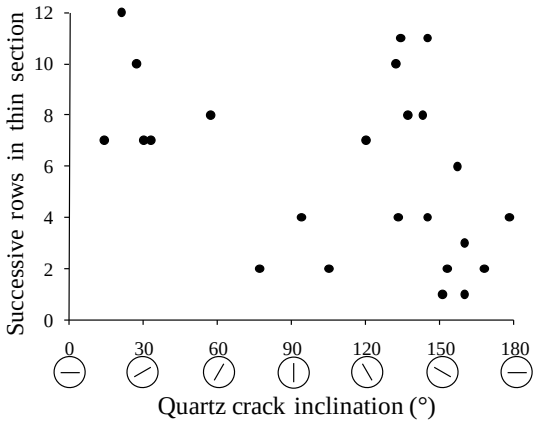
Successive rows in thin section
Quartz crack inclination (°)

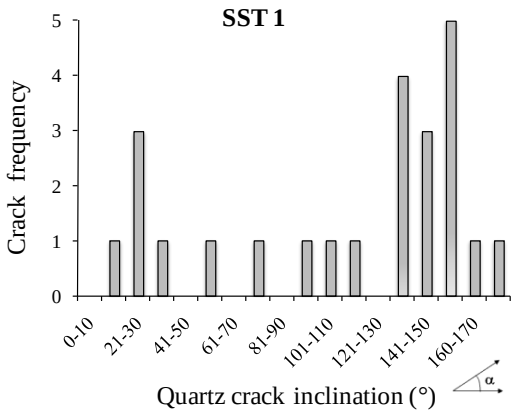
SST 1
Crack frequency
0-10
21-30
41-50
61-70
81-90
101-110
121-130
141-150
160-170
α
Quartz crack inclination (°)

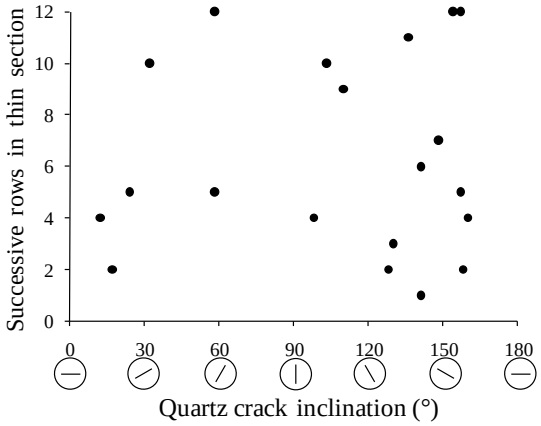
Successive rows in thin section
Quartz crack inclination (°)

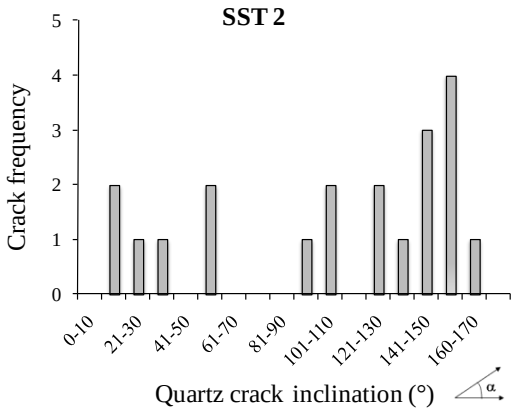
SST 2
Crack frequency
0-10
21-30
41-50
61-70
81-90
101-110
121-130
141-150
160-170
α
Quartz crack inclination (°)

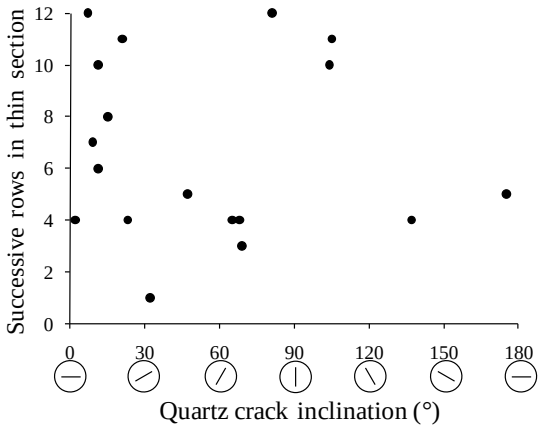
Successive rows in thin section
Quartz crack inclination (°)

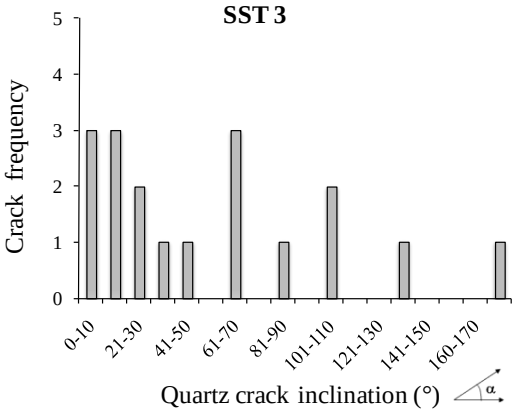
SST 3
Crack frequency
0-10
21-30
41-50
61-70
81-90
101-110
121-130
141-150
160-170
α
Quartz crack inclination (°)

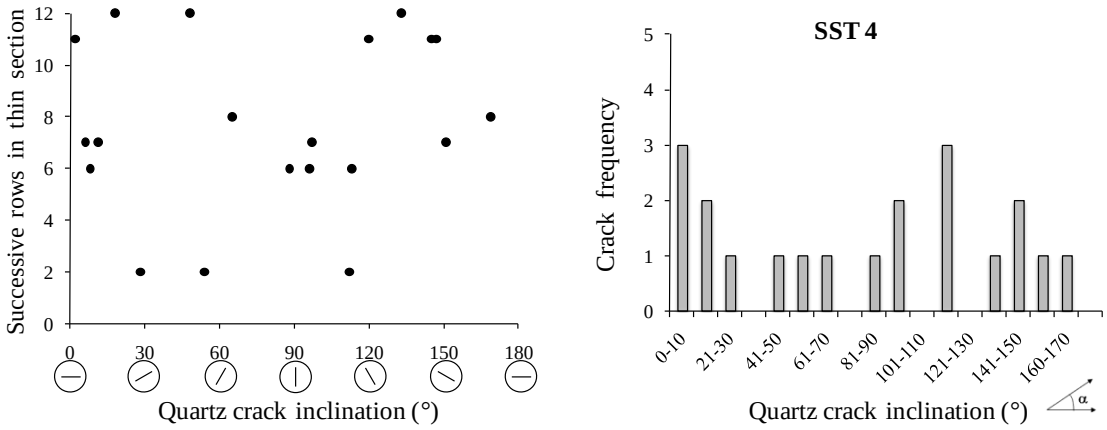

Figure 3.18 Quartz grains with intragranular crack as a function of their crack inclination for untested samples of Modave sandstone sub-types (SST) 1 to 4. The graphs on the left side present the micro-cracks in quartz grains which are searched in the thin sections through 12 rows. The graphs on the right side present the crack frequency as a function of crack inclination for intervals of 10°. In all the samples layer orientation is 70°.

3.2 Structure and methodology

In this study tests are conducted on layered sandstone (Psammite of Condroz) and the Brazilian tensile method (diametrical loading of cylindrical discs) is applied. The disc-shaped samples are positioned as in Figure 3.19 and compressed vertically until failure. Five relatively similar blocks of layered sandstone are taken from a quarry in Modave in the South of Belgium. The blocks are taken at very short distance (from 1 to 10 m) from each other. This sandstone is characterized by numerous thin and parallel layers. The stratified or layered rock material is sometimes called transversely isotropic rock material. The number of layer boundaries over 1 cm of the five sandstone blocks is not the same and consequently as already mentioned the five blocks are called the five sandstone sub-types.

The summary of consecutive steps in this research is presented in Figure 3.20. The experimental research in this study first focuses at macro-scale on the effect of the layer orientation on failure strength and failure pattern of this type of layered sandstone. Sandstone sub-types 1 (reference) has the maximum number of layer boundaries over 1 cm; therefore, the effect of layer orientation on conducted samples of the reference sub-type should be more pronounced. The effect of layer orientation is investigated in detail for samples of sandstone sub-types 1 (see detail A in Figure 3.20). 31 samples of reference sub-type are tested under Brazilian test conditions, whereby their layer orientation varies between perpendicular and parallel to the loading direction. These tests illustrate the effect of layer orientation on failure behaviour at macro-scale. In sandstone sub-type 1, layer activation is dominantly observed while layer orientation, θ, varies between 60 and 90°.
The effect of layer orientation in samples from other sub-types (see detail B in Figure 3.20) is investigated. However, test results of samples from the four other sub-types do not show the same effect of layer orientation. Therefore further research at micro-scale is being conducted to quantify the reason for the different behaviour on relatively similar rock materials (see detail C in Figure 3.20). For each sub-type of sandstone a thin section is prepared and studied under the microscope (Ganne and Vervoort 2006 and Van de Steen et al. 2002). It is observed

that relatively similar rock materials are different at micro-scale. It should be stated again that all five sandstone sub-types are normally classed as Psammite of Condroz and to a non-trained or a non-geologic eye, like the author, they looked more than the same. While conducting tests, differences in the behaviour between blocks were observed. After a microscopical study, the geological expert based on the gained knowledge could indeed indicate also the different characteristics on the hand samples. So, the author is pretty sure now that each block (about 30 × 30 × 30 cm^3) can be considered as homogeneous but there is a (slight) difference between the individual blocks.

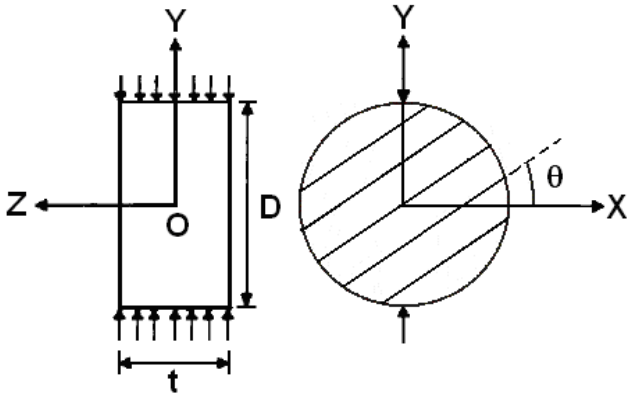

Figure 3.19 Disc-shaped sample and configuration of layers in Brazilian tests. θ varies between 0° and 90°. Set of inclined parallel lines symbolises average layer direction (bedding).

To study the effect of the differences at micro-scale on the failure behaviour obtained in the Brazilian test, a thin section from the loaded samples is needed (see detail D in Figure 3.20). To be able to quantify the damage induced at microstructural level in the samples (due to loading), damaged but not completely failed samples are needed. Using acoustic emission (AE) monitoring, effort has been made to stop the sample loading just before its final failure. 17 samples from different sub-types of sandstone are tested under Brazilian test conditions and with AE monitoring. Several thin sections from these loaded samples are prepared. Observation of the thin sections is done and it is tried to find and explain the correlations between the micro-scale parameters and the macro-scale behaviour of the studied sub-types of Modave sandstone.

A scale effect is also studied (see detail E in Figure 3.20). 46 disc-shaped samples with different diameters from 30 to 115 mm and constant thickness of 25 mm are prepared to verify the effect of sample diameter on failure behaviour of tested samples.

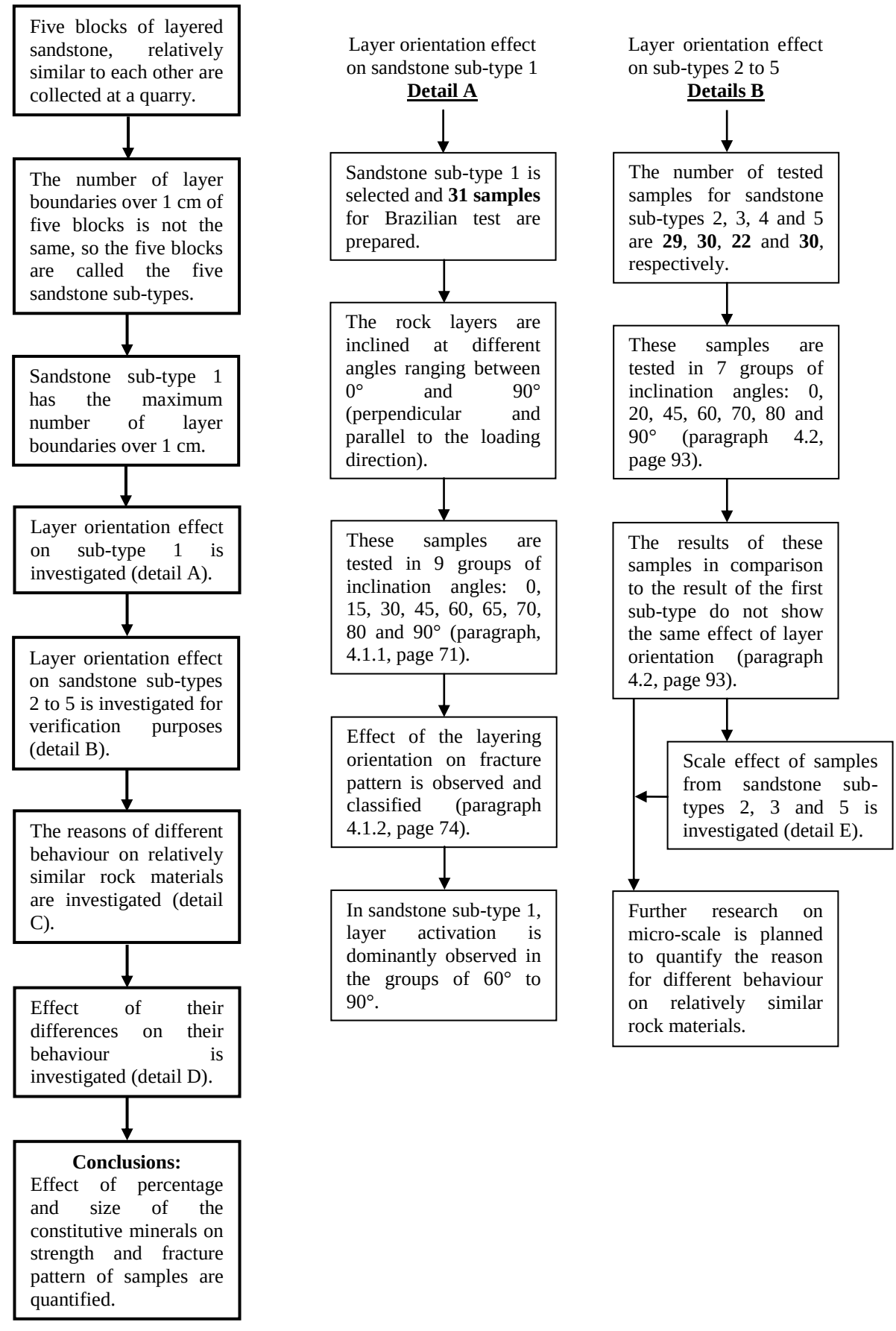
Five blocks of layered sandstone, relatively similar to each other are collected at a quarry.
The number of layer boundaries over 1 cm of five blocks is not the same, so the five blocks are called the five sandstone sub-types.
Sandstone sub-type 1 has the maximum number of layer boundaries over 1 cm.
Layer orientation effect on sub-type 1 is investigated (detail A).
Layer orientation effect on sandstone sub-types 2 to 5 is investigated for verification purposes (detail B).
The reasons of different behaviour on relatively similar rock materials are investigated (detail C).
Effect of their differences on their behaviour is investigated (detail D).
Conclusions:
Effect of percentage and size of the constitutive minerals on strength and fracture pattern of samples are quantified.
Layer orientation effect on sandstone sub-type 1
Detail A
Sandstone sub-type 1 is selected and 31 samples for Brazilian test are prepared.
The rock layers are inclined at different angles ranging between 0° and 90° (perpendicular and parallel to the loading direction).
These samples are tested in 9 groups of inclination angles: 0, 15, 30, 45, 60, 65, 70, 80 and 90° (paragraph, 4.1.1, page 71).
Effect of the layering orientation on fracture pattern is observed and classified (paragraph 4.1.2, page 74).
In sandstone sub-type 1, layer activation is dominantly observed in the groups of 60° to 90°.
Layer orientation effect on sub-types 2 to 5
Details B
The number of tested samples for sandstone sub-types 2, 3, 4 and 5 are 29, 30, 22 and 30, respectively.
These samples are tested in 7 groups of inclination angles: 0, 20, 45, 60, 70, 80 and 90° (paragraph 4.2, page 93).
The results of these samples in comparison to the result of the first sub-type do not show the same effect of layer orientation (paragraph 4.2, page 93).
Scale effect of samples from sandstone sub-types 2, 3 and 5 is investigated (detail E).
Further research on micro-scale is planned to quantify the reason for different behaviour on relatively similar rock materials.

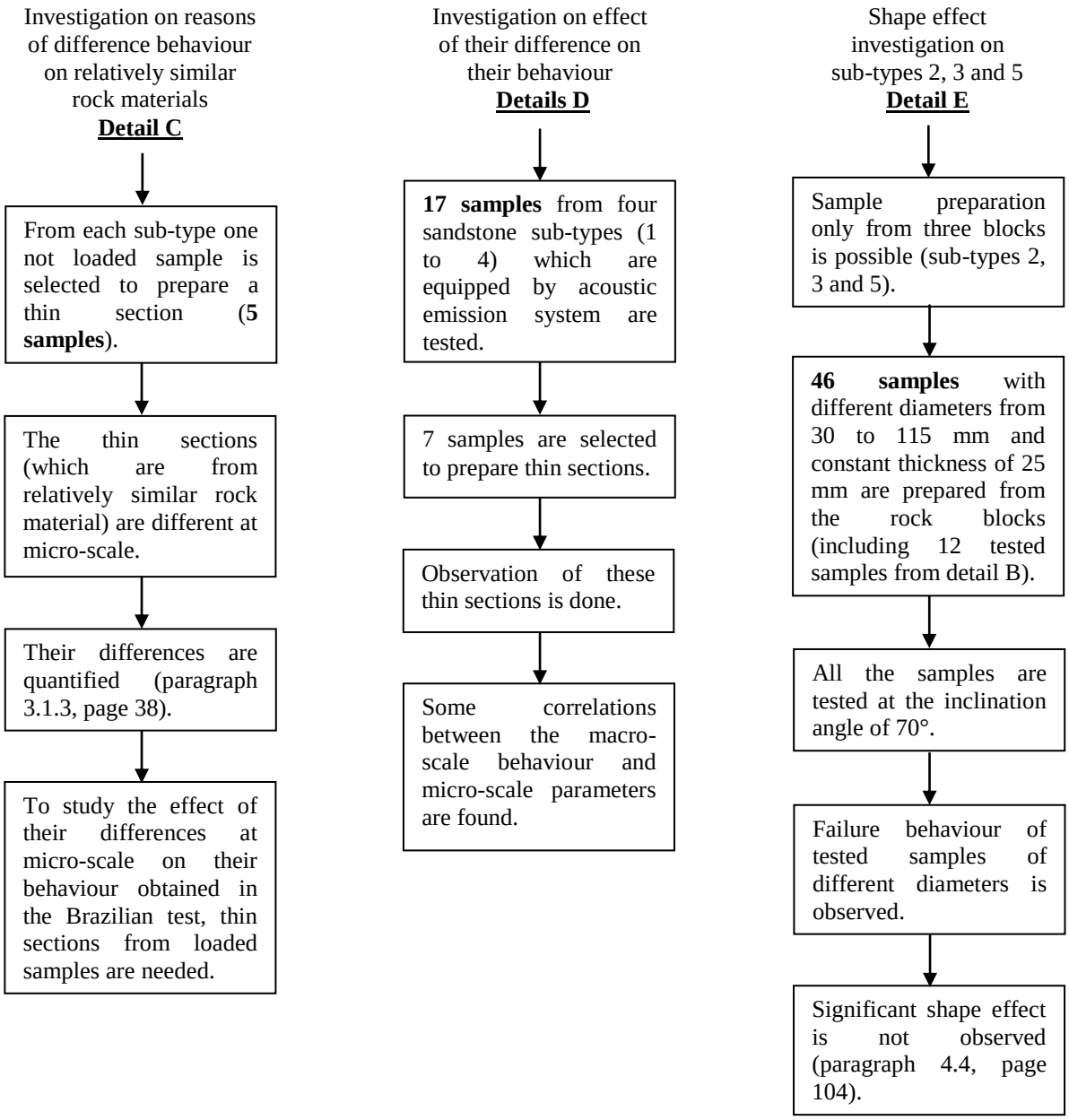

Figure 3.20 Flow chart of the current research on five blocks of stratified sandstone (Psammite of Condroz) which are from a quarry in Modave in the South of Belgium. 202 disc-shaped samples from five sub-types (blocks) of relatively similar sandstone are conducted. The Brazilian tensile method is applied. Diameter and thickness of samples are 50 and 25 mm respectively, except for scale effect experiments (diameter varies from 30 to 115 mm).

3.3 Experimental techniques

The experimental techniques that are used in this study are as follows: the Brazilian tensile test (diametrical loading of cylindrical discs) with and without acoustic emission monitoring, the microscopic observation of a thin section with optical microscope (transmitted polarized light and incident fluorescent light) and finally the microscopic observation with the environmental scanning electron microscopy (ESEM).

3.3.1 Brazilian tensile test

The rock is cored in the laboratory by using a 50 mm diameter drill bit. The direction of coring is parallel to the layer. For the tests, a thickness-to-diameter ratio (t/D) of 0.5 is taken. All tests are carried out by using a loading machine with a loading capacity of 100 kN, at a constant displacement rate of 1 mm/min. Layer orientation for the tested samples varies between perpendicular and parallel to the loading direction (see Figure 3.19).
Samples after a Brazilian test split in at least two parts. The failure of studied sub-types of Modave sandstone is often dynamic and violent with releasing a large amount of energy. The results of tested samples at macro-scale are failure load and fracture pattern. However, for micro-scale quantification stopping the sample loading before its final failure is necessary and this can be managed using acoustic emission (AE) monitoring (see further).

3.3.2 Acoustic emission monitoring

17 samples are prepared for micro-scale quantification to understand how cracks initiate and propagate. The Brazilian loading for these 17 samples is tried to be stopped just before final failure of the samples, in order to have samples that contain many induced micro-cracks, but are not completely fractured. Once a macro-fracture occurs, displacements of the fractured parts of the sample make it difficult or even impossible to recognise what happens at micro-scale. Therefore, the samples are loaded as close as possible to its final strength. Acoustic emission (AE) is continuously measured throughout the tests. Simultaneous analysis of the recorded AE hits helps to determine the moment the tests should be stopped. To have a non-fractured sample that contains many micro-cracks, the best moment to stop the sample loading is the time that cracks start to coalesce. The samples are loaded as close as possible to its final strength, as it would be better for crack visualisation. But when the curve of the cumulated AE events becomes semi vertical, it is very difficult to save the sample from final failure. In the mentioned condition the crack propagation becomes unstable and some parameters such as crack growth velocity govern the crack propagation. In several tests of the current research, the final failure is detected after stopping the sample loading (which is explained later). However, sufficient samples (10 from 17) could be stopped, just prior to the macro-failure.
For conducting Brazilian test with acoustic emission monitoring sandstone sub-types 1 to 4 are considered (sub-type 5 has the secondary plane of weakness, ripples, in addition to the layer boundaries). For sample preparation the rock is cored in the laboratory by using a 50 mm diameter drill bit. The direction of coring is parallel to the layers. Disc-shaped samples have a diameter of 50 mm and a thickness of approximately 18 mm. It should be noted that the thickness-to-diameter ratio of about 0.36 used in this research does not match with ISRM recommendations for Brazilian test (i.e. around 0.5). However, for research purposes, it is better to use smaller thickness-to-diameter ratio specimens in order to make the state of the disc closer to plane stress rather than plane strain. This makes the stress distribution along the thickness of the disc more similar (Lavrov et al. 2002).

The loading of disc-shaped samples are carried out using a displacement-controlled testing machine with a loading capacity of 100 kN (same machine that is already mentioned in paragraphs 3.3.1). The displacement rate is constant, i.e. 0.2 mm/min. All the samples are tested at a layer orientation of 70°. Acoustic emission (AE) is continuously measured throughout the tests using an AMSY-5 system by Vallen-Systeme GmbH. One wide-band AE sensor of type B1025 (Digital Wave Corp., USA) having a frequency range from 50 kHz to 2MHz is attached to the samples as shown in Figure 3.21. The AE sensor is placed not on the very edge of the disc but about 5 mm towards the centre as shown schematically in Figure 3.21. The sensor is attached to the sample with plastic tape, using vacuum grease as the couplant. As it is discussed before, the purpose of this AE monitoring is getting an idea about the changes in the microstructure and the failure process of loaded sample to stop the test just before the final failure. Only one sensor is used, as the aim is not the localization of the AE sources.

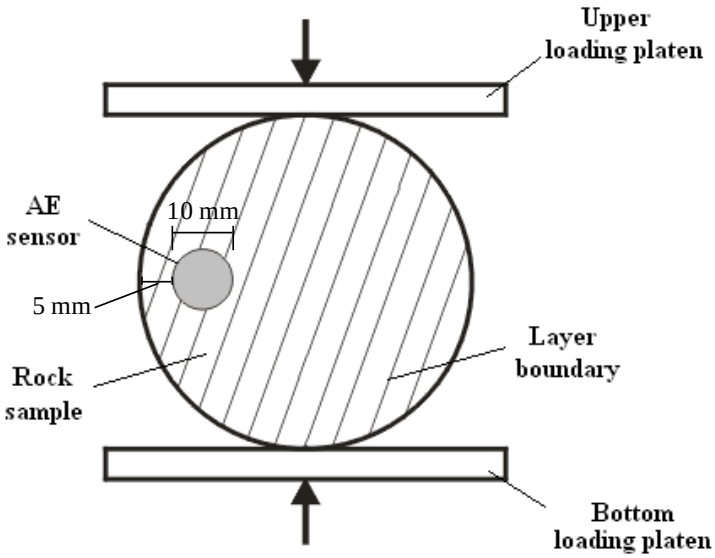

Figure 3.21 Disc-shaped sample loaded in diametrical compression with the location of acoustic emission sensor. Layer orientation is 70° and sandstone sub-types 1 to 4 are tested. Sample diameter is 50 mm.

The piezoelectric crystal inside the AE sensors converts the detected elastic stress waves into analogue electrical signals. AE signals (hits) are amplified by preamplifier with a gain of 34 dB. This means that the signals from the AE sensors (μV) are amplified as in the following equation:

$$34\ dB = 20\ \log\left(\frac{Amplified\ \ signal\ [\mu V]}{Signal\ \ from\ \ AE\ sensor\ \ [\mu V]}\right)$$

A 16 bit analogue to digital converter incorporated in the AMSY-5 system digitises the amplified analogue signal with a sampling rate of 5 MHz. To have an idea of signals (noise) coming from the testing machine, an aluminium cylinder with an attached AE sensor is first loaded. A threshold level of 21.9 dB is used. The aluminium cylinder is loaded more than the expected sample load but much less than its plastic deformation level. It is loaded up to 30 kN. This load is supposed to be at least the maximum load applied to the samples. Considerable AE activity is recorded from the beginning of loading on the aluminium cylinder. The registered hits are not from the aluminium cylinder but from the loading

machine. These hits are noise coming from frictions between different moving parts of the loading machine. After loading the aluminium cylinder, it is unloaded and reloaded again up to 30 kN. It is observed that in the second cycle of loading no signal is recorded and the mentioned noises are eliminated after the first loading cycle. Therefore, before starting the experiments always this dummy test (an experiment of 30 kN) on aluminium cylinder for elimination of noises (of loading machine) is conducted. This is a practice which is followed by all previous researchers within the Research Unit Mining.

Normally in the AE measurements, the threshold level should be high enough to get rid of the environmental noise and low enough to register the AE activity of loaded sample. In this study the main aim is to have a non-fractured sample containing as many micro-cracks as possible, i.e. as close as possible to its final strength. Therefore in this particular case threshold setting is very delicate as testing and analysing should be done simultaneously to save the loaded sample before its final failure. The data processing is carried out using Visual AE Vallen Software (Release R2006).
In testing the samples by AE measurement, a few levels of threshold (21.9, 30.6 and 35.5 dB) are examined on the samples from sandstone sub-type 4 (see later in Table 3.4). After four tests, 30.6 dB is selected as the threshold for the other tests. The threshold measured in dB has to be referred to the 1 µV preamplifier input. A threshold of 30.6 dB corresponds to 33.9 µV (with reference signal of 1 µV). Therefore only signals with peak amplitude higher than a threshold value of 33.9 µV are registered. Figure 3.22 shows that the used threshold is well above the noise level and well below the peak amplitude of a typical AE signal.

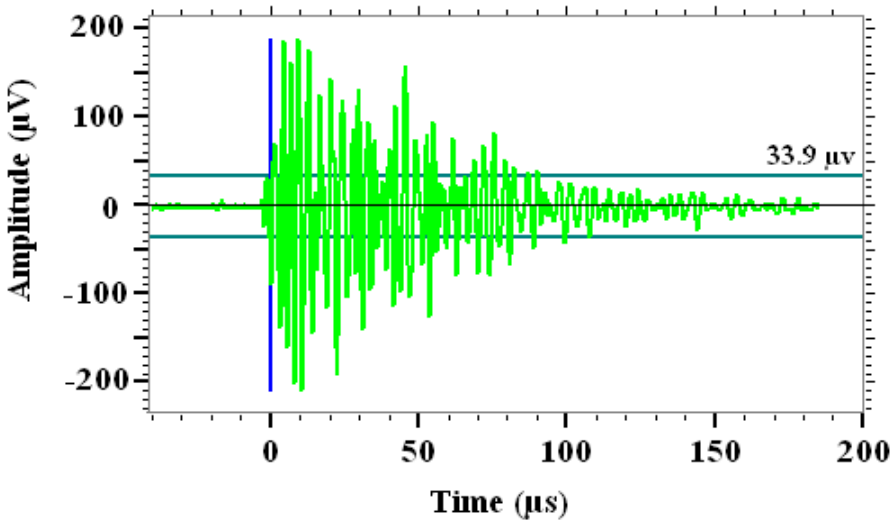

Figure 3.22 Example of a recorded AE signal. Threshold of 30.6 dB corresponds to 33.9 µV (with reference signal of 1 µV).

Table 3.4 gives the diameter D, the thickness t, the maximum applied load F, the threshold level and some other information about the tested samples. The cumulative AE curves for the samples are presented in Appendix A. For micro-scale quantification thin sections from tested samples which are given introduced in Table 3.4 should be prepared. As it is already discussed, non-fractured samples are considered for thin section preparation. But the question is: from which of the non-fractured samples it is better to prepare thin section or in other words from which of them, better and more useful information could be extracted?

Table 3.4 Brazilian test results of samples from sandstone sub-types 1-4, monitored by acoustic emission sensor

Group	Sample N°	D (mm)	t (mm)	ρ (t/m³)	L/D	Th (dB)	F (kN)	Condition	BTS (MPa)
1 (Ref)	1	49.3	17.8	2.6	0.36	30.6	12.1	BFF	8.8
	2	49.3	19.1	2.6	0.39	30.6	13.1	BFF	8.9
2	1	49.3	18.5	2.6	0.37	30.6	11.7	BFF	8.2
	2	49.3	18.8	2.6	0.38	30.6	16.0	FF	11.0
	3	49.3	18.7	2.6	0.38	30.6	15.1	BFF	10.4
	4	49.3	18.7	2.6	0.38	30.6	11.8	FF	8.2
3	1	49.3	18.5	2.6	0.37	30.6	16.0	FF	11.2
	2	49.3	18.8	2.5	0.38	30.6	17.8	BFF	12.2
	3	49.3	18.8	2.5	0.38	30.6	16.7	BFF	11.5
	4	49.3	18.8	2.5	0.38	30.6	18.5	BFF	12.7
4	1	49.3	19.2	2.6	0.39	21.9	16.5	FF	11.1
	2	49.3	17.8	2.6	0.36	21.9	15.0	FF	10.9
	3	49.3	18.9	2.6	0.38	30.6	14.8	FF	10.1
	4	49.3	18.5	2.6	0.38	35.5	11.7	FF	8.2
	5	50.0	17.3	2.6	0.35	30.6	10.9	BFF	8.0
	6	50.0	17.3	2.6	0.35	30.6	11.8	BFF	8.7
	7	50.0	17.1	2.6	0.34	30.6	13.8	BFF	10.3

In all the samples layer orientation is 70° from horizontal. D = Diameter, t = Thickness, Th = Threshold level and F = the maximum experienced load (which is not always the failure load). Presented density is measured in the laboratory condition. Samples after the test have one of the two following conditions: FF = Final Failure, which means that sample is failed and split into two or more parts or BFF = Before Final Failure, which means that sample loading is stopped prior to final failure and the sample is not failed.

Among all the 17 samples introduced in Table 3.4, the second sandstone sample of the reference sub-type is an exception. Although in this sample final failure occurs, the sample is not split and a fracture corresponding to an activated layer boundary is not easily visible (see Figure 3.23). In the mentioned sample crack coalescence and initiation of macro-scale failure occur and fortunately sample loading is stopped few milliseconds prior to the splitting. The condition of this sample is ideal and consequently from the reference sub-type this sample is selected for thin section preparation.

In the other three sub-types (sub-types 2 to 4) non-failed samples (BFF condition in Table 3.4) are considered. For each sub-type of sandstone, the sample with the highest amount of AE activity (hit) is selected for thin section preparation. These samples are the third for sandstone sub-type 2; the fourth for sub-type 3 and the seventh sample for sub-type 4 (corresponding to Table 3.4). Coincidently these samples in their groups among the other non-failed samples have the highest loading values. For micro-scale quantification, selecting the sample to prepare thin section by only considering the applied stress is not a reliable criterion. Because between two samples from one sub-type of sandstone, the one on which higher stress is applied has not necessarily more changes in its microstructure.

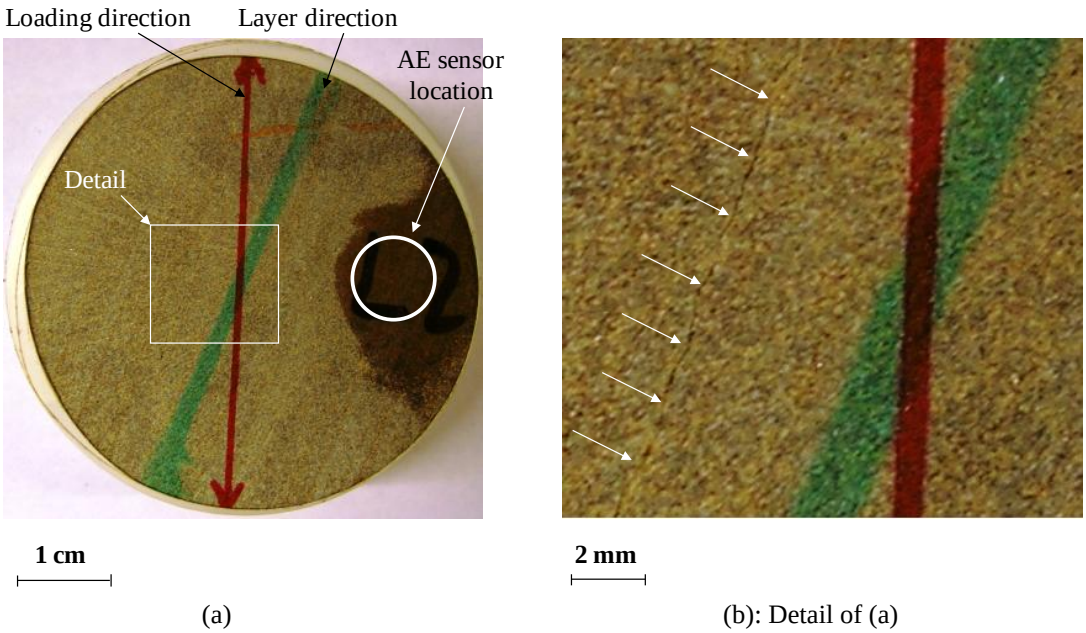

Figure 3.23 Digital photos of a sandstone sample from reference sub-type after conducting Brazilian test. Acoustic emission monitoring is done during the test. Angle of layer direction from horizontal is 70°. Brazilian tensile strength of the sample is 8.9 MPa. This sample is 1.2 in Table 3.4. (a) Picture of tested sample with a fracture (activated layer boundary) that is not easily visible, (b) Magnified central part of the sample. Fracture path is indicated by white arrows.

For the selected samples of sandstone sub-types 2, 3 and 4 there is no certainty that the micro-cracks could be visible under microscope. Therefore from each sub-type of sandstone one failed sample is also selected to prepare a thin section (except reference sub-type). In the fractured samples, the crack width is considerably more than the grain size and consequently the changes in microstructure cannot be followed. But near the main fracture, existence of some other fracture paths is probable. This kind of fractures can be monitored and some information can be extracted from them. The criterion for selecting the failed samples (to prepare thin section) is the degree of fracturing and the distance between fractured parts of the sample. The sample with the smallest fractures and the shortest distance between the different parts is considered. In this condition it is more probable to have more fractured grain minerals. When a sample is totally fractured, losing the zone in which micro-cracks exist is more probable. By considering the mentioned criterion, the selected samples are the fourth for sandstone sub-type 2, the first for sub-type 3 and the fourth sample for sub-type 4 with referring to Table 3.4.

3.3.3 Microscopic observation of thin sections with optical microscope

In total 7 samples from 17 are selected to prepare thin sections for micro-scale quantification. For each of the sandstone sub-types 2, 3 and 4, two samples are selected (one before and one after final failure). For reference sub-type only one sample which was exactly at its failure state is selected.

The fractured samples are twice impregnated under vacuum with a fluorescent (FITC) dyed epoxy resin to enhance the contrast between the grains and the spaces of grain boundaries and also the cracks. A multiple impregnation is necessary to avoid falling out of damaged grains during cutting, grinding and polishing. For the three non-fractured samples only one

impregnation is done. Thin sections with a thickness of 30 µm are prepared from all these 7 samples. For the fractured samples the thin sections are from the fractured part. For the three non-fractured tested samples the thin sections are from the central part of the samples in the direction of loading (see Figure 3.24). Because in this zone whether the micro-fractures are in the layer direction or in the loading direction, they could be visualised on the thin section.
It is very important to consider the cracks which are only induced due to the loading. It is possible that cracks occur during the process of thin section preparation. Figure 3.25 shows a crack induced in the preparation process of a thin section. In all the (17) thin sections 3 induced cracks (corresponding to preparation process) with a limited length are observed. The crack edges in Figure 3.25 are not sharp. This kind of cracks induces by some dirt or loos separated quartz in the last part of thin section preparation. The last part is polishing the thin section in order to make it more flat and shiny.

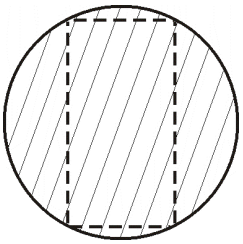

Figure 3.24 Location of thin section in a non-fractured tested sample. Layer orientation is indicated (thin lines).

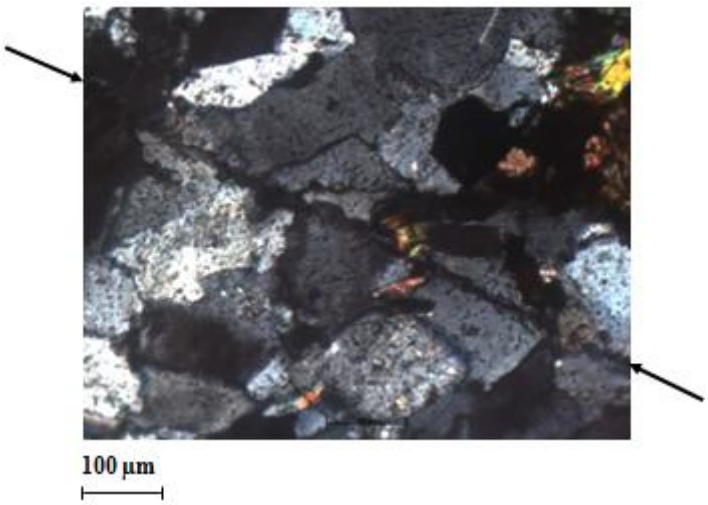

Figure 3.25 Example of a crack induced in the process of thin section preparation. The crack is located between the two arrows. Pixel resolution is 0.54 µm.

In these sub-types of Modave sandstone, quartz as the strong element is the main constitutive mineral while carbonate and mica are the two weak minerals. In these sub-types, the observed mineral percentage of carbonate is higher than mica (see further). Furthermore as the mica minerals are very thin (20-30 µm), detecting the crack in them is very difficult in the non-fractured samples. Therefore, to be able to quantify the changes in the microstructure of these sub-types of sandstone, the quartz and the carbonate grains which have intragranular cracks are considered.

As loading the samples is stopped prior to the final macro-failure, micro-changes in the carbonates are in the form of activated cleavages. The activated cleavages in the carbonate grains are much more visible than crack(s) in quartz grains. The process of crack detection in quartz grains is rather problematic. Therefore to find the micro-changes in the quartz and carbonate grains, two different procedures are used which are explained separately.

3.3.3.1 Activated cleavages in carbonate grains

The microscopic observation of minerals is done by a Zeiss petrographical microscope with transmitted light. The images (micrographs) of the thin sections are digitally acquired using an Axio-Cam Zeiss digital camera attached to the mentioned petrographical microscope. The micrographs are processed with the software MRGrab from Carl Zeiss Vision GmbH. In order to have a systematic map of grains observed, the apparatus of the point-counting method is used. The activated cleavage of carbonate grains are searched through 1500 points in each thin section. These points are in a regular pattern with a fixed interval of 400 µm between the points. The direction of counting is perpendicular to the layers. The distance of 800 µm is taken between the lines of point-counting. The carbonate grains are weak in strength and the cleavages (see Figure 3.26a) can be activated even during the process of thin section preparation. Therefore, the carbonate grains with one single activated cleavage are not considered as cracked carbonates (see Figure 3.26b). Only the carbonate grains that have several activated cleavages are considered as cracked carbonates. Figure 3.27 presents two micrographs of carbonate grains from thin section of the non-failed sample of sandstone sub-type 2 which are considered as cracked carbonate. In the mentioned figure several parallel cleavages in both carbonate minerals are activated due to the applied load in the diametrical compression test. In the untested samples the presence of several parallel activated cleavages is never observed, while a single activated cleavage is observed (i.e. due to sample preparation).

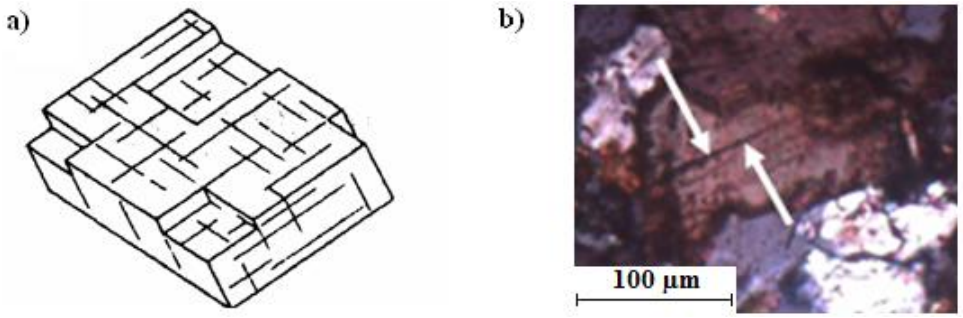

Figure 3.26 Carbonate cleavages: a) A schematic view of rhombohedral cleavage system of calcite (Klein & Hurlbut, 1993). Calcite is a carbonate mineral. b) A view of carbonate in the thin section of the non-failed sample from sandstone sub-type 2. White arrows show a single activated cleavage plane in the carbonate but the grain is not considered as a cracked carbonate (induced by the sample loading), because this kind of activated cleavage is also observed in untested samples. Pixel resolution is 0.54 µm.

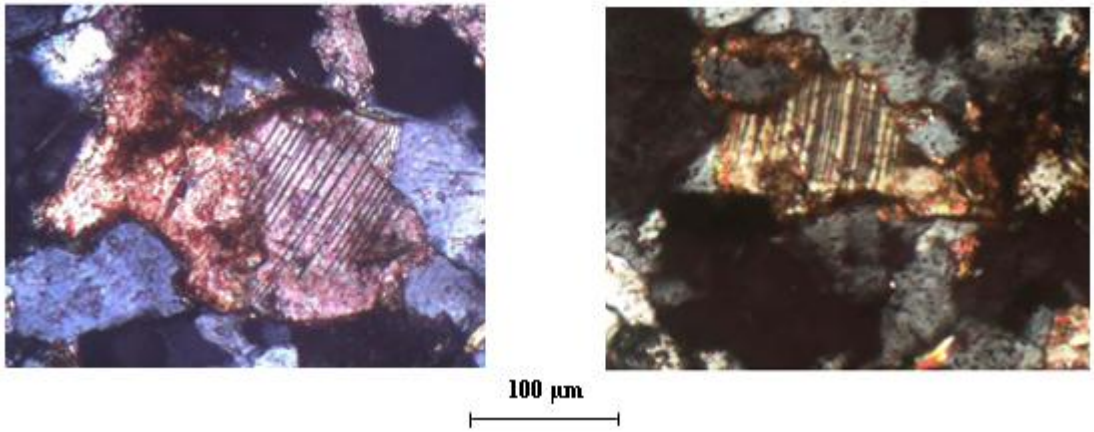

Figure 3.27 Dominant activated cleavages in carbonate. The micrographs are from the thin section of the non-failed sample from sandstone sub-type 2. Both grains are considered as a cracked carbonate (induced by the sample loading) as many cleavages are activated together. Furthermore, similar cleavage patterns to these cases are never observed in untested samples. Pixel resolution is 0.54 µm.

3.3.3.2 Micro-cracks in quartz grains

The microscopic observation of minerals in this part is done by a Zeiss petrographical microscope with incident fluorescent light and also by transmitted polarized light. The images (micrographs) of the thin sections are digitally acquired using an Axio-Cam Zeiss digital camera attached to the Zeiss petrographical microscope. The micrographs are processed with the software AxioVision version 4.

Detection of micro-cracks in quartz grains needs a particular process as these micro-cracks are very small in their width and even in their length. In order to have a systematic map of grains observed, the thin sections (24×33 mm) are divided into 12 rows as shown in Figure 3.28. This is done by using the apparatus of the point-counting method. The intracrystalline cracks in quartz grains are searched through 160 points along the centre line of each row of the thin section. The points in each row are in a regular pattern with a fixed interval of 200 µm. The width of the rows is 1750 µm. In total the intracrystalline cracks in quartz grains are searched through 1920 points.

Figure 3.28 Detection of micro-cracks in quartz grains. Dividing the thin section into 12 rows. The dimensions of the thin sections are 24×33 mm. The width of each row is 1750 µm. The intracrystalline cracks are searched through 160 points along the centre line of each row. The points in each row are in a regular pattern with a fixed interval of 200 µm. This is done by point-counting apparatus.

Micro-cracks in quartz grains are sharp and are presented by small open lines which are filled by resin under vacuum. Unfortunately, it is impossible to detect this kind of cracks only by observation of the microscopic view of the thin section with incident fluorescent light, because they show no characteristic difference with the planar grain to grain contacts. Therefore, when a feature (as a possible micro-crack) is observed with incident fluorescent light, it is verified with the transmitted polarized light. Planar grain to grain contacts are easily detectable by transmitted polarized light. If that feature is not a planar grain to grain contact, it is considered as a micro-crack in a quartz grain. The procedure of micro-cracks detection in quartz grains is illustrated with some micrographs, presented in Figure 3.29. This figure presents the verification of micro-cracks in quartz grains of tested samples.

In Figure 3.29a the micrograph which is obtained with incident fluorescent light (left photo) shows a sharp line of penetrated resin. This could be a micro-crack. To verify this feature (possible micro-crack) the incident fluorescent light should be changed to the transmitted polarized light. The micrograph of the same position by using transmitted polarized light (right photo) shows that the mentioned line is a planar contact of two quartz grains and not a micro-crack. This is important to note that finding the micro-cracks by only microscopic observation with transmitted polarized light is not possible due to the same polarization effect within one grain. This is proved by the micrographs in Figure 3.29c. The left photo which is obtained with incident fluorescent light shows two straight lines of resin penetration. But in the right photo which is obtained with transmitted polarized light, only the planar contact of two quartz grains is clearly visible while the micro-crack is not visible. As already noted micro-cracks are very small (short and thin) and for example the length of the mentioned micro-cracks is less than 50 μm (see micro-crack in Figure 3.29c). Another example in Figure 3.29b shows two parallel micro-cracks in a quartz grain. These two micro-cracks are slightly visible in the photo which is obtained with transmitted polarized light. In this quartz grain the direction of the two parallel micro-cracks are close to the loading direction (middle photos in Figure 3.29) while in the photos of Figure 3.29c, the direction of micro-crack and loading axis are nearly perpendicular.

Defects existence is considered as an important factor that influences rock behaviour. Willard and McWilliams (1969) regard defects as either open or closed cracks or as loci at which cracks most likely would occur with sufficient tensile or shear stress. They mention that defects appear as small visible or microscopic planar and linear discontinuities associated with specific minerals and groups of minerals in a rock fabric. Willard and McWilliams (1969) identify the defects in the study of granite and limestone. They mention the quartz defects in granite as: 1) Grain elongation, 2) Cleavage (if present), 3) Micro-fractures and 4) Inclusion trains and planes. It can be concluded that cleavage in quartz grain is not often observed.
In the current study among the five sub-types of stratified Modave sandstone only in sub-type 3, one quartz grain with cleavage is observed. Figure 3.30 presents the cleavages in the quartz grain. In this figure the micrograph acquired by incident fluorescent light presents an activated cleavage. The activated cleavage in the quartz grain is indicated by two white arrows. In Figure 3.30 the micrograph acquired by transmitted polarized light, does not show clearly the cleavage activation.

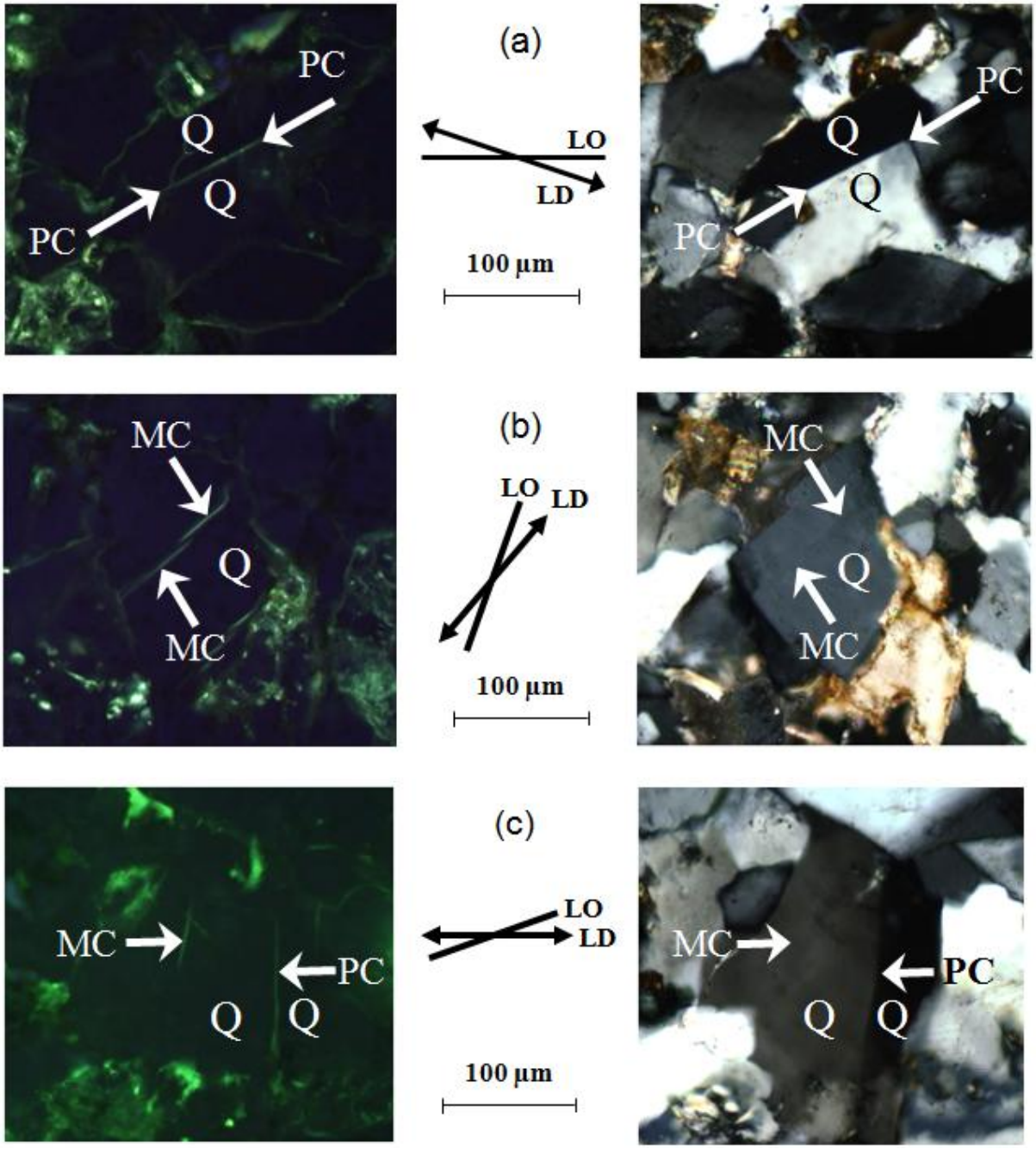

Figure 3.29 Verification of micro-cracks in quartz grain (left: incident fluorescent light; right: transmitted polarized light) [Q = Quartz grain, PC = Planar contact, MC = Micro-crack, LO = Layer orientation, LD = Loading direction. Pixel resolution is 0.27 µm].
The sharp line of penetrated resin (left) is a possible micro-crack, as:
(a) Sandstone sub-type 1: no micro-crack but planar contact of two quartz grains.
(b) Sandstone sub-type 4: two parallel micro-cracks.
(c) Sandstone sub-type 3: a micro-crack and a planar contact of two quartz grains.

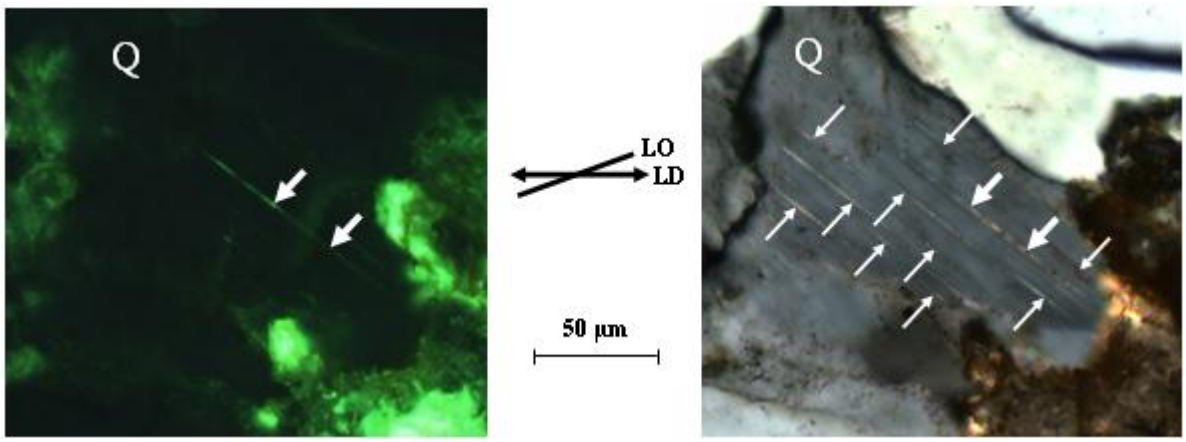

Figure 3.30 Observed cleavages in a quartz grain of Modave sandstone sub-type 3 (left: incident fluorescent light; right: transmitted polarized light) [Q = Quartz, LO = Layer orientation, LD = Loading direction. Pixel resolution is 0.27 µm]. White arrows show the quartz cleavages and the two thicker ones indicate the activated quartz cleavage.

3.3.4 Microscopic observation of thin section using ESEM

The environmental scanning electron microscopy (ESEM) is an instrument for studying the solids surfaces at high magnifications. Although the images are qualitatively similar to the images obtained by an optical microscope, ESEM possesses much greater resolution (Aligizaki 2006). As an alternative, ESEM is used for the detection of micro-cracks in quartz grains. ESEM is used as there is no need to cover the thin section with gold or carbon. The ESEM has become popular in microstructural research in cement-based materials and mainly on backscattered electron (BSE) images of plane polished surfaces of epoxy-impregnated specimen (Aligizaki 2006) are studied. In this study BSE imaging is used to take the images from the thin section of an impregnated non-failed sandstone sample.
The intensity with which electrons are backscattered depends principally on the local atomic number of the specimen. Backscattering is more likely to occur for higher atomic numbers of a material (Aligizaki 2006). Thus as a beam passes from a low atomic number to a high atomic number area, the signal due to backscattering, and consequently the image brightness increases. Impregnated areas with epoxy resin appear black and provide an easy identification of porosity and cracks (see Figure 3.31).

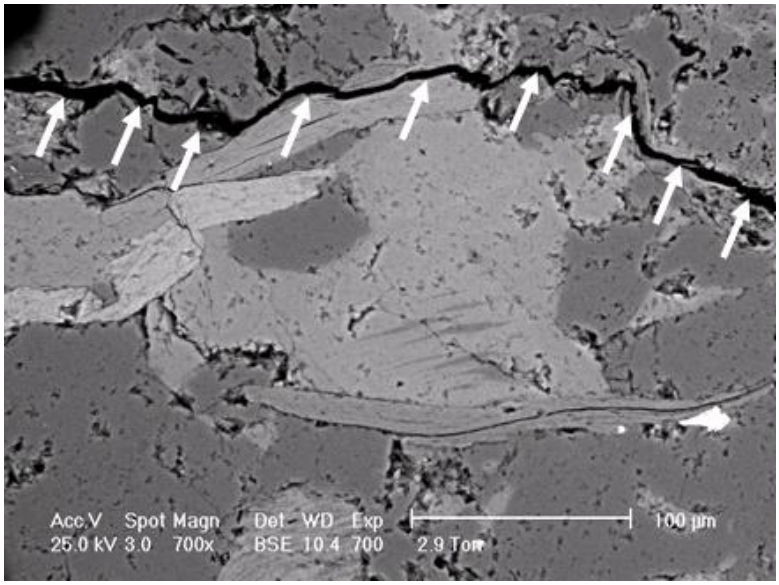

Figure 3.31 A crack in the reference sandstone sub-type (1). The white arrows indicate the (black) crack. The contrast of the crack (black) and rock material (greyish) is obvious.

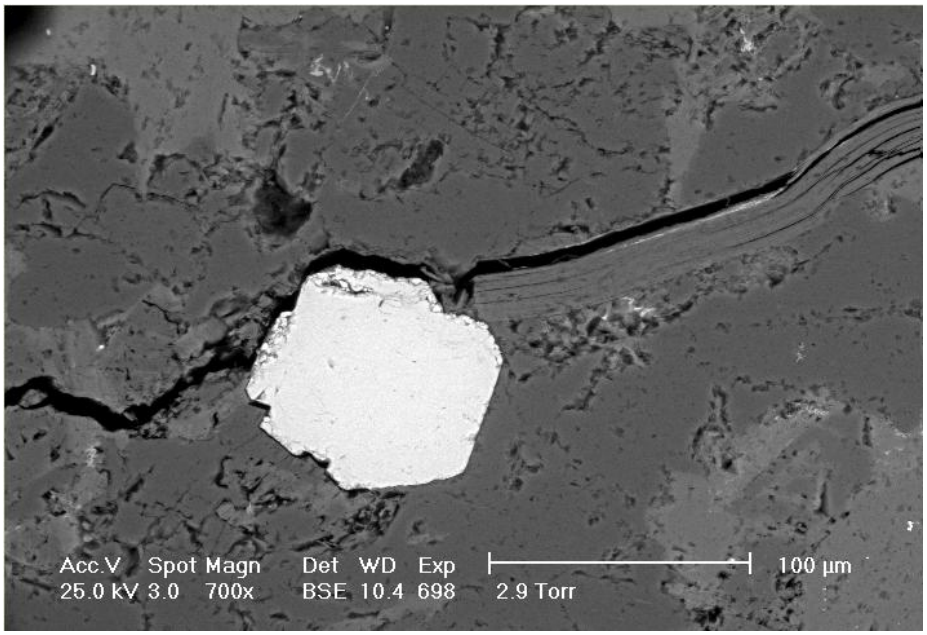

Figure 3.32 BSE image from a thin section of the impregnated non-failed sample of sandstone sub-type 1 by ESEM. The bright mineral in the middle is pyrite with the specific gravity of 5 (quartz grain and the matrix material have a specific gravity of around 2.7). An intergranular crack (black strip) is extended over the whole image and is deflected by pyrite.

The density of the main constitutive minerals of the studied Modave sandstones is close to each other (around 2.7 gr/cm^3). Therefore the ESEM in this study presents the rock material as a greyish view and it is not easy to detect the quartz grain within the matrix material due to similar densities. However, ESEM can help to investigate small heterogeneities.
The bright mineral in the middle of Figure 3.32 is pyrite with a specific gravity of 5. As can be seen in this figure rock material is presented as a greyish view and it is not easy to detect the quartz grains. In Figure 3.32 an intergranular crack (black strip) is observed and deflected

by pyrite. This type of cracks is longer and often wider than the intragranular cracks (in quartz grain).

BSE images of a fracture surface have a high quality and, hence, they are suitable for micro-structural analysis. The resolution of a BSE image is comparable to the resolution of optical microscopy; however, the better image contrast in BSE images allows better definition of the constituents than with optical microscopy imaging (Powers 1955, Stutzman 1994). Figure 3.33 presents the delamination of mica in the non-failed sample of sandstone sub-type 1. In this figure the delamination of mica is indicated by white arrows and also an opened planar contact of mica with another grain is indicated by a white star. Although studied rock material is presented as a greyish view, mica is visible because of its particular shape (thin and long).

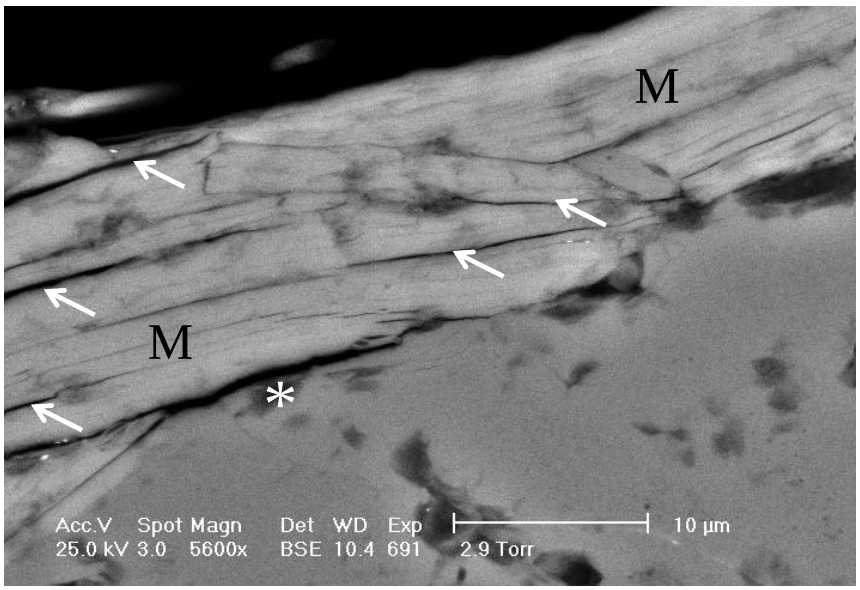

Figure 3.33 BSE image of delamination of mica in the fractured sample of sandstone sub-type 1. Mica is indicated by M and its delamination is indicated by white arrows. An opened planar contact of mica with another grain is indicated by a white star.

The wavelength of electrons is not as limited as the wave length of visible light; therefore, the images obtained by ESEM can be magnified much more than optical microscopy (Aligizaki 2006). However it is important to note that ESEM images are formed by a quite different mechanism than in an optical microscope. Unlike the light in an optical microscope, the electrons in an ESEM never form a real image of the sample (Johnson 1996). In ESEM, no objective lens is used, but instead, virtual images are built up point by point, in a way similar to that used in a television display.

3.4 Overview of findings

In this study layered or stratified rock material as a specific form of anisotropy is considered. The tests are conducted on layered sandstone. Studied sandstone is from a quarry in Modave in the South of Belgium. This type of sandstone is known as “Psammite of Condroz”, characterized by numerous thin and parallel layers. Five blocks of layered sandstone are taken from the mentioned quarry at very short distance (from 1 to 10 m) from each other and

visually they seem similar. However, the number of layer boundaries (over 1 cm on hand sample) is not the same for all blocks; therefore, the five blocks are further called the five sub-types.
The layered sandstone sub-types have low effective porosity (from 2% to 3.2%) with dry density of 2.6 g/cm^3. Minimum and maximum wave velocities are always measured perpendicular and parallel to the layers, respectively. Measured average wave velocities for sandstone sub-type 1 to 5, respectively vary from 4.7 to 5.1, 4.6 to 4.9, 4.4 to 4.5, 4.5 to 4.9 and 4.5 to 5.0 km/s. In different configurations, slight differences of wave velocity are recorded for all samples. So, one can conclude that they are in a similar range.

The five sandstone sub-types are macroscopically relatively similar. However, microscopic observation of the five thin sections shows that the samples from a microscopic view are different. Thin sections show that samples have different microscopic parameters such as grain size, quantity and quality of weak elements, etc. Also sub-type 5 has second planes of weakness, namely ripples. For this reason, further on most microscopic study focuses on sandstone sub-types 1 to 4. Although quartz grain size ranges for the five sandstone sub-types are different, all the sub-types are in the size range of fine sand. The numbers of observed pre-existing micro-cracks in quartz grains in the untested samples of four sandstone sub-types (1 to 4) are close to each other.

It is also important to mention that in this chapter a method for detection of micro-cracks in quartz grains is presented. This method is summarised by the following 6 points:
1- Micro-cracks in quartz grains are small openings which are filled by resin under vacuum.
2- Sharp lines of penetrated resin are searched by petrographical microscope with incident fluorescent light.
3- The lines determined in that way are either a micro-cracks or planar grain to grain contact.
4- Incident fluorescent light is changed to transmitted polarized light.
5- Planar contact of two grains because of their different polarization effect is easily detectable.
6- If the sharp line (see point 3) is not a planar contact, it is a micro-crack which is not generally visible by transmitted polarized light due to the same polarization effect within one grain.
As quartz is the main constitutive mineral in the studied layered sandstone, observation of its behaviour due to loading is important.

4 Results of Brazilian Test: Macro-scale Behaviour

Sandstone sub-type 1 (reference) has the maximum number of layer boundaries among the five Modave sandstone sub-types. Furthermore the amount of weak minerals (mainly mica and carbonate) is the largest for sub-type 1. Therefore, as expected, a more dominant effect of layer orientation on conducted samples of the reference sub-type is observed.
This chapter is focused on the tensile strength and the fracture pattern of the tested samples under Brazilian test conditions. The results are presented in the following four main topics: (1) Results for sandstone sub-type 1 (reference sub-type), (2) Results for sandstone sub-types 2 to 5, (3) A comparison in Brazilian test results for sandstone sub-types 1 to 5 for an inclination angle of 70° and finally (4) Shape effect investigation.

4.1 Effect of layer orientation for sandstone sub-type 1

4.1.1 Tensile strength

The samples are tested at different layer inclination angles (see Figure 3.19) ranging between 0° (perpendicular to the loading direction) and 90° (parallel to the loading direction). It should be highlighted that the orientation of the layers with respect to loading direction is evaluated. As the loading direction in this study is always vertical, changing the layer orientation implies that the angle between the layer direction and the load direction changes. Nine different values for the reference sub-type are considered: 0, 15, 30, 45, 60, 65, 70, 80 and 90°. Since one sample is not necessarily representative for the failure behaviour corresponding to a specific inclination angle, two to five samples are tested per inclination angle value. 31 samples for the reference sub-type are tested. Table 4.1 gives the inclination angle θ, the diameter D, the thickness t, the failure load F and some other information about the tested samples. As a reminder it is important to note that, in this study Brazilian tensile strength, BTS, is considered as $\frac{2F}{\pi Dt}$. Of course this formula is considered for the loaded diameter (see paragraph 2.2.1) and a typical vertical fracture, which is often not the case (see further, Figure 4.5). In other words the formula is used just to compare the Brazilian strength of samples in different layer orientations. This formula is applied for all the samples regardless of their fracture pattern (failing through the loaded diameter or following other parts).

Table 4.1 Brazilian test results for Modave sandstone sub-type 1

Group	θ(°)	Sample N°	D (mm)	t (mm)	ρ (t/m³)	t/D	F (kN)	BTS (MPa)
I 	0	4	49.8	26.6	2.5	0.53	29.4	14.1
	0	5	49.9	26.9	2.5	0.54	25.6	12.1
	0	6	49.8	26.6	2.6	0.53	33.1	15.9
II	15	24	49.8	26.7	2.5	0.54	30.8	14.7
	15	25	49.9	24.4	2.6	0.49	29.7	15.5
III	30	7	49.7	26.4	2.6	0.53	24.8	12.0
	30	8	49.8	26.3	2.6	0.53	24.4	11.9
	30	9	49.9	26.5	2.5	0.53	23.6	11.3
IV	45	21	49.9	25.7	2.6	0.52	29.9	14.8
	45	22	49.9	25.9	2.6	0.52	33.0	16.3
	45	23	49.8	25.3	2.6	0.51	28.3	14.3
V	60	10	49.9	26.4	2.6	0.53	22.9	11.1
	60	11	49.9	26.1	2.6	0.52	29.8	14.6
	60	12	49.9	25.7	2.6	0.52	22.7	11.3
	60	17	49.8	26.1	2.5	0.52	14.3	7.0
	60	31	49.3	25.6	2.5	0.52	18.8	9.5
VI	65	27	49.9	27.1	2.5	0.54	26.9	12.7
	65	28	49.9	26.4	2.6	0.53	38.0	18.4
	65	29	49.9	26.2	2.6	0.52	23.5	11.4
	65	30	49.2	24.7	2.5	0.50	18.4	9.7
VII	70	18	49.9	26.4	2.6	0.53	18.6	9.0
	70	19	49.9	25.5	2.6	0.51	18.3	9.2
	70	20	49.8	26.2	2.6	0.53	19.5	9.5
	70	26	49.9	26.2	2.5	0.53	30.7	14.9
VIII	80	13	49.9	26.2	2.6	0.53	18.0	8.8
	80	15	49.9	26.9	2.5	0.54	17.4	8.3
	80	16	49.8	26.3	2.6	0.53	23.8	11.5
IX 	90	1	49.8	26.4	2.6	0.53	22.5	10.9
	90	2	49.9	26.3	2.6	0.53	23.7	11.5
	90	3	49.9	26.3	2.6	0.53	25.3	12.2
	90	14	49.8	26.2	2.6	0.53	13.8	6.7

θ is the angle of layer direction from horizontal. D = Diameter, t = Thickness and F = Failure load of the samples. Presented density is measured in laboratory conditions.

The variation in Brazilian tensile strength (BTS) with the inclination angle θ is plotted in Figure 4.1 for all the samples of the reference sub-type. This figure shows two groups located at both sides of θ = 50°. The average BTS-values of the samples with θ < 50° (13.9 MPa) is slightly larger than that for the samples with θ > 50° (10.9 MPa). Normally one would expect that when the layers are horizontal or semi-horizontal the fracture is mainly through the stronger material, while by increasing the inclination angle the fracturing processes make use of the layers, which have weaker mechanical properties. Also in the latter cases samples fail also in shear and not purely in tension. For the tested samples of sub-type 1 that θ < 50°, the

fractures through the intact material are dominant. While, for the samples with $\theta > 50°$, the fracture parallel to the layers is dominant.

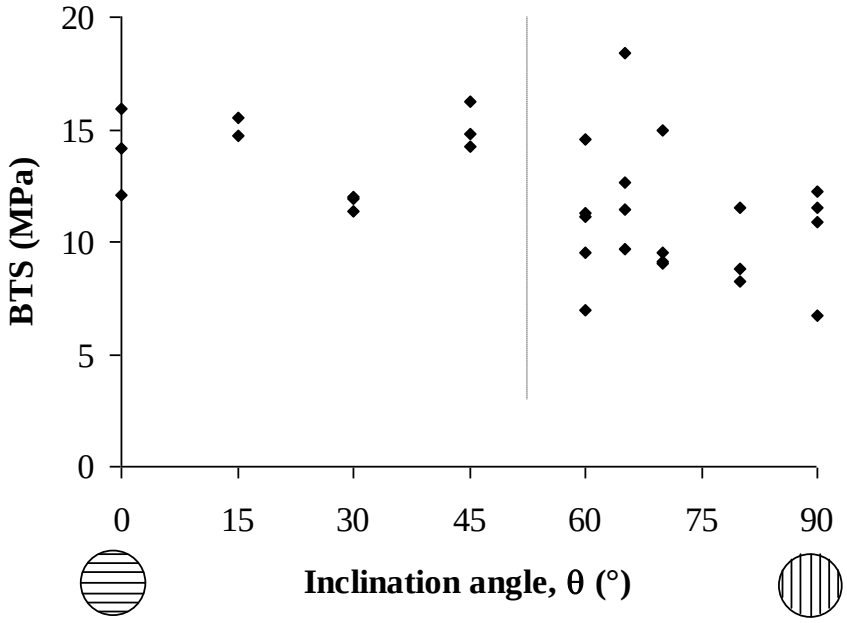

Figure 4.1 Variation in Brazilian tensile strength, BTS, as a function of the inclination angle θ for all the samples of reference sub-type.

Figure 4.2 presents the variation in the average Brazilian tensile strength (BTS) with the inclination angle θ for the reference sub-type. The graph shows a small downward trend. For the reference sub-type the average BTS varies between 15.1 MPa (45°) and 9.5 MPa (80°). This seems to be consistent with the experimental results of Chen et al. (1998) on two kinds of transversely isotropic sandstone. However, for one of the sandstone types the maximum value of BTS is more than four times of the minimum value for the experiments of Chen et al. (1998), while in this study a relatively small difference is observed. In the experiments of Chen et al. (1998), the BTS-values for an angle of 0° and 90° were close.

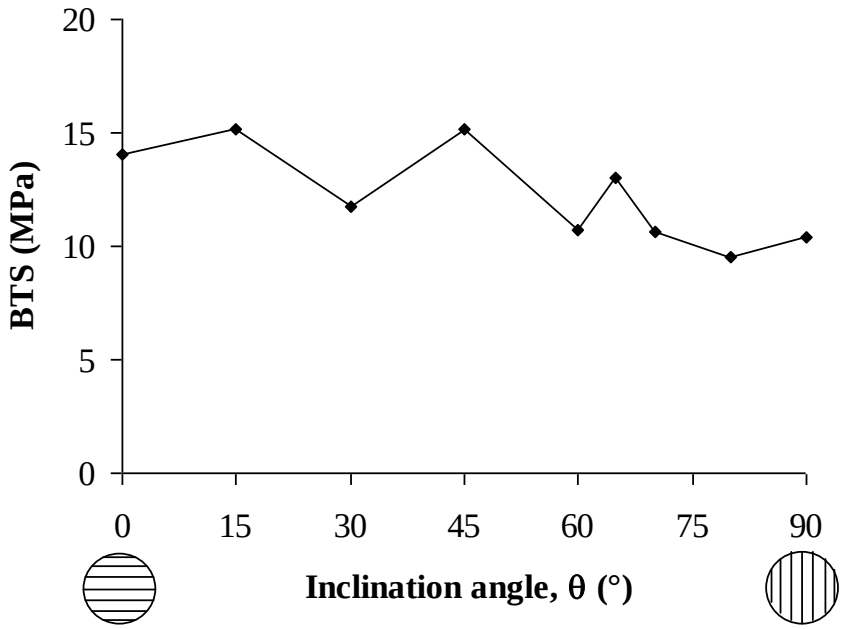

Figure 4.2 Variation in average Brazilian tensile strength, BTS, as a function of the inclination angle θ for the reference sub-type.

4.1.2 Fracture analyses

Similar to the idea introduced by Szwedzicki (2007) for UCS-tests (see paragraph 2.3), different failure modes are suggested. By considering the samples after failure different types of fractures are observed (see Figure 4.3):
(1) Some fractures are parallel to the isotropic layers which are further called "layer activation" (LA).
(2) Some fractures are roughly parallel to the loading direction and they are located in the central part of the sample between the two loading lines. The central part is arbitrarily defined as 10% of the diameter on both sides of the central line. These fractures are further called "central fractures" (CF).
(3) Fractures outside the central part are also observed. If they do not correspond to layer activation, they are further called "non-central fractures" (NCF). The latter are often curved lines, starting at or around the loading platens.
In most cases, two or three different fracture types occur in the same experiment (see Figure 4.4). It is good to note that in case of θ = 90° and when a straight fracture parallel to the layers between both loading platens is induced, this is classed as layer activation and not as central fracture. However, if in that case (θ = 90°), a fracture locates in the central part but does not follow the layer direction, it is classed as central fracture.

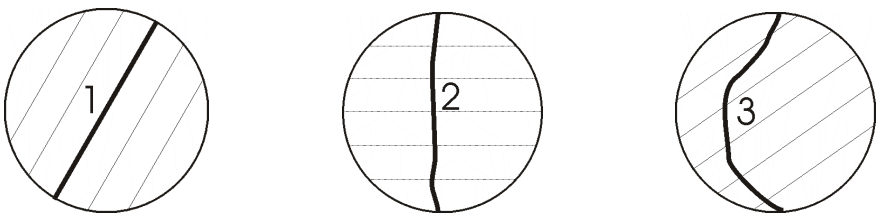

Figure 4.3 Schematic representation of different fracture types in Brazilian test. (1) Layer activation, (2) Central fracture, and (3) Non-central fracture.

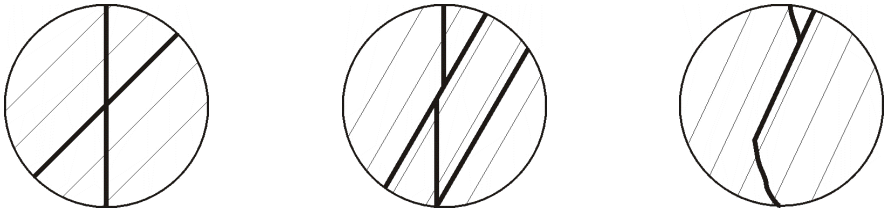

Figure 4.4 Schematic representation of combinations of different failure modes (layer activation and central fracture) in Brazilian test.

The failure patterns (one side) of all the samples after failure are digitalised and shown in Figure 4.5 in different groups of the inclination angle for the reference sandstone sub-type. Apart from the predominant failure mode some secondary fractures are also observed. The descriptions of the samples after failure are presented in Table 4.2. The predominant failure mode of the reference sub-type samples are observed as follows: (1) central fracture(s) when inclination angle is equal to 0°, 15° or 30°, (2) combination of central fracture(s) and layer activation when this angle is equal to 45° or 60° and (3) layer activation when the inclination angle is equal to 65°, 70°, 80° or 90°.
The failure patterns corresponding to $\theta = 0°$ and $\theta = 90°$ look similar. However for $\theta = 0°$ (layers perpendicular to the loading direction) the average BTS is 14.1 MPa, which should rather correspond to the tensile strength of the "intact" material. As already mentioned predominant failure mode for $\theta = 0°$ is central fracture(s). For $\theta = 90°$ (layers parallel to the loading direction), the average BTS is 10.4 MPa. The latter should rather correspond to the tensile strength of the "layers" and the predominant failure mode in this case ($\theta = 90°$) is the layer activation.

Figure 4.5 shows that for inclination angles situated between 45° and 60°, both failure modes (central fracture and layer activation) are present, but as this angle increases, layer activation becomes more dominant. So it can be concluded for this layered sandstone that below a certain transition angle, fractures are mainly in the central zone (central fracture mode). Above that transition angle, fractures are parallel to the isotropic layers (layer activation mode). To determine more precisely the transition angle, the failure modes are quantified by estimating the fracture length.

In sample 25 ($\theta = 15°$) a part of layer activation is observed; the predominant failure mode in that sample is central fracture. In this sample layer activation is not considered as a secondary failure mode because fracture length corresponding to layer activation is very small in comparison to fracture length corresponding to central fracture (see further, Table 4.3). In sample 21 ($\theta = 45°$) both central fracture and layer activation are dominantly observed. In this sample fracture length corresponding to central fracture is larger than fracture length corresponding to layer activation, therefore central fracture is considered as the predominant failure mode while layer activation is the secondary failure mode. In the next paragraph (fracture analyses) quantification of predominant and secondary failure modes is presented and discussed in detail.

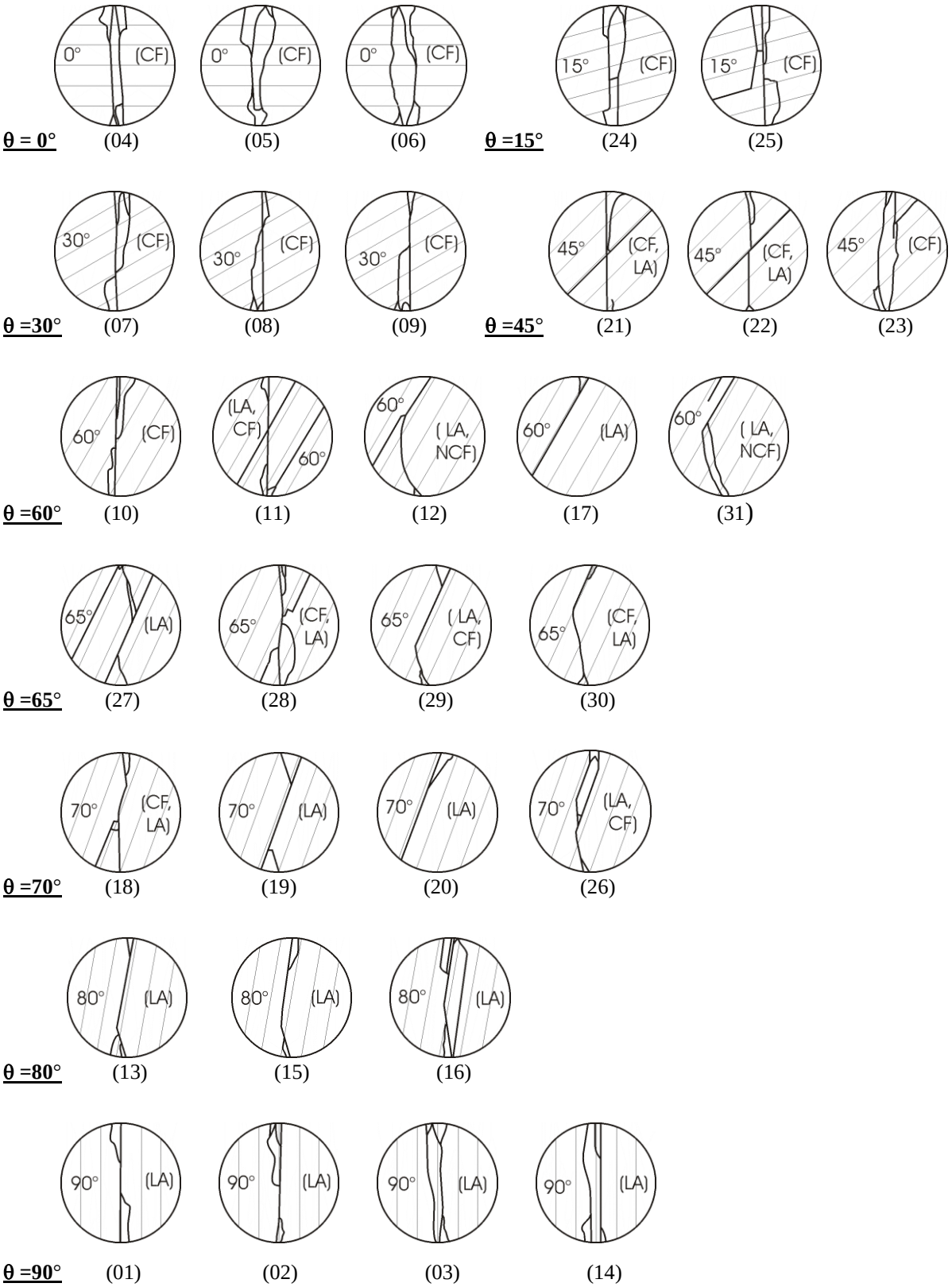

Figure 4.5 Observed failure patterns (one side) of samples for different values of the inclination angle θ for Modave sandstone sub-type 1 after conducting Brazilian tests. Sample number and the predominant mode are put in parentheses, CF = Central fracture, NCF = Non-central fracture, LA = Layer activation. Quantification of predominant and secondary failure modes is presented further (Table 4.3).

Table 4.2 Description of the samples after failure in Brazilian tests for Modave sandstone sub-type 1

Group	Sample No.	θ (°)	Description
I 	4 5 6	0	**Central fracture.** One main fracture, another secondary and semi-parallel to the main one.
II	24 25	15	**Central fracture.** In sample 25 an activated layer with a length of d/3 is connected to the central fracture.
III	7 8 9	30	**Central fracture.** One main fracture, another secondary and semi-parallel to the main one.
IV	21 22 23	45	**Both types of central fracture and layer activation.** In samples 21 and 22 a layer with the angle of 45° to the central fracture is activated.
V	10 11 12 17 31	60	**Both types of layer activation and central fracture.** Central fracture in sample 10. In sample 11 a central fracture with two activated layers. In samples 12 and 31 combination of layer activation and non-central fracture(s).
VI	27 28 29 30	65	**Both types of layer activation and central fracture.** In sample 27 fractures from the loading points are connected to one of the activated layers. In sample 28 combination of central fracture and layer activation. In samples 29 and 30 activated layer is connected to the central fracture.
VII	18 19 20 26	70	**Both types of layer activation and central fracture.** In sample 18 combination of central fracture and layer activation. In sample 26 two activated layers are connected to the central fracture.
VIII	13 15 16	80	**Layer activation.**
IX 	1 2 3 14	90	**Layer activation.**

The fracture length within various rock samples is estimated and used as a tool to distinguish between the different failures modes. First, the length of all fractures in the sample is measured. Second, the length corresponding to various fracture types is considered. When a fracture is classified as layer activation the entire length, including the part within the central zone, is put into the total sum of layer activation. In a similar way, if the major part of a curved shape fracture (e.g. the non-central fracture in Figure 4.3) is outside the central zone, the entire length including the small portion in the central zone is put into the total sum of non-central fractures.

The fracture pattern in most of the samples is similar on both sides (i.e. front and back; however, they are not exactly the same). It means that the fracture pattern can mostly be considered as two-dimensional. Therefore, all the fractures lengths in these cases are measured on one side. The fracture pattern in a few samples (numbers 16 and 31) is true three-dimensional and on both sides of the sample, the fracture pattern is significantly different. In such cases, averages of the fracture lengths on both sides are considered. To have a better understanding, Figure 4.6 presents a schematic sample with two different failure patterns on both sides. On one side of the sample 48 mm layer activation is observed while on the other side 38 mm layer activation and 12 mm non-central fracture are observed. For this sample, layer activation length, non-central fracture length and the total fracture length are considered as 43, 6 and 49 mm, respectively.

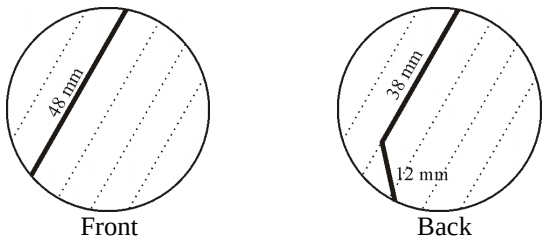

Figure 4.6 Different failure patterns on both sides of a schematic sample after conducting a Brazilian test.

Table 4.3 presents the fracture length of all samples of sandstone sub-type 1 in the nine groups. In this table fracture lengths corresponding to layer activation, central fracture(s) and non-central fracture(s) are presented.

Variation of the fracture lengths corresponding to layer activation, central fracture(s), non-central fracture(s) and the total fracture length as a function of the inclination angle θ are plotted in Figure 4.7 for individual samples. Figure 4.7a shows that when the inclination angle θ exceeds 60°, a considerable decrease in the length corresponding to central fracture(s) is observed. Figure 4.7b shows that for an inclination angle θ smaller than 45°, the length corresponding to layer activation is very small, sometimes even negligible. When this angle exceeds 45°, layer activation becomes significant. For an inclination angle between 45° and 90°, there is an increasing trend for this length. In other words, central fracture(s) is predominant for an inclination angle of 0° to 45°, while layer activation is the main failure mode above 60°.
The presented results in Figure 4.7a and b can be also explained from the fracture mechanics viewpoint (He and Hutchinson 1989; He et.al 1994). Figure 4.7a and b show the variation in fracture length corresponding to the fractures which occur between the two loading lines in the intact material (central fracture) or deflect to the layer boundaries (layer activation). In other words, there is a competition between central fracture and layer activation (He and Hutchinson 1989; Carpinteri and Paggi 2007). For inclination angles less than 45° the crack propagation through the central part needs less energy to dissipate and occurs at a lower load than that for deflecting in the layer boundary. However, when inclination angles exceed 60°, the cracks tend to deflect to the layer boundaries as the fractures grow and propagate along a path that needs less energy to dissipate. Crack deflection along the layer boundary is a material property that contrary to the fracture toughness of the bulk material depends on the inclination angle (He and Hutchinson 1989; He et.al 1994; Wang 1997).

From the above explanation, it can be concluded that the transition angle, which indicates the change of failure mode from central fracture to layer activation, is in the range between 45° and 60° for the reference sub-type of layered sandstone (sub-type 1). Figure 4.7d in comparison to Figure 4.7a and b shows that the variation of total fracture length is not as explicit as the variation of layer activation length and central fracture length. Figure 4.7c presents a nearly constant value for the non-central fracture length for different values of the inclination angle θ.

Table 4.3 Fracture length of samples of Modave sandstone sub-type 1(Brazilian tests)

Group	θ (°)*	Sample	Fracture length						
			Layer activation		Central fracture		Non-central fracture		Total
			(mm)	(%)	(mm)	(%)	(mm)	(%)	(mm)
I 	0	4	0	0	136	100	0	0	136
		5	4	3	109	81	21	16	134
		6	0	0	93	64	53	36	145
		Average	1	1	113	82	25	17	138
II	15	24	8	6	116	94	0	0	124
		25	18	12	106	72	24	16	148
		Average	13	9	111	83	12	8	136
III	30	7	9	7	81	68	30	25	120
		8	3	3	94	97	0	0	96
		9	5	6	85	94	0	0	90
		Average	5	5	87	87	10	8	102
IV	45	21	54	41	78	59	0	0	131
		22	51	46	60	54	0	0	111
		23	16	12	118	88	0	0	134
		Average	40	33	85	67	0	0	125
V	60	10	9	8	101	92	0	0	110
		11	99	58	73	42	0	0	171
		12	44	53	3	3	36	44	83
		17	48	86	8	14	0	0	55
		31	38	46	15	18	29	35	81
		Average	47	50	40	34	13	16	100
VI	65	27	94	67	46	33	0	0	140
		28	49	37	65	49	19	14	133
		29	36	54	31	46	0	0	68
		30	28	43	36	57	0	0	64
		Average	52	50	45	46	5	4	101
VII	70	18	34	42	46	58	0	0	80
		19	50	68	24	32	0	0	74
		20	55	90	6	10	0	0	61
		26	51	61	33	39	0	0	84
		Average	48	65	27	35	0	0	75
VIII	80	13	50	74	18	26	0	0	68
		15	50	73	19	27	0	0	69
		16	96	75	33	25	0	0	129
		Average	65	74	23	26	0	0	88
IX 	90	1	71	80	18	20	0	0	89
		2	95	93	8	7	0	0	103
		3	100	82	23	18	0	0	123
		14	110	84	21	16	0	0	131
		Average	94	85	17	15	0	0	111

* Inclination angles θ is the angle of layer direction from horizontal. In all the samples, the length of fractures is measured from one side, except samples 31 and 16 which is the average from both sides.

Dark gray indicates the predominant failure mode and light gray indicates the secondary failure mode. The change of the predominant and the secondary failure mode is clearly observed for the range of θ between 45° and 60°. The second percentage of either fracture is arbitrarily called the secondary failure mode only if it is equal or more than half of the largest percentage.

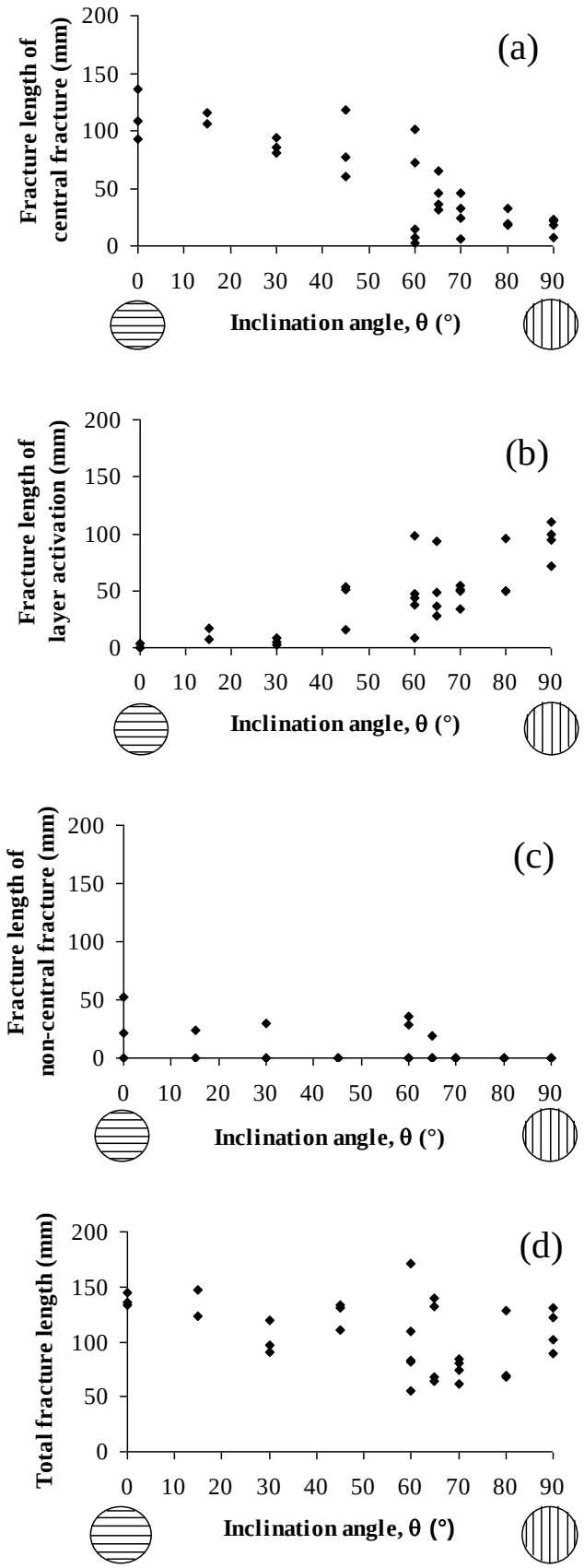

Figure 4.7 Variation in fracture length as a function of the inclination angle θ for Modave sandstone sub-type 1, (a) Central fracture(s), (b) Layer activation, (c) Non-central fracture(s), and (d) Total fracture.

For all samples corresponding to a single angle value, the average fracture length is calculated (Table 4.3). For the samples of the reference sub-type, variation in three types of fractures, as well as the total fracture length is plotted as a function of the inclination angle θ in Figure 4.8. It shows that for inclination angles θ smaller than 45°, the fracture length corresponding to layer activation is very small, sometimes even negligible. When this angle exceeds 45°, layer activation becomes significant. For an inclination angle between 45° and 90°, there is an increasing trend for this length. Figure 4.8 also shows that when inclination angles exceed 70° the fracture length corresponding to central fracture(s) becomes small. This figure also illustrates that the non-central fracture length is nearly constant and thus independent of θ, at least for the interval 0° to 65°. When the inclination angle θ increases from 30° to 90°, the length of central fracture(s) decreases while the length corresponding to layer activation increases. Variation in total fracture length in comparison to variation in layer activation length and central fracture length shows that the variation in total fracture length is not as explicit in comparison to the individual classes.

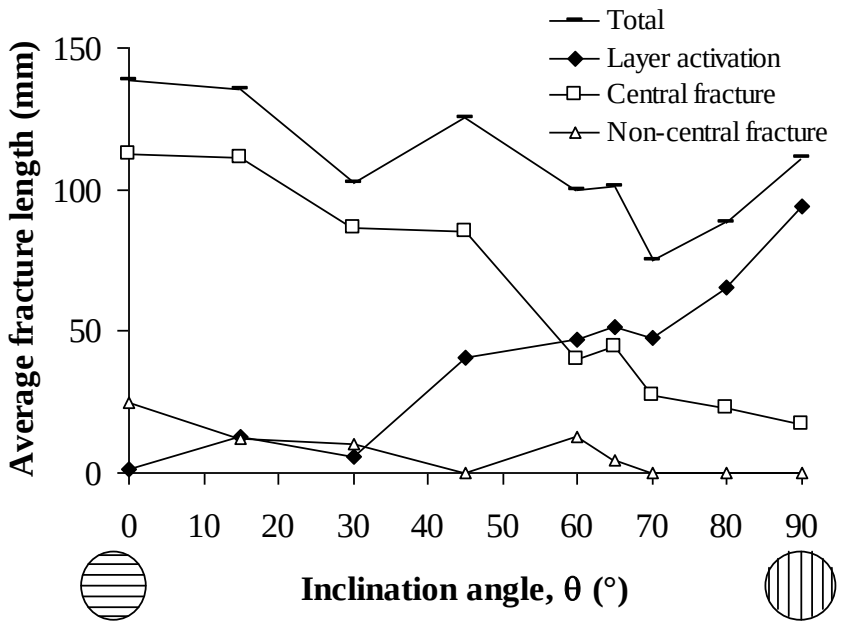

Figure 4.8 Variation in average fracture length as a function of the inclination angle θ, for reference sub-type.

It can be useful to consider also the percentage of central fracture(s) and layer activation compared to the total fracture length. The failure pattern of samples 22 (θ = 45°) and 11 (θ = 60°) in Figure 4.5 are discussed as an example. In both samples one central fracture is observed. In sample 22 (θ = 45°), only one layer is activated while in sample 11 (θ = 60°) two layers are activated. Therefore the percentage of the central fracture for sample 22 is higher (54%) in comparison to sample 11 (42%), although in both samples one central fracture is observed. The averages in Table 4.3 show clearly the predominant mode of failure. The largest percentage of either fracture in the form of layer activation or as central fracture(s) indicates the predominant failure mode. The second percentage of either fracture is arbitrarily called the secondary failure mode only if it is equal or more than half of the

largest percentage. The change in the predominant failure mode in the range of θ between 45° and 60° for the reference sub-type is remarkable and needs more attention.

In Figure 4.9, the percentage of central fracture(s) and layer activation compared to the total fracture length is given as a function of the inclination angle for the reference sub-type. Central fracture(s) is predominant for an inclination angle of 0° to 45°, while layer activation is the main failure mode above 60°. It is important to mention that it is not always correct to interpret layer activation as the shear failure mode. For example, in the case of θ = 90° layer activation is due to pure tension. Rock samples under Brazilian test conditions can fail in tension, in shear or in both tension and shear. Depending on the stress redistribution, the failure is initiated in one of these modes. It is very difficult to determine this by only observing the failure pattern.

From the above explanation, it can be concluded that the transition angle, which indicates the change in failure mode from central fracture to layer activation, is in the range of 45° and 60° for the reference sub-type of the layered Modave sandstone.

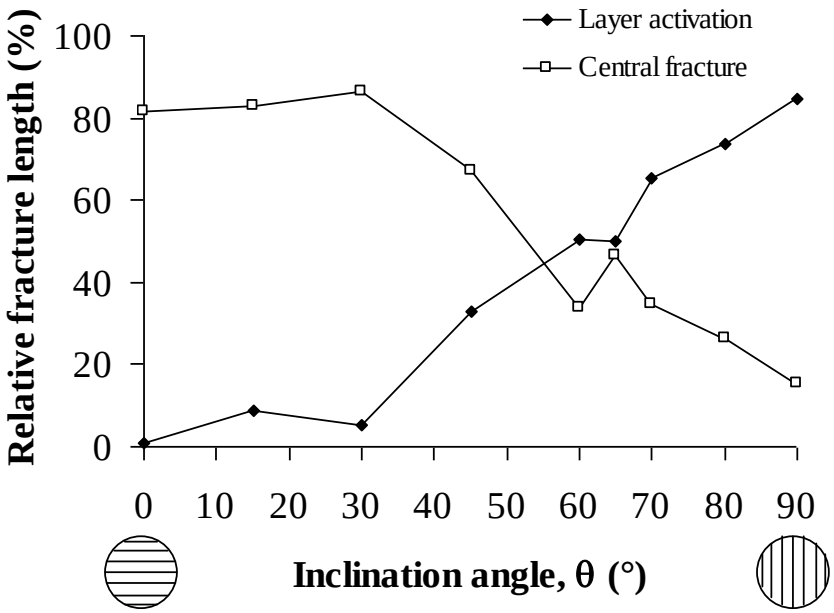

Figure 4.9 Variation in fracture length percentage corresponding to central fracture(s) and layer activation as a function of the inclination angle θ, for reference sub-type.

4.1.3 Fracture strength correlation

By comparing the variation in the average Brazilian tensile strength (BTS) to the average total fracture length of samples as a function of the inclination angle θ (Figure 4.10), it is observed that the trend of both diagrams is similar. So, it can be assumed that a correlation between the total fracture length and BTS may exist.

Table 4.4 presents the total fracture length and the BTS-values for all samples of the reference sub-type. This table is sorted by the maximum fracture length in each group. It is interesting to note that in some groups such as I, II, III (θ = 0°, 15°, 30°), the BTS-values are exactly in the same sorting order as the total fracture length. In 4 additional groups (60°, 65°, 80° and 90°), nearly identical sequences are observed between both parameters. For example in group VI (θ = 65°), if sample 28 is not considered, total fracture length and BTS-values of the three other samples are in the same sorting order. These results show that there could be a relation between the total fracture length and the failure stress in Brazilian test. In the 2 other groups (IV, VII) sorting order is different. In group IV (θ = 45°) as total fracture length decreases, BTS-value increases. In group VII (θ = 70°) among 4 samples, sample 26 has indeed the largest value of the total fracture length and the BTS-value; but for the other samples the trend is different.

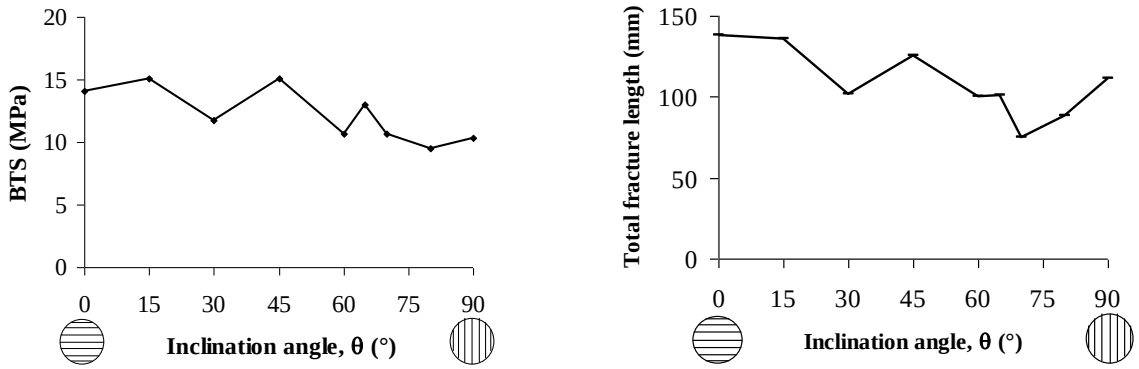

Figure 4.10 Variation in average Brazilian tensile strength, BTS, and average total fracture length as a function of the inclination angle θ, for reference sub-type.

The variation in BTS-values as a function of total fracture length for all samples of the reference sub-type is plotted in Figure 4.11. For the samples of the reference sub-type the total fracture length varies between 55 mm and 175 mm or in other words between 1 and 3 and half times the diameter. It can be concluded from Figure 4.11 that larger fracture length correlates with higher strength. Already from Figure 4.1 (variation in BTS-values as a function of inclination angle) it is concluded that by increasing the inclination angle, a slight decrease in tensile strength occurs. Consequently the samples with low inclination angles, which are more fractured, should have the higher values of strength. From the above explanation it can be concluded that strength is smaller for larger inclination angles and smaller total fracture lengths (see Figure 4.12). Figure 4.12 presents the variation on the three mentioned parameters (inclination angle, total fracture length and Brazilian tensile strength) in a three dimensional diagram.

Table 4.4 Total fracture length (TFL) and Brazilian tensile strength (BTS) of the samples of Modave sandstone sub-type 1.

Group	θ (°)*	Sample	TFL (mm)	BTS (MPa)	Group	θ (°)*	Sample	TFL (mm)	BTS (MPa)
I 	0	6	145	15.9	VI	65	27	140	12.7
		4	136	14.1			28	133	18.4
		5	134	12.1			29	68	11.4
II	15	25	148	15.5			30	64	9.7
		24	124	14.7	VII	70	26	84	14.9
III	30	7	120	12.0			18	80	9.0
		8	96	11.9			19	74	9.2
		9	90	11.3			20	61	9.5
IV	45	23	134	14.3	VIII	80	16	129	11.5
		21	131	14.8			15	69	8.3
		22	111	16.3			13	68	8.8
V	60	11	171	14.6	IX 	90	14	131	6.7
		10	110	11.1			3	123	12.2
		12	83	11.3			2	103	11.5
		31	81	9.5			1	89	10.9
		17	55	7.0					

This Table is sorted by maximum fracture length in each group.
* θ is the angle of layer direction from horizontal.

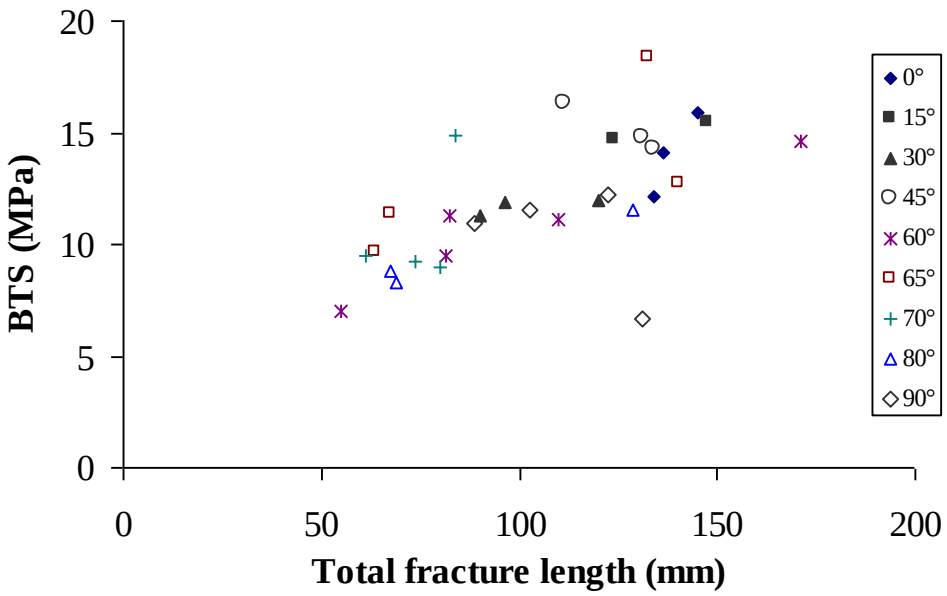

Figure 4.11 Variation in Brazilian tensile strength, BTS, as a function of total fracture length for all the samples of reference sub-type.

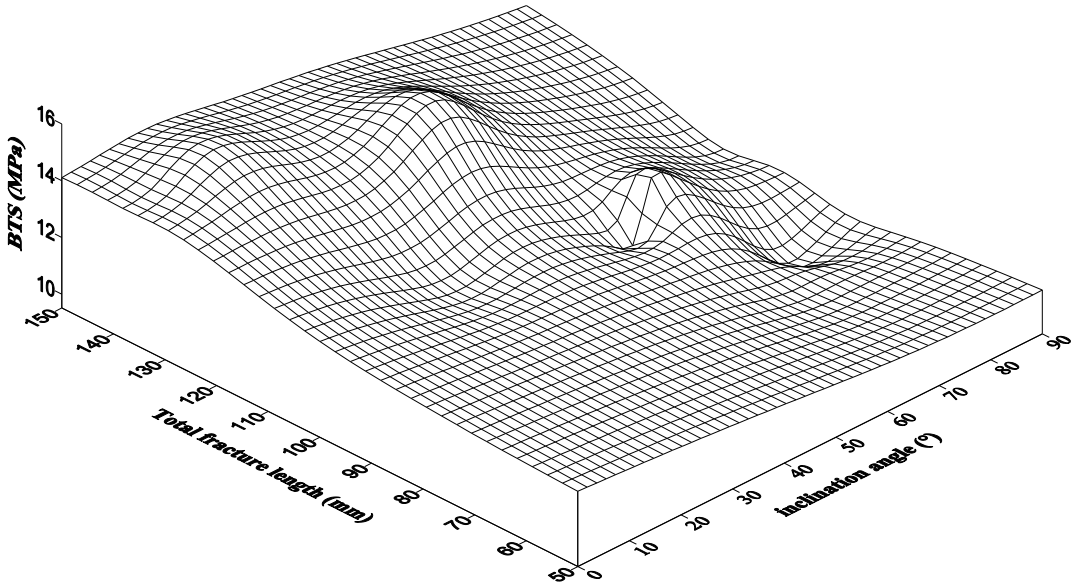

Figure 4.12 Variation in Brazilian tensile strength, BTS, as a function of inclination angle and total fracture length for all the samples of reference sub-type.

A comparison between Figure 4.11 and Figure 4.1 is interesting. The latter shows the variation in BTS-values as a function of inclination. This comparison highlights that the variation in BTS-values as a function of the total fracture length (see Figure 4.11) is considerably more significant than when the BTS-values are plotted as a function of the inclination angle (see Figure 4.1). It means that difference in values of BTS for samples with the same fracture pattern may be relatively small (even with different inclination angles). However, for samples with the same inclination angle but different fracture patterns, variation in BTS-values can often be remarkable.
As an example (see Figure 4.13) three samples are presented. Two samples (No. 17 and 15) have a different inclination, but similar strength and fracture length. However, samples 11 and 17 have the same inclination but significant different strengths and fracture lengths. Sample 17 ($\theta = 60°$) and sample 15 ($\theta = 80°$) are failed dominantly by one activated layer. Their BTS-values are respectively 7.0 MPa and 8.3 MPa. However, if sample 17 is compared to sample 11 which has the same inclination angle ($\theta = 60°$) a different fracture pattern is observed and a considerable difference in BTS-values is noted. The value of BTS for sample 11 is 14.6 MPa which is more than twice the BTS-value of sample 17.

Variation in BTS as a function of total fracture length for group V ($\theta = 60°$) is plotted in Figure 4.14. Sample 11 failing by the combination of layer activation and central fracture corresponds to the largest BTS-value and to the largest fracture length. Sample 17 which is failing by layer activation corresponds to the lowest BTS-value and to the lowest fracture length.

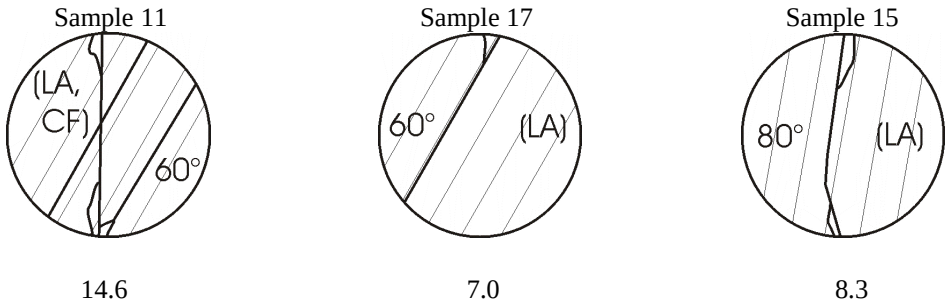

BTS (MPa): 14.6 7.0 8.3

Figure 4.13 Correlation of Brazilian tensile strength, BTS, and fracture pattern. The predominant modes are mentioned, CF = Central fracture, LA = Layer activation.

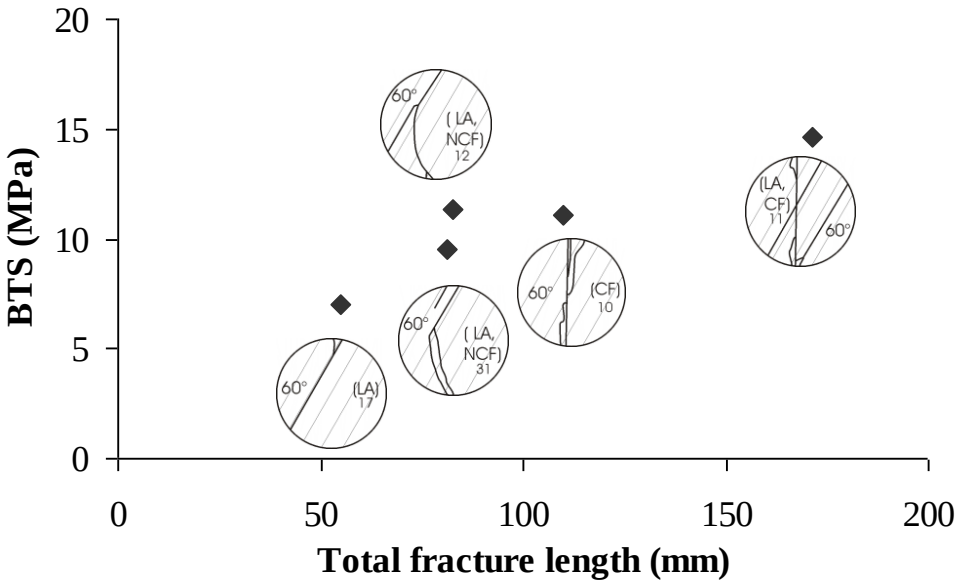

Figure 4.14 Variation in Brazilian tensile strength, BTS, as a function of total fracture length for group V (θ = 60°) of reference sub-type. The predominant modes are put in parentheses, CF = Central fracture, NCF = Non-central fracture, LA = Layer activation. Sample number is written below the predominant mode.

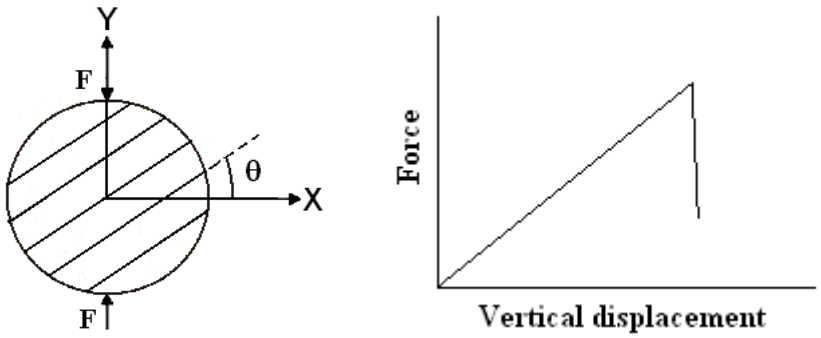

Figure 4.15 Schematic behaviour of layered Modave sandstone samples while conducting Brazilian test.

28 samples from 31 samples of the reference sub-type (> 90%) show brittle failure with monotonic load increase till a sudden failure. The loading of these samples ends suddenly after failure in a brittle way (see Figure 4.15). All the graphs of the applied load as a function of vertical displacement for all the 31 samples in different groups of inclination angle are presented in Appendix B. In a similar study by Debecker and Vervoort (2007 and 2009) on layered slate, brittle failure with monotonic load increase is not observed. In the mentioned studies, the applied force increases up to a local failure. After a local failure the applied force decreases, but increases rapidly up to another local failure. This phenomenon occurs several times before final failure. That is because the strength of mentioned slate in layer direction is remarkably less than in other directions. In the study of Debecker (2009), the BTS-value for the typical slate samples of $\theta = 0$ and 90° is 20.0 and 0.4 MPa, respectively. As the strength of layer boundaries in the mentioned slate is very low, many local failures in layer direction occur before the final failure (independent of loading direction). In this research on layered Modave sandstone sub-type 1, local and final failure cannot be distinguished as they occur almost simultaneously (except for three samples 11, 14 and 20).

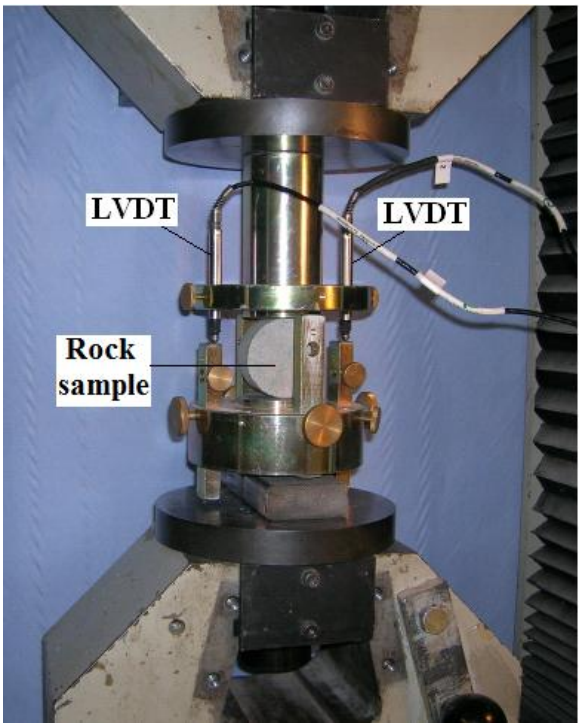

Figure 4.16 Measuring and calibration set up of the vertical displacement of a sample under Brazilian test conditions by two linear variable differential transformers (LVDTs). Loading machine is Schenck.

Also in this part, effort has been made to find the energy that is applied on a rock sample till its failure. Two parameters of force and displacement are needed for calculation of applied energy. These two parameters are registered by the loading machine; however, a correction is applied on the registered displacement by calibration (see Figure 4.16).
For the tested sandstone samples of the reference sub-type, the failure applied force varies from 13.8 kN to 38.0 kN while the final vertical displacement varies between 0.05 mm and 0.18 mm. For each sample the diagram of the applied force as a function of the vertical displacement is considered. The area under the diagram in the interval from 0 to the final vertical displacement is considered as the applied energy. As an example, consider a sample

(D = 50 mm and t = 25 mm) showing brittle failure with monotonic load increase. Mentioned sample has failed by applying 20 kN force while its vertical displacement is 0.15 mm. For this sample the BTS-value and applied energy are 10.2 MPa and 1.5 J, respectively.
For the samples whereby the load increase is not monotonic, the entire area under the load-displacement diagram is not considered as the applied energy. For these samples, it is observed that with increasing the vertical displacement, the load remains constant or even decreases in certain parts of the test. The areas in load-displacement diagram corresponding to constant or decreasing load are deducted from the entire area (under the diagram in the interval from 0 to the final vertical displacement).

Figure 4.17 shows the variation in applied load as a function of displacement for group V ($\theta = 60°$) which contains one of the three exceptions (sample 11). By comparing the diagram of sample 11 with the other diagrams, different behaviour is observed. For sample 11, the load increase is not monotonic and before final failure three peaks can be distinguished.

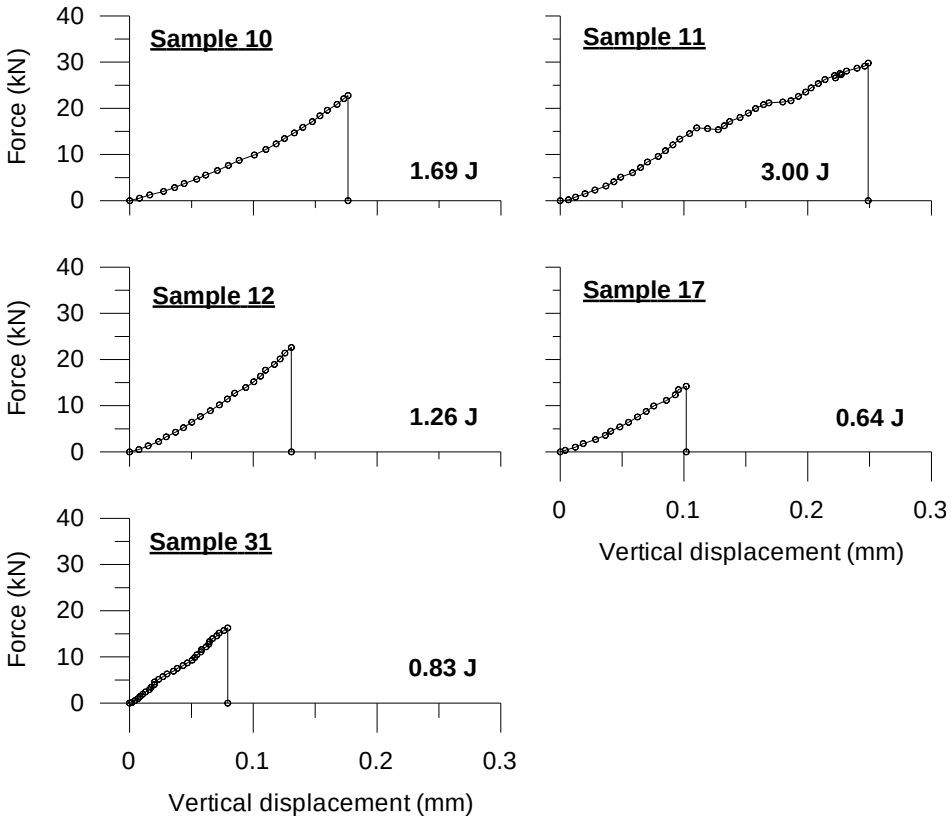

Figure 4.17 Variation in applied load as a function of displacement for group V ($\theta = 60°$) of reference sub-type. Applied energy is also mentioned.

Table 4.5 Total fracture length (TFL) and applied energy (APE) of the samples of Modave sandstone sub-type 1.

Group	θ (°)*	Sample	TFL (mm)	APE (J)	Group	θ (°)*	Sample	TFL (mm)	APE (J)
I 	0	4	136	1.92	VI	65	27	140	1.03
		5	134	1.73			28	133	1.71
		6	145	2.27			29	68	0.46
II	15	24	124	2.21			30	64	0.86
		25	148	1.74	VII	70	18	80	0.97
III	30	7	120	1.12			19	74	0.65
		8	96	1.73			20	61	1.96
		9	90	1.84			26	84	1.36
IV	45	21	131	1.70	VIII	80	13	68	0.41
		22	111	2.23			15	69	0.77
		23	134	1.62			16	129	1.17
V	60	10	110	1.69	IX 	90	1	89	1.03
		11	171	3.00			2	103	1.62
		12	83	1.26			3	123	1.79
		17	55	0.64			14	131	0.65
		31	81	0.83					

* θ is the angle of layer direction from horizontal.

Table 4.5 presents the total fracture length and the applied energy for all samples of the reference sub-type. Figure 4.18 shows the variation in applied energy as a function of the total fracture length for samples of reference sub-type. The total fracture length is correlated with the applied energy. The variation in applied energy as a function of the total fracture length (see Figure 4.18) is considerably more significant than when the applied energy is plotted as a function of the inclination angle (see Figure 4.19). Figure 4.19 (similar to Figure 4.1, variation in BTS-values) shows two groups located at either side of $\theta = 50°$. The average applied energy of the samples with $\theta < 50°$ (1.8 J) is slightly larger than that for the samples with $\theta > 50°$ (1.3 J).

Figure 4.20 presents the variation in the average applied energy with the inclination angle θ, where the graph shows a slight negative trend. For the reference sub-type, the average applied energy varies between 0.8 and 2.0 J. The smallest value (which is not significant) corresponds to an inclination angle equal to 80°. This is similar to Figure 4.2 that presents the variation in the average Brazilian tensile strength with the inclination angle.

Variation in BTS as a function of applied energy for all the samples of reference sub-type in a Brazilian test is plotted in Figure 4.21. In this figure the three samples without a monotonic load increase are indicated (samples 11, 14 and 20). For all the other 28 samples a monotonic load increase is observed. Although the load increase in 31 samples is different, it can be concluded that the samples, which need more energy to fail, have higher values of BTS. This results in a very good correlation for all samples (of reference sub-type) in Figure 4.21.

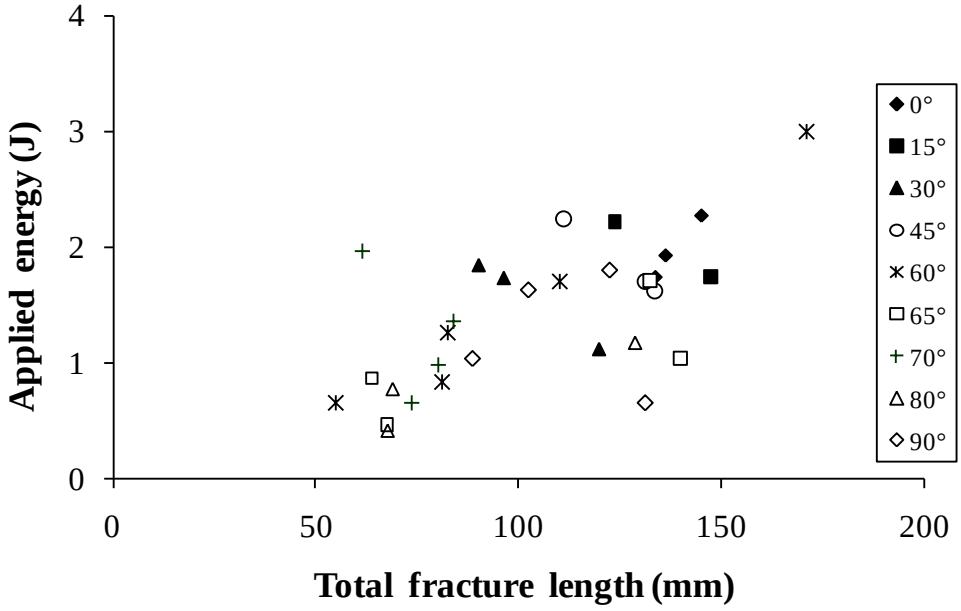

Figure 4.18 Variation in applied energy as a function of total fracture length for all the samples of reference sub-type (Brazilian test).

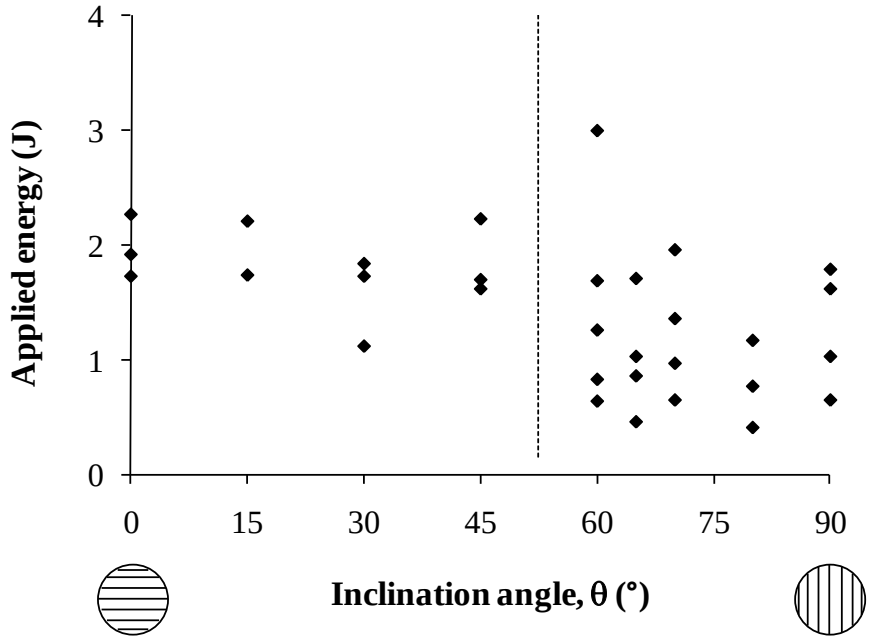

Figure 4.19 The applied energy as a function of the inclination angle θ for all the samples of reference sub-type.

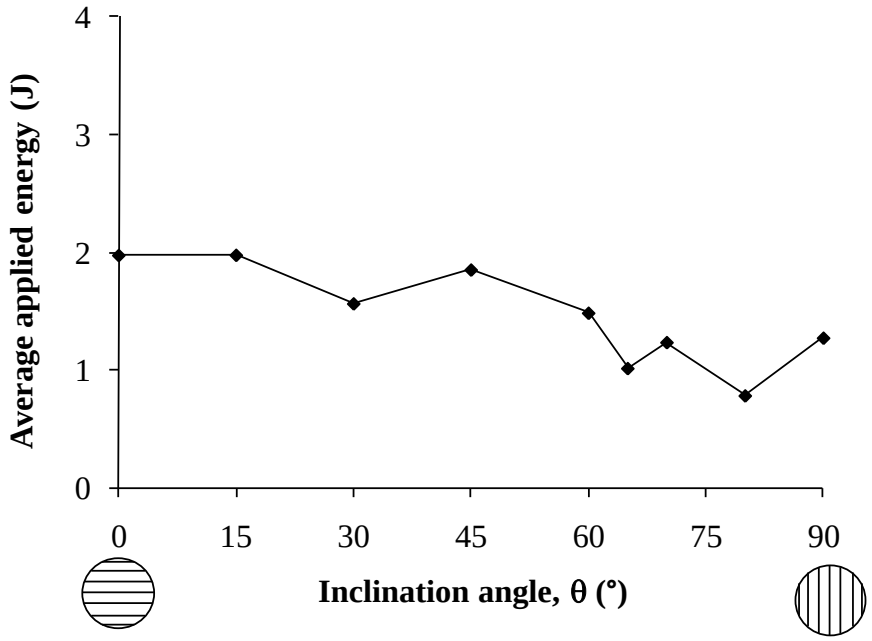

Figure 4.20 The average applied energy as a function of the inclination angle θ for reference sub-type.

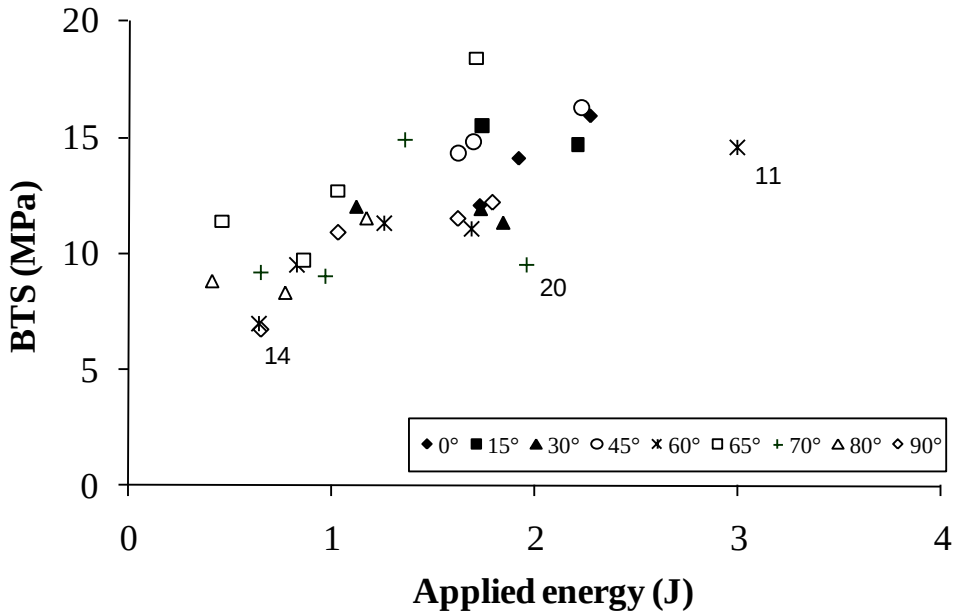

Figure 4.21 Variation in Brazilian tensile strength, BTS, as a function of applied energy for all the samples of reference sub-type. Load increase in samples 11, 14 and 20 is not monotonic (see Figures B.5, B.7 and B.9 in Appendix B), while in the other 28 samples a monotonic load increase is observed.

4.2 Effect of layer orientation for sandstone sub-types 2 to 5

For sub-type 1, nine groups of the inclination angle are tested. For the other sub-types (2-5), seven different values are considered: 0, 20, 45, 60, 70, 80 and 90°. Since one sample is not necessarily representative for the failure behaviour corresponding to a specific inclination angle, two to six samples are tested per inclination angle value per sub-type. The number of tested samples for sandstone sub-types 2, 3, 4 and 5 are 29, 30, 22 and 30, respectively. By considering the tested samples of the reference sub-type, 142 samples (in total) are tested. In Appendix C for each sandstone sub-types (2-5), a table gives the inclination angle θ, the diameter D, the thickness t, the failure load F and some other information about the tested samples.

The variation in the average Brazilian tensile strength (BTS) with the inclination angle θ for the sandstone sub-types is presented in Figure 4.22. All the graphs show a small downwards trend. The largest average BTS corresponds to the samples of sandstone sub-type 3, which varies between 11.3 and 15.1 MPa, while the lowest corresponds to the samples of sandstone sub-type 2, which varies between 5.3 and 14.2 MPa.
It is interesting to note that sandstone sub-type 3 has the highest average grain size (107 μm) and sub-type 2 the lowest average (69 μm). Furthermore sandstone sub-type 3 with the highest BTS-value has the largest range of grain sizes among the five sandstone sub-types.

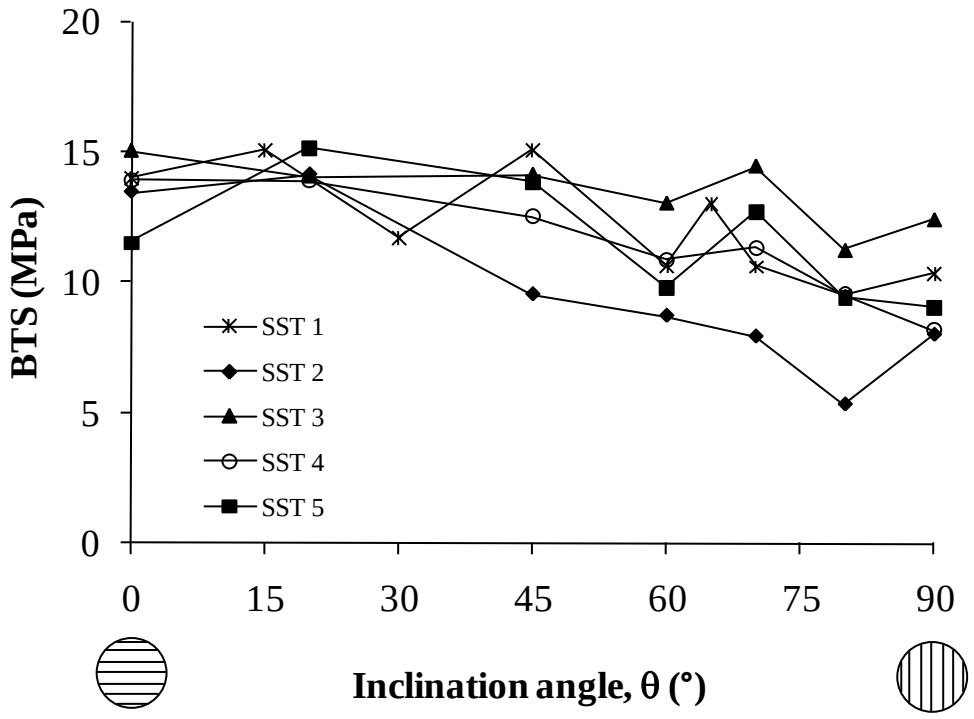

Figure 4.22 Variation in average Brazilian tensile strength, BTS, as a function of the inclination angle θ for sandstone sub-types (SST) 1-5.

Similar to sandstone sub-type 1, the fracture analysis is done for all the tested samples of sub-type 2 to 5. In Figure 4.23, the percentage of central fracture(s) and layer activation compared to the total fracture length is given as a function of the inclination angle for the four sub-types (2-5) of the layered sandstone. The graph corresponding to sub-type 2 shows that for an

inclination angle of 0° to 70° central fracture(s) is the main failure mode, while layer activation is predominant for 80° and 90°. Relative fracture length of sub-type 3 shows that for inclination angles θ smaller than 50°, the fracture length corresponding to layer activation is negligible. When inclination angle exceeds 50°, fracture length corresponding to layer activation increases and only for 90° becomes predominant. Layer activation for the inclination angle of 0° and 20° for sub-types 4 and 5 is negligible. Then by increasing the inclination angle, layer activation increases but only for 90° becomes the main failure mode in sub-types 4 and 5.

From the above explanation, it can be concluded that for all sandstone sub-types as inclination angle increases from 0° to 90°, the fracture length corresponding to central fracture(s) decreases while layer activation increases. However, the decreasing and the increasing rates (of fractures length) for the five studied sub-types are different. Consequently the transition angle, which indicates the change in failure mode from central fracture to layer activation, is not the same for all sub-types of studied layered sandstone. It is important to remind that the number of layer boundaries over 1 cm of five sub-types is not the same. However, for a further understanding of different behaviour from similar rocks, detailed microscopic study is needed.

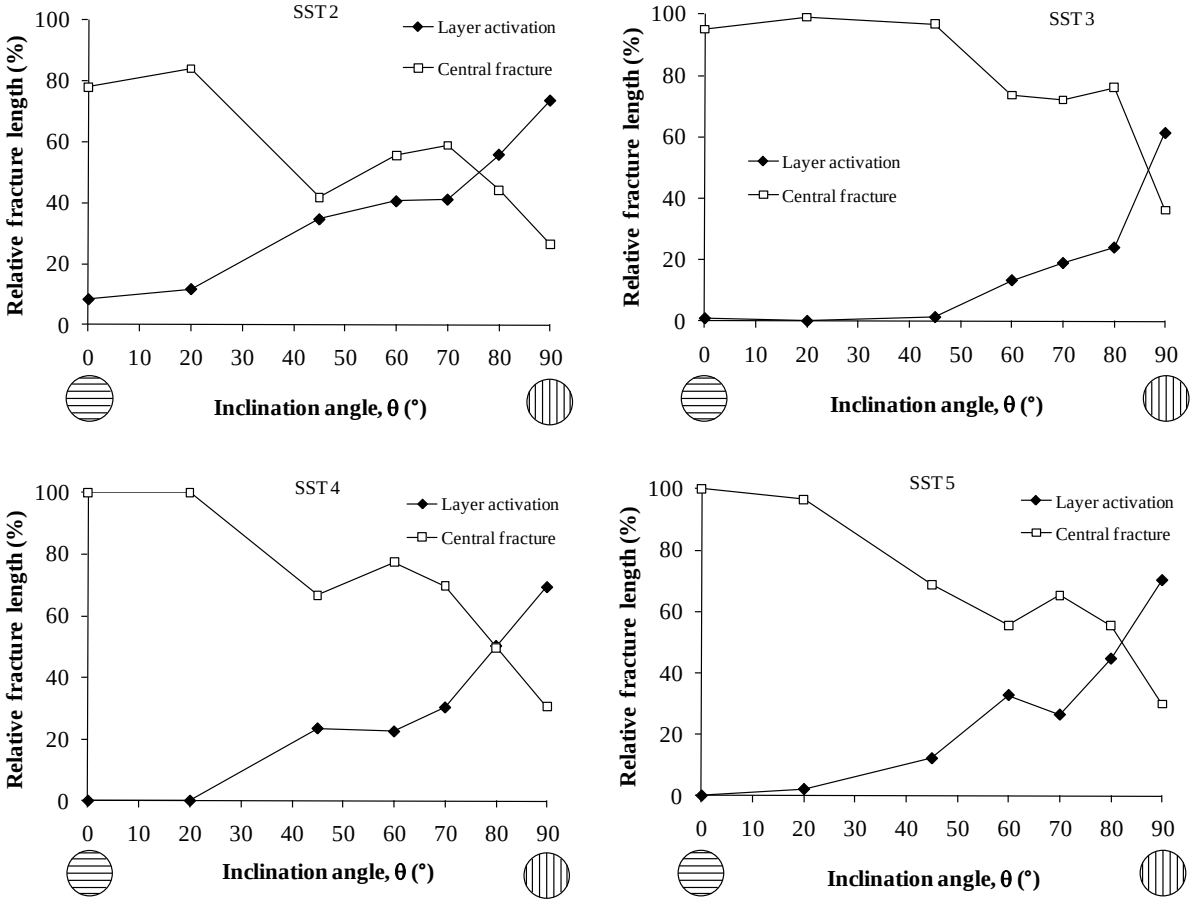

Figure 4.23 Variation in fracture length percentage corresponding to central fracture(s) and layer activation as a function of the inclination angle θ, for sandstone sub-types (SST) 2-5.

In this research on Modave sandstone sub-types (1-5), one-hundred thirty-five samples out of one-hundred forty-two total samples (> 95%) show brittle failure with monotonic load increase till a sudden failure (for the reference sub-type 28 samples from 31 samples). For the mentioned one-hundred thirty-five samples, local and final failure cannot be distinguished as they occur almost simultaneously. For each sample from the one-hundred thirty-five samples, all the fractures have occurred simultaneously in the final failure. Only for seven of the samples the load increase is not monotonic and some local fractures are observed before final failure. For mentioned exceptions the length of the fractures that have occurred in a local failure (before final failure) are not considered. In other words, for all the samples only the fractures that have occurred in the final failure are considered.
For all the tested sandstone samples the failure applied force varies from 1.7 kN to 38.0 kN while the final vertical displacement varies between 0.02 mm and 0.22 mm. Variation in BTS as a function of applied energy for all the samples of four sub-types (2-5) tested in a Brazilian test is plotted in Figure 4.24. From Figure 4.24, it can be concluded that the samples which, need more energy to fail, have higher values of BTS. This results in a very good correlation for all the sub-types of the layered sandstone of Modave.

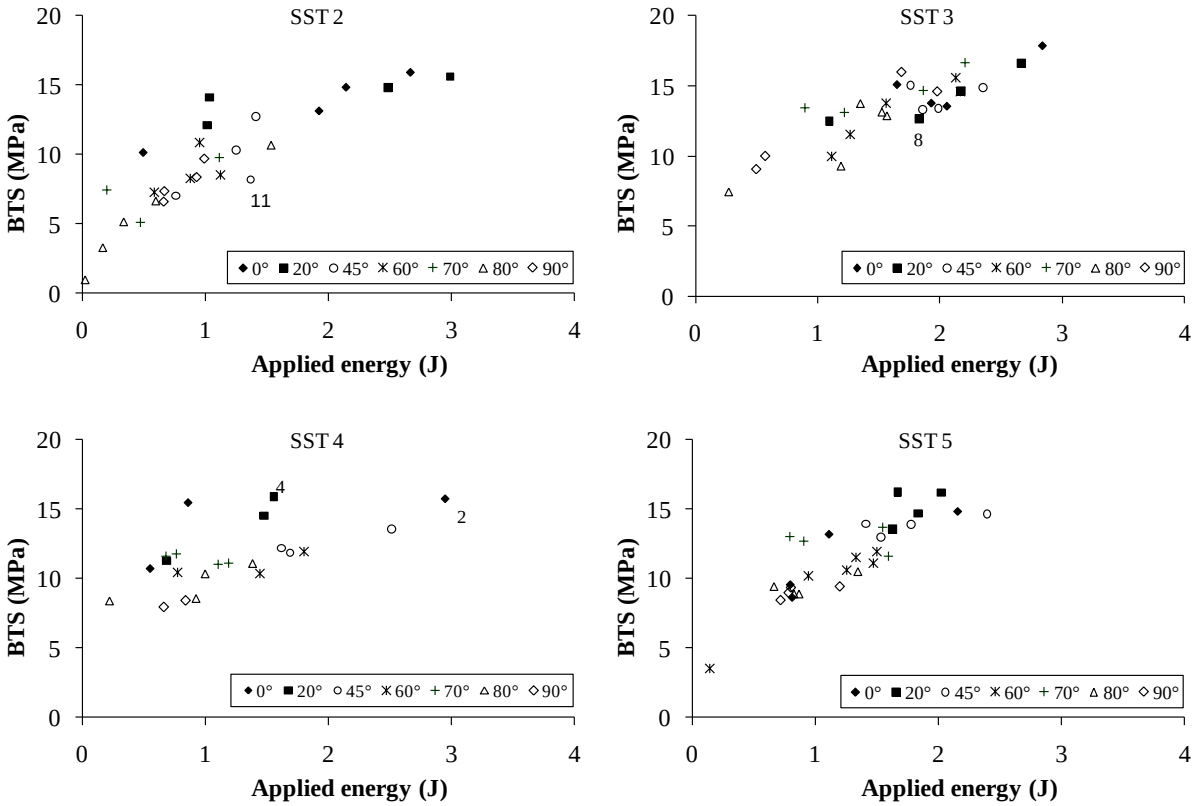

Figure 4.24 Brazilian tensile strength, BTS, as a function of applied energy for all the samples of Modave sandstone sub-types 2-5. Load increase in samples 11 of sub-type 2, 8 of sub-type 3 and, 2 and 4 of sub-type 4 is not monotonic, while in the other samples a monotonic load increase is observed (see Appendix C, for samples information).

4.3 A comparison in Brazilian test results for sandstone sub-types 1 to 5 for an inclination angle of 70°

For sub-type 1, nine groups of the inclination angle are tested. In five groups (60°, 65°, 70°, 80° and 90°) layer activation is the predominant failure mode (see paragraph 4.1). It was originally assumed that different blocks of sandstone from the same quarry which are taken at very short distance (from 1 to 10 m) from each other, would behave in a similar way. It is decided to verify the similarity in behaviour for one inclination angle (i.e. 70°) using samples of the five sandstone sub-types. Contrary to what was assumed originally, this resulted in different behaviour between samples of five blocks (sub-types) cored. In this paragraph their different macro-scale behaviour is discussed.

4.3.1 Tensile strength

For five sub-types of Modave sandstone, four samples are tested under an angle of 70° for each sub-type. Table 4.6 gives the diameter D, the thickness t, the failure load F and some other information about the tested samples.

The value of the Brazilian tensile strength (BTS) for all the samples is plotted in Figure 4.25. The average value of Brazilian tensile strength for sandstone sub-types 1 to 5 are 10.7, 7.9, 14.5, 11.4 and 12.8 MPa, respectively. At a macroscopic scale the blocks look similar, but there is about 6.6 MPa difference between the smallest and largest average value of BTS. Figure 4.26 presents the variation in upper and lower limits of Brazilian tensile strength, BTS, for sandstone sub-type 1 as a function of the other inclination angles. This figure shows that by increasing the inclination angle a slight decrease in tensile strength of sandstone sub-type 1 occurs.
The variation in BTS-values of the different sandstone sub-types for an inclination angle θ of 70° is also presented in Figure 4.26. This figure shows that the Brazilian tensile strength of one sample from sandstone sub-type 3 (16.7 MPa) and two samples from sandstone sub-type 2 (5.1 and 7.4 MPa) are out of the range of BTS-values of the reference sub-type (1) at the inclination angle of 70° (9.0-14.9 MPa). However, Brazilian tensile strength of one sample from sandstone sub-type 2 (5.1 MPa) is out of the range of BTS-values of the reference sub-type for all the inclination angles ($0° \leq \theta \leq 90°$) which vary from 6.7 to 18.4 MPa.

By summarising the above observations, it can be concluded that considerable difference exists among the BTS-values. This is more obvious when one compares sandstone sub-type 2 to sub-type 3 where the average value of Brazilian tensile strength for sub-type 3 (14.5 MPa) is about two times that for sub-type 2 (7.9 MPa). The effective porosity of all the samples is similar and no correlation between effective porosity and BTS-values is found (see Figure 4.27). The effective porosity of fractured samples of Table 4.6 is measured similar to the method explained in paragraph 3.1.2. The variation in BTS-values of samples (in Table 4.6) as a function of their effective porosity is presented in Figure 4.27.

Table 4.6 Brazilian tests result for layered Modave sandstone sub-types 1 to 5 (inclination angle of 70°)

Sub-type	Sample N°	D (mm)	t (mm)	ρ (t/m^3)	t/D	F (kN)	BTS (MPa)
1 (Ref)	18	49.9	26.4	2.6	0.53	18.6	9.0
	19	49.9	25.5	2.6	0.51	18.3	9.2
	20	49.8	26.2	2.6	0.53	19.5	9.5
	26	49.9	26.2	2.5	0.53	30.7	14.9
2	1	50.1	24.9	2.6	0.50	18.6	9.5
	2	50.0	24.8	2.6	0.50	9.9	5.1
	3	50.1	24.9	2.6	0.50	14.5	7.4
	4	50.1	25.0	2.6	0.50	19.2	9.8
3	1	50.1	25.0	2.5	0.50	28.9	14.7
	2	50.2	24.8	2.6	0.49	26.2	13.4
	3	50.2	24.6	2.6	0.49	32.3	16.7
	4	50.1	24.5	2.6	0.49	25.4	13.1
4	1	50.1	25.1	2.6	0.50	23.2	11.8
	2	50.1	24.7	2.6	0.49	21.4	11.0
	3	50.1	25.2	2.6	0.50	23.0	11.6
	4	50.1	25.2	2.6	0.50	22.1	11.1
5	1	50.1	25.3	2.6	0.50	25.3	12.7
	2	50.1	25.6	2.6	0.51	23.4	11.6
	3	50.1	25.4	2.6	0.51	27.3	13.7
	4	50.1	25.2	2.6	0.50	25.8	13.0

D = Diameter, t = Thickness and F = Failure load of the samples. Presented density is measured in laboratory conditions.

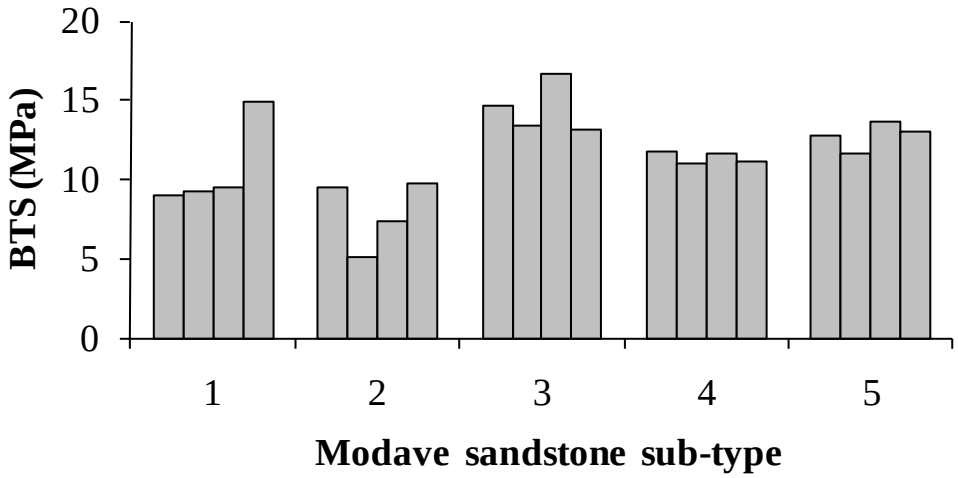

Figure 4.25 Variation of Brazilian tensile strength, BTS, for the different sandstone sub-types. The inclination angle θ for all the samples is 70°.

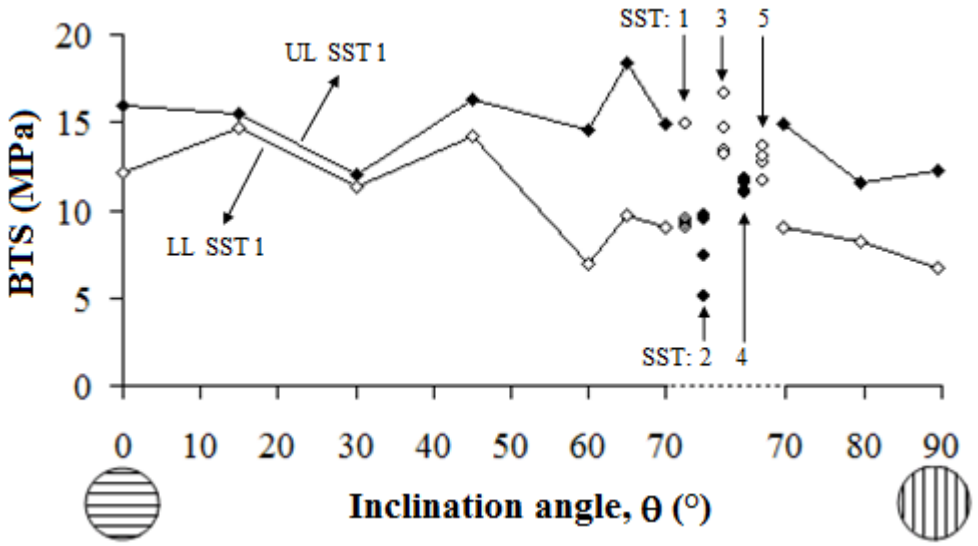

Figure 4.26 Variation in upper limit (UL) and lower limit (LL) of Brazilian tensile strength, BTS, as a function of inclination angle for sandstone sub-type 1. Variation in BTS as a function of sandstone sub-type (SST) for an inclination angle θ of 70° is also presented.

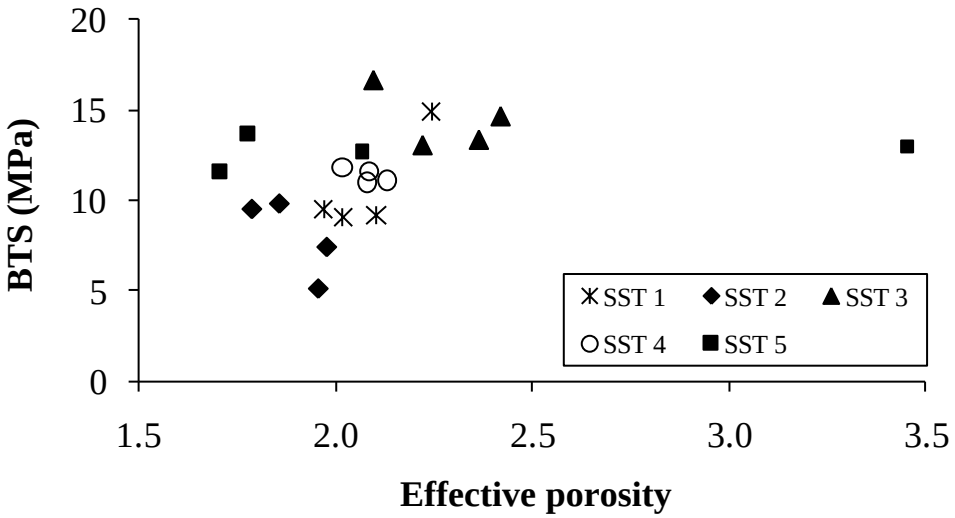

Figure 4.27 Variation in Brazilian tensile strength, BTS, as a function of effective porosity for all Modave sandstone sub-types (SST). The inclination angle for all the samples is 70°.

4.3.2 Fracture analyses

The failure pattern (one side) of all the samples after failure is shown in Figure 4.28 for five sandstone sub-types. As already mentioned all the samples are tested under an angle of 70°. Similar to paragraph 4.1.2 the failure modes are quantified by estimating the fracture length. Table 4.7 presents the fracture length of all samples of the five groups. In this table the fracture lengths corresponding to layer activation, central fracture(s) and non-central fracture(s) are presented, as well as the total fracture length. The fracture patterns in Figure 4.28 and the fracture analysis in Table 4.7 show clearly that the predominant failure mode is not only layer activation as for sub-Type 1. All the samples from the four blocks show a failure by either central fracture(s) only or a combination of central fracture(s) and layer activation.

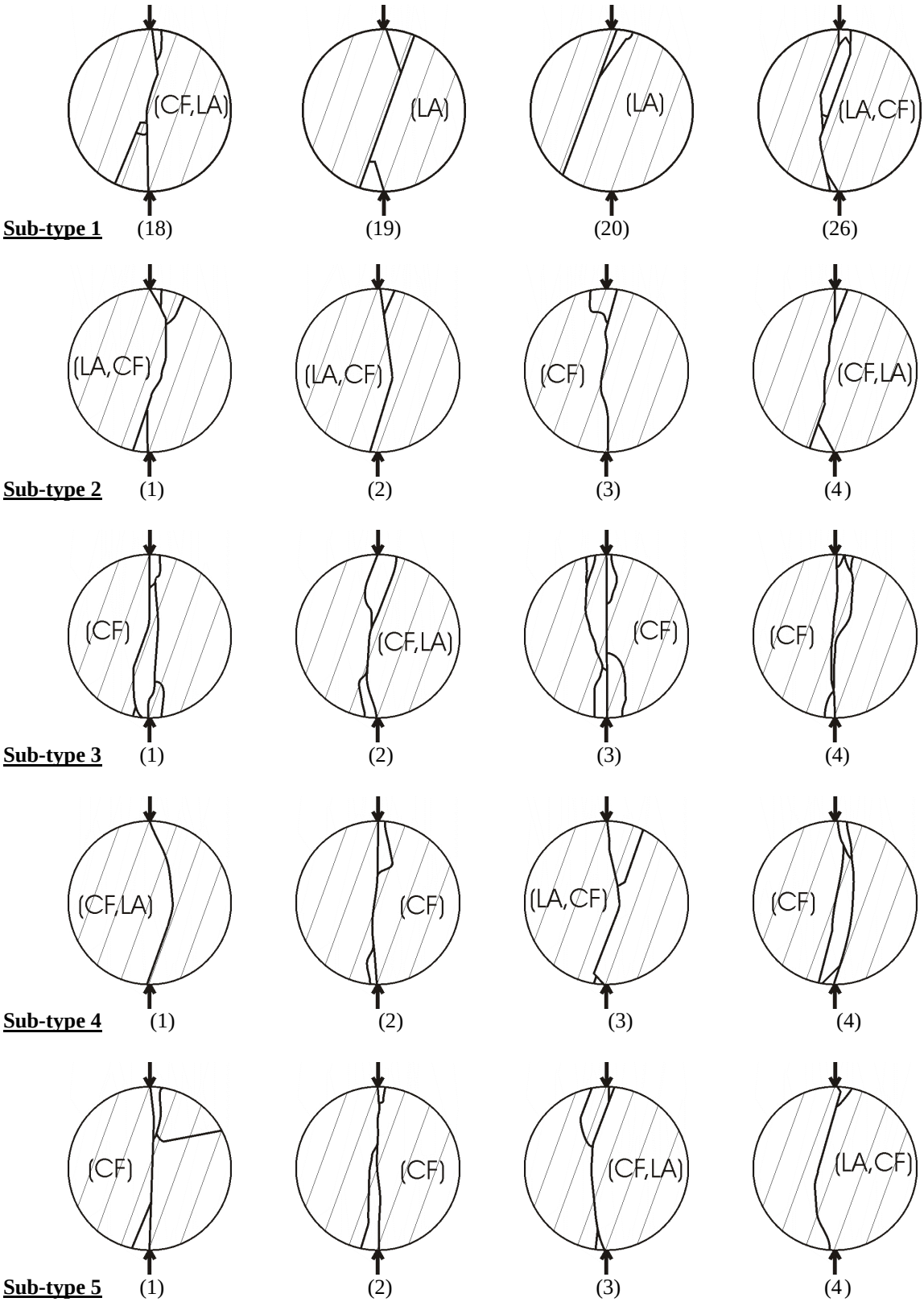

Figure 4.28 Observed failure patterns (one side) of samples from different sub-types of Modave sandstone under Brazilian test conditions. Inclination angle for all samples is 70°. Sample number and the predominant failure mode are given in parentheses, CF = Central fracture, LA = Layer activation.

Table 4.7 Fracture length of samples of Modave sandstone sub-types 1 to 5 (Brazilian tests, inclination angle of 70°)

Sub-type	Sample	Fracture length						
		Layer activation		Central fracture		Non-central fracture		Total
		(mm)	(%)	(mm)	(%)	(mm)	(%)	(mm)
1	18	34	42	46	58	0	0	80
	19	50	68	24	32	0	0	74
	20	55	90	6	10	0	0	61
	26	51	61	33	39	0	0	84
	Average	48	65	27	35	0	0	75
2	1	40	51	39	49	0	0	79
	2	31	53	28	47	0	0	59
	3	14	21	51	79	0	0	65
	4	28	39	43	61	0	0	70
	Average	28	41	40	59	0	0	68
3	1	16	14	101	86	0	0	118
	2	35	41	38	43	14	16	86
	3	21	14	98	66	30	20	149
	4	8	7	101	93	0	0	109
	Average	20	19	84	72	11	9	115
4	1	24	46	28	54	0	0	51
	2	0	0	80	100	0	0	80
	3	38	52	35	48	0	0	73
	4	26	23	86	77	0	0	113
	Average	22	30	57	70	0	0	79
5	1	14	14	66	65	21	21	101
	2	8	9	80	91	0	0	88
	3	28	33	45	55	10	12	83
	4	29	50	29	50	0	0	58
	Average	19	26	55	65	8	8	82

Dark gray indicates the predominant failure mode and light gray indicates the secondary failure mode. The second percentage of either fracture is arbitrarily called the secondary failure mode only if it is equal or more than half of the largest percentage. The change of the predominant and the secondary failure mode is clearly observed from sandstone sub-type 1 to other four sub-types of Modave sandstone.

Variation of the fracture length corresponding to layer activation, central fracture(s), non-central fracture(s) and the total fracture length for the different sandstone sub-types are plotted in Figure 4.29 for individual samples. Figure 4.29a in comparison to Figure 4.29b shows that almost for all the samples of sub-types 2 to 5, the fracture length corresponding to central fracture(s) is larger than the fracture length corresponding to layer activation. For the reference samples Figure 4.29d presents a relatively identical total fracture length for all the samples. However, samples of sandstone sub-type 3 show larger values. Figure 4.29c shows that a non-central fracture only exists in some samples of sandstone sub-types 3 and 5. The samples of sub-type 3 have the maximum fracture length corresponding to non-central fracture (see later their differences in micro-scale).

For all samples corresponding to each sub-type of sandstone, the average fracture length is calculated (Table 4.7). In Figure 4.30, the percentage of layer activation, central fracture(s) and non-central fracture(s) compared to the total fracture length is given for the different sandstone sub-types. Central fracture(s) is predominant for all four sub-types (2, 3, 4, and 5)

of Modave sandstone, while layer activation is the main failure mode for the reference sandstone. Also it is interesting to mention that minimum layer activation is observed in sandstone sub-type 3 (see Figure 4.30) or in other words this sub-type has the lowest degree of transverse isotropy. It can be noted that this sub-type shows the smallest difference in wave velocities measured between the directions perpendicular and parallel to the layer (see paragraph 3.1.2).
From the above explanation, it can be concluded that samples from different blocks (which are relatively similar) behave differently at macro-scale. Therefore, further study on micro-scale by preparing thin sections is necessary to be able to explain the differences.

The variation in Brazilian tensile strength (BTS) as a function of total fracture length for all the sandstone sub-types is plotted in Figure 4.31 for individual samples. The total fracture length varies between 51 mm and 149 mm or in other words between one and three times the diameter. It can be concluded from Figure 4.31 (similar to Figure 4.11) that larger fracture length correlates with higher strength (although the BTS-values of samples of sandstone sub-types 4 and 5 are nearly constant and do not change significantly by the variation in total fracture length).

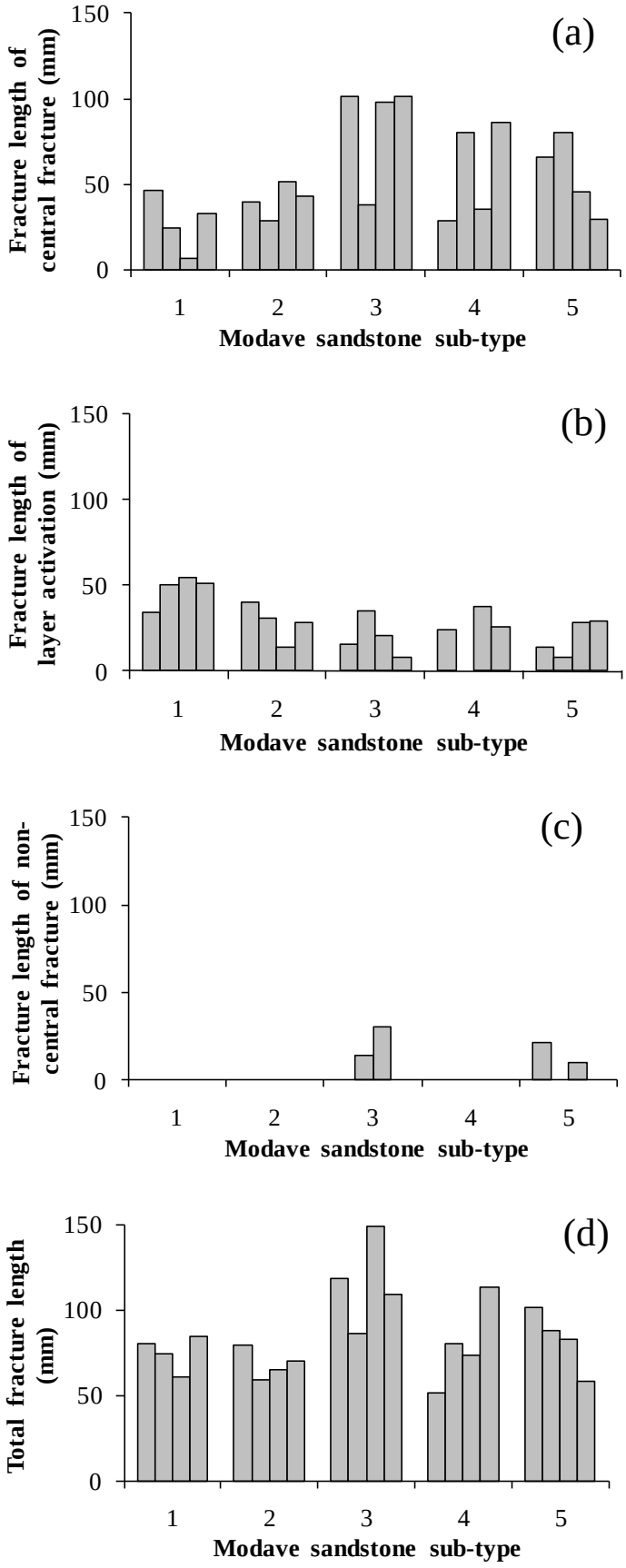

Figure 4.29 Variation in fracture length for different Modave sandstone sub-types, (a) Central fracture(s), (b) Layer activation, (c) Non-central fracture(s) and (d) Total fracture. Inclination angle for all samples is 70°.

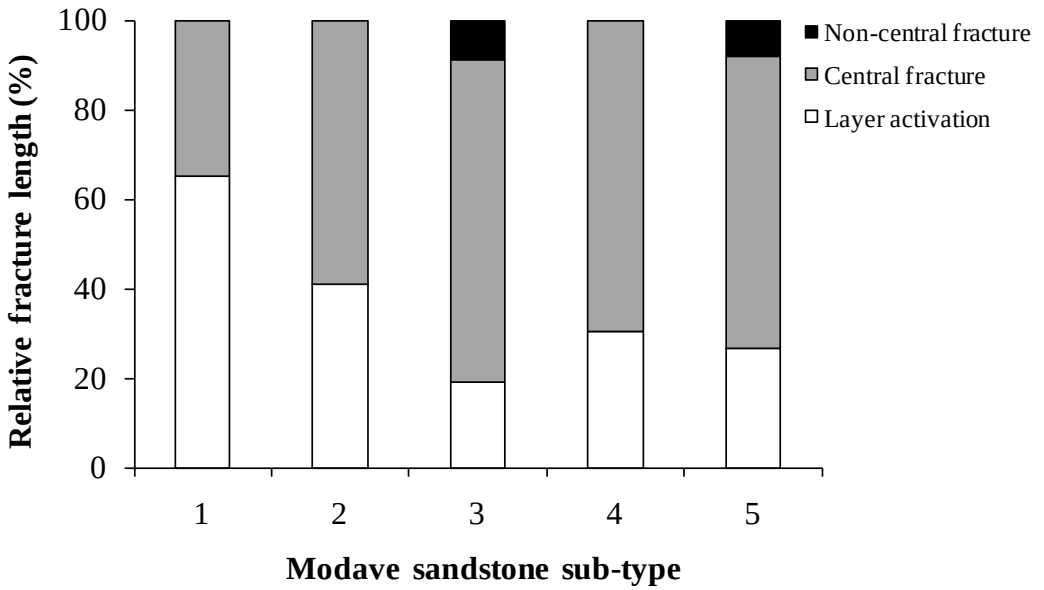

Figure 4.30 Variation in fracture length percentage corresponding to layer activation, central fracture(s) and non-central fracture(s) for different sandstone sub-types.

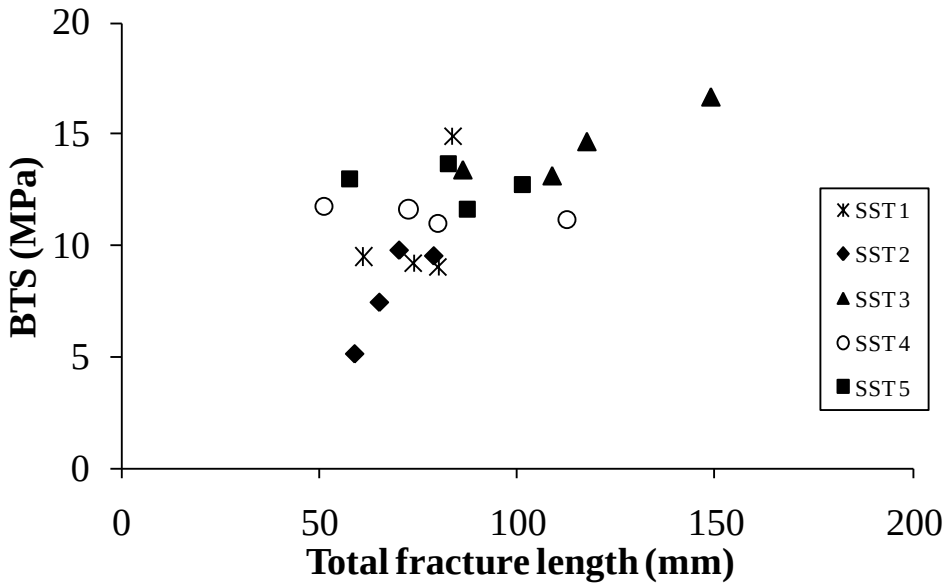

Figure 4.31 Variation in Brazilian tensile strength, BTS, as a function of total fracture length for all the sandstone sub-types after conducting Brazilian tests. Inclination angle for all samples is 70°.

4.4 Shape effect for Modave sandstone sub-types

In this part of study, the effect of sample shape on the failure behaviour of (disc-shaped) samples after conducting Brazilian test is investigated for some Modave sandstone. To be sure that the same material is tested (and not incorporating other parameters), the samples coming from each sub-type are considered separately. So, in one way, with this condition, the amount of rock material is limited. Therefore, size effect experiments are not possible, as for the same length/diameter (or thickness/diameter) ratio a large amount of rock material is needed for larger diameters (> 50 mm). Therefore only the shape effect is investigated.

It is observed that number of layer boundaries (e.g. over 1 cm) of five sandstone sub-types is not the same, and also their failure patterns are different. It is essential to know that whether the number of layer boundaries per sample is important or the distance between the layers play the main role in failure behaviour. By preparing larger samples, the number of layer boundaries per samples increase; however, the distance between them does not change. For example the number of layer boundaries over 1 cm for sandstone sub-type 2 (5.4) is about two times than that for sandstone sub-type 3 (2.6). It means that a sample from sub-type 2 with "d" in diameter has the same number of layer boundaries as a sample from sub-type 3 with "2d" in diameter. However, the distance between the layer boundaries in the sample from sub-type 3 is two times larger than that for the sample from sub-type 2.
The above explanations can be summarised in two following questions, which arise during the experimental tests on different sub-types of Modave sandstone.
1) What is the effect of sample diameter on failure behaviour of disc-shaped samples from a particular sandstone sub-type?
2) Is there any similarity in failure pattern of samples from different sub-types which have (roughly) the same number of layer boundaries?
An effort has been made to answer these questions. For this purpose several samples with different diameters from different sub-types of sandstone should be tested. By observing the studied blocks of sandstone, samples preparation from three blocks is feasible (sandstone sub-types 2, 3 and 5).
The rock blocks of sandstone sub-types 2, 3 and 5 are cored in the laboratory by using drill bits with different diameters from 30 to 115 mm. The direction of coring is parallel to the layering. For all samples a constant thickness of 25 mm is taken. Therefore the thickness-to-diameter ratio varies from 0.2 to 0.9. Variation in mentioned ratio in the study of Thuro et al. 2001 and Pan et al. 2009 are executed by changes in the thicknesses, while keeping the diameter as a constant value. However, for purposes of this study changes in diameter are needed (in order to have different number of layer boundaries per sample) and the samples thickness is kept constant.

From the three mentioned sandstone sub-types 46 samples are prepared for conducting Brazilian tests in order to investigate the shape effect and also to find the answer of the mentioned two questions. All the samples are tested under an inclination angle of 70° (similar to paragraph 4.2). Sample quantities with different diameters from sandstone sub-types 2, 3 and 5 are presented in Table 4.8. It should be noted that all samples with 50 mm are already tested, presented and described in paragraph 4.2. These samples are integrated in this part of study.

Table 4.8 Quantity of sandstone samples for shape effect observation

SST = Sandstone sub-type, D = Sample diameter (cm)

SST	Samples quantity						
	D = 3	D = 4	D = 5	D = 8	D = 10	D = 11.5	Total
2	4	4	4	2	2	-	16
3	4	-	4	3	-	4	15
5	4	-	4	-	3	4	15

The failure pattern (one side) of the samples after failure from the three sandstone sub-types is shown in Figure 4.32 (one typical sample for each diameter). Apart from the predominant failure mode in some samples (such as in sandstone sub-type 2) some secondary modes are also observed (see Figure 4.32). Although in samples 80-2 and 115-3 of sandstone sub-types 3 some parts of layer activation are also observed, the predominant failure mode in these samples is central fracture. In these samples layer activation is not considered as a secondary failure mode because fracture length corresponding to layer activation is very small in comparison to fracture length corresponding to central fracture.

Table 4.9 gives the diameter D, the thickness t, the failure load F and some other information about all the tested samples. After executing the Brazilian tests the fracture analysis is done for all the samples. Table 4.10 presents the fracture length of the 46 tested samples for the three sandstone sub-types. In this table fracture lengths corresponding to layer activation, central fracture(s) and non-central fracture(s) are presented, as well as the total fracture length.

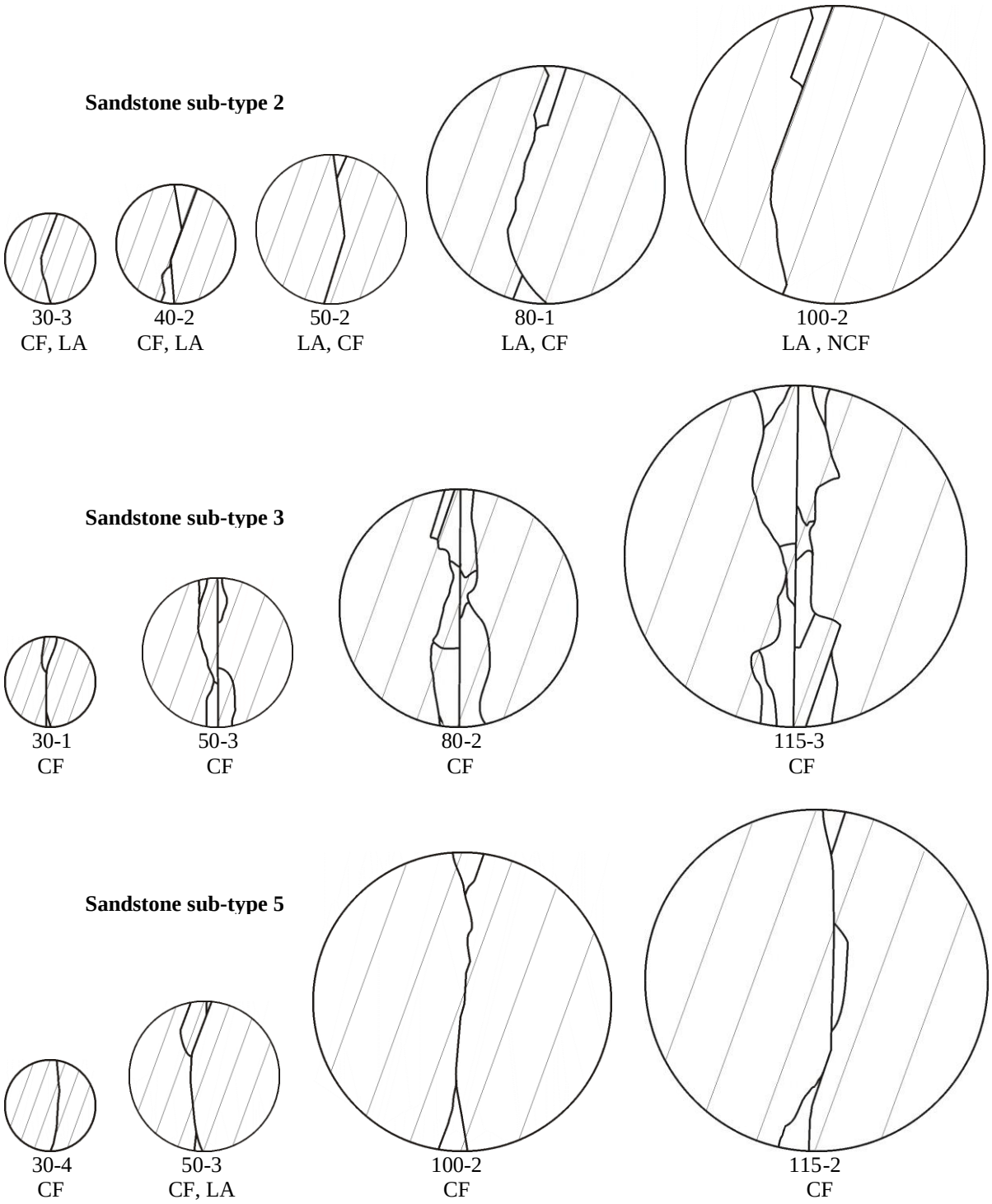

Figure 4.32 Observed failure patterns (one side) of Brazilian test for samples in different diameters from Modave sandstone sub-types 2, 3 and 5 (one typical sample for each diameter). Inclination angle for all samples is 70°. Sample number and the predominant failure mode are put under the samples. The first part of the numbers is the sample diameter in mm. CF = Central fracture, LA = Layer activation. Quantification of predominant and secondary failure modes is presented in Table 4.10.

Table 4.9 Brazilian test results for Modave sandstone sub-types (SST) 2, 3 and 5 for shape effect observation (inclination angle of 70°). D = Diameter, t = Thickness and F = Failure load. Presented density is measured in the laboratory condition.

SST	Sample N°	D (mm)	t (mm)	ρ (t/m³)	t / D	F (kN)	BTS (MPa)
2	30-1	28.8	25.1	2.6	0.87	14.1	12.4
	30-2	28.9	25.6	2.5	0.89	13.2	11.4
	30-3	28.8	25.7	2.6	0.89	11.1	9.5
	30-4	28.8	25.4	2.6	0.88	10.3	9.0
	40-1	39.4	25.4	2.6	0.65	13.5	8.6
	40-2	39.4	25.6	2.6	0.65	20.9	13.2
	40-3	39.5	25.4	2.6	0.64	17.7	11.2
	40-4	39.4	25.3	2.6	0.64	22.0	14.0
	50-1	50.1	24.9	2.6	0.50	18.6	9.5
	50-2	50.0	24.8	2.6	0.50	9.9	5.1
	50-3	50.1	24.9	2.6	0.50	14.5	7.4
	50-4	50.1	25.0	2.6	0.50	19.2	9.8
	80-1	79.6	25.6	2.6	0.32	25.8	8.1
	80-2	79.7	25.1	2.6	0.31	24.0	7.6
	100-1	99.7	24.5	2.6	0.25	39.1	10.2
	100-2	99.8	24.9	2.5	0.25	30.5	7.8
3	30-1	28.8	24.4	2.6	0.85	18.2	16.4
	30-2	28.8	25.3	2.5	0.88	16.9	14.8
	30-3	28.7	25.2	2.5	0.88	19.3	16.9
	30-4	28.7	25.3	2.5	0.88	20.0	17.5
	50-1	50.1	25.0	2.5	0.50	28.9	14.7
	50-2	50.2	24.8	2.6	0.49	26.2	13.4
	50-3	50.2	24.6	2.6	0.49	32.3	16.7
	50-4	50.1	24.5	2.6	0.49	25.4	13.1
	80-1	79.7	26.1	2.5	0.33	45.6	13.9
	80-2	80.3	24.3	2.5	0.30	43.9	14.3
	80-3	79.9	26.4	2.5	0.33	43.5	13.2
	115-1	114.1	25.6	2.5	0.22	71.7	15.6
	115-2	114.1	25.9	2.6	0.23	69.2	14.9
	115-3	114.2	25.5	2.6	0.22	70.7	15.4
	115-4	114.2	25.1	2.5	0.22	60.2	13.4
5	30-1	28.7	25.3	2.5	0.88	12.4	10.9
	30-2	28.7	25.0	2.6	0.87	14.1	12.5
	30-3	28.7	25.3	2.5	0.88	10.9	9.5
	30-4	28.7	25.1	2.6	0.87	14.7	13.0
	50-1	50.1	25.3	2.6	0.50	25.3	12.7
	50-2	50.1	25.6	2.6	0.51	23.4	11.6
	50-3	50.1	25.4	2.6	0.51	27.3	13.7
	50-4	50.1	25.2	2.6	0.50	25.8	13.0
	100-1	99.6	24.7	2.6	0.25	41.5	10.7
	100-2	99.7	25.4	2.6	0.25	46.7	11.7
	100-3	99.8	24.5	2.6	0.25	43.6	11.4
	115-1	114.3	24.9	2.6	0.22	55.0	12.3
	115-2	114.2	25.5	2.6	0.22	45.9	10.0
	115-3	114.2	25.4	2.6	0.22	52.6	11.5
	115-4	114.2	25.3	2.6	0.22	53.9	11.9

Table 4.10 Fracture length of samples after conducting Brazilian tests for Modave sandstone sub-types (SST) 2, 3 and 5 for shape effect observation (inclination angle of 70°).

SST	Sample N°	Fracture length						
		Layer activation		Central fracture		Non-central fracture		Total
		(mm)	(%)	(mm)	(%)	(mm)	(%)	(mm)
2	30-1	9	21	34	79	0	0	43
	30-2	19	48	20	52	0	0	39
	30-3	14	46	16	54	0	0	30
	30-4	6	21	24	79	0	0	30
	Average	12	34	24	66	0	0	36
	40-1	8	19	33	81	0	0	40
	40-2	29	48	31	52	0	0	60
	40-3	9	22	0	0	31	78	40
	40-4	25	40	38	60	0	0	63
	Average	18	32	25	48	8	20	51
	50-1	40	51	39	49	0	0	79
	50-2	31	53	28	47	0	0	59
	50-3	14	21	51	79	0	0	65
	50-4	28	39	43	61	0	0	70
	Average	28	41	40	59	0	0	68
	80-1	61	51	59	49	0	0	120
	80-2	72	65	39	35	0	0	111
	Average	66	58	49	42	0	0	115
	100-1	49	40	6	5	66	54	122
	100-2	83	63	4	3	44	34	131
	Average	66	52	5	4	55	44	127
3	30-1	0	0	44	100	0	0	44
	30-2	0	0	29	100	0	0	29
	30-3	0	0	61	100	0	0	61
	30-4	0	0	42	100	0	0	42
	Average	0	0	44	100	0	0	44
	50-1	16	14	101	86	0	0	118
	50-2	35	41	38	43	14	16	86
	50-3	21	14	98	66	30	20	149
	50-4	8	7	101	93	0	0	109
	Average	20	19	84	72	11	9	115
	80-1	13	6	186	94	0	0	199
	80-2	34	11	259	89	0	0	293
	80-3	22	16	84	61	32	23	138
	Average	23	11	176	81	11	8	210
	115-1	40	10	348	85	22	5	410
	115-2	58	11	322	64	123	24	502
	115-3	69	14	383	77	44	9	496
	115-4	12	2	478	93	24	5	514
	Average	45	9	383	80	53	11	480

Continue of Table 4.10

SST	Sample N°	Fracture length						
		Layer activation		Central fracture		Non-central fracture		Total
		(mm)	(%)	(mm)	(%)	(mm)	(%)	(mm)
5	30-1	6	17	30	83	0	0	37
	30-2	0	0	29	100	0	0	29
	30-3	0	0	29	100	0	0	29
	30-4	4	13	25	87	0	0	29
	Average	3	8	28	92	0	0	31
	50-1	14	14	66	65	21	21	101
	50-2	8	9	80	91	0	0	88
	50-3	28	33	45	55	10	12	83
	50-4	29	50	29	50	0	0	58
	Average	19	26	55	65	8	8	82
	100-1	40	30	95	70	0	0	135
	100-2	29	21	110	79	0	0	139
	100-3	14	10	125	90	0	0	139
	Average	28	20	110	80	0	0	138
	115-1	59	19	248	81	0	0	307
	115-2	36	19	156	81	0	0	192
	115-3	37	22	105	61	29	17	172
	115-4	12	7	151	93	0	0	163
	Average	36	17	165	79	7	4	208

The failure pattern is measured from one side of all the samples after failure except two samples (80-3 in SST3 and 30-1 in SST5). For the exceptions fracture length is the average of fractures length on the both sides of the samples. Dark gray indicates the predominant failure mode and light gray indicates the secondary failure mode. The second percentage of either fracture is arbitrarily called the secondary failure mode only, if it is equal or more than half of the largest percentage.

To observe the effect of sample diameter on failure behaviour of disc-shaped samples, relative layer activation fracture length and also Brazilian tensile strength are considered. Figure 4.33 presents the variation in the mentioned two factors (relative layer activation fracture length and Brazilian tensile strength) as a function of sample diameter for sandstone sub-types 2, 3 and 5. For sandstone sub-types 3 and 5 a clear difference in layer activation and also in BTS-values of samples with different diameter is not distinguished (see Figure 4.33).

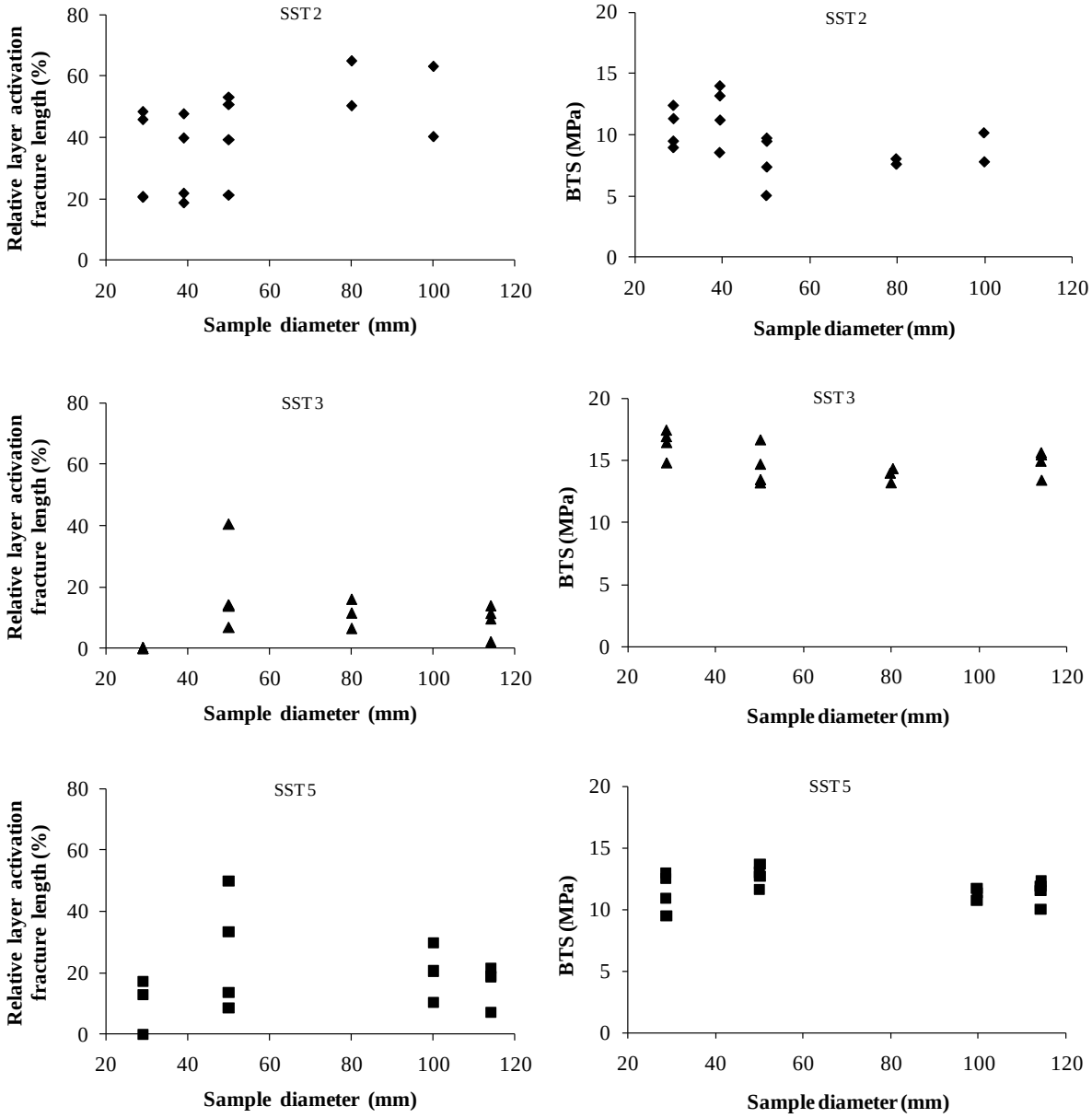

Figure 4.33 Shape effect on failure behaviour of disc-shaped samples after conducting Brazilian test. Samples with different diameters but constant thickness (25 mm) from sandstone sub-types (SST) 2, 3 and 5 are tested. The inclination angle for all the samples is 70°. Left diagrams: Variation in relative layer activation fracture length as a function of the sample diameter. Right diagrams: Variation in Brazilian tensile strength, BTS, as a function of the sample diameter.

Variation in BTS-values as a function of sample diameter for sandstone sub-type 2 is also not significant, especially when sample diameter varies among 50, 80 and 100mm. The condition for relative layer activation fracture length of samples from sandstone sub-type 2 is slightly different. The samples with diameter of 30, 40 and 50 mm have similar layer activation; however, for larger diameter (80 and 100 mm) layer activation is slightly increased. For each of the diameter 80 and 100 mm from sandstone sub-type 2, two samples are tested (see Table 4.9 and Table 4.10). Relative layer activation fracture length of one sample in each of these two diameters is in the range of layer activation of the other samples with diameters of 30, 40 and 50 mm. In other words only one sample with diameter of 80 and one sample with diameter of 100 mm show higher relative layer activation fracture length. Therefore it is

difficult to judge about the layer activation trend in sandstone sub-type 2 as sample diameter is increased. From the above explanation it can be concluded that, the shape effect is limited in the tested diameter range for the studied sandstone sub-types.

Mean values of relative layer activation fracture length and of Brazilian tensile strength are calculated from 2 to 4 samples for each diameter in sandstone sub-types 2, 3 and 5 (see Table 4.9 and Table 4.10). Figure 4.34 shows the variation in mean values of relative layer activation fracture length and also Brazilian tensile strength as a function of sample diameter for sandstone sub-types 2, 3 and 5. As stated earlier, Figure 4.34 shows that the shape effect on failure behaviour of disc-shaped samples is limited, particularly on Brazilian tensile strength in the tested diameter range.

By observing the presented results in Figure 4.34, another interesting conclusion is achieved. Brazilian tensile strength is inversely correlated with relative layer activation fracture length for the tested diameter range. Samples of sandstone sub-type 2 have the highest relative layer activation fracture length and the lowest Brazilian tensile strength in the tested diameter range. Samples of sandstone type 3 have the lowest relative layer activation fracture length and the highest Brazilian tensile strength. The inverse correlation of Brazilian tensile strength and relative layer activation fracture length for the tested samples is clearly presented by Figure 4.35. This figure shows that higher strength corresponds to the samples with lower layer activation fracture length.

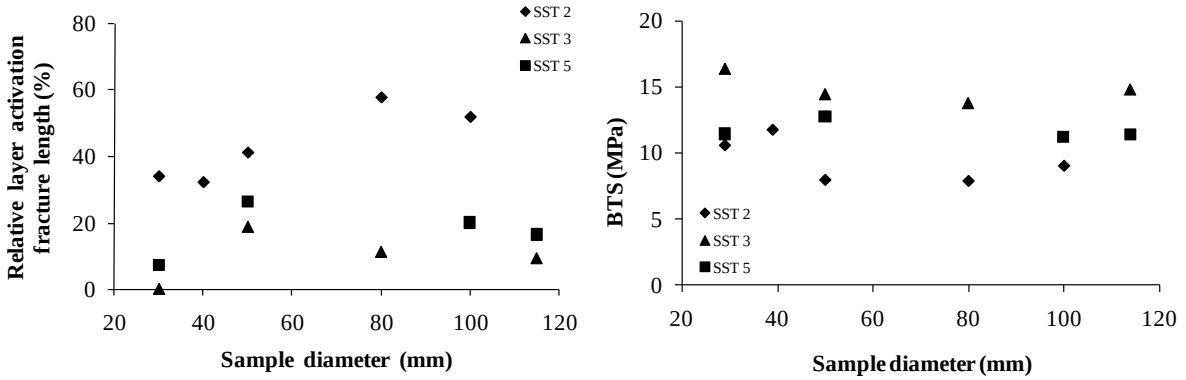

Figure 4.34 Shape effect on failure behaviour of disc-shaped samples after conducting Brazilian test. Mean values are calculated from 2 to 4 samples for each diameter (see Table 4.9 and Table 4.10). Samples with different diameters but constant thickness (25 mm) from sandstone sub-types (SST) 2, 3 and 5 are tested. The inclination angle for all the samples is 70°. Left diagram: Variation in relative layer activation fracture length as a function of the sample diameter. Right diagram: Variation in Brazilian tensile strength, BTS, as a function of the sample diameter.

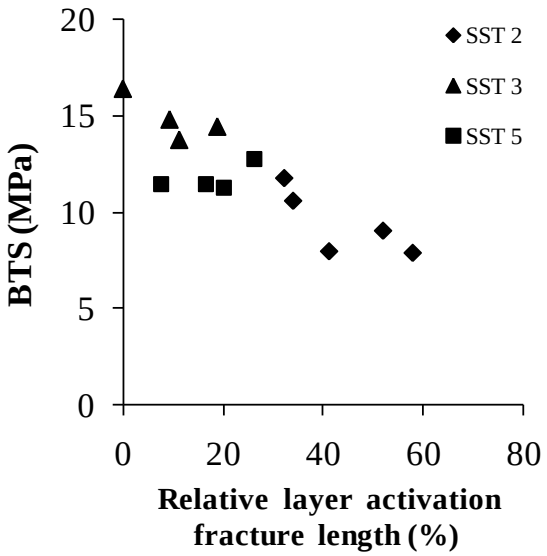

Figure 4.35 Correlation of Brazilian tensile strength and relative layer activation fracture length

As can be seen in Figure 4.34 although the number of layer boundaries is increased in samples of sandstone sub-types 3 and 5 by increasing the samples diameter, their relative layer activation fracture length do not changed considerably. It means that the failure patterns of samples from different sub-types of sandstone which have (roughly) the same number of layer boundaries are not similar. Mentioned conclusion is verified by comparing the failure patterns of samples with similar number of layer boundaries.

Table 4.11 Modave sandstone samples for shape effect investigation. SST = Sandstone sub-type, D = Sample diameter (cm)

a) Number of layer boundaries (LB) of different sandstone samples

SST	# LB / cm	Number of layer boundaries (LB) per sample					
		D = 3	D = 4	D = 5	D = 8	D = 10	D = 11.5
2	5.4	15.7	21.1	27.0	43.2	54.0	-
3	2.6	7.5	-	13.0	20.8	-	29.6
5	1.4	4.1	-	7.0	-	14.0	16.0

b) Sandstone samples with (roughly) the same number of layer boundaries

Item	SST	D (cm)	# LB / sample		D (cm)	SST	Item
1	5	5	7.0	7.5	3	3	1
2	3	5	13.0	14.0	10	5	2
3	2	3	15.7	16.0	11.5	5	3
4	3	8	20.8	21.1	4	2	4
5	2	5	27.0	29.6	11.5	3	5

By knowing the number of layer boundaries per cm for each sub-type of sandstone, number of layer boundaries in the samples with different diameter is calculated. Table 4.11a presents the number of layer boundaries of samples in the tested diameter range for sandstone sub-types 2, 3 and 5. From this table the samples with similar numbers of layer boundaries are grouped. For example the numbers of layer boundaries in the samples with 3 cm diameter from sandstone sub-type 2 is (15.7) close to the numbers of layer boundaries in the samples with 11.5 cm diameter from sandstone sub-type 5 (16.0). The samples with 8 cm diameter from sandstone sub-type 3 and the samples with 4 cm diameter from sandstone sub-type 2 are the other example (see Table 4.11a and also item 4 in Table 4.11b). Five pairs with relatively similar numbers of layer boundaries can be found in Table 4.11a. These five pairs are presented in Table 4.11b as item 1 to 5 with their sandstone sub-types (SST), diameters (D) and individual numbers of layer boundaries (# LB / sample).

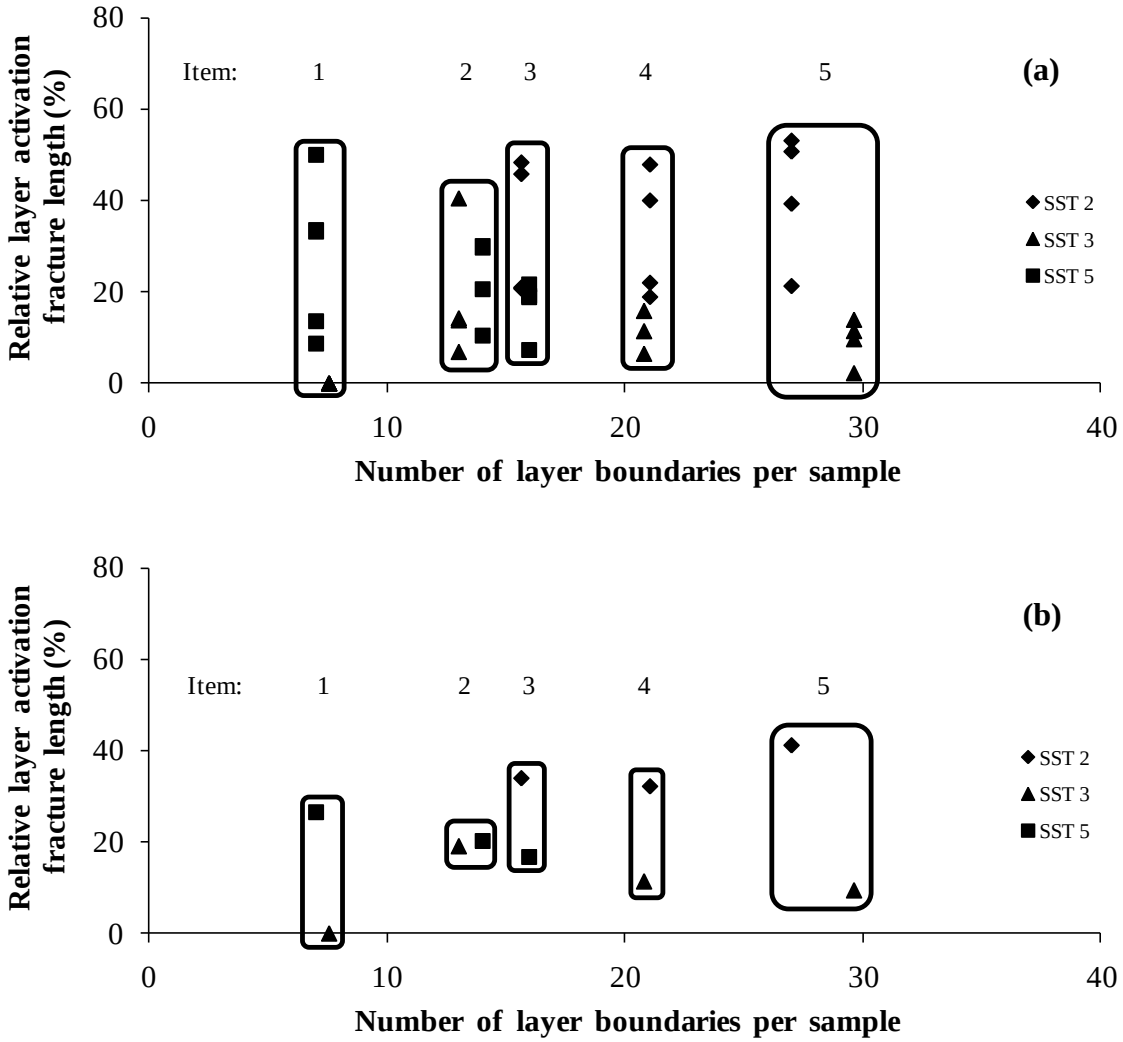

Figure 4.36 Variation in relative layer activation fraction length as a function of number of layer boundaries per sample. Items 1 to 5 show the samples with (roughly) the same number of layer boundaries (see Table 4.11 b). SST = Sandstone sub-type.
a) All the samples which are mentioned in Table 4.11 b. b) Average for 3 to 4 samples.

Variation in relative layer activation fraction length for samples with (roughly) the same number of layer boundaries (item 1 to 5 in Table 4.11b) is presented in Figure 4.36. Figure 4.36a shows that for all items except item 2, the effect of the number of layer boundaries on layer activation cannot be observed. Furthermore, this figure shows that by increasing the number of layer boundaries per sample (by increasing the sample diameter), any positive trend of relative layer activation fraction length does not exist. Figure 4.36b presents the variation in average relative layer activation fraction length as a function of number of layer boundaries per sample in every item. In this figure only item 2 shows the same average relative layer activation fraction length for the samples with roughly the same number of layer boundaries and for the other four items no correlation can be observed. Observation of Figure 4.36b similar to Figure 4.36a leads to the same conclusion that increasing the number of layer boundaries by enlarging the samples does not have influence on the layer activation. For each particular sandstone sub-type some parameters (e.g. mineral composition) do not change in the samples with different diameters. This point is the reason of relatively the same layer activation of the samples with different diameters (from each sandstone sub-type).

Observed weak mineral percentage in sandstone sub-types 2, 3 and 5 is 23.5%, 7.9% and 12.4%, respectively. By reviewing Figure 4.36 it can be stated that most of the samples from sandstone sub-type 2 are in the highest range of layer activation while most of the samples from sub-type 3 are in the lowest range of layer activation. This observation is compatible with their weak mineral percentage. Among mentioned Modave sandstone sub-types, sub-type 2 has the largest amount of weak minerals (23.5%) and sub-type 3 has the lowest (7.9%). Therefore, it is logic to conclude that layer activation depends on weak mineral percentage or number of layer boundaries in the condition of identical diameter.

It is interesting to redraw the graphs of Figure 4.36 with only the samples of sandstone sub-types 2 and 3, as in these sub-types layer the boundaries are the only planes of weakness. In sandstone sub-type 5 apart from the layer boundaries, the ripples exist as the secondary plane of weakness. Figure 4.37a shows the variation in relative layer activation fraction length as function of number of layer boundaries per samples for sandstone sub-types 2 and 3. As expected, Figure 4.37a shows that similarity in number of layer boundaries of samples with different diameter does not affect the relative layer activation. Figure 4.37b presents the variation in average relative layer activation fraction length for samples of sandstone sub-types 2 and 3. In Figure 4.37b both sub-types present relatively identical rate of relative layer activation as a function of number of layer boundaries per samples.

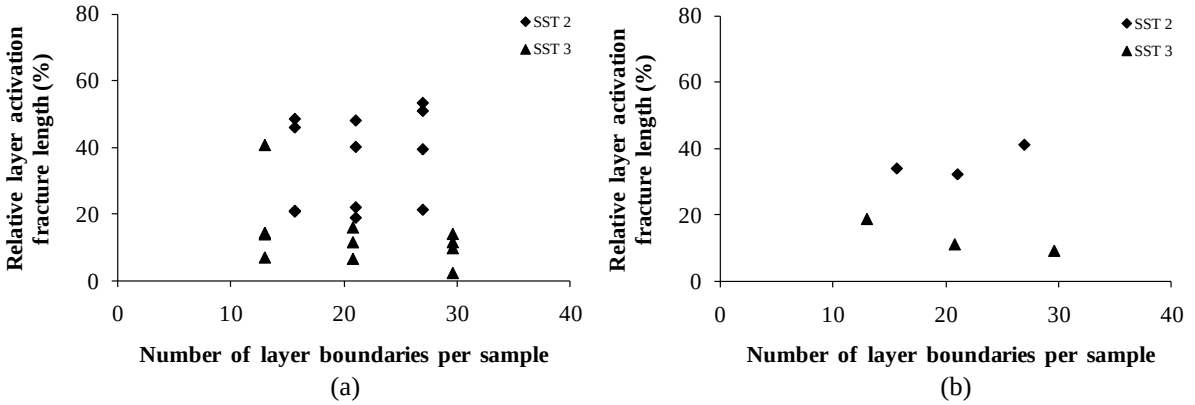

Figure 4.37 Variation in relative layer activation fraction length as a function of number of layer boundaries per sample for Modave sandstone sub-types (SST) 2 and 3. a) All the samples from sandstone sub-types 2 and 3 which are mentioned in Table 4.11 b. b) Average for 3 to 4 samples.

4.5 Overview of findings

The experimental study on the sandstones from Modave in the South of Belgium, which is a layered rock, shows that the failure stress and fracture pattern are considerably affected by the layer orientation. However, measurements of P-wave velocity show small differences in wave velocity parallel (4.5-5.1 km/s) and perpendicular to the layers (4.4-4.7 km/s).
For the reference sub-type of this layered sandstone it is observed that a change in failure mode from central fracture to layer activation is in the range of 45° and 60°. Central fracture(s) is predominant for $\theta < 45°$, while layer activation is the main failure mode for $\theta > 60°$. However, variation in the total fracture length is not as explicit in comparison to the individual classes.
For the reference sub-type, the average BTS-values and the average applied energy of the samples with $\theta < 50°$ (13.9 MPa and 1.8 J, respectively) are slightly larger than that for the samples with $\theta > 50°$ (10.9 MPa and 1.3 J, respectively). It seems logic as in the case of $\theta < 50°$ fracturing is mainly through the stronger material; while as in the case of $\theta > 50°$ fracturing makes use of the layers that normally have weaker mechanical properties. In other words the strength of the first group ($\theta < 50°$) rather corresponds to the tensile strength of the "intact" material, while for the second group ($\theta > 50°$) it rather corresponds to the shear and/or tensile strength of the "layers". The results show that larger fracture length correlates with higher strength and higher applied energy. In other words that the variation in BTS-values and applied energy as a function of the total fracture length is considerably more significant than when they are considered as a function of the inclination angle. This is the reason why for the samples with different inclination angles but the same fracture pattern, relatively the same BTS is achieved. From the above explanation it is concluded that the samples with low inclination angles which are more fractured have the higher values of strength.

The influence of layer orientation is verified by four other sub-types of the layered sandstone of Modave. These samples are taken from other blocks in the same quarry, collected at close distance (1 to 10 m). The global behaviour is similar; however, they do not behave exactly the same. For all sandstone sub-types as inclination angle increases from 0° to 90°, the fracture length corresponding to central fracture(s) decreases while layer activation increases. However the decreasing and the increasing rates (of fractures length) for the five studied sub-types are different.
Brazilian test results for one inclination angle (i.e. 70°) for a few samples from five sub-types are noted. The average value of Brazilian tensile strength for the five sub-types varies from 7.9 MPa, to 14.5 MPa. Although at a macroscopic scale the blocks look similar, but there is about 6.6 MPa difference between the smallest and largest average value of BTS. All the samples from sandstone sub-types 2 to 5 show a failure by either central fracture(s) only or a combination of central fracture(s) and layer activation. However, the predominant failure mode for sandstone sub-types 1 is only layer activation.
In this study sandstone sub-type 3 has the highest average quartz size (107 μm) and sub-type 2 the lowest average (69 μm). It is interesting to note that the average value of the Brazilian tensile strength (BTS), the total fracture length and fracture length corresponding to non-central fracture(s) are the highest for sub-type 3 of Modave sandstone, while these three parameters are the lowest for sandstone sub-type 2 which corresponds to the lowest average grain size.
From the above explanation it can be concluded that, even observing different failure behaviour of two blocks of layered sandstone from the same quarry is probable. In that case,

to be able to answer the question “Why relatively similar natural rocks behave differently?” more detailed microscopic study is needed.

The aim of this paragraph is presenting the classification of fractured samples after conducting Brazilian tests whereby the samples have one specific form of anisotropy. Furthermore, it is tried to highlight the effect of layer orientation on strength, applied energy and fracture pattern of layered sandstone (Psammite of Condroz). How these factors are correlated to each other is also illustrated.

Also in this chapter on scale effect analysis, only the shape effect is investigated and not the size effect, as not enough material was available. Disc-shaped samples with a constant thickness of 25 mm and with a diameter varying from 30 to 115 mm are prepared. An effort is done to observe the effect of samples diameter on failure behaviour of samples from Modave sandstone sub-types. Also it is interesting to find if samples from different sandstone sub-types which have (roughly) the same number of layer boundaries have the similar failure pattern.

The shape effect in the tested diameter range is limited and the failure behaviour of samples is not influenced by their diameter. Also no obvious similarity of failure behaviour of sandstone samples from different sub-types which have the same number of layer boundaries is observed. It means that increasing the number of layer boundaries by enlarging the samples does not influence layer activation. By enlarging the samples (in diameter range of 30 to 115 mm) weak mineral percentage does not change and this is probably the main reason of having relatively the same layer activation in each sandstone sub-type. Above explanation can be summarised as follows: layer activation depends on weak mineral percentage and the number of layer boundaries plays only a role in the case of identical diameter.

It is also observed that Brazilian tensile strength is inversely correlated with relative layer activation fracture length for the tested diameter range. Samples of sandstone sub-type 2 with the highest weak minerals percentage (23.5%) have the highest relative layer activation fracture length and the lowest Brazilian tensile strength in the tested diameter range. Samples of sandstone sub-type 3 with the lowest weak minerals percentage (7.9%) have the lowest relative layer activation fracture length and the highest Brazilian tensile strength.

5 Results of Petrographical Analyses on Modave Sandstone

In the macro-scale study of different blocks of Modave sandstone (Psammite of Condroz) from the same quarry some different behaviour is recognised especially in their fracture patterns. Fracture patterns for the different sub-types of sandstone show an essential difference between the reference material, i.e. layer activation, and the other sandstone sub-types, i.e. central fracture(s). To explain the reason for the differences in macro-scale behaviour, as discussed in chapter 4, micro-scale quantification is necessary. In this chapter micro-scale quantification is presented for tested samples. The tested samples are divided into two categories, the samples for which prior to their failure loading is stopped and the samples that fail and whereby macro-fracture(s) occur.

5.1 Micro-scale quantification of tested non-failed samples

As it is already discussed in chapter 4, rock samples from different blocks of Modave sandstone which are relatively similar by visual inspection, have different behaviour at macro-scale. Petrographical analysis of thin sections from the untested material shows differences at micro-scale, where the microstructure of rock is known to influence its macro-scale behaviour. Therefore, to be able to understand the effect of micro-scale parameters on macro-scale behaviour of different sub-types of sandstone, it is necessary to analyse the thin sections of tested samples.
Generally a small displacement (about few hundred µm) of fractured parts is inevitable due to the violent brittle fracture of these sub-types of sandstone. This small displacement which is presented in thin section as the crack width, are enough for losing the detail information about the crack path among the grains. Because the grain size of all sub-types of studied sandstone is much smaller than the crack width. Therefore, to detect micro-cracks, stopping the sample loading (by the help of AE monitoring) prior to failure is necessary. However, the closer the maximum applied load is to the final strength of a sample, the micro-cracks are more frequent and more easily detectable.

5.1.1 Result of acoustic emission monitoring

It is important to note that the curve of cumulative AE hits for this type of rock material is not a semi-parabola as can be observed in many studies (Lavrov et al. 2002) on homogeneous rock materials. In the referred study on crinoïdal limestone, the cumulative AE hits diagram starts with a relatively small slope which is followed by a steep slope. At the end of this stage crack initiation, stable crack growth and crack coalescence have occurred and the sample is going to final failure. For the studied layered sandstone the diagrams of cumulative AE hits in

most cases can be divided into two successive parts: one for relatively small loading forces, another prior to the final failure. This type of sandstone mainly consists of quartz and weak minerals. Therefore the first part can be related to the cleavage activation in the weak minerals.

Although the quantity of weak minerals is considerably less than quartz as the strong mineral, they can have some major effect on the behaviour of rock samples. For most samples both parts are clearly distinguishable, however for some other samples they are not that clear and easily detectable. The reason of being different is that all the studied blocks of layered sandstone have not the same mineralogical composition. Furthermore, for micro-scale quantification, thin sections from tested samples are prepared and analysed for fracture observation.

As already shown in Figure 3.12 the amount of weak minerals (carbonate and mica) in sandstone sub-types 1 to 4 is 33%, 23.5%, 7.9% and 14.3%, respectively. In total 17 samples from four sub-types are tested under the Brazilian test conditions. For 10 of them loading is stopped just prior to the macro-failure. From these 10 samples, one typical sample is presented per sub-type. It should be mentioned that loading for the tested non-failed samples are stopped (arbitrary) close to the sample ultimate strength and consequently the curves in Figure 5.1 and in the appendix A are not totally similar. Furthermore, in few samples large quantity of mica located in a small part of the samples is observed. These mica cause high amount of registered hits during the sample loading and also reduce the sample strength. A sample with this type of exception is not considered as a typical sample for a sub-type.
The diagrams of the cumulative AE hits as a function of applied load for the four representative samples are presented in Figure 5.1. As already mentioned the presented diagram can be divided into two successive parts. The dotted lines in Figure 5.1 separate and show the two parts. As the sensor is attached manually for different samples, the emphasis should be on the curve shapes, rather than on the number of hits. Normally, when the sensors are reinstalled in a new position or on other samples, the coupling conditions can change which makes it difficult to draw a comparison between absolute values of the AE activity in different tests (Lavrov et al. 2002).

It is explained that the two successive parts correspond to the changes in the microstructure of weak and strong minerals respectively. In all the studied Modave sandstone sub-types, sub-type 1 has the highest percentage (33%) of weak minerals. The percentage of weak minerals in sandstone sub-type 1 is considerable. In microscopic observation of thin section of this sub-type, carbonate minerals can be seen everywhere. High percentage of weak minerals in sandstone sub-type 1 in comparison to the other sub-types makes it more homogeneous. In other words everywhere a combination of weak and strong elements can be observed. Therefore from the beginning of loading the sample of sandstone sub-type 1, carbonate cleavages can be activated (see the first part in Figure 5.1). As carbonate minerals are frequent in sub-type 1, cleavage activation can continue during the stage of activation of quartz bonds (or quartz fracturing) which occurs before the final failure (see the second part in Figure 5.1). This can be the reason that for the diagram of sub-type 1 a clear distinction between the two parts is not observed (in comparison to the diagrams corresponding to sub-types 2 and 4).

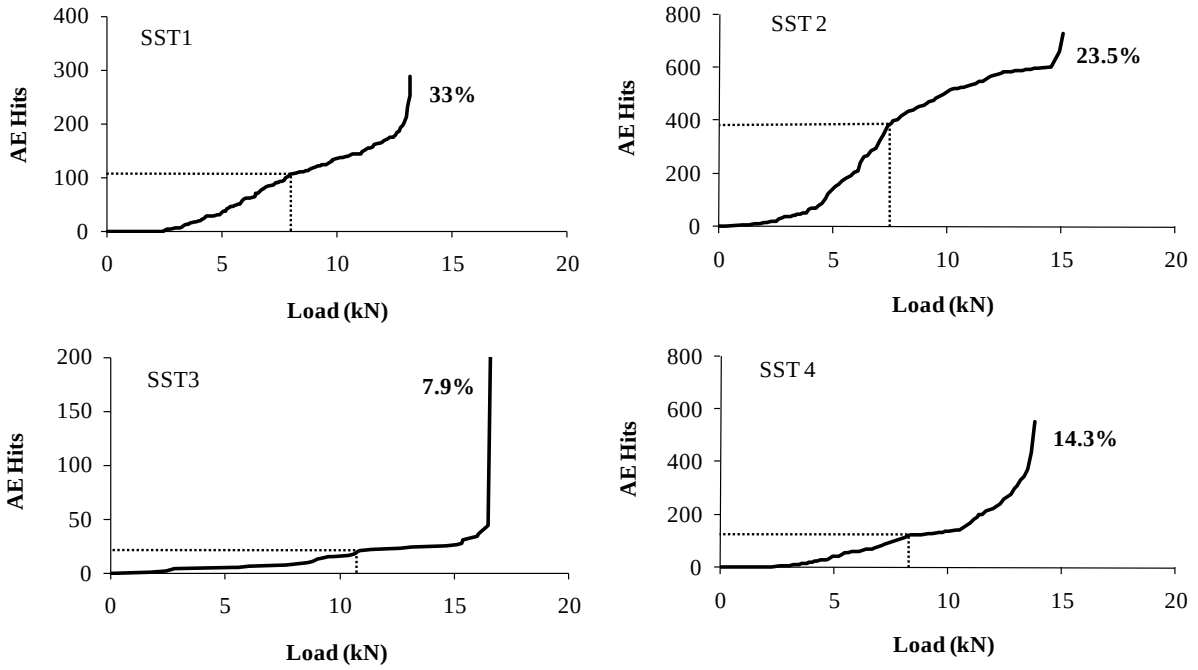

Figure 5.1 Cumulative AE hits as a function of applied load for Modave sandstone sub-types (SST) 1-4. The amount of weak minerals (%) is presented. The two parts are separated by dotted lines. As weak minerals percentage decreases, the mentioned two parts converge more towards one part. Loading the sample is stopped prior to the final failure. The displacement rate is 0.2 mm/min.

Sandstone sub-type 3 has the lowest percentage (7.9%) of weak minerals. The registered AE hits in the first part of the diagram corresponding to sub-type 3, is small in comparison to the first part of the other diagrams. When the applied load becomes adequate for activation of the quartz bonds, a sudden increase of AE hits is registered while the sample is going to fail. The difference of weak mineral percentage in sandstone sub-types 1 and 3 is the reason that for sub-type 1 more AE hits are registered from the beginning of loading in comparison to sub-type 3. This seems logic, as weak minerals in sandstone sub-type 3 (7.9%) in comparison to sub-type 1 (33%) are less frequent.
By only considering the first part for sub-type 2, one can be mislead that crack initiation, stable crack growth and crack coalescence occur and that the sample is going to final failure. But as loading continues, the second part appears.
The diagrams in Figure 5.1 give an indication that as the weak minerals percentage increases the first part of cumulative AE hits diagram becomes more important and more pronounced. Even the mentioned part in sandstone sub-type 3 with 7.9% weak minerals percentage have nearly disappeared.
The above conclusions (from Figure 5.1) are verified by microscopic investigation on thin sections from the three non-failed sandstone samples (sub-types 2 to 4) and the only thin section from sub-type 1 (reference sub-type).

The above explanations can be linked to the changes in the microstructure of weak and strong minerals, respectively. The first part is related to the cleavage activation in the weak minerals. This is illustrated by analysing a sample, whereby the loading is stopped just prior to the second part (see Figure 5.2). A sample (from sub-type 2) with a diameter of 49.4 mm and thickness of 19.0 mm is prepared and tested under Brazilian test conditions, with an inclination angle of 70°. The conditions of this sample are similar to the other 17 tested

samples (presented in Table 3.4). A thin section from the central part of the sample in the direction of loading is prepared and investigated under the microscope. The microscopic results of mentioned sample from sub-type 2 are compared to the results of the samples whereby loading is stopped (close to the ultimate strength) just prior to the macro-fracture.

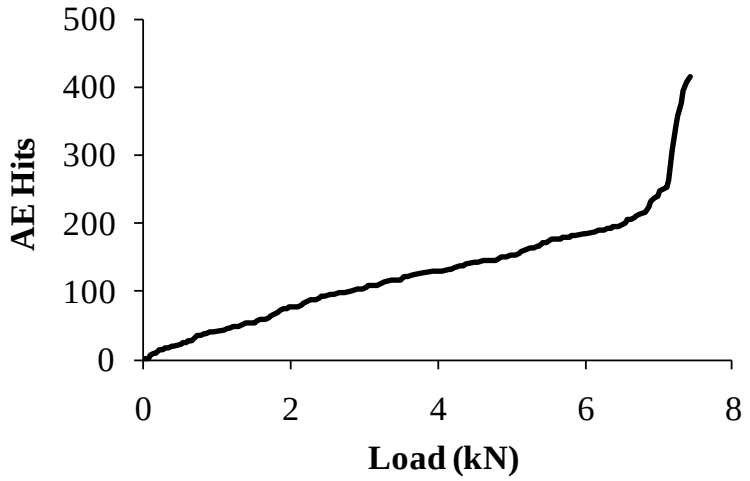

Figure 5.2 Cumulative AE hits as a function of applied load for Modave sandstone sub-type 2. Loading the sample is stopped prior to the beginning of the second part. The displacement rate is 0.2 mm/min.

5.1.2 Activated cleavages in carbonate grains

Carbonate grains with the activated cleavages are observed by petrographical microscope. Figure 5.3 presents the number of carbonates with activated cleavages for Modave sandstone sub-types 1-4, after Brazilian tests (close to ultimate strength). The number of carbonates with activated cleavages for sandstone sub-types 1, 2, 4 and 3 is 21, 18, 15 and 5 grains, respectively. The observed carbonate percentage for these four sub-types of Modave sandstone from maximum to minimum percentage is exactly in the same order. It can be concluded that more carbonates with activated cleavages exist in the sandstone sub-types with higher carbonate content. Carbonate minerals in comparison to quartz grains fail at lower stress state. Therefore before the final failure of samples the carbonate minerals are already fractured. It means that for higher carbonate content, the number of fractured carbonates in a lower stress state increases and consequently causes a higher perturbation in the shape of the accumulative AE hits curve.

Above explanations are validated by the result of a sample from sub-type 2 whereby the loading is stopped roughly at half of the sample ultimate strength. The number of carbonates with activated cleavages of mentioned sample is also presented in Figure 5.3. It is interesting to compare the fractured carbonates in the two samples from sandstone sub-type 2. For one of them loading is stopped roughly at half of the sample ultimate strength (17 fractured carbonates) and for the other one loading is continued and stopped, just prior to the macro-failure (18 fractured carbonates). The similarity in the number of carbonates with activated cleavages for the mentioned two samples shows that the carbonates fracture in the first half of sample loading (see Figure 5.3).

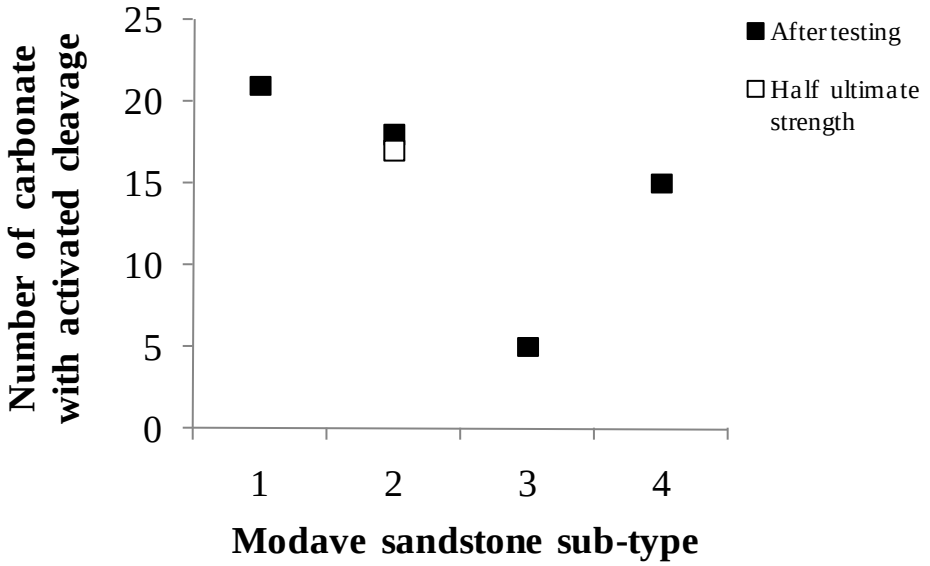

Figure 5.3 The number of carbonates with activated cleavages for Modave sandstone sub-types 1-4, after Brazilian tests (close to ultimate strength). Also a sample from sub-type 2 whereby loading is stopped roughly at half of the sample strength is presented. Inclination angle for all samples is 70°.

When a carbonate grain with the activated cleavages is observed, the orientation of them is also recorded. Figure 5.4 presents the carbonate grains with the activated cleavages (cracked carbonate) as a function of their orientations for sandstone sub-types 1 to 4. This figure shows that the activated cleavage inclination of different cracked carbonate grains are scattered all over the range of inclination angles from 0° to 180°. Even for sandstone sub-type 1 which is failed through an activated layer boundary, a preferential inclination of activated cleavages is not observed. The reason can be explained by fracture observation at macro-scale and its differences at micro-scale. At macro-scale observation an activated layer boundary is a straight line, while at micro-scale observation it can be a combination of several zigzag or fragmented lines that each part has an inclination angle independent of other parts.
By visual inspection, the fracture in reference sample is a straight line parallel to the layer direction (bedding). Figure 5.5 shows a microscopic view of a small part of the fracture in the reference sub-type. At microscopic observation, this part of the fracture is neither straight nor parallel to the layer direction and even shows a zigzag form in the carbonate grain which is not in contradiction of layer activation of this sample. The fracture in passing through the carbonate mineral is combined of several cracks with different directions. However, at a larger scale the fracture can have a single direction, different from the mentioned local directions. Furthermore, when two layer boundaries are partially activated, the connection of them cannot be parallel to the layer boundaries.

For sandstone sub-type 3 only five carbonate grains with activated cleavages are observed. Figure 5.4 shows that in sandstone sub-type 3, the inclination angle of activated cleavage plane in four carbonate grains is about 159°. The fifth activated cleavage plane has an inclination angle of 49°. The difference between the inclination angles of these two sets is 110°. It is interesting to mention that rhombohedral cleavage angle in carbonate grain is about 105° (Klein and Hurlbut 1993) which is comparable to mentioned difference. However, it is important to note that in this study the projection of activated cleavages on thin section plane is considered and orientation of carbonate grain in three dimensions is not studied.

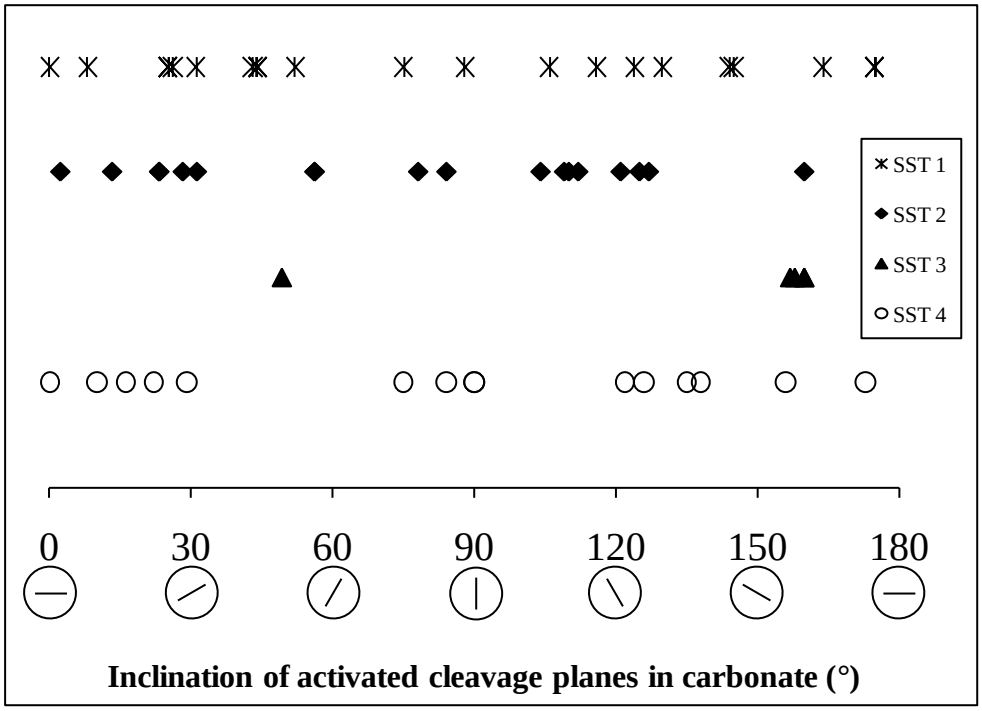

Figure 5.4 Carbonate grains with activated cleavages (cracked carbonate) for Modave sandstone sub-types (SST) 1-4. They are sorted as a function of their activated cleavage inclination. In these diametrical compression tests loading direction is 90° and layer orientation is 70°. The number of carbonates with activated cleavages for sandstone sub-types 1, 2, 3 and 4 is 21, 18, 5 and 15 grains, respectively.

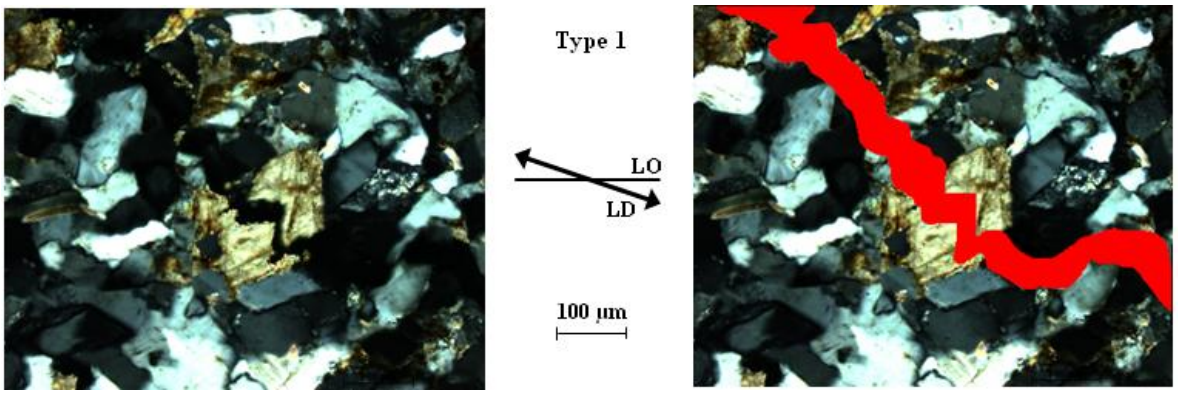

Figure 5.5 A part of a fracture in sandstone sub-type 1 (reference sample). The fractured area of the left micrograph is shown by red scale in the right picture. Carbonate grain is in the centre of the micrograph and fracture passes through this grain in a zigzag format. In this sample crack coalescence and initiation of macro-scale failure occurs and fortunately sample loading is stopped few milliseconds prior to splitting. LO = Layer orientation, LD = Loading direction. Pixel resolution is 0.27 µm.

Observed carbonate percentage and hence the amount of carbonates with activated cleavages (cracked carbonates) in the different sub-types of Modave sandstone are important in their failure behaviour. However, the orientation of activated cleavages in carbonate grains is not representative of the fracture pattern in macro-scale observation.

5.1.3 Micro-cracks in quartz grains

When a micro-crack in a quartz grain is observed, its orientation is also measured. The micro-cracks in quartz grains are searched through 12 rows in the thin sections. The results are presented on the left side of Figure 5.6. In the mentioned graphs all the quartz grains with intergranular crack(s) are presented as a function of their crack orientations for Modave sandstone sub-types 1 to 4. These graphs are summarized as the number of cracked quartz grain for successive intervals of 10 degrees (Figure 5.6, right).

The inclination of micro-cracks in quartz grains are scattered over all inclination angles between 0° and 180°. If the loaded sample would be a single crystal without any cleavages or preferential direction, one would expect a crack inclination around 90°. If that crystal would have several planes of weakness (transversely isotropic) with the orientation of 70° (the same as orientation of layer boundaries in the loaded samples), one would expect that crack inclination is 70°. However, by considering all the graphs of Figure 5.6, it can be observed that the quartz crack orientation is less frequent in the ranges around 70°.
In sandstone sub-types 1, 2 and 3 the crack frequency in the inclination range around 70° is obviously less than the other inclination angles. The graphs correspond to sandstone sub-type 3 in Figure 5.6 show that the cracked quartz grains with horizontal and semi-horizontal cracks are more frequent in comparison to other crack inclination angles.
The layer orientation in these tested samples is 70°. In this direction weak minerals such as mica are more frequent. Therefore, in this direction loading energy can fracture weak minerals much easier than quartz grains. This is why cracks in quartz grains which need much higher energy to induce, are less frequent in this direction.

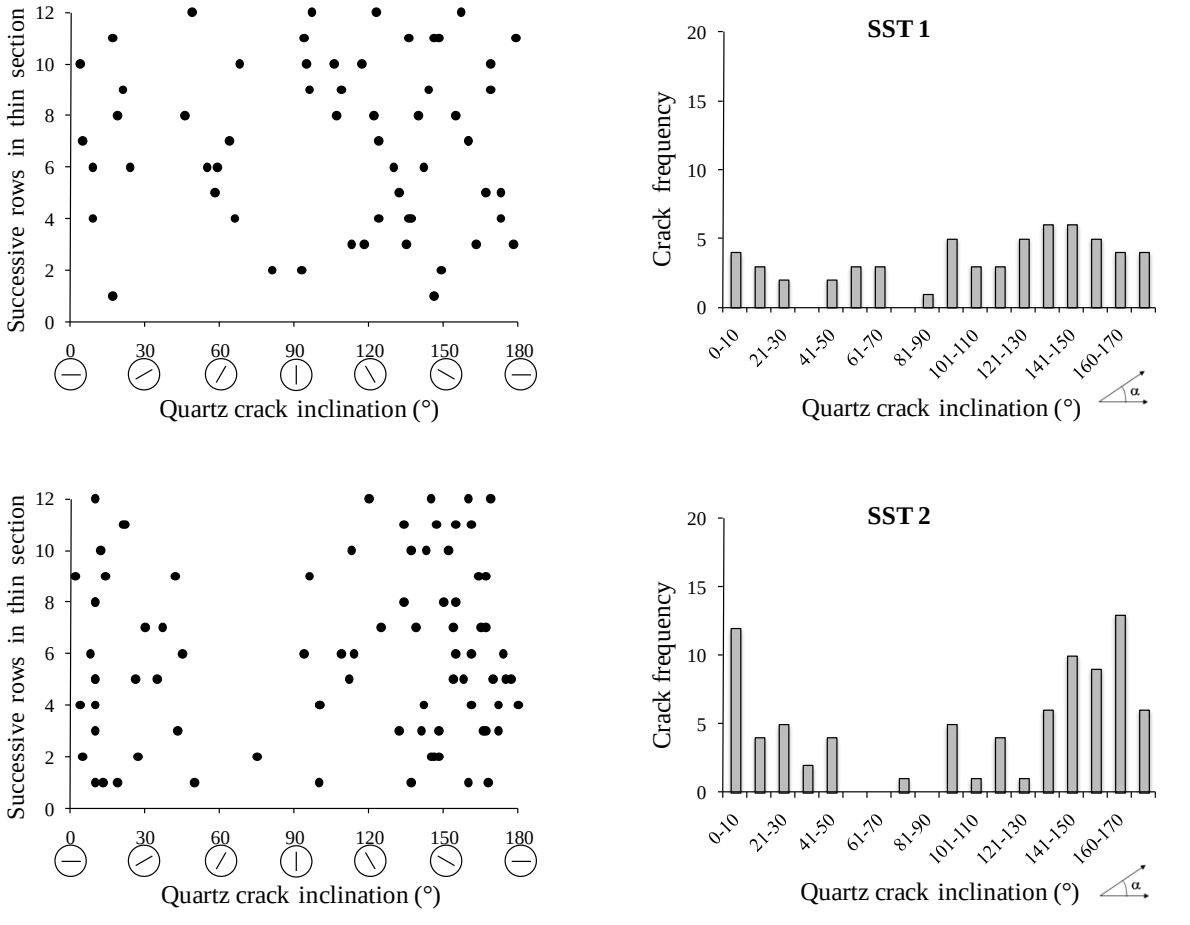

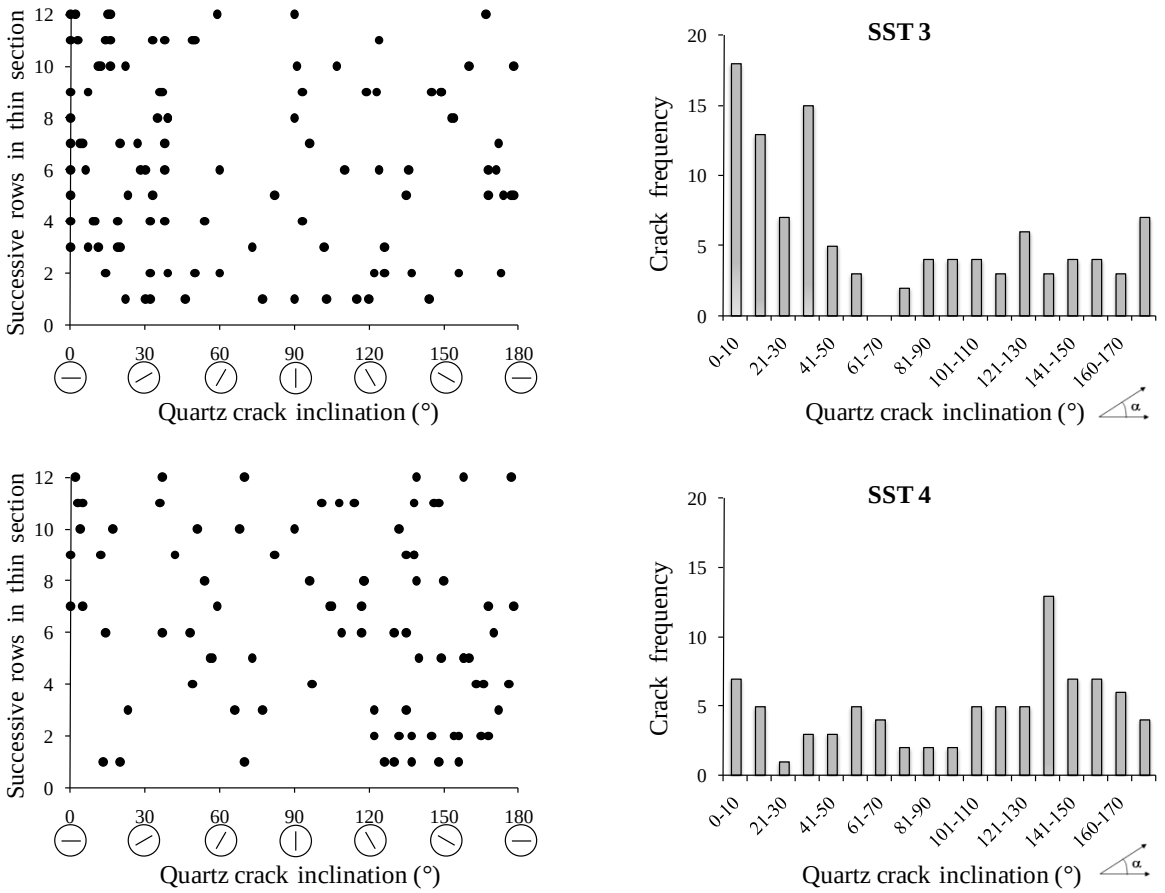

Figure 5.6 Quartz grains with intragranular crack as a function of their crack inclination for Modave sandstone sub-types (SST) 1-4. The graphs in the left side present the micro-cracks in quartz grains which are searched in the thin sections through 12 rows. The graphs in the right side present the crack frequency as a function of crack inclination. Right side graphs are the summary of the left side graphs. In these diametrical compression tests loading direction is 90° and layer orientation is 70°.

The number of quartz with intragranular cracks for sandstone sub-types 3, 4, 2 and 1 is 105, 86, 83 and 59 grains, respectively. Figure 5.7 presents the number of observed fractured quartz grains in the sandstone sub-types 1 to 4, before and after the tests. The number of pre-existing micro-cracks in quartz grains of different sub-types of studied sandstone is relatively similar. However, after the test significantly more micro-cracks in quartz grains are observed for all sub-types.

In Figure 5.7 the number of observed fractured quartz grains in the sample of sandstone sub-type 2 whereby loading is stopped roughly at half of the sample ultimate strength is also presented. In that sample 41 quartz grains with intracrystalline cracks are observed. In the mentioned sample the number of quartz grains with intragranular cracks (41) is more close to the number of pre-existing cracks (20) rather than the induced cracks (83). In the sample from sandstone sub-type 2 whereby loading is stopped, just prior to the macro-failure 83 quartz grains with intracrystalline cracks are observed. The difference between the numbers of quartz grain with intragranular cracks in an untested sample (pre-existing cracks) and a tested sample of sub-type 2 whereby loading is stopped, just prior to macro-failure can be considered as the induced cracks due to the loading under Brazilian test condition. In this case 63 fractured quartz grains are considered. Therefore it can be concluded that one-third of the fractured quartz grains occur in the first half of loading and the other two-third of them occur in the second half of sample loading. In other words it shows that quartz fracturing needs more energy which is achieved in the second half of the sample loading.

Figure 5.7 shows also significant differences in quantities of fractured quartz grains in the tested samples of different sub-types. Maximum and minimum numbers of fractured quartz grains correspond to sandstone sub-types 3 and 1, respectively. Sandstone sub-type 3 has the highest percentage of quartz content (88.2%), while sub-type 1 has the lowest percentage of quartz content (63.3%). Also it is interesting to note that sub-type 3 has the largest quartz grains size (107 μm) and presents the highest Brazilian tensile strength (14.5 MPa). Furthermore, the observed quartz percentage for Modave sandstone sub-types from maximum to minimum percentage are sub-types 3, 4, 2 and 1, respectively. It is interesting to note that in these four sub-types of sandstone as shown in Figure 5.7, the number of cracked quartz grains from maximum to minimum percentage is exactly in the same order.

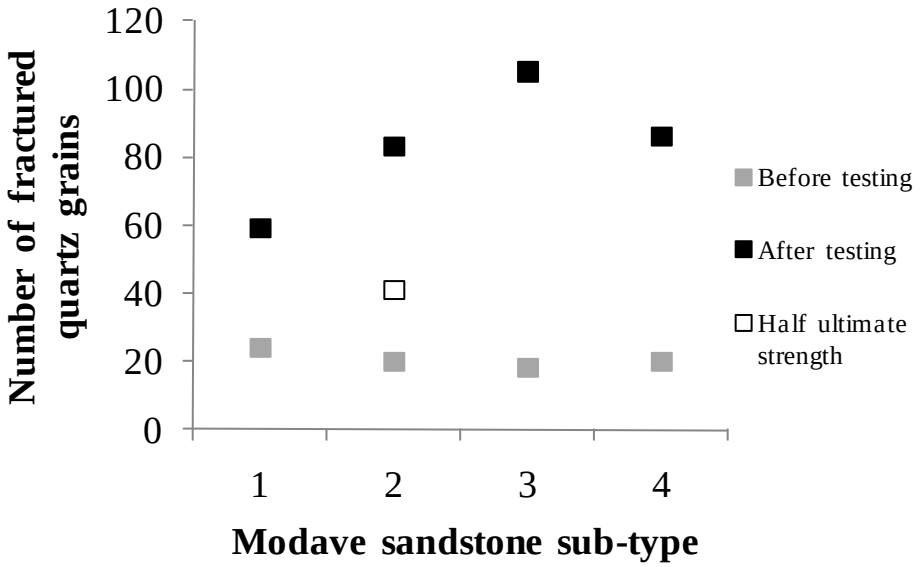

Figure 5.7 The number of observed fractured (intragranular cracks) quartz grains for sandstone sub-types 1-4, before and after (close to ultimate strength) Brazilian tests. The result of a sample from sub-type 2 that loading is stopped roughly at half of the sample ultimate strength is also presented. Inclination angle for all samples is 70°.

It is also observed from Figure 5.7 that the minimum difference of number of fractured quartz grains before and after the test, belongs to the reference sub-type. Sandstone sub-type 1 has the minimum percentage of quartz content (63.3%) and consequently a larger part of applied load (in comparison to the other sub-types) can be distributed on other grains. Therefore the least fractured quartz grains are observed.

During the detection of the micro-cracks in quartz grains, sometimes few dots in the quartz grains are observed (see Figure 5.8). These are inclusions. In mineralogy, an inclusion is any material that is trapped inside a mineral during its formation. Inclusions are usually other minerals or rocks, but may also be liquid or gas. Liquid or gas inclusions are known as fluid inclusions. Fluid inclusions are microscopic bubbles of liquid and gas that are trapped within crystals. Generally from a liquid or aqueous medium, minerals form. Therefore tiny blebs of that liquid can become trapped within the crystal structure or in healed fractures within a crystal. Because of the nature of inclusions, they may be considered as the weak points which is not the case, as the inclusions are very small in all three dimensions. It is important to note that although layer boundary is presented as a line in thin section observation, in three dimensions it is a plane and this plane of weakness affect the fracture pattern.

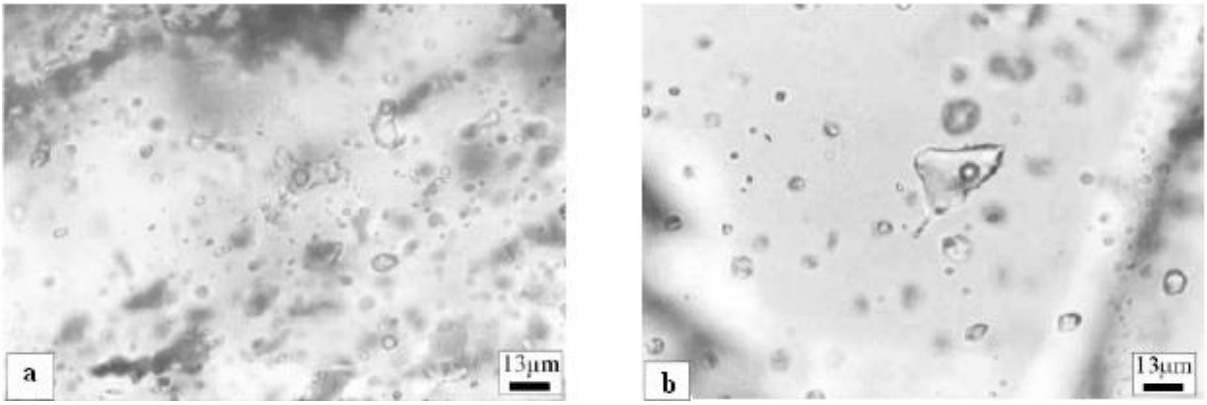

Figure 5.8 Inclusions in the quartz grain (Dewaele et al. 2004). a) Detail of the primary fluid inclusions. In the Marcq area in Anglo-Brabant fold belt (after De Vos et al. 1993), primary inclusions are clearly defined in quartz growth zones. b) Detail of the fluid inclusions in the vein quartz at Quenast. In the post-compressive quartz veins, only secondary inclusions have been identified.

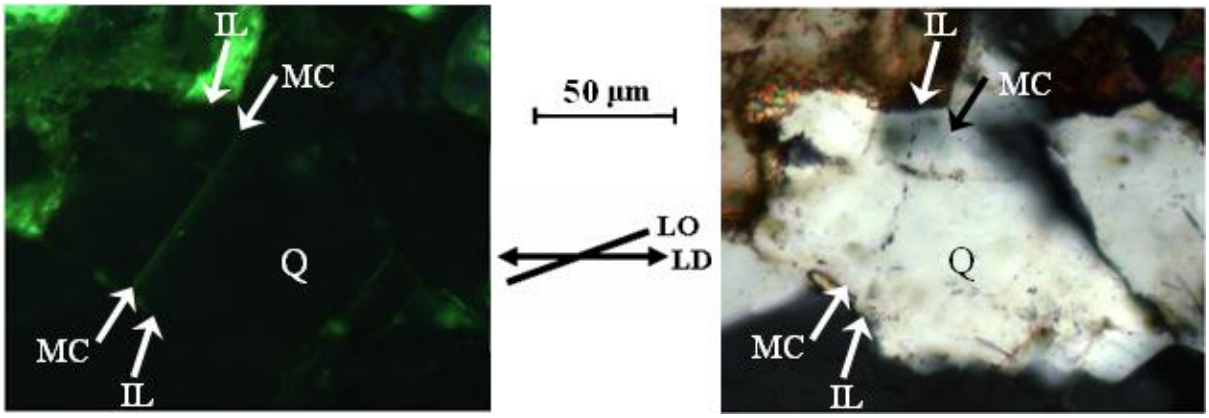

Figure 5.9 Micro-crack and inclusions in quartz grain of Modave sandstone sub-type 3 (left: incident fluorescent light; right: transmitted polarized light) [Q = Quartz grain, MC = Micro-crack, IL = Inclusion line, LO = Layer orientation, LD = Loading direction. Pixel resolution is 0.27 µm].
The sharp line of penetrated resin in the left micrograph is a micro-crack. In the right micrograph the inclusions are visible and they do not show any effect on the cracked quartz grain.

In the micrographs of Figure 5.9 (right photo) the inclusions are aligned and they form a line from one side of the quartz grain to the other side. However, they do not play the role of weak direction. An induced crack which is observed in the mentioned grain (left photo in Figure 5.9), is near the inclusion line but not in that direction. In other words, influence of the inclusion line is not observed in that cracked quartz grain.

Rock can be represented as a heterogeneous material composed of cemented grains. Therefore some of the complexities of load distribution among the grains are due to their differences in deformability and strength of the grains and the cement, grain size, grain shape, grain packing, degree of cementation (i.e. how much of the intergrain space is filled with cement) and the way in which they are connected to each other. All of these items influence the mechanical behaviour of rock materials. Both in the laboratory and in situ, fracturing of rock is due to many complicated microscopic processes. Experimental observations reveal that most of the induced cracks nucleate at initial defects, such as grain boundaries or crack and cavities. The micro-mechanism responsible for the formation of these cracks is not fully understood. However, many models exist that can reproduce some features of the brittle failure phenomena (Potyondy and Cundall 2004, Yuang and Harrison 2006).

In this study it is observed that a sharp end of a grain (corner) in load transferring can produce an enormous stress. This stress concentration can be the reason for the induced crack in the neighbouring grain (see Figure 5.10). The induced crack can have different orientations depending on the configuration of the neighbouring grains. Micro-crack direction in the quartz grain presented in Figure 5.10 is in the direction of one of the boundaries which are highlighted with white lines. As it can be seen in this figure, micro-crack orientation in this quartz grain is not the same as layer orientation or loading direction. Therefore mentioned micro-crack illustrates the importance of the pattern of grain locations and also the importance of the way that they are connected to each other.

The following two simplified models which are presented in Figure 5.11 show that the crack orientation can have the extreme values of 0° (= 180°) and 90°. Consequently the crack orientation between these extreme values is also probable.

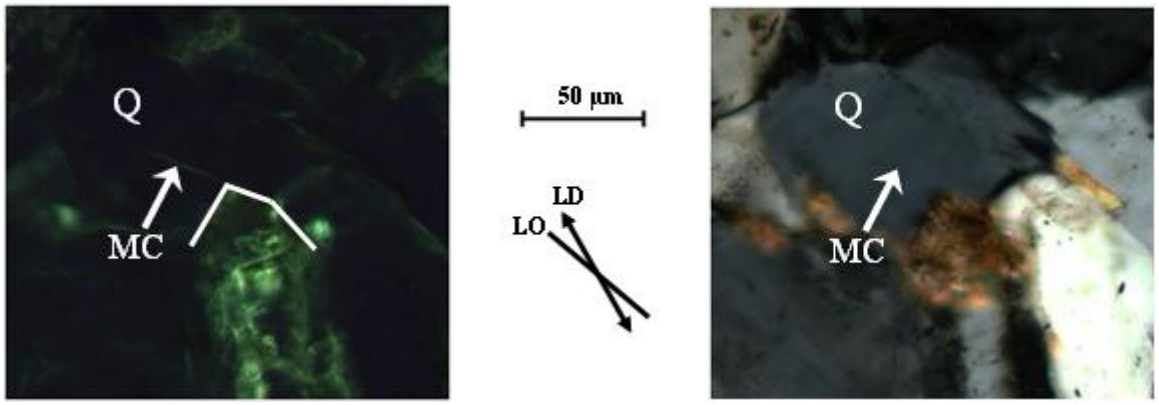

Figure 5.10 Induced micro-crack in quartz grain as a result of stress concentration at the corner of neighbouring grain in sandstone sub-type 1 (left: incident fluorescent light; right: transmitted polarized light) [Q = Quartz grain, MC = Micro-crack, LO = Layer orientation, LD = Loading direction. Pixel resolution is 0.27 µm].
The boundaries of the grain below the quartz grain are highlighted by the white lines. The micro-crack is in the direction of a boundary. This micro-crack shows that the way the grains are connected to each other is important.

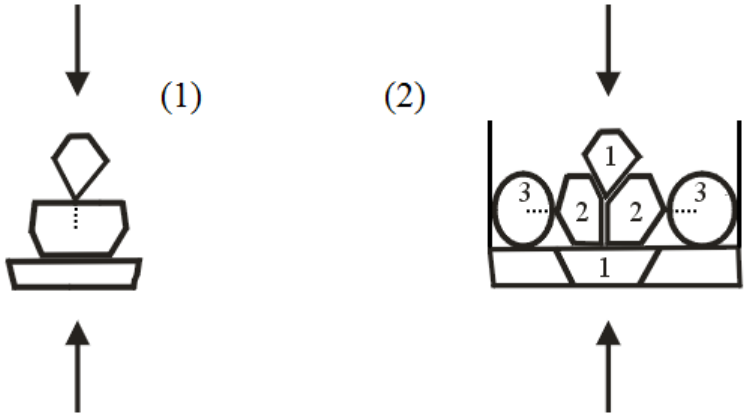

Figure 5.11 Illustrating the dependency of induced crack orientation on the grains configuration by two simplified models. All the induced cracks (pointed lines) are due to the point loading and stress concentration. In the first model loading axis and induced crack are in the same direction. In the second model induced crack direction is perpendicular to the loading axis.

In the first model all the three grains are in vertical direction. The induced crack in the middle grain by tension is the result of stress concentration which is produced by the sharp corner of the upper grain. The orientation of this crack is in the direction of the external loading (90°). In the second model the grains 1 are in compression. These two grains open the planar contact of the grains 2. Therefore in this configuration mentioned crack is induced due to tension. Consequently the two grains 2 move to the sides and stress concentration is made at their sharp ends. These point loads of the grains 2, along their direction induce two cracks in the grains 3 by tension. The orientation of the induced cracks in the grains 3 (0°) is perpendicular to the external loading direction (90°). It is important to note that in the first model presented in Figure 5.11, the induced crack is considered and counted, where in the second model only the horizontal cracks are considered and the vertical crack which occurs in the planar contact bond is not taken into account. As already mentioned (for in Figure 5.6), only the intragranular cracks in the quartz grains are considered.

Kemeny (1991) asserts that although the actual growth of cracks under compression may be due to many complex mechanisms, as revealed by laboratory tests, it appears that they can all be approximated by the crack with a central point load. The results of these "point" loads in rock under compression are small regions of tension that develop in the direction of the least principal stress. The idea of the presented models in Figure 5.11 is initiated from the research of Potyondy and Cundall (2004). They introduced a mechanism for the formation of compression-induced tensile cracks as shown in Figure 5.12c, in which a group of four circular particles is forced apart by axial load, causing the restraining bond to experience tension (Cundall et al. 1996). These axially aligned "micro-cracks" occur during the early loading stages of compression tests on bonded assemblies of circular or spherical particles. Potyondy and Cundall (2004) also introduced similar crack-inducing mechanisms even when different conceptual models for rock microstructure are used. For example, ''wedges'' and ''staircases'' also induce local tension if angular grains replace circular grains as presented in Figure 5.12a and b. Most of the models that reproduce essential features of the brittle failure phenomena are governed by tensile induced cracks. As an example, one of the interesting features of the program code PFC^{2D} (Particle Flow Code) is the ability to simulate compression-induced tensile cracks (Itasca 2004, Yuang and Harrison 2006).

Figure 5.13 presents the number of observed fractured quartz grains (with intragranular crack) for Modave sandstone sub-types 1 to 4, before and after loading as a function of their crack orientation. This figure is presented for successive intervals of 10 degrees of crack orientations. Any remarkable correlation between pre-existing and induced micro cracks as a function of crack inclination is not observed for all sub-types of Modave sandstone. Figure 5.13 shows that for sandstone sub-types 2, 3 and 4, quartz grains with pre-existing micro-cracks in comparison to quartz grains with induced micro-cracks are least pronounced (nearly for the entire range of crack orientations). However, in sandstone sub-type 1, pre-existing micro-cracks are more pronounced.

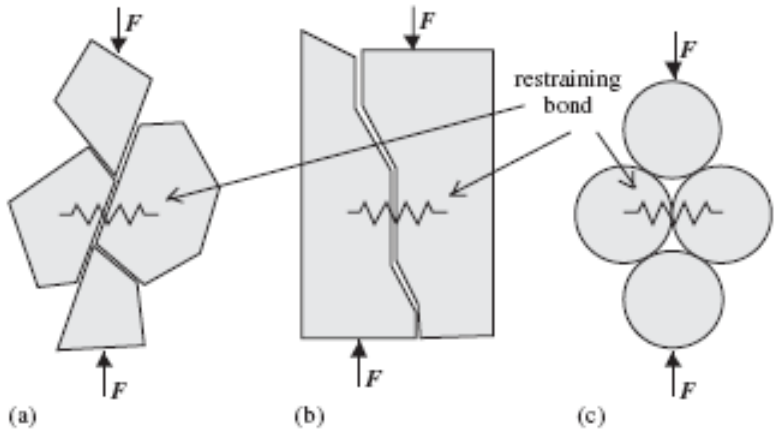

Figure 5.12 Physical mechanisms for compression-induced tensile cracking (a and b) and idealisation as a bonded assembly of circular particles (c) (Potyondy and Cundall 2004).

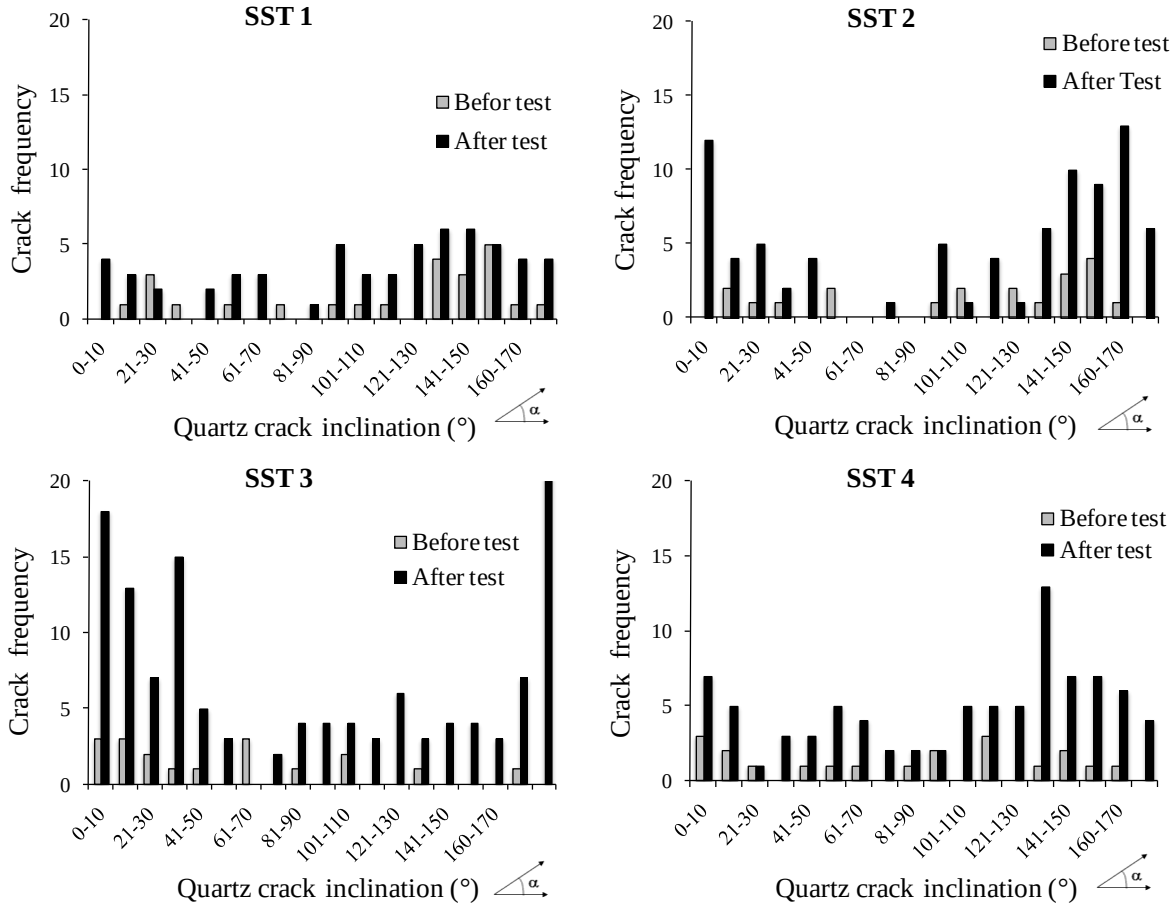

Figure 5.13 Quartz grains with an intragranular crack as a function of their crack inclination for Modave sandstone sub-types (SST) 1-4 before and after Brazilian tests. For the loaded samples loading direction is 90° and for all the samples layer orientation is 70°.

5.2 Micro-scale quantification of failed samples (macro-fractures)

Brittle fracturing of these sub-types of sandstone is often dynamic and violent with large amounts of energy being released. Therefore, when a macro-fracture occurs, displacements of the fractured parts of the sample are inevitable. The displacement (crack width) makes it difficult or even impossible to recognize what does happen at micro-scale. Although, it is complicated and difficult to clarify the fracture growth procedure at micro-scale (because of the macro-crack occurrence in the fractured samples) effort has been made to extract some information concerned its behaviour. In this paragraph five examples are introduced. For the examples of 1 to 3, the sandstone sample of the reference sub-type which is already mentioned as the exception in the tested samples is considered. For the tested sample of sub-type 1 final failure has occurred but it does not split and therefore the cracks width is limited. For the examples 4 and 5, the sandstone sample of sub-type 2 is considered. It is tried to get some detail information from these tested samples.

Example 1
A fracture encountering a quartz grain, behaves differently depending on the quartz grain size. In the microscopic investigation it is observed that mostly a fracture deflects or splits on the grain boundaries of a quartz grain. A relatively large quartz grain deflects the fracture whereby fracture direction before and after the large quartz grain is different. While a fracture after passing through the grain boundary around a relatively small quartz grain continues along the same line. When a fracture in a layer boundary deflects due to a small quartz grain, it returns to the layer boundary in order to dissipate less energy for growing. However, fracture deflection in the case of a relatively large quartz grain tends to grow in a new direction with less energy (He and Hutchinson 1989) and consequently the fracture length corresponding to layer activation decreases. Figure 5.14 shows how a fracture line passes along the boundaries of a small quartz grain. In this figure the fracture line before and after the small quartz grain continues in the same direction (roughly parallel to the loading direction). It shows that grain size can have an influence on the fracture pattern.

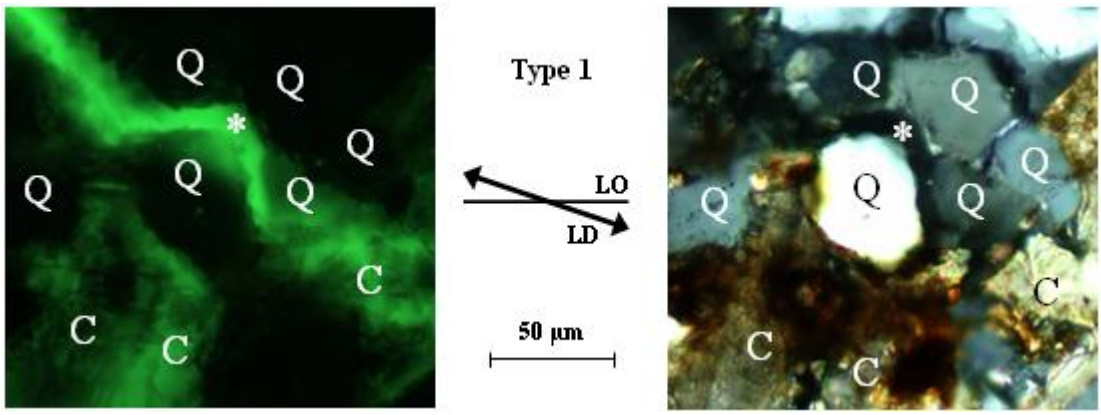

Figure 5.14 A view of a crack line encountering a small quartz grain in the fractured sample of sandstone sub-type 1 (left: incident fluorescent light; right: transmitted polarized light) [Q = Quartz grain, C = Carbonate, LO = Layer orientation, LD = Loading direction. Pixel resolution is 0.27 µm]. Fracture which is filled by resin looks light in the left picture and dark in the right picture.
The fracture encounters a small quartz grain and passes through its boundaries. The fracture before and after the small quartz grain continues along the same line. The fracture opens the planar and interpenetrating contacts of the small quartz grain with the three neighbouring quartz grains. The interpenetrating contact is indicated by a white star.

Example 2

Figure 5.15 shows a large view of crack propagation in the failed sample of sandstone sub-type 1. In this figure two layers which are partially activated are shown. In this figure the crack propagation is described from the right to the left side of the micrograph (which is not necessary the direction of fracture growth). Detail a shows that the micas aligned in the lower layer boundary are activated; however, it is not the main fracture (the crack width from the right to the left side of the micrograph decreases). The width of penetrated resin is representative of the crack width. The fracture in this part is going to disappear (see the left side of Figure 5.15). In detail a of Figure 5.15, comparing the crack width of the lower activated layer on the left side (6 μm) with the right side (52 μm) illustrates that the continuation of lower activated layer (to the left side) is not the main fracture line. It is also interesting to note that, crack width of upper activated layer is also about 52 μm.

In detail a of Figure 5.15, it becomes more visible that the lower activated layer on the left side of the micrograph is composed of several mica minerals which are indicated by white points. Although the energy of applied stress causes the main fracture toward the upper layer (in the photo), the planar contacts of mica with quartz grains in the lower layer are enough weak to be activated. Contact of mica with other minerals (similar to itself) is weak in strength and can be activated (opened) easily.

It is important to note that although the quartz grains have a high strength, they can also be fractured. In detail a in the main upper fracture line, two parts of a fractured quartz grain are observed and they are indicated by two white arrows.

In detail b the fracture encounters a quartz grain. The quartz grain as a strong mineral resists fracturing and splits the fracture on the grain boundaries (see point 1). At the left side of point 2 in detail b, the mica and carbonate minerals which are aligned in the (direction of) layer boundary, are fractured. As they are weak in strength, they are fractured easily. By these fractures, the activation of lower layer in Figure 5.15 is continued, however it is not the main fracture. This part after fracturing of several carbonate minerals encounters a quartz grain in point 3 (see detail a and c in Figure 5.15). The fracture due to the high strength of quartz grain splits on quartz grain boundaries (see the white arrows in detail c of Figure 5.15). The lower crack in point 3 fractures the carbonate mineral and passes through it but the upper crack opens the interpenetrating contact of two quartz grains (this contact is indicated by a white star in detail c). Mentioned detail clearly illustrates the difference of grain strength in quartz and carbonate. As can be seen in detail c of Figure 5.15, the quartz grain is not fractured by the main crack, while a (smaller) part of that splits the carbonate mineral. Also mentioned detail shows that for the quartz grains, even an interpenetrating contact has less strength than the quartz grain itself and can be activated.

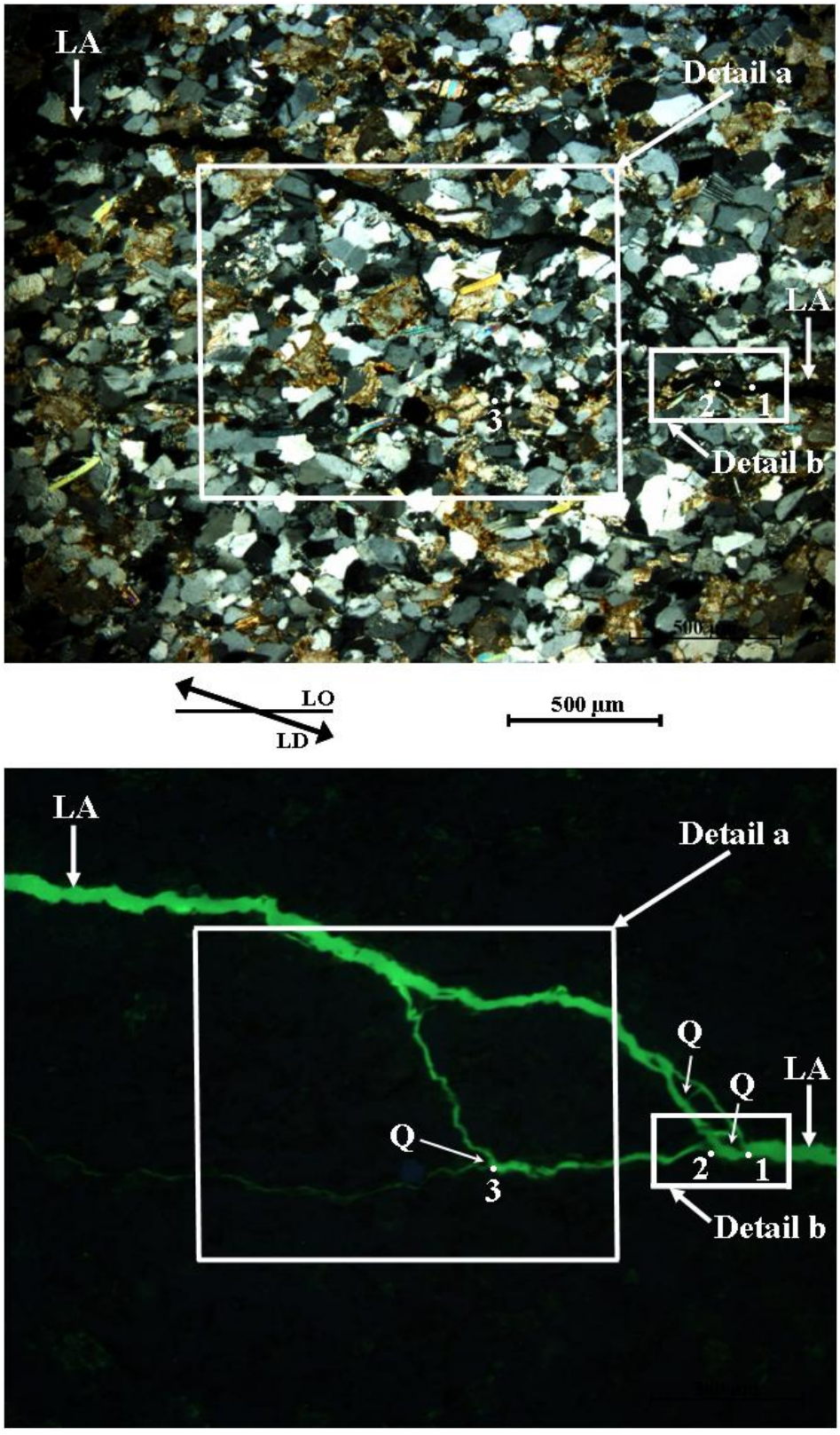

(See Figure 5.15 on the next page)

Detail a

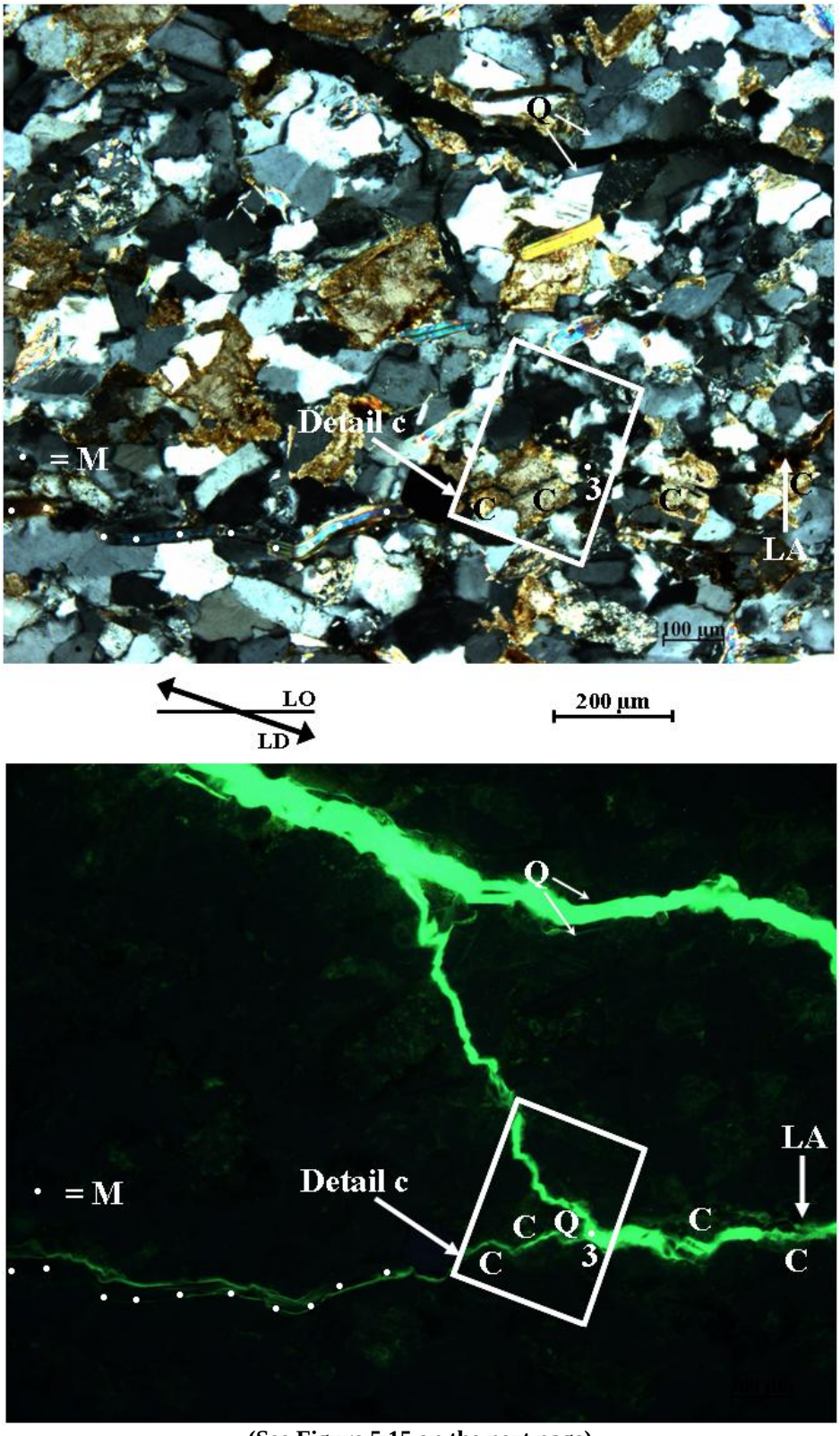

(See Figure 5.15 on the next page)

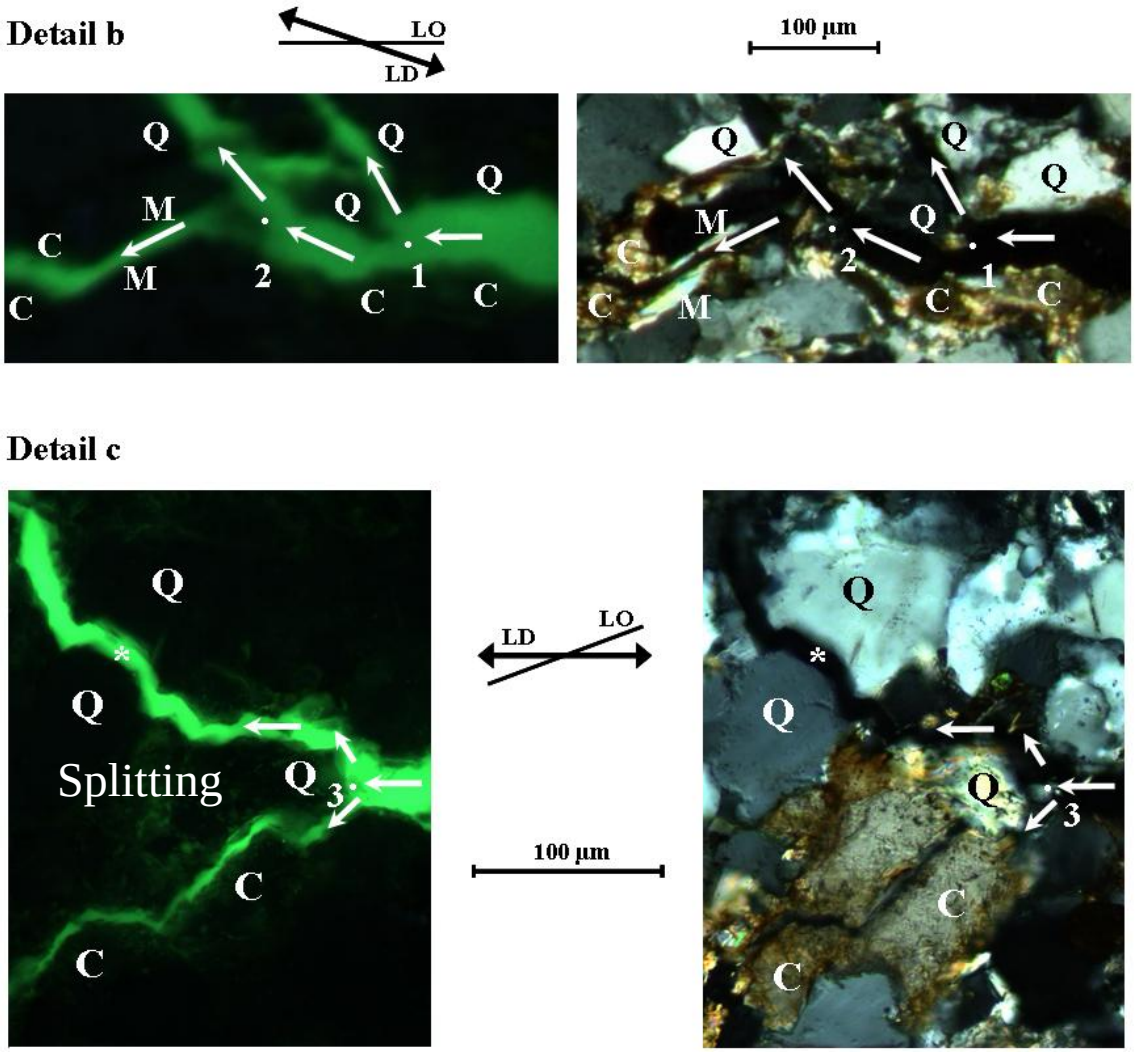

Figure 5.15 A large view of crack propagation in the fractured sample of sandstone sub-type 1 (top: transmitted polarized light; bottom: incident fluorescent light) [Q = Quartz grain, M = Mica, C = Carbonate, LO = Layer orientation, LD = Loading direction, LA = Layer activation]. These micrographs show two layers which are partially activated. Pixel resolution is 1.06 µm.
Detail a) Magnified area of lower activated layer. Mica minerals are indicated by white spots. Two parts of a fractured quartz grain are indicated by two white arrows. Pixel resolution is 0.53 µm.
Detail b) Magnified area, where the fracture encounters a quartz grain. Pixel resolution is 1.06 µm.
Detail c) Magnified fracture. The fracture encounters a quartz grain and splits on quartz grain boundaries. All the fractures are indicated by the white arrows. The lower part fractures the carbonate mineral but the upper part opens the interpenetrating contact of two quartz grains which is indicated by a white star. The micrographs of detail c are acquired after rotation of detail a at 20° counter-clockwise. As can be seen in detail a the two quartz grains and their opened interpenetrating contact are dark while in detail c they have different colour and can be easily recognized. Pixel resolution is 0.27 µm.

Example 3

Figure 5.16 presents the propagation of parallel cracks in the fractured sample of sandstone sub-type 1. In Figure 5.16 an interpenetrating contact of two quartz grains is opened in the main crack. The main crack to dissipate less energy for propagation locally changes its direction from a quartz grain to a contact of two quartz grains. Also in neighbouring of the main fractures, grain contacts can be opened. The other two cracks which are parallel to the main crack are mainly induced by opening the planar quartz to quartz and quartz to mica contacts. These parallel induced cracks can increase the final fracture length, where the applied stress does not need to be increased.

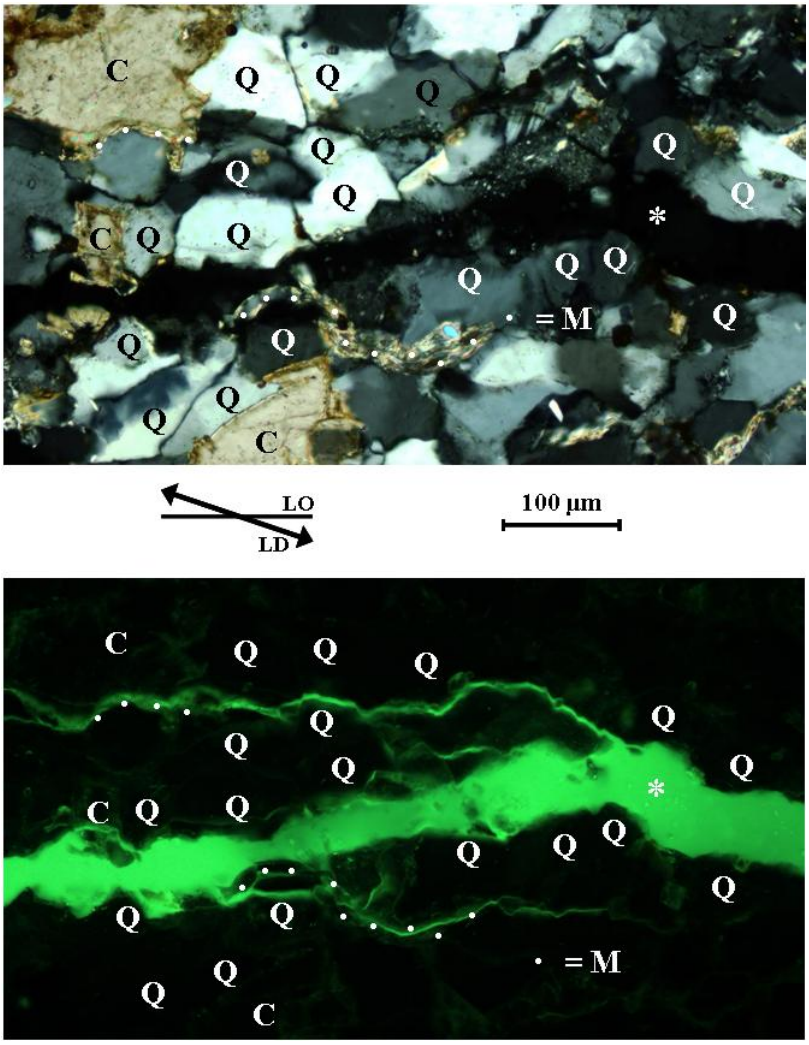

Figure 5.16 Parallel cracks propagation in the failed sample of sandstone sub-type 1 (top: transmitted polarized light; bottom: incident fluorescent light) [Q = Quartz grain, M = Mica, C = Carbonate, LO = Layer orientation, LD = Loading direction. Pixel resolution is 0.27 µm]. The micas are indicated by white spots. The main (middle) fracture at the right side of the micrograph opens an interpenetrating contact of two quartz grain which is indicated by a white star.

Example 4

Figure 5.17 presents a macro-crack in a failed sample. On both sides of the crack, weak minerals (carbonate and mica) are observed. It shows that it is easier for a crack to propagate through the weak minerals where it needs less energy to dissipate rather than through a quartz grain. Consequently the path of the macro-crack as it is shown in this photo is in the direction of mica's orientation. Therefore when the weak minerals are well aligned in a direction (see Figure 5.18) such as the layer boundaries, they have the potential for cracks to propagate through and along them. This direction of weakness is activated in Figure 5.17.

The cracks can be extended through the weak minerals or through the connection of them with quartz grains. Planar contacts of the weak minerals (carbonate and mica) with quartz grains can also be activated. For the quartz grains, the activation of the planar grain to grain contact is much easier than fracturing a quartz grain.

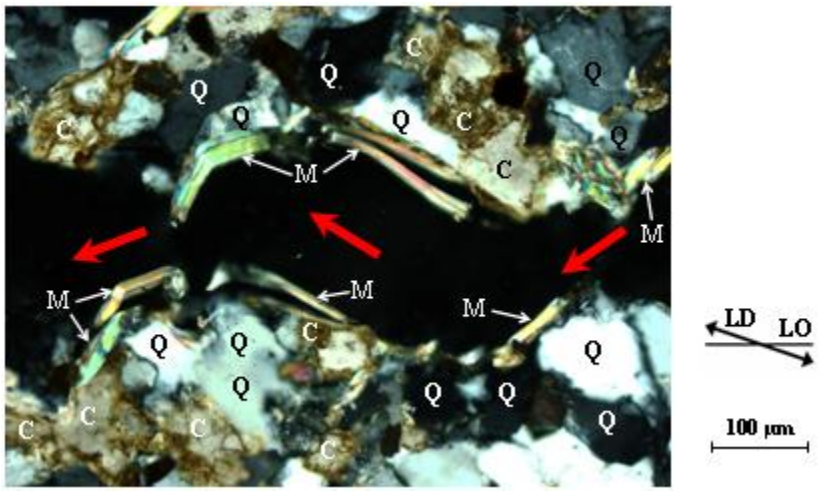

Figure 5.17 Micrograph of induced macro-crack in a failed sample [Q = Quartz, M = Mica, C = Carbonate, LO = Layer orientation, LD = Loading direction. Pixel resolution is 0.27 µm]. Dark wide macro-crack located in the middle of the micrograph is indicated by large arrows. The crack width is much larger than the grains size [sandstone sub-type 2].

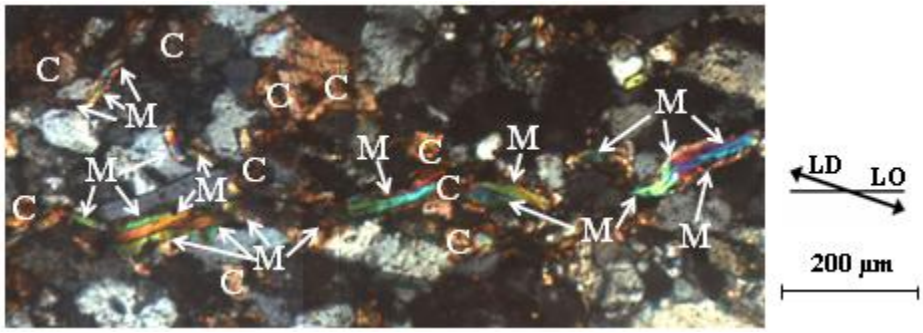

Figure 5.18 Weak minerals which are continuously aligned form a narrow strip of weakness in between the quartz grain. This micrograph is taken from a failed sample. The grains which are white, grey and dark grey are quartz [M = Mica, C = Carbonate, LO = Layer orientation, LD = Loading direction. Pixel resolution is 0.54 µm] [sandstone sub-type 2].

Example 5

Figure 5.19 presents a view of crack propagation in a failed sample. In this Figure the crack propagation is described from the right to the left side of the micrograph indicated by the grey lines. Entire shape of the presented macro-crack is aligned parallel to the layer orientation. The crack presented in Figure 5.19, first is divided into two cracks at the right side and finally these cracks join together at the left side of the micrograph (or vice versa, as the direction of the fracture growth is not monitored). The direction of these two cracks is also parallel to the layer orientation. Another crack parallel to the loading direction connects the two mentioned cracks. Therefore, the crack propagation produces two islands of grains in between the fractured area. The mentioned islands which are in the centre of the photos are explicitly presented in the Figure 5.19b which is acquired with incident fluorescent light.

At the right edge of the micrographs the carbonate grains are fractured. After that two quartz grains are observed at the top and the bottom of the crack. The shape of the two quartz grains at the border of the crack is rounded. Also the extinction colour of them is different in Figure 5.19a which is acquired with transmitted polarized light (upper quartz grain is white and the lower grain is grey). Therefore it can be concluded that the crack has opened its contact and they are not the two parts of a fractured quartz grain. After that the crack splits on the boundaries of a quartz grain. Fracturing the quartz grain needs lots of energy to dissipate.

Therefore, the crack chooses another way to propagate, in order to expend less energy. The crack is divided into two cracks and they are continuing the propagation at the boundaries of that quartz grain as can be seen in Figure 5.19a. The lower crack continues by opening the contacts of the grains up to the left side. The upper crack finds an easy way to continue. The crack has opened the planar mica to mica contact, and also the planar mica to quartz contact as can be seen in detail in Figure 5.19c. By observing this part of the fracture, it is interesting to note that the mica minerals locally change the orientation of the crack and cause a zigzag instead of a straight line. After that the crack line continues relatively parallel to the layer orientation and deflects on a quartz grain boundary to the bottom side. Finally the upper crack joins to the lower crack as shown it the left side of the micrographs.

In Figure 5.19 the two islands are mostly composed of the quartz grains. Between the islands two micas are observed (see the lower part of the detail in Figure 5.19c). These two micas form weak zones, which could be the reason for separation of the two islands of quartz grains. By observation of the micrograph in Figure 5.19b, even a small space which is filled by resin cannot be found in the two quartz islands. Because the planar contact of the two mentioned micas with quartz grains are activated and make the stress to relief between the two quartz islands. Therefore, the stress passes through the crack without pushing the quartz grains and their bonds in the two mentioned islands. Some of the conclusions from these micrographs can be summarized as follows:

- A quartz grain can split and even can deflect the fracture.
- A growing crack prefers to open the grain bonds (point contacts, planar contacts and even interpenetrating contacts) rather than fracturing the minerals.
- The fractures in order to dissipate less energy prefer to pass through a path with a higher amount of weak minerals.
- The weak minerals can locally change the direction of a fracture.

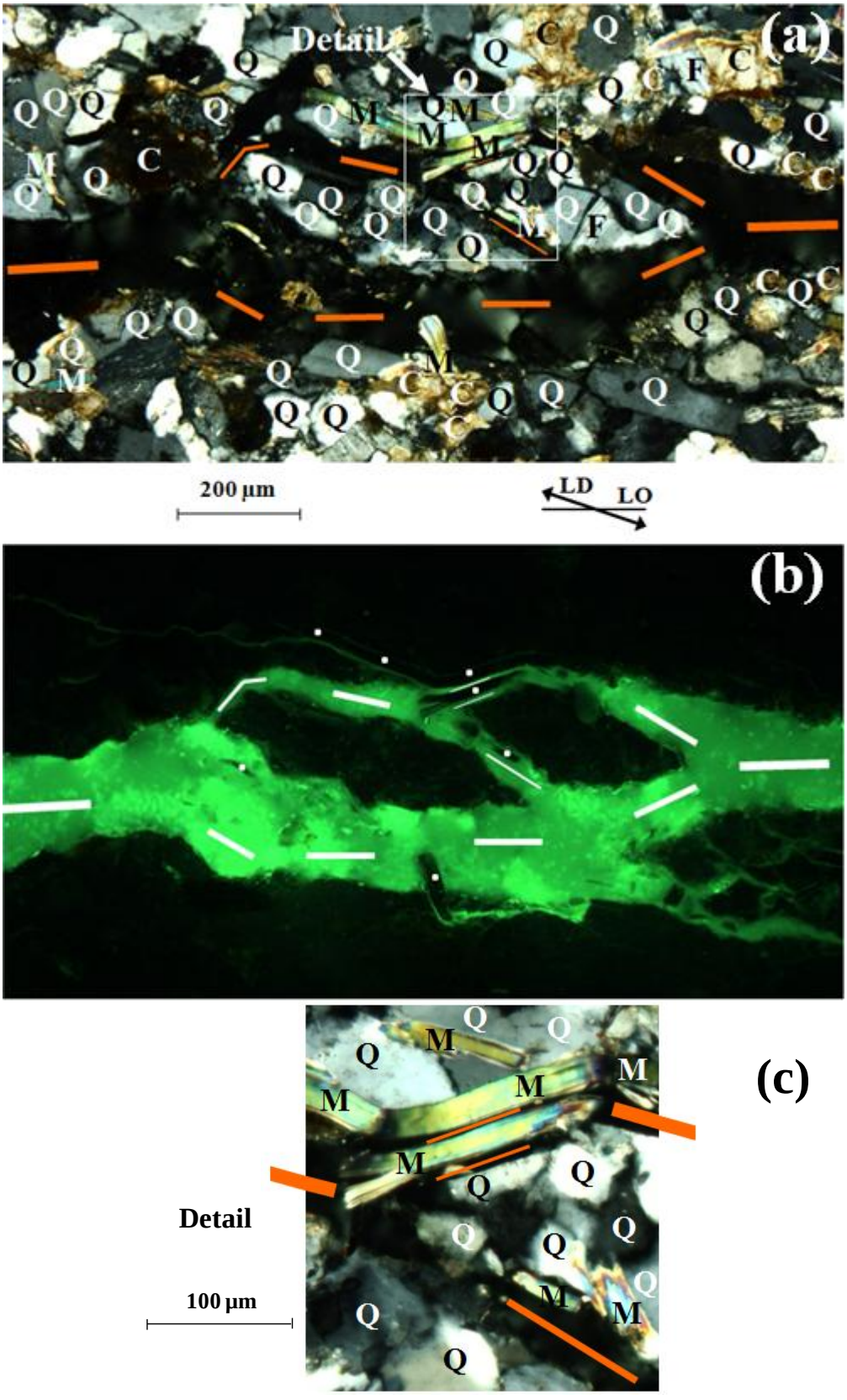

(See the caption of Figure 5.19 in the next page)

5.3 Overview of findings

By comparing the five sandstone sub-types which are macroscopically relatively similar, it is observed that their Brazilian tensile strength is different, but mainly that the fracture pattern is different.
Microstructure of rock is known to influence its macro-scale behaviour. As the thin sections of untested material show some micro-scale differences, petrographical analysis on thin sections of tested samples is done. As only sandstone sub-type 5 has second planes of weakness (ripples), most microscopic study focuses further on sandstone sub-types 1 to 4.
Thin sections are prepared from samples after a Brazilian test is completed, but also from samples which are just stopped prior to the final failure. On these thin sections petrographical analysis is done.

In micro-scale observation of non-failed samples, activated cleavages in carbonate grains and (induced) micro-cracks in quartz grain are quantified. In Modave sandstone sub-types 1 to 4 it is illustrated that the one with lower observed carbonate percentage has less cracked carbonate grains. It is also observed that maximum and minimum number of fractured quartz grains correspond to the sub-types with the highest and the lowest percentage of quartz content, respectively. Between the four sub-types of Modave sandstone, it is observed that as the quartz percentage is higher, more fractured quartz grains are observed, while higher strength is also achieved.

Inclination angles of the activated cleavages of carbonate grains and also of micro-cracks in quartz grains are scattered over all inclination angles between 0° and 180°. The grain contacts pattern is complicated and it is not easy to present the grain loading conditions as a function of the external loading. Therefore, the grain stress state becomes complicated. However, it is observed that the quartz crack orientation is less frequent in the ranges around layer orientation. Because in layer direction weak minerals such as mica are more frequent and loading energy can fracture them much easier than quartz grains.

Although it is complicated and difficult to observe the changes in microstructure of failed samples, some interesting conclusions from obtained micrographs are retrieved. It is observed that growing crack prefers to activate the grain contacts rather than fracturing the minerals. Activated (opened) contacts of point contacts, planar contacts and even interpenetrating contacts are observed in the fractured samples. The fractures prefer to grow through a path with a higher amount of weak minerals; however, the weak minerals locally change the direction of a fracture (it seems easier for the fractures to grow in order to dissipate less energy). Also it is observed that a fracture encountering a quartz grain changes its direction or splits on the boundaries of the quartz grain. Because the quartz grain as a strong mineral resists fracturing.

Figure 5.19 A view of crack propagation in the fractured sample of sandstone sub-type 2, [(a): transmitted polarized light; (b): incident fluorescent light)] [Q = Quartz grain, F = Feldspar, M = Mica, C = Carbonate, LO = Layer orientation, LD = Loading direction. Pixel resolution is 0.53 µm]. Dark wide macro-crack located over the entire length of the upper micrograph is indicated by large grey lines. The crack propagation is obviously clear in (photo) b. Also in this photo two islands of quartz grains are observed and the micas are indicated by white spots. The two lines on both sides of the detail c show the crack orientation before and after the mica minerals. These two crack orientations with the crack in mica locally make a small zigzag.

6 Effect of Micro-scale Parameters on Macro-scale Behaviour of Modave Sandstone

It this chapter, an attempt is made to find and explain the correlations between the micro-scale parameters and macro-scale behaviour of all sub-types of the studied Modave sandstone. The variability in strength and fracture patterns seems to be closely related to the changes in the mineral composition and microstructures of rock samples. Therefore, in the beginning of this chapter it is useful to summarize the parameters which are taken into account in this study. Three categories are considered as follows:

- The macro-scale behaviour of tested samples is described by both their strength and fracture pattern. For the fracture pattern, the focus is on the relative fracture length corresponding to layer activation and central fracture (see paragraph 4.3).

- The micro-scale quantifications of untested samples (petrographical properties) are: number of layer boundaries, grain size, presence of ripples and mineral composition (see paragraph 3.1.3).

- The micro-scale quantifications of non-failed tested samples are number of fractured quartz grains and number of fractured carbonate grains (carbonate with activated cleavages) (see paragraph 5.1).

6.1 Effect of micro-scale parameters on BTS

In this part the relationships between petrographical properties and rock strength of studied layered sandstone are investigated. In chapter 4 it is shown that the BTS-values of studied sandstones change as a function of layer orientation. By fixing the layer orientation (i.e. 70°) for the test samples of this part of study, layer orientation effect is eliminated. Therefore, the effects of micro-scale parameters on strength of different sub-types of layered sandstone can be monitored.

6.1.1 Effect of grain size on BTS

The experimental results in this work as well as the data from other studies suggest that the relationship between grain size and strength is very important. As already mentioned, quartz grains are the major rock-forming mineral in all the studied Modave sandstone sub-types. Therefore, the term ‘grain size’ is applied for the average quartz grain size. The grain size range of studied Modave sandstones in the current research is small. The grain sizes of all studied sub-types correspond to fine sand (see paragraph 3.1.3.4). The range of grain size is

from 69 to 107 µm which fits in the range of fine sand (from 63 to 210 µm). The variation in Brazilian tensile strength (BTS) as a function of grain size for all the sandstone sub-types is plotted in Figure 6.1. From Figure 6.1 it can be concluded that Brazilian tensile strength of low porosity Modave sandstones is higher for larger grain size and this corresponds to a very good correlation (correlation factor of 0.9).
As can be observed in Figure 6.1 sandstone sub-type 2 has the minimum tensile strength, with the minimum quartz grain size. In the size range of quartz grains in the studied sandstone, smaller quartz grains in comparison to larger quartz grains need less energy to be fractured, because in the larger grains more strong internal bonds should be fractured (Kannien and Poperlar 1985, Lawn 1993). Furthermore fractures can easily turn around a small quartz grain (see Figure 5.14). Fractures encountering a large quartz grain, split or divert (see Figure 5.19). In both cases of splitting or diversion of fractures, fracture length increases, more energy should be applied and consequently larger strength is recorded.
In the mentioned limited grain size range (69 to 107 µm), the most important factor that has influence on the rock strength is grain size.

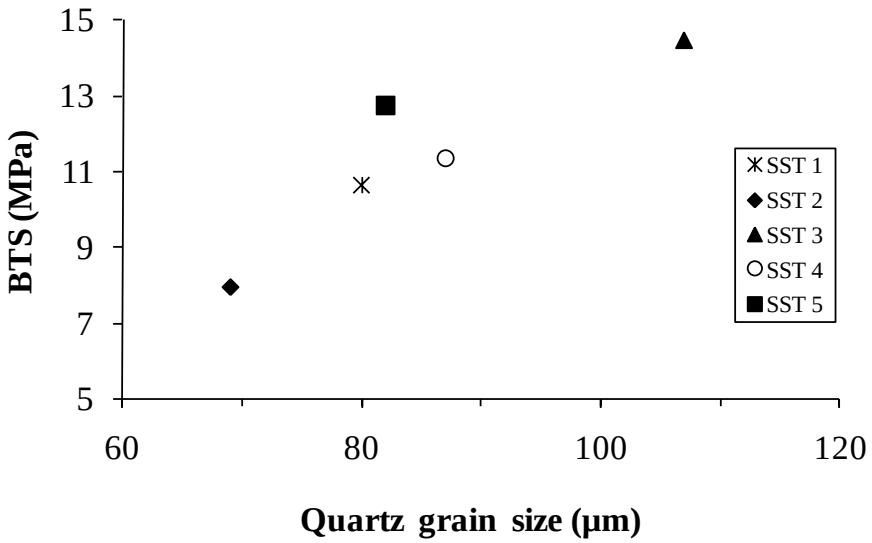

Figure 6.1 Variation in Brazilian tensile strength, BTS, as a function of grain size for all the sandstone sub-types (SST). Inclination angle for all samples is 70°.

6.1.2 Effect of mineral composition on BTS

The experimental results in this study as well as the data from other studies (see paragraph 2.2.4.1) show that rock strength is considerably affected by the existence of different minerals. In this research and for all the studied sub-types of Modave sandstone, the majority of the grains are quartz which is considered as strong in rock material. In addition to quartz as the main constitutive mineral, weak minerals such as mica and carbonate are observed (see Figure 3.12). As already mentioned, all the five sub-types of studied sandstone have relatively the same density and low effective porosity (2.0 to 3.2%), however the percentage of their constitutive minerals is not the same. Therefore it is possible to find the mineral composition effect on the rock strength as there is no interference of porosity effect.
Figure 6.2 shows the variation in Brazilian tensile strength as a function of strong and weak minerals content. Weak minerals' content is the sum of carbonate and mica minerals content. Figure 6.2a shows that as the quartz content is larger, higher tensile strength is presented.

Also Figure 6.2b shows that for larger weak minerals percentage, tensile strength decreases. It is widely accepted that even a limited amount of fine flaky minerals or easy cleavable minerals can considerably reduce the rock strength. This is also observed in the numerical simulation of uniaxial compressive tests introducing some weaker elements with 10% of the other element strength (Debecker et al. 2008). In the mentioned studies even a small amount of weaker elements caused a much larger effect than one would expect from a weighted average. For example introducing 5% weak elements in a sample by a random distribution, reduces the uniaxial compressive strength from 252 to 198 MPa. In other words 5% weak elements decrease the rock strength by more than 20%. It is interesting to mention that for example the weak mineral content in sandstone sub-types 3 and 4 is 7.9% and 14.3%, respectively. Their tensile strength is 14.5 and 11.4 MPa, respectively. In other words by an increase of 6.4% in the amount of weak minerals, 21.4% of tensile strength is decreased.

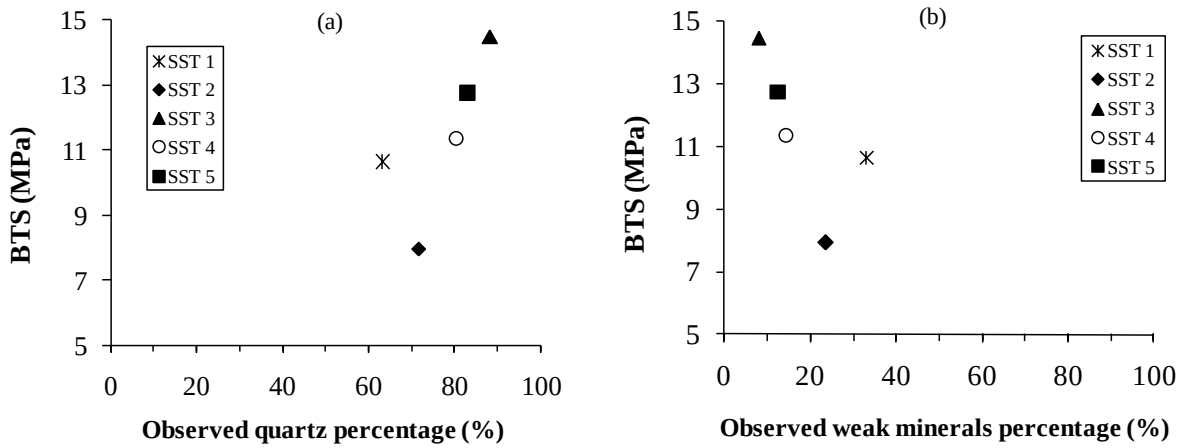

Figure 6.2 Variation in Brazilian tensile strength, BTS, as a function of constitutive minerals percentage for all the sandstone sub-types (SST). Inclination angle for all samples is 70°. (a) Variation in BTS as a function of observed quartz content. (b) Variation in BTS as a function of observed weak mineral content. Weak mineral content is the sum of carbonate and mica content.

It is good to mention that the effect of number of layer boundaries on BTS is similar to the effect of observed weak mineral percentage on BTS.
Figure 6.3 presents the variation in BTS as a function of number of fractured grains. In Figure 6.3a variation in BTS as a function of number of fractured quartz grains is presented. From this figure it can be observed that more fractured quartz grains are in the sample with higher strength. Figure 6.3b shows the variation in BTS as a function of carbonate grains with activated cleavages. From this figure it can be concluded that as the carbonate grains with activated cleavages become more frequent, the tensile strength decreases. It seems logic, because if it is needed to fracture more quartz grains in a sample to reach the final failure, more energy should be applied and consequently higher strength is recorded. However, in a sample where fracture grows through the weak and easy cleavable minerals such as carbonate, less energy is needed to reach the final failure. In the mentioned case, more carbonates with activated cleavages are produced and consequently smaller strength values are recorded.

It is interesting to note that the numbers of observed fractured grains are proportional to their content percentages. As can be seen in Figure 6.4a more observed fractured quartz grains are

in the sandstone sub-types with higher quartz content. Also more carbonates with activated cleavages are observed in the sandstone sub-types with higher carbonate content (see Figure 6.4b). Carbonate minerals in comparison to quartz grains are weaker in strength and consequently fails at lower stress state. Therefore, before the final failure of samples the carbonate minerals are already fractured. It means that for higher carbonate content, the number of fractured carbonates in a lower stress state increases and consequently causes a higher perturbation in the semi-parabola shape of cumulative AE hits curve (see Figure 5.1).

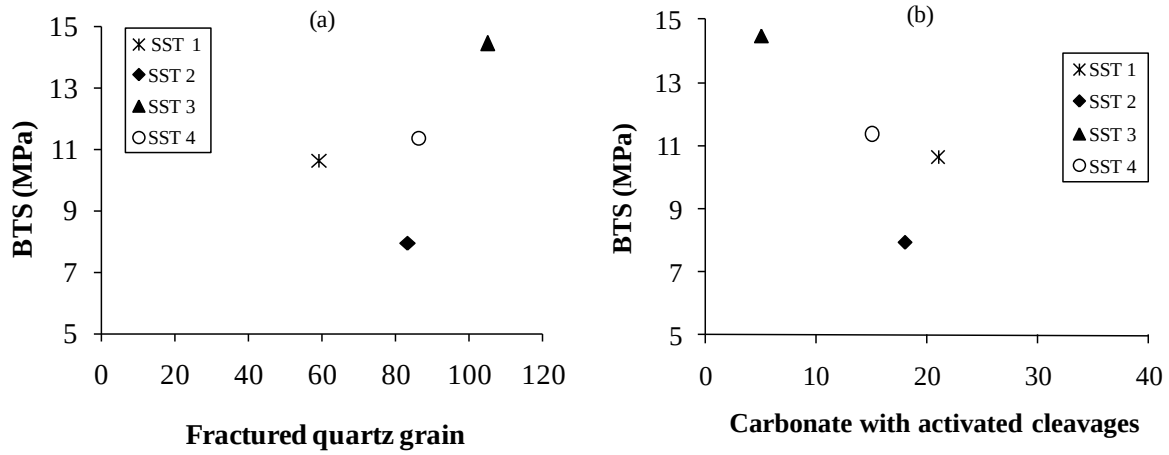

Figure 6.3 Variation in Brazilian tensile strength, BTS, as a function of number of fractured grains for the sandstone sub-types (SST) 1 to 4. Inclination angle for all samples is 70°. (a) Variation in BTS as a function of number of observed fractured quartz grains. (b) Variation in BTS as a function of number of observed carbonates with activated cleavages.

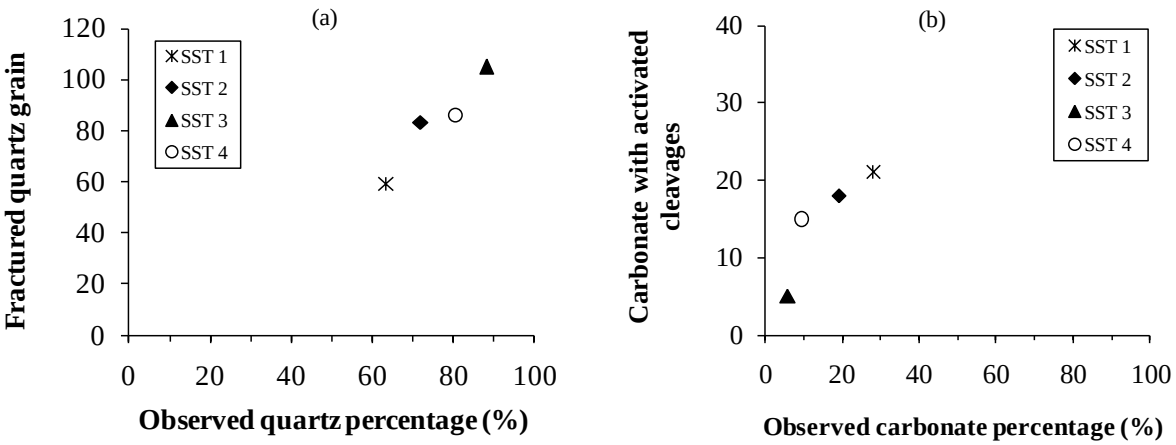

Figure 6.4 Variation in observed fractured grains as a function of their composition content in the sandstone sub-types (SST) 1 to 4. Inclination angle for all samples is 70°. (a) Variation in observed fractured quartz grains as a function of quartz content. (b) Variation in observed carbonates with activated cleavages as a function of carbonate content.

6.2 Effect of micro-scale parameters on fracture pattern

Micro-fractures, grain boundaries, mineral cleavages act as surfaces of weakness which control the failure direction. This subject in literature (see paragraph 2.2.4) is expressed in an uncertain way because expressing an exact rule on the effect of micro-scale parameters on fracture pattern is really complex. In this study, effort has been made to shed light on the effects of layer orientation and material properties on fracture patterns of layered sandstone. The purpose of this part of the study is to investigate the relationships between petrographical properties and fracture patterns of studied layered sandstone. The aim is to quantify the effect of petrographical properties on fracture patterns.

It is already observed that in the reference sub-type of Modave sandstone, layer activation is the predominant failure mode when layers are inclined from 60° to 90° (see Figure 4.8 and Figure 4.9 in paragraph 4.1.2). In Brazilian tests of different sandstone sub-types, an inclination angle of 70° is chosen and it is observed that their predominant failure mode is not only layer activation as for sub-type 1 (see paragraph 4.3.2). Hence, this part particularly focuses on the effect of micro-scale parameters on relative layer activation fracture length in different sandstone sub-types.

6.2.1 Effect of grain size on fracture pattern

The rock material in this study is from stratified sandstones which are characterized by numerous thin and parallel layers. The grains tend to be elongated parallel to the foliation (Willard and McWilliams 1969) and fine quartz grains do not perturb the continuous path of weakness (see Figure 5.14) in comparison to coarser quartz grains (see Figure 5.19). In a limited range of grain size such as the sandstone sub-types in the current research where the grain size range is from 69 to 107 µm, grains size can have an effect on fracture pattern.

Figure 6.5 presents the variation in fracture pattern as a function of average grain size. From this figure it can be observed that the fracture length corresponding to layer activation is smaller for larger grain size. It is observed that a relatively large quartz grain deflects or splits a fracture whereby fracture direction before and after the large quartz grain is different (see Figure 5.19). While for a relatively small quartz grain, a fracture after passing through the grain boundary, continues along the same line (see Figure 5.14).
In Figure 6.5, layer activation fracture length of the reference sandstone sub-type (1) is higher than the considered trend of the other four sub-types.

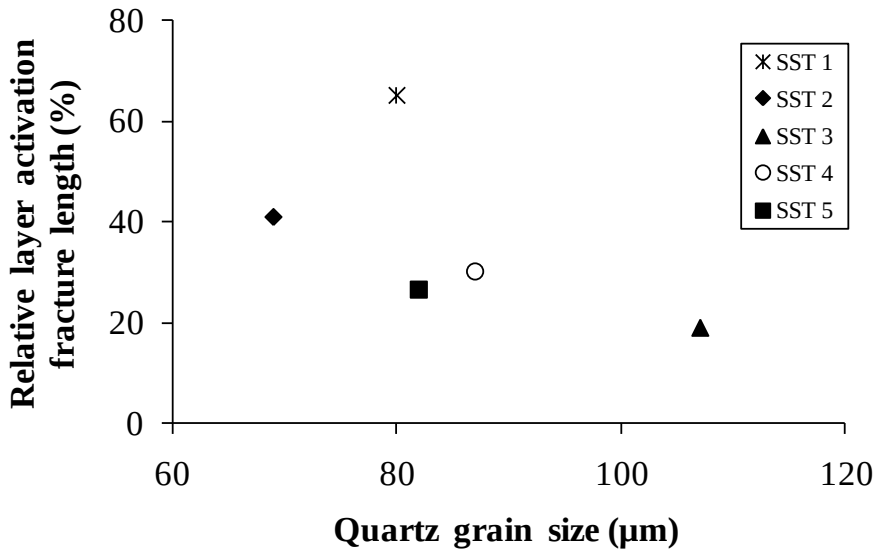

Figure 6.5 Variation in relative layer activation fracture length as a function of quartz grain size for all the sandstone sub-types (SST). Inclination angle for all samples is 70°.

6.2.2 Effect of mineral composition on fracture pattern

The rupture of a chain occurs at the weakest link. It is a law of nature that a fracture grows and propagates along a path and direction that needs less energy to dissipate. In a layered rock, layer boundaries are considered as the planes of weakness. When mentioned planes are frequent, it is logical that fractures use one or more of them to propagate. Fractures grow through weak planes (such as layer boundaries) in order to dissipate less energy. Of course this is so for the case that the direction of plane of weakness and loading axis are close to each other (e.g. a layer orientation of 70°, close to the 90° of the loading axis). For example in the case that layer orientation and loading axis are perpendicular, weak planes do not show any effect on fracture pattern (see the fractured samples in Figure 4.5, when layer orientation varies between 0° and 30°).

In the case that direction of layer orientation and loading axis are close to each other, for higher frequency of the layer boundaries, existence of them at both ends of rock sample becomes more probable. Both ends of a rock sample in a Brazilian test are the regions where load is applied. Therefore, initiated fractures can directly propagate in a plane of weakness. However, for lower frequency of the layer boundaries, initiated fracture should grow through the intact material to reach a plane of weakness, where propagation is easier and needs less energy to dissipate. In the recent case fracture length corresponding to layer activation is smaller.

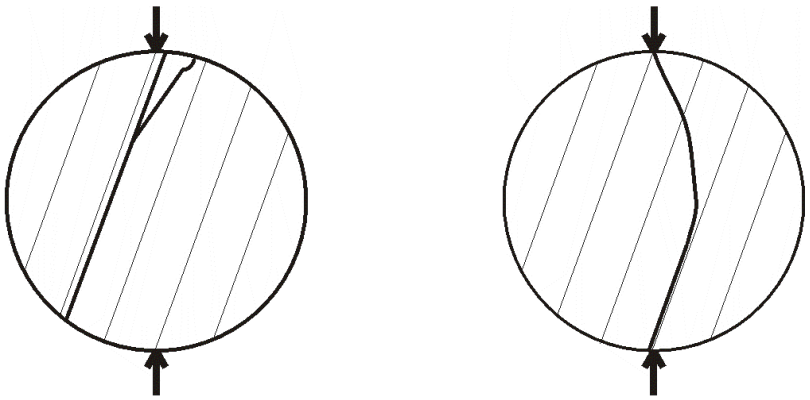

SST:	1	4
LB/cm:	8.8	4.2
LA (%):	90	46

Figure 6.6 Comparison of fracture pattern in two samples with different number of layer boundaries. Thin lines symbolize average layer direction (bedding) while the bold lines are the observed fractures. Inclination angle for both samples is 70°. For both samples, sandstone sub-type (SST), number of layer boundaries (LB) per cm and also relative layer activation fracture length (LA (%)) are mentioned. Higher relative layer activation fracture length for the sample with more layer boundaries is remarkable.

In Figure 6.6, layer activation of a sample from sandstone sub-type 1 is compared to another sample from sandstone sub-type 4. The number of layer boundaries per centimetre for sandstone sub-types 1 and 4 is 8.8 and 4.2, respectively. It is observed that relative layer activation fracture length of the sample from sandstone sub-type 1 is 90%, while for the sample from sandstone sub-type 4 it is 46% (where the layer boundaries are less frequent).

Figure 6.7 presents the variation in relative layer activation fracture length as a function of the number of layer boundaries per cm. As expected, a direct relationship between these two parameters exists and higher frequency of layer boundaries causes higher amount of layer activation. This figure shows that maximum layer activation in the reference sandstone sub-type is due to the maximum number of layer boundaries which exist in that sub-type. It is good to note that the ripples in sandstone sub-type 5 are not considered as layer boundaries.

Already in paragraph 3.1.3.3 it is observed that the number of layer boundaries and observed weak mineral percentage are directly proportional to each other (see Figure 3.13). Therefore, variation in relative layer activation fracture length as a function of observed weak minerals content should be interesting. Figure 6.8 presents the mentioned variation where weak mineral percentage is the sum of the carbonate and mica content. As expected, for higher relative quantity of weak minerals, layer activation becomes more predominant and this corresponds to a very good correlation. In Figure 6.8, all the mica and carbonate content are considered and compared to each other. Figure 6.8 is presented independent of the number of layer boundaries (or ripples).

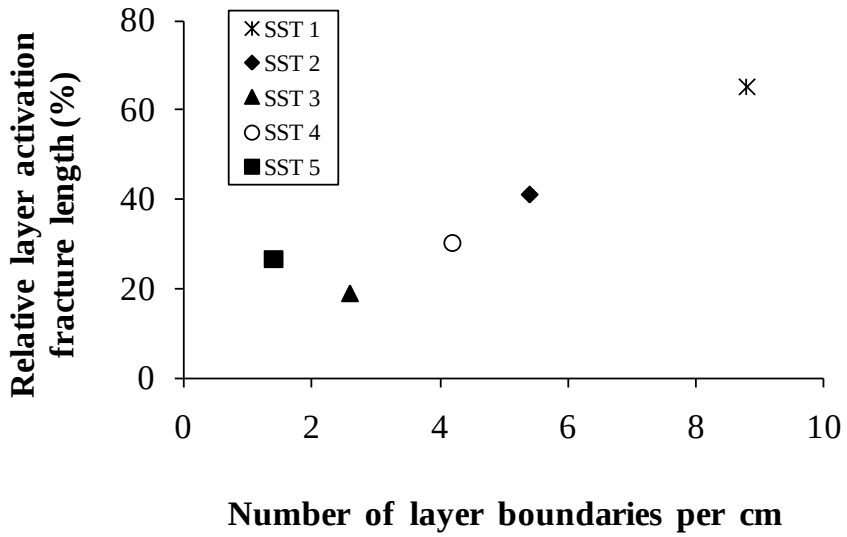

Figure 6.7 Variation in relative layer activation fracture length as a function of the number of layer boundaries for all the sandstone sub-types (SST). Inclination angle for all samples is 70°. Ripples in sandstone sub-type 5 are not considered as layer boundaries.

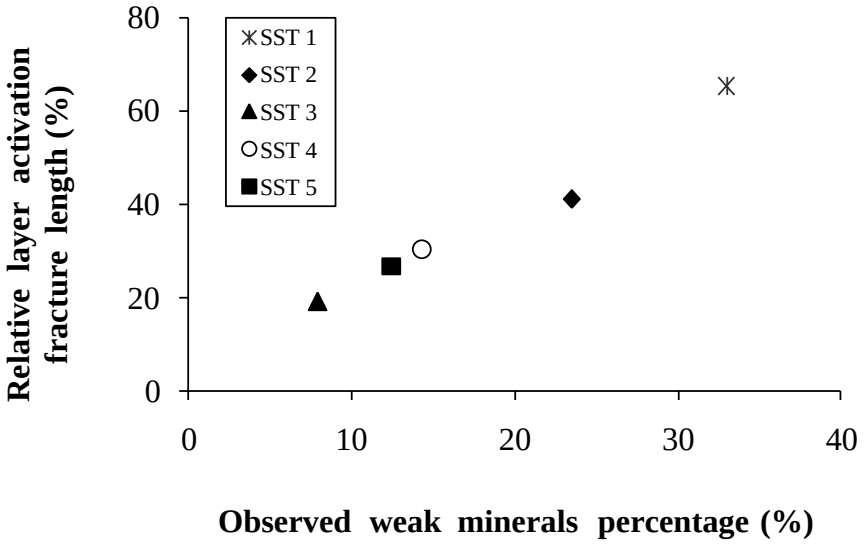

Figure 6.8 Variation in relative layer activation fracture length as a function of observed weak mineral percentage for all the sandstone sub-types (SST). Weak mineral percentage is the sum of the carbonate and mica content. Inclination angle for all samples is 70°.

Observed weak minerals' content and number of layer boundaries per cm (which are linearly proportional to each other) are observed as the dominant parameters that influence the fracture pattern. Mentioned explanations clarify the effect of weak minerals on fracture pattern. More weak minerals cause layer activation, becoming more dominant in the fracture pattern.

Figure 6.9 shows the variation in fracture pattern as a function of observed fracture grains in sandstone sub-type 1 to 4. For a large number of carbonates with activated cleavages, relative layer activation fracture length is higher (see Figure 6.9a) and consequently relative central

fracture length is smaller (see Figure 6.9c). However, when weak minerals become less frequent, the number of observed fractured quartz grains increases and therefore relative layer activation fracture length decreases (see Figure 6.9b). In this case, it is concluded that layer boundaries become less frequent and consequently, fracture length corresponding to central fracture increases (see Figure 6.9d).
Figure 6.9 illustrates that by observing more carbonates with activated cleavages, relative layer activation fracture length becomes more dominant and as a result relative central fracture length becomes smaller. However, when more fractured quartz grains are observed, it shows that the weak mineral content is small and therefore relative layer activation fracture length becomes less remarkable and consequently relative central fracture length becomes more dominant.

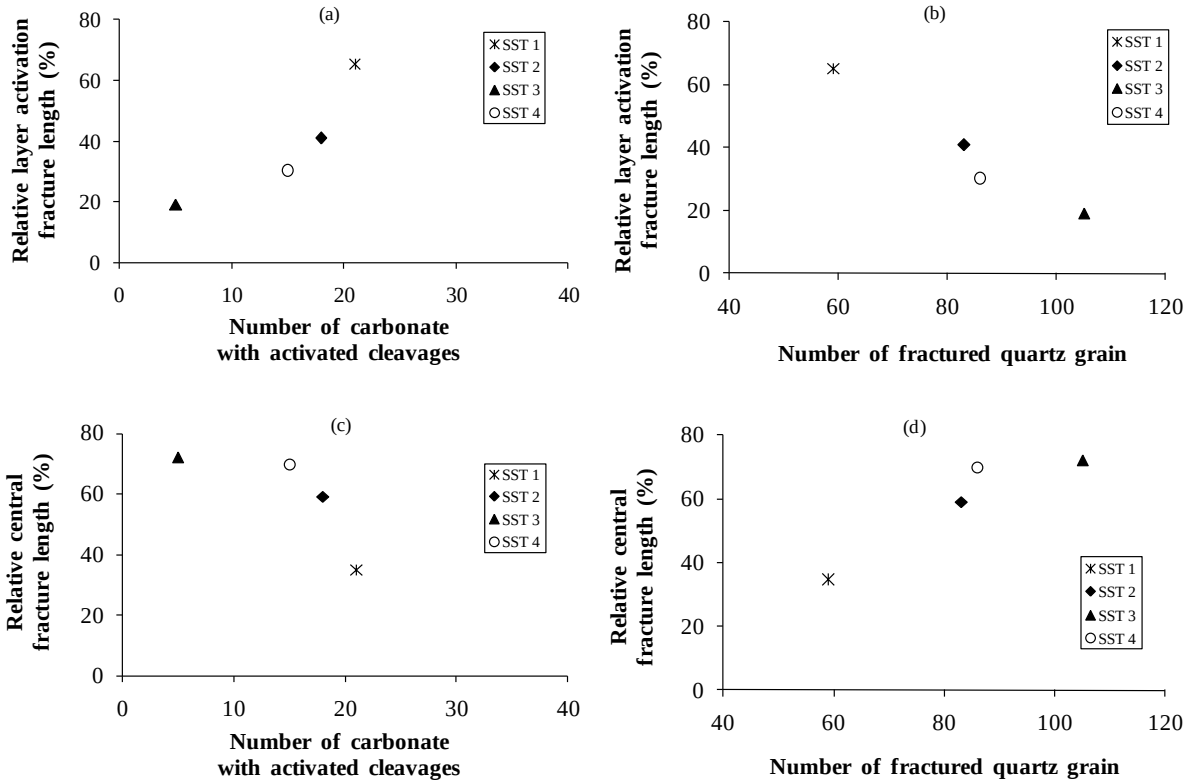

Figure 6.9 Variation in fracture pattern as a function of the number of observed fractured grains in the sandstone sub-types 1 to 4 (SST). Inclination angle for all samples is 70°. (a) Variation in relative layer activation fracture length as a function of number of carbonates with activated cleavages. (b) Variation in relative layer activation fracture length as a function of number of fractured quartz grains. (c) Variation in relative central fracture length as a function of number of carbonates with activated cleavages. (d) Variation in relative central fracture length as a function of number of fractured quartz grains.

In other words it can be concluded that layer activation and the number of carbonates with activated cleavages have a direct relationship, while layer activation and the number of fractured quartz grains have reverse relationship. Strong and weak minerals have an opposite effect not only on the rock strength but also on the fracture pattern. Figure 6.10a shows that in these sub-types of layered sandstone for larger quartz content, carbonate content is smaller. Consequently, after loading the samples, their carbonate and quartz fractured grains become reversely proportional.

Figure 6.10b shows the variation in number of carbonates with activated cleavages as a function of number of fractured quartz grains. This figure shows that more carbonates with activated cleavages are observed in a sample that has less fractured quartz grains. In Figure 6.10b the data of the sample from sandstone sub-type 2 whereby loading is stopped roughly at half of the ultimate strength is also presented. By considering the samples from sub-type 2, this figure clearly shows that the carbonates fracture at a lower stress state and their quantity can reach the maximum possible amount before quartz grains are fractured. In other words the similarity in the number of carbonates with activated cleavages for the two samples of sub-type 2 proves that the carbonates fracture in the first half of sample loading.
Figure 6.10b also shows that by increasing the loading on the sample from sub-type 2, the number of fractured quartz grains increases; however, the number of fractured carbonates stays roughly constant. It shows that quartz fracturing needs more energy which is achieved in the second half of the sample loading.

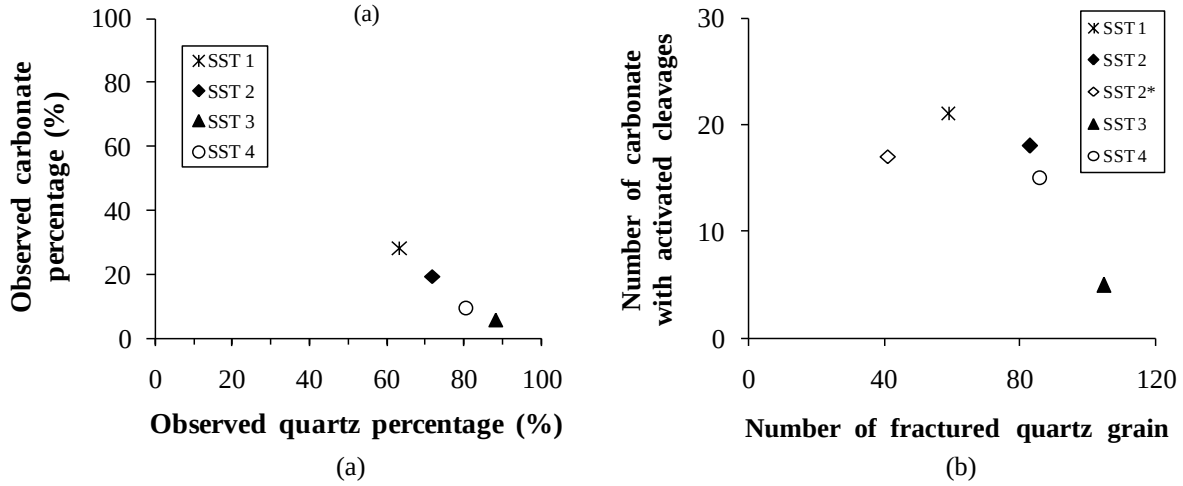

Figure 6.10 Relationships between quartz and carbonate in the sandstone sub-types 1 to 4 (SST). (a) Variation in carbonate content as a function of quartz content. (b) Variation in number of carbonates with activated cleavages as a function of number of fractured quartz grains. Also the result of a sample from sub-type 2 (SST 2*) that loading is stopped roughly at half of the sample ultimate strength is presented.

7 Conclusions and Recommendations for Future Research

7.1 Overview of findings

The experimental study on the layered sandstone (Psammite du Condroz) from Modave in the South of Belgium shows that the failure stress and fracture pattern are considerably affected by the layer orientation. However, measurements of P-wave velocity show slight differences in wave velocity parallel and perpendicular to the layers. In this research all sub-types of studied layered sandstone have nearly identical physical properties (porosity and density). They were all taken at very short distances from each other (between 1 and 10 m). Their density is about 2.6 t/m^3 and their porosity varies from 2.4 to 3%.
It is observed that for all sandstone sub-types as inclination angle increases from 0° to 90°, the fracture length corresponding to central fracture(s) decreases while layer activation increases. In the mentioned variation range of the inclination angle, the decreasing and the increasing rates (of fractures length) for the five studied sub-types are different. Therefore, the transition angle (the change of failure mode from central fracture to layer activation) is not the same for all sub-types.
As inclination angle increases from 0° to 90°, the average Brazilian tensile strength for the sandstone sub-types shows a small downwards trend. It is also observed that larger fracture length correlates with higher strength. Therefore, the samples with low inclination angles, which are more fractured, show the higher values of strength. It is concluded that strength is smaller for larger inclination angles and smaller total fracture lengths. Fracture lengths of samples with larger inclination angles mostly correspond to layer activation.

The global behaviour of five studied sandstone sub-types is similar, however looking at microscopic scales differences are noted. In this study the importance of the effect of micro-scale parameters at macro-scale behaviour of layered Modave sandstone is highlighted. If in a quarry by visual inspection several rock blocks seem similar, one should not expect the same behaviour in strength and fracture pattern.
It is important to note that numerous micro-scale parameters can have some effect on rock properties. Furthermore, their influences can be similar or act in opposite directions. Therefore, not the influence of a single parameter, but all parameters should be considered when studying the rock behaviour. It is important to consider the range of variation for the different parameters. As the range of variation of one parameter is broader than for the other parameters, one would expect a larger influence of that particular parameter. Hence, declaring the effects of any micro-scale parameters on the rock behaviour, without mentioning the range of the variation of the parameters is incomplete.

The effect of micro-scale parameters on macro-scale behaviour can be summarised as follows:

1- Brazilian tensile strength of low porosity layered sandstones is observed to be higher for larger average grain size. For the grain size measurements, quartz grains as the main constitutive mineral are considered. Coarser quartz becomes the main stress-bearing skeleton and as it has higher strength, accumulates larger quantities of elastic strain energy. The variation in grain size in the studied Modave sandstone is from 69 to 107 μm which is classified as fine sand.

2- Brazilian tensile strength of studied layered sandstone is higher for larger observed quartz content and also for smaller weak minerals content. In the studied sandstone quartz content varies from 63 to 88% of mineral composition, while weak minerals' (carbonate and mica) content varies from 8 to 33%.

3- Both parameters of grain size and mineral content have an obvious effect on Brazilian tensile strengths. However, grain size effect is more dominant than the effect of mineral content.

4- Fracture length corresponding to layer activation is less for larger grain sizes (in the range of 69 to 107 μm), linked to smaller observed weak mineral percentage.

5- Fracture length corresponding to layer activation is larger, firstly if more layer boundaries are observed (e.g. per cm) and secondly, for more observed weak minerals percentage. For these studied layered sandstones, the number of layer boundaries per centimetre varies from 1.4 to 8.8, and weak minerals content varies from 8 to 33%.

6- All the parameters of number of layer boundaries, weak minerals percentage and grain size have an obvious effect on layer activation. However, grain size effect is less dominant than the others.

7.2 Recommendations for future research

These days, numerical modelling is applied for many geotechnical problems. However, the characteristics of host rock are simplified to be able to introduce them in numerical codes and therefore, the microstructure of rock is most of the time not fully taken into account.
In this Ph.D. a detailed experimental study is conducted on failure of layered sandstone under Brazilian test conditions. This type of rock material is sometimes introduced in numerical codes by considering a weak direction (Alam et al. 2007, Debecker and Vervoort 2009). However, it is understood that the weak layer direction is not the only factor that affect the behaviour of transversely isotropic rock material. The number of layer boundaries; mineral composition; grain size of major rock-forming mineral and existence of other weak direction (i.e. ripples) have major influence on macro-scale behaviour (strength and fracture pattern) of rock materials. Hence, introducing the micro-scale parameters (as much as possible) in the numerical modelling has become a necessity to simulate real rock.
In the Research Unit "Mining" of K.U.Leuven studying the fracturing process in brittle rock has been a primary focus of research (Vervoort et al. 2008) and over the years an expertise is developed in the fields of experimental work (e.g. current research and Debecker (2009)) and numerical simulations of individual fracture growth (Van de Steen at al. 2001, Lavrov et al.

2003, Ganne 2007, Debecker 2009) using advanced numerical codes (DIGS, UDEC and PFC). In this Ph.D., it is experimentally observed that micro-scale parameters play a significant role in the rock behaviour.

In this paragraph the main focus is on transversely isotropic rock material as one specific form of anisotropy. It is a form of anisotropy that is often present in geological material. Introducing the micro-scale parameters in numerical simulations is the main recommended objective for further research as it improves the interpretation of modelling results. The micro-scale parameters which can be considered are:
- Frequency of number of layer boundaries
- Mineral composition percentage
- Grain size of major mineral
- Contact pattern of constitutive minerals

Some researchers apply ubiquitous-joint models to incorporate a weak direction. This type of models considers the weak direction as part of a continuum, which makes it difficult to simulate transversely isotropic rock material like layered sandstone, as it is composed of thin layers from a few millimetres to a few centimetres (i.e. for graded bedding of shallow-water environment is generally from 1 mm to 2 cm) (Reineck and Singh 1986). In other words the layer boundaries are not everywhere and furthermore they do not have exactly the same geomechanical properties. The experimental observations about the number of layer boundaries of layered rock material should be classified and effort should be made to introduce them into the numerical models. The results can be compared with experimental results (of this Ph.D.).
In numerical simulations of a sample, an individual weak direction should be considered. A line or interface as a layer boundary should be introduced to the model and failure behaviour should be monitored. The second weak line (in the same direction) should be introduced to observe the changes in sample behaviour. The distance between the two weak lines can have a variation range to see its effect on sample behaviour. By considering the other weak lines, the effect of their frequency and the distances between them can be monitored.

For mineral composition the same procedure as for the number of layer boundaries can be applied. Different percentage of strong and weak elements should be introduced to the model. Also it will be interesting to introduce the heterogeneities (pores and weak element) to observe the effect of different percentage of them in rock behaviour.

The plan and prospective results presented in this paragraph could be a good base for further and more complex research.

References

1. Alam M.R., Swamidas S.J., Munaswamy K. Experimental and numerical studies on dynamic crack growth in layered slate rock under wedge impact loads: part I - plane strain problem. Fatigue Fract. Eng. Mater. Struct. Vol. 30: 844-862, 2007
2. Aligizaki Kalliopi K. Pore structure of cement-based materials, testing, interpretation and requirements. London, Taylor & Francis Group, 388 p., 2006.
3. Andreev G.E. Brittle failure of rock materials, test results and constitutive models. Can. Geotech. J. Vol. 33: 378, 1996.
4. Andreev G.E. Brittle failure of rock materials, test results and constitutive models. Balkema, Rotterdam, 446 p, 1995.
5. Anderson T.L. Fracture mechanics, fundamentals and applications. CRC Press, London, 621 p, 2005.
6. Attewell P.B., Farmer I.W. Principles of engineering geology. London: Chapman and Hall Ltd., 30–4, 1976.
7. Bailey L.K., Peters E. Decomposition of pyrite in acids by pressure leaching and anodization: the case for an electrochemical mechanism. Can. Metall. Q. Vol. 15(4): 333, 1976.
8. Bell F.G. The physical and mechanical properties of the Fell sandstones, Northumberland, England. Eng. Geol. Vol. 12: 1–29, 1978.
9. Bieniawski Z.T. The effect of specimen size on compressive strength of coal. Int. J. Rock Mech. Min. Sci. & Geomech. Abstr. Vol. 5: 325-335, 1968.
10. Bieniawski Z.T. Mechanism of brittle rock fracture: Part I- Theory of the fracture process. Int. J. Rock Mech. Min. Sci. Geomech. Abstr. Vol. 4 (4): 395-406, 1967.
11. Blott S.J., Pye K. Technical communication, Gradistat: a grain size distribution and statistics package for the analysis of unconsolidated sediments. Earth Surf. Process. Landforms Vol. 26: 1237–1248, 2001.
12. Brace C.H., Paudling B.W. Jr., Scholtz, C.H. Dilatancy in the fracture of crystalline rocks. J. Geophys. Res. Vol. 71: 3939-3953, 1966.
13. Brace W.F. Brittle fracture of rocks. In: State of stress in the earth's crust: Proceeding of International Conference, Santa Monica, 110-178, 1964.
14. Brace W.F., Walsh J.B. Some direct measurements of the surface energy of quartz and orthoclase. Am. Mineral. Vol. 47: 1111-1122, 1962.
15. Brace W.F. Dependence of fracture strength of rocks on grain size. Proceedings of the 4th Symposium Rock Mechanics, University Park, USA: 99–103, 1961.
16. Brady B.H.G., Brown E.T. Rock mechanics for underground mining. London, Chapman & Hall, 571 p., 1994.
17. Butler I., Rickard D., Grimes S. Framboidal pyrite: self-organisation in the Fe-S system. J. Conf. Abst. Vol. 5(2): 276–277, 2000.

18. Cai M., Kaiser P.K., Tasaka Y., Maejima T., Morioka H., Minami M. Generalized crack initiation and crack damage stress thresholds of brittle rock masses near underground excavations. Int. J. Rock Mech. Min. Sci. Vol. 41: 833–847, 2004.
19. Carpinteri A., Paggi M. Numerical analysis of fracture mechanisms and failure modes in bi-layered structural components. Finite Elem. Anal. Des. Vol. 43: 941-953, 2007.
20. Chayes F. Petrographic modal analysis: an elementary statistical appraisal. New York, Wiley, 113 p., 1956.
21. Chen Y., Nishiyama, T., Kusunda H., Kita H., Sato T. Correlation between microcrack distribution patterns and granitic rock splitting planes. Int. J. Rock Mech. Min. Sci. Vol. 36: 535-541, 1999.
22. Chen C.S., Pan E., Amadei B. Determination of deformability and tensile strength of anisotropic rock using Brazilian tests. Int. J. Rock Mech. Min. Sci. Vol. 35 (1): 43-61, 1998.
23. Clatworthy D.E., Sellers E.J., Scheele F. Investigation of splitting tensile test. Report No. 225, FRD/UCT Centre for research in computational and applied mechanics, University of Cape Town, 1993.
24. Colback P.S.B. An analysis of brittle fracture initiation and propagation in the Brazilian test. Proceedings of the first Congress of the International Society of Rock Mechanics (ISRM 1966), Lisbon, Portugal, 385-391, 1966.
25. Craig R.F. Soil mechanics, 4th ed. London: Chapman and Hall, 410 p., 1990.
26. Compston W. Interpretation of SHRIMP and isotope dilution zircon ages for the Palaeozoic time-scale: II. Silurian to Devonian, Mineral. Mag. Vol. 64: 1127-1146, 2000.
27. Cundall P.A., Potyondy D.O., Lee C.A. Micromechanics-based models for fracture and breakout around the mine-by tunnel. In: Martino JB, Martin CD, editors. Proceedings of the excavation disturbed zone workshop, designing the excavation disturbed zone for a nuclear repository in hard rock, Toronto, Canada. Canadian Nuclear Society, 113–122, 1996.
28. Debecker B. Influence of planar heterogeneities on the fracture behaviour of rock. PhD thesis, KULeuven, Leuven, 168 p., 2009.
29. Debecker B., Vervoort A. Numerical simulation of the fracture process in layered rock. Costa Neves L.F., Barros R.C. (Eds.). Proceeding of the 12th int. conf. on civil, structural and environmental engineering computing, Civil-Comp Press, Madeira, September 2009, paper 227, 2009.
30. Debecker B., Vervoort A. Experimental observation of fracture patterns in layered slate. Int. J. Fract. Vol. 159: 51-62, 2009.
31. Debecker B., Vervoort A. Observation de fracturation dans des roches stratifiées par images de vidéo. Proceedings of horizons de l'optique, Grenoble, 2-5 July 2007, 116-117, 2007.
32. Debecker B., Vervoort A., Napier J.A.L. Fracturing in and around a natural discontinuity in rock: a comparison between boundary and discrete element models. Topping B.H.V., Montero G. and Montenegro R. (Eds.). Proceeding of the 5th Int. Conf. Eng. Comp. Tech. Paper 168, Las Palmas de Gran Canaria, 12-15 September 2006. Civil-Comp press LTD, 387-388, 2006.
33. Debecker B., Tavallali A., Vervoort A. Probability distribution of rock properties: effect on the rock behaviour. Stacey T.R., Malan D.F. (Eds.), Proceeding of the 6th international symposium on ground support in mining and civil engineering construction, Cape Town, South Africa. The Southern African Institute of Mining and Metallurgy Publications, 357-368, 2008.

34. Delannay F. Fracture mechanics: theory and application to materials. UCL, Louvain-la-Neuve, 97 p., 1994.
35. De Vos W., Verniers J., Herbosch A., Vanguestaine M. A new geological map of the Brabant Massif, Belgium. Geological Magazine Vol. 130: 605–11, 1993.
36. Dewaele S., Muchez P.H., Banks D.A. Fluid evolution along multistage composite fault systems at the southern margin of the Lower Palaeozoic Anglo-Brabant fold belt, Belgium. Geofluids Vol. 4: 341-356, 2004.
37. Dey T.N., Wang C.Y. Some mechanisms of microcrack growth and interaction in compressive rock failure. Int. J. Rock Mech. Min. Sci. & Geomech. Abstr. Vol. 18: 199-209, 1981.
38. Eberhardt E. Numerical modelling of three-dimension stress rotation ahead of an advancing tunnel face. Int. J. Rock Mech. Min. Sci. Vol. 38: 499–518, 2001.
39. Eberhardt E., Stimpson B., Stead D. Effects of grain size on the initiation and propagation thresholds of stress-induced brittle fractures. Rock Mech. Rock Eng. Vol. 32 (2): 81–99, 1999.
40. Fairhurst C. On the validity of the Brazilian test for brittle materials. Int. J. Rock Mech. Min. Sci. Vol. 1: 535-546., 1964.
41. Fairhurst C., Cook N.G.W. The phenomenon of rock splitting parallel to the direction of maximum compression in the neighbourhood of a surface. Proceedings of the First Congress of the International Society of Rock Mechanics, Lisbon, Portugal. Vol. 1: 687–692, 1966.
42. Falls S.D., Chow T., Young R.P., Hutchins D.A. Acoustic emission analysis and ultrasonic velocity imaging in the study of rock failure. In: Sachse W., Roget J., Yamaguchi K., editors. Acoustic emission: current practice and future directions, ASTM STP 1077. Philadelphia: American Society for Testing and Materials: 381–91, 1991.
43. Falls S.D., Chow T., Young R.P., Hutchins D.A. Acoustic emission analysis and ultrasonic velocity imaging in the study of rock failure. J. Acoust. Emission Vol. 9(1/2):S166–9, 1989.
44. Fang Z., Harrison J.P. Development of a local degradation approach to the modelling of brittle fracture in heterogeneous rocks. Int. J. Rock Mech. Min. Sci. Vol. 39: 443–457, 2002.
45. Fujii Y., Takemura T., Takahashi M., Lin W. Surface features of uniaxial tensile fractures and their relation to rock anisotropy in Inada granite. Int. J. Rock Mech. Min. Sci. Vol. 44: 98-107, 2007.
46. Gallagher J.J., Friedman M., Handin J., Sowers G.M. Experimental studies relating to microfracture in sandstone. Tectonophysics Vol. 21: 203-247, 1974.
47. Ganne P. Assessing the influence of stress sequence on the fracturing of rock. PhD thesis, KULeuven, Leuven, 169 p., 2007.
48. Ganne P., Vervoort A. Effect of stress path on pre-peak damage in rock induced by macro-compressive and -tensile stress fields. Int. J. Fract. Vol. 144: 77-89, 2007.
49. Ganne P., Vervoort A. Characterisation of tensile damage in rock samples induced by different stress paths. Pure appl. geophys. Vol. 163: 2153-2170, 2006.
50. Ganne P., Vervoort A., Wevers M. Quantification of pre-peak brittle damage: Correlation between acoustic emission and observed micro-fracturing. Int. J. Rock Mech. Min. Sci. Vol. 44: 720-729, 2007.
51. Geological Society Engineering Group. Working party report on the logging of rock cores for engineering purposes. Q.J. Eng. Geol., Vol. 3: 1-24, 1970.
52. Gradstein F.M., Ogg J.G., Bleeker W., Lourens L.J. A new Geologic Time Scale with special reference to Precambrian and Neogene. Episodes Vol. 27: 83-100, 2004.

53. Griffith A.A. The theory of rupture. Proceeding of the First International Congress for Applied Mechanics, Delft: 55-63, 1924.
54. Griffith A.A. The phenomena of rupture and flow in solids. Philos. Trans. Roy. Soc. London, Series A, Math. Phys. Sci. 221 (587): 163-198, 1920.
55. Gunsallus K.L., Kulhawy F.H. A comparative evaluation of rock strength measures. Int. J. Rock Mech. Min. Sci. Geomech. Abstr. Vol. 21: 233–248, 1984.
56. Hallbauer D.K., Wagner H., Cook N.G.W. Some observations concerning the microscopic and mechanical behaviour of quartzite specimens in stiff, triaxial compression tests. Int. J. Rock Mech. Min. Sci. & Geomech. Abstr. Vol. 10: 713-726, 1973.
57. Han G., Preat A., Chamley H., Deconinck J.F., Mansy J.L. Palaeozoic clay mineral sedimentation and diagenesis in the Dinant and Avesnes Basins (Belgium, France): relationships with Variscan tectonism. Sedimentary Geol. Vol. 136: 217–238, 2000.
58. Hatzor Y.H., Palchik V. The influence of grain size and porosity on crack initiation stress and critical flaw length in dolomites. Int. J. Rock Mech. Min. Sci. Vol. 34(5): 805–16, 1997.
59. Hawkes I., Mellor M. Uniaxial testing in rock mechanics laboratories. Eng. Geol. Vol. 4:177-285, 1970.
60. He M.Y., Hutchinson J.W. Crack deflection at an interface between dissimilar elastic materials. Int. J. Solids Struct. Vol. 25: 1053-1067, 1989.
61. He M.Y., Evans A.G., Hutchinson J.W. Crack deflection at an interface between dissimilar elastic materials: role of residual stresses. Int. J. Solids Struct. Vol. 31: 3443-3455, 1994.
62. Hoek E., Brown E.T. Underground Excavation in Rock. London: The Institution of Mining and Metallurgy, 527 p., 1980.
63. Hoxha D., Lespinasse M., Sausse J., Homand F. A microstructural study of natural and experimentally induced cracks in a granodiorite. Tectonophysics Vol. 395: 99-112, 2005.
64. Hudson J.A., Brown E.T., Rummel F. The failure of rock discs and rings loaded in diametral compression. Int. J. Rock Mech. Min. Sci. Vol. 9: 241-248, 1972.
65. Hudson J.A., Brown E.T. Fairhurst C. Shape of the complete stress–strain curve for rock. Stability of rock slopes. Proceedings of the 13th symposium rock mechanics, University of Illinois, 773–795, 1971.
66. Hudson J.A, Fairhurst C. Tensile strength, Weibull's theory and a general statistical approach to rock failure. Te'eni M., editor. Structure, solid Mechanics and engineering design: Proceedings of Southampton Civil Engineering Materials Conference, Part I, Univ. Southampton, 901–14, 1969.
67. Humphreys G.S., Mitchell P.B. A preliminary assessment of the role of bioturbation and rainwash on sandstone hillslopes in the Sydney Basin, in Australian and New Zealand Geomorphology Group, 66-80, 1983.
68. İrfan T.Y., Mineralogy, fabric properties and classification of weathered granites in Hong Kong. Q. J. Eng. Geol. Vol. 29: 5–35, 1996.
69. ISRM Suggested Methods. Suggested method for determining tensile strength of rock materials. Int. J. Rock Mech. Min. Sci. & Geomech. Abstr. Vol. 15: 99-103, 1978.
70. ISRM, The complete ISRM suggested methods for rock characterization, testing and monitoring. Editors: Ulusay R., Hudson J.A., 628 p., 2007.
71. Itasca Consulting Group Inc. PFC2D (Particle Flow Code in 2 Dimensions), theory and background, version 3.1. Minneapolis, USA, 120 p., 2004.
72. Itasca Consulting Group Inc. FLAC (Fast Lagrangian Analysis of Continua), theory and background, version 5.0. Minneapolis, USA, 218 p., 2005.

73. Jackson R., Lau J.S.O. The effect of specimen size on the laboratory mechanical properties of Lac du Bonnet grey granite. Cunha P. (Ed.), Scale Effect in Rock Masses. Balkema, 165–174, 1990.
74. Jaeger J.C., Cook, N.G.W. Fundamentals of Rock Mechanics. London, Chapman and Hall, 593 p., 1979.
75. Jaeger J.C., Cook, N.G.W. Fundamentals of Rock Mechanics. London, Methuen & Co. Ltd, 513 p., 1969.
76. Jianhong Y., Wu F.Q., Sun J.Z. Estimation of the tensile elastic modulus using Brazilian disc by applying diametrically opposed concentrated loads. Int. J. Rock Mech. Min. Sci. Vol. 46: 568-576, 2009.
77. Johnson R. Environmental scanning electron microscopy, an introduction to ESEM. 2nd printing, Eindhoven: Philips Electron Optics, 55 p., 1996.
78. Kanninen M.V., Popelar C.H. Advanced Fracture Mechanics. Oxford University Press, New York. 563p., 1985.
79. Kemeny J.M. A model for non-linear rock deformation under compression due to sub-critical crack growth. Int. J. Rock Mech. Min. Sci. Geomech. Abstr. Vol. 28(6): 459–467, 1991.
80. Klein C., Hurlbut C.S. Manual of mineralogy. John Wiley and Sons, New York, 549 p., 1993.
81. Kožušníková A., Marečková K. Analysis of rock failure after triaxial testing. Int. J. Rock Mech. Min. Sci. Vol. 36: 243-251, 1999.
82. Kranz R.L. Microcracks in rocks: a review. Tectonophysics Vol. 100: 449-480, 1983.
83. Kranz R.L. Crack-crack and crack-pore interactions in stressed granite. Int. J. Rock Mech. Min. Sci. & Geomech. Abstr. Vol. 16: 37-47, 1979.
84. Lavrov A. The Kaiser effect in rocks: principles and stress estimation techniques. Int. J. Rock Mech. Min. Sci. Vol. 40: 151–171, 2003.
85. Lavrov A., Vervoort A. Theoretical treatment of tangential loading effects on the Brazilian test stress distribution. Int. J. Rock Mech. Min. Sci. Vol. 39: 275-283, 2002.
86. Lavrov A., Vervoort A. Effect of a non-uniform radial load distribution on stress field in Brazilian test. J. Rock Mech. Tunnelling Tech. Vol. 7(2): 79-92, 2001.
87. Lavrov A., Vervoort A., Wevers M., Napier J.A.L. Experimental and numerical study of the Kaiser effect in cyclic Brazilian tests with disk rotation. Int. J. Rock Mech. Min. Sci. Vol. 39: 287–302, 2002.
88. Lawn B.R. Fracture of brittle solids. Cambridge: Cambridge University Press, 378 p., 1993.
89. Long H., Dixon D.G. Pressure oxidation of pyrite in sulfuric acid media: a kinetic study. Hydrometallurgy, Vol. 73: 335–349, 2004.
90. MacKenzie W.S., Guilford C. Atlas of rock-forming minerals in thin section. New York: Longman Scientific & Technical, 98 p., 1993.
91. McWilliams J. The Role of Microstructure in the Physical Properties of Rock, ASTM Special Technical Publication 402: 175-189, 1966.
92. Mellor M., Hawkes I. Measurement of tensile strength by diametral compression of discs and annuli. Eng. Geol. Vol. 5, 173-225, 1971.
93. Meng Z., Pan J. Correlation between petrographic characteristics and failure duration in clastic rocks. Eng. Geol. Vol. 89: 258–265, 2007.
94. Moore D.E., Lockner D.A. The role of microcracking in shear-fracture propagation in granite. J. Struct. Geol. Vol. 17: 95-114, 1995.
95. Moura A., Lei X., Nishisawa O. Prediction scheme for the catastrophic failure of highly loaded brittle materials or rocks. J. Mech. Phys. Solids, Vol. 53: 2435–2455, 2005.

96. Nasseri M.H.B., Mohanty B., Robin P.Y.F. Characterization of microstructures and fracture toughness in five granitic rocks. Int. J. Rock Mech. Min. Sci. Vol. 42: 450-460, 2005.
97. Napier J.A.L., Hildyard M.W. Simulation of fracture growth around openings in highly stressed, brittle rock. J. S. Afr. Inst. Min. Metall. Vol. 92: 159-168, 1992.
98. Nguyen D.C. and Derkx F. Méthode de mesure des caractéristiques rhéologiques d'un matériau au moyen de la compression diamétrale: application aux matériaux routiers. Bulletin des laboratoires des Ponts et Chaussées Vol. 207: 21-32, 1997.
99. Olempska, E. The Late Devonian Upper Kellwasser Event and entomozoacean ostracods in the Holy Cross Mountains, Poland. Acta Palaeontol. Pol. Vol. 47 (2): 247–266, 2002.
100. Olsson W.A., Peng S.S. Microcrack nucleation in marble. Int. J. Rock Mech. Min. Sci. & Geomech. Abstr. Vol. 13: 53-59, 1976.
101. Onodera T.F., Asoka Kumara H.M. Relation between texture and mechanical properties of crystalline rocks. Bull. Int. Assoc. Eng. Geol. Vol. 22: 173–177, 1980.
102. Pan P.Z., Feng X.T., Hudson J.A. Study of failure and scale effects in rocks under uniaxial compression using 3D cellular automata. Int. J. Rock Mech. Min. Sci. Vol. 46: 674-685, 2009.
103. Paterson M.S. Experimental rock deformation-the Brittle Field. Berlin, Springer, 254 p., 1978.
104. Paton T.R., Humphreys G.S., Mitchell P.B. Soils: A new global view. London: UCL Press Limited, 1995.
105. Paul B., Gangal M. Initial and subsequent fracture curves for biaxial compression of brittle materials. Proceedings of the 8th US Symposium on Rock Mechanics, Baltimore, 131–141, 1966.
106. Poty E., Chevalier E. L'activité extractive en Wallonie, Situation actuelle et perspectives. Belgium, Ouvrage publié par le Ministère de la Region Wallonne, 85 p., 2004.
107. Potyondy D.O., Cundall P.A. A bonded-particle model for rock. Int. J. Rock Mech. Min. Sci. Vol. 41: 1329-1364, 2004.
108. Powers M.C. A new roundness scale for sedimentary particles. J. Sediment. Petrol. Vol. 23: 117-119, 1953.
109. Powers T.C. Void spacing as a basis for producing air-entrained concrete. Research bulletin no. 49 of the Portland Cement Association, reprint from the Journal of the American Concrete Institute, in Proceedings Vol. 50: 741-760, 1954.
110. Přikryl R. Some microstructural aspects of strength variation in rocks. Int. J. Rock Mech. Min. Sci. Vol. 38: 671–682, 2001.
111. Reineck H.E., Singh I.B. Depositional sedimentary environments, Germany, Springer-Verlag, 552 p., 1986.
112. Reinhart J.S. Fracture of rocks. Int. J. Fract. Mech. Vol. 2: 534–590, 1966.
113. Rocco C., Guinea G.V., Planas J., Elices M. Size effect and boundary conditions in the Brazilian test: experimental verification. Mater. Struct. Vol. 32: 210-217, 1999a.
114. Rocco C., Guinea G.V., Planas J., Elices M. Size effect and boundary conditions in the Brazilian test: theoretical analysis. Mater. Struct. Vol. 32: 437-444, 1999b.
115. Savanick G.A., Johnson D.I. Measurements of the strength of grain boundaries in rock. Int. J. Rock Mech. Min. Sci. Vol. 11: 173-180, 1974.
116. Scotese C.R., McKerrow W.S. Revised world maps and introduction. Palaeozoic Palaeogeography and Biogeography, Geological Society of London Memoir. Editors: W.S.McKerrow and C.R. Scotese, Vol. 51:1–21, 1990.

117. Singh V.K., Singh D., Singh T.N. Prediction of strength properties of some schistose rocks from petrographic properties using artificial neural networks. Int. J. Rock Mech. Min. Sci. Vol. 38: 269-284, 2001.
118. Shakoor A., Bonelli R.E. Relationship between petrographic characteristics, engineering index properties, and mechanical properties of selected sandstones. Bull. Int. Assoc. of Eng. Geol. XXVIII (1): 55–71, 1991.
119. Shaler N.S. The origin and nature of soils. Powell J.W. (Ed.), USGS 12th Annual report 1890-1891: Washington, D.C., Government Printing Office, 213-245, 1891.
120. Shepard F.P. Submarine geology. New York, Harper & Row, 557 p., 1963.
121. Simmons G., Richter D. Microcracks in rock. In: The physics and chemistry of minerals and rocks. Strens R.G.J., ed. John Wiley & Sons, London, 105-137, 1976.
122. Sprunt E.S., Brace W.F. Direct observation of microcavities in crystalline rocks. Int. J. Rock Mech. Min. Sci. & Geomech. Abstr. Vol. 11: 139-150, 1974.
123. Stutzman P.E. Applications of scanning electron microscopy in cement and concrete petrography. Petrography of cementitious materials, ASTM STP 1215. De Hayes S.M., Stark D. (Eds.), American Society for Testing and Materials, West Conshohocken, PA, 74-90, 1994.
124. Szwedzicki T. A hypothesis on modes of failure of rock samples tested in uniaxial compression. J. Rock Mech. Rock Eng. Vol. 40 (1): 97-104, 2007.
125. Szwedzicki T., Shamu W. The effect of material discontinuities on strength of rock samples. Proceeding of Australasian Institute of Mining and Metallurgy. Vol. 304(1): 23–28, 1999.
126. Takemura T., Oda M. Stereology-based fabric analysis of microcracks in damaged granite. Tectonophysics Vol. 387: 131-150, 2004.
127. Tejchman J., Górski J. FE-investigations of a deterministic and statistical size effect in granular bodies within a micro-polar hypoplasticity. Granular Matter Vol. 9: 439-453, 2007.
128. Thorez J., Dreesen R., Streel M. Famennian. Geologica Belgica Vol. 9/1-2: 27-45, 2006.
129. Thorez J., Goemare E., Dreesen R. Tide- and wave-influenced depositional environments in the Psammites du Condroz (Upper Famennian) in Belgium. In: De Boer, P.L., Van Gelder A., Nio S.D. (Eds.). Tide-Influenced Sedimentary Environments and Facies, Sedimentology and Petroleum Geology, D. Reidel, Dordrecht, 389–415, 1988.
130. Thuro K., Plinninger R.J., Zäh S., Schütz S. Scale effects in rock strength properties. Part 1: Unconfined compressive test and Brazilian test. Särkkä P., Eloranta P. (Eds.), Proceedings of ISRM regional symposium EUROCK 2001: Rock Mechanics – A Challenge for Society, Espoo, Finland. Swets & Zeitlinger Lisse, 169-174, 2001.
131. Tien Y.M., Kuoa M.C., Juang G.H. An experimental investigation of the failure mechanism of simulated transversely isotropic rocks. Int. J. Rock Mech. Min. Sci. Vol. 43: 1163-1181, 2006.
132. Tien Y.M., Tsao P.F. Preparation and mechanical properties of artificial transversely isotropic rock. Int. J. Rock Mech. Min. Sci. Vol. 37: 1001–1012, 2000.
133. Tucker M. Techniques in sedimentology. Avon, The Bath Press, 394 p., 1995.
134. Tuğrul A., Zarif I.H. Correlation of mineralogical and textural characteristics with engineering properties of selected granitic rocks from Turkey. Eng. Geol. Vol. 51: 303-317, 1999.
135. Tuğrul A., Gürpinar O. The effect of chemical weather on the engineering properties of Eocene basalts in north-eastern Turkey. Environmental Eng. Geosci. Vol. 3 (2): 225–234, 1997.

136. Uysal I.T., S.D. Golding, Glikson A.Y., Mory A.J., Glikson M. K-Ar evidence from illitic clays of a Late Devonian age for the 120 km diameter Woodleigh impact structure, Southern Carnarvon Basin, Western Australia. Earth and Planetary Science Letters, Vol. 192: 281-289, 2001.
137. Van de Steen B. Effect of heterogeneities and defects on the fracture pattern in brittle rock. PhD thesis, KULeuven, Leuven, 250 p., 2001.
138. Van de Steen B., Vervoort A. Non-local stress approach to fracture initiation in laboratory experiments with a tensile stress gradient. Mech. Mater. Vol. 33: 729-740, 2001.
139. Van de Steen B., Vervoort A., Napier J.A.L. Numerical modelling of fracture initiation and propagation in biaxial tests on rock samples. Int. J. fract. Vol. 108: 165–191, 2001.
140. Van de Steen B., Vervoort A., Sahin K. Influence of internal structure of crinoidal limestone on fracture paths. Eng. Geol. Vol. 67: 109-125, 2002.
141. Vervoort A., Ganne P., Van de Steen B. Effect of stress state on fracture initiation and growth around circular openings. Stacey T.R., Malan D.F. (Eds.), Proceeding of the 6th international symposium on ground support in mining and civil engineering construction, Cape Town, South Africa. The Southern African Institute of Mining and Metallurgy Publications, 381-390, 2008.
142. Vervoort A., Govaerts A. Kaiser effect in tri-axial tests of limestone samples. Lu M., Li C.C., Kjørholt H., Dahle H. (Eds.), Proceeding of the international symposium on in-situ rock stress, Trondheim, Norway. Taylor & Francis Group, 143-149, 2006.
143. Wang C.H. Fracture of interface cracks under combined loading. Eng. Fract. Mech. Vol. 56: 77-86, 1997.
144. Wevers M. Identification of fatigue failure modes in carbon fibre reinforced composites. PhD thesis, KULeuven, Leuven, 1987.
145. Whittaker B.N., Singh R.N., Sun G. Rock fracture mechanics. Amsterdam: Elsevier, 570 p., 1992.
146. Willard R.J., McWilliams J.R. Microstructural techniques in the study of physical properties of rock. Int. J. Rock Mech. Min. Sci. Vol. 6: 1–12, 1969.
147. Wong R.H.C., Chau K.T., Wang P. Microcracking and grain size effect in Yuen Long marbles. Int. J. Rock Mech. Min. Sci. Geomech. Abstr. Vol. 33(5): 479–485, 1996.
148. Wong T.F. Micromechanics of faulting in Westerley granite. Int. J. Rock Mech. Min. Sci. Geomech. Abstr. Vol. 19: 49-64, 1982.
149. Yanagidani T., Sano O., Terada M., Ito I. The observation of cracks propagating in diametrically-compressed rock discs. Int. J. Rock Mech. Min. Sci. Geomech. Abstr. Vol. 15(5): 225–35, 1978.
150. Yoshinaka R., Osada M., Park H., Sasaki T., Sasaki K. Practical determination of mechanical design parameters of intact rock considering scale effect. Eng. Geol. Vol. 96: 173–186, 2008.
151. Yu Y., Zhang J., Zhang J. A modified Brazilian disk tension test. Int. J. Rock Mech. Min. Sci. Vol. 46: 421–425, 2009.
152. Yu Y. Question the validity of the Brazilian test for determining tensile strength of rock. Chin. J. Rock. Mech. Eng. Vol. 24(7): 1150–1157, 2005.
153. Yuan S.C., Harrison J.P. A review of the state of the art in modelling progressive mechanical breakdown and associated fluid flow in intact heterogeneous rocks. Int. J. Rock Mech. Min. Sci. Vol. 43: 1001-1022, 2006.
154. Yuan S.C., Harrison J.P. Development of a hydro-mechanical local degradation approach and its application to modelling fluid flow during progressive fracturing of heterogeneous rocks. Int. J. Rock Mech. Min. Sci. Vol. 42: 961–984, 2005.

Appendix A:
Diagrams of AE Hits

Variation in cumulative AE hits as a function of applied load for all 17 samples of sandstone sub-types 1 to 4 (Table 3.1) is presented in this Appendix. For the first sample of sandstone sub-type 4, variation in cumulative AE hits is presented as a function of applied load duration. Threshold level for all the graphs is fixed on 30.6 dB, except for the graph of sample 4 in sandstone sub-type 4 which is fixed on 35.5 dB.

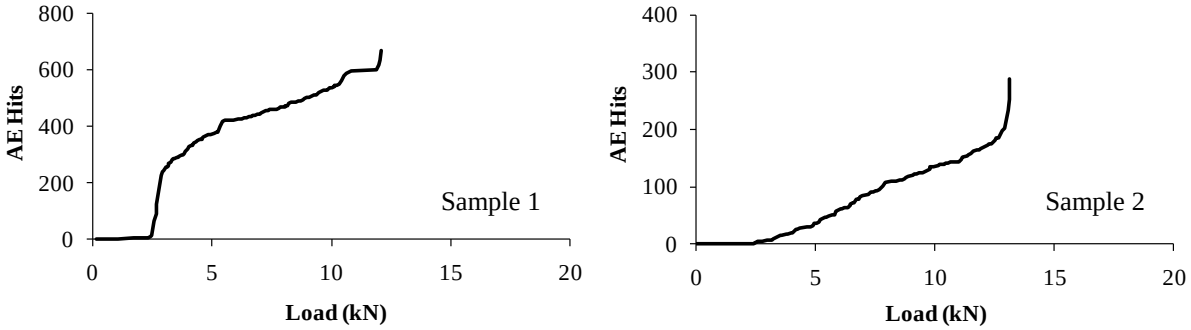

Figure A.1. Variation in cumulative AE hits as a function of applied load for the two samples of sandstone sub-type 1. Threshold level for all the graphs is fixed on 30.6 dB.

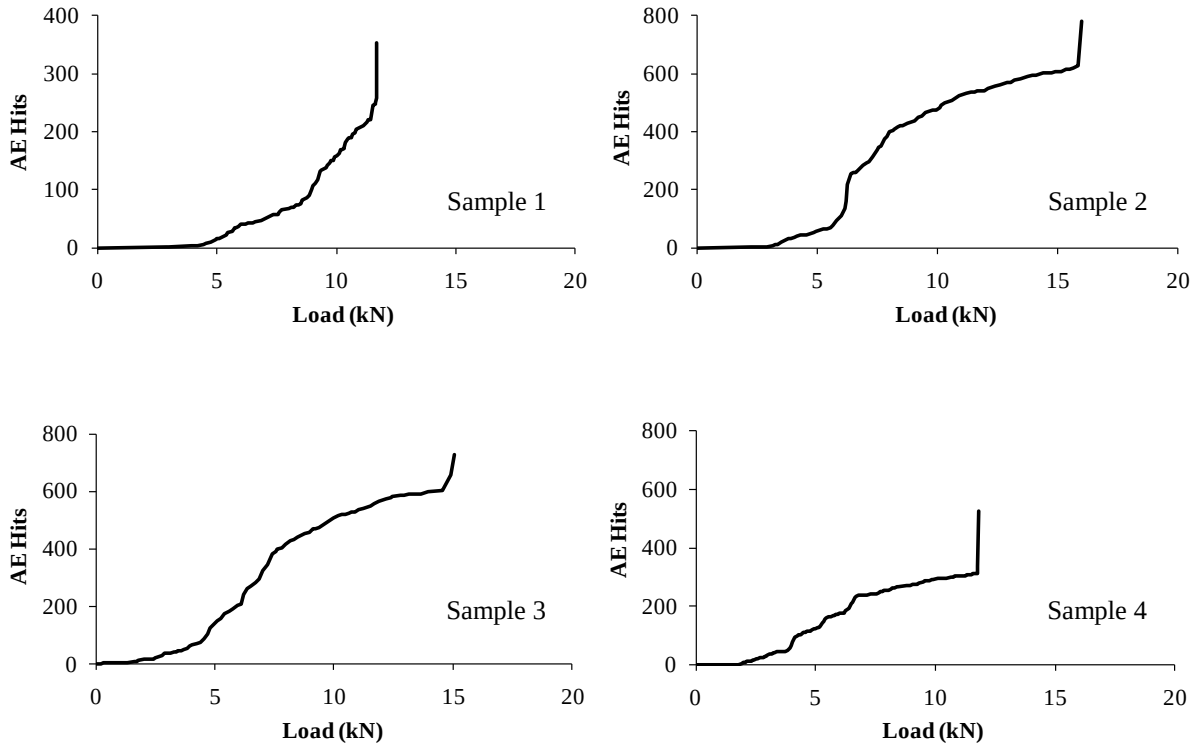

Figure A.2. Variation in cumulative AE hits as a function of applied load for the four samples of sandstone sub-type 2. Threshold level for all the graphs is fixed on 30.6 dB.

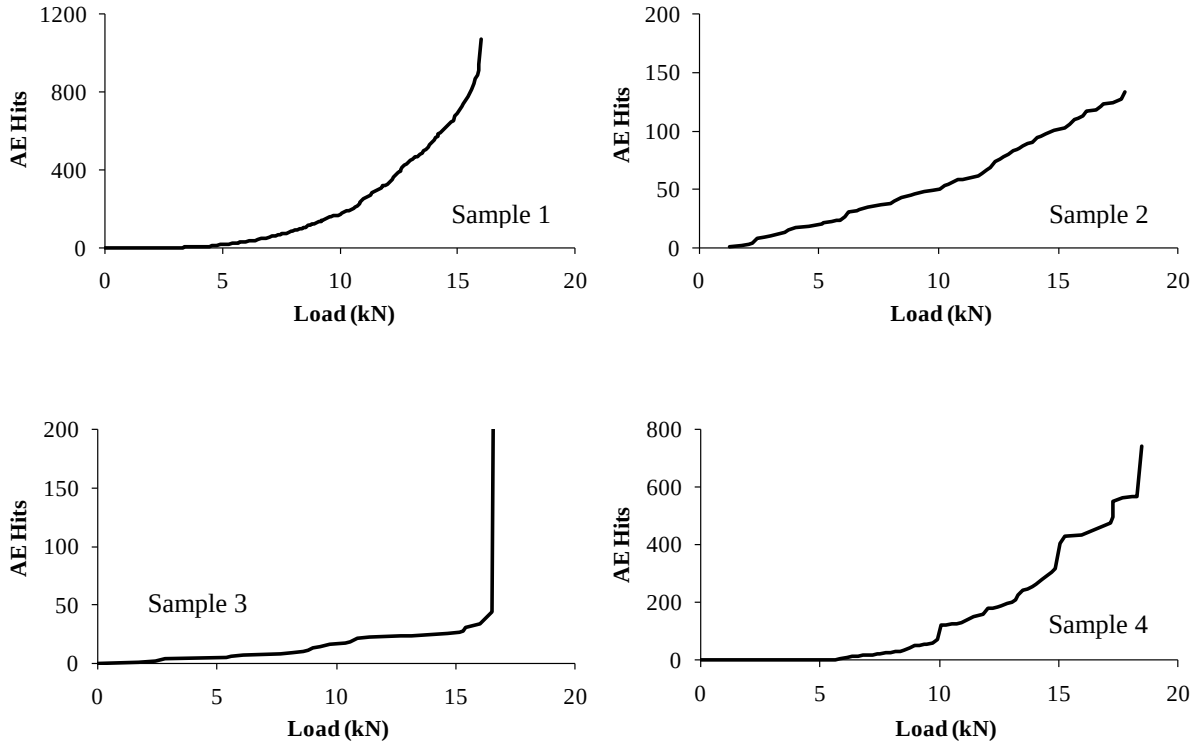

Figure A.3. Variation in cumulative AE hits as a function of applied load for the four samples of sandstone sub-type 3. Threshold level for all the graphs is fixed on 30.6 dB.

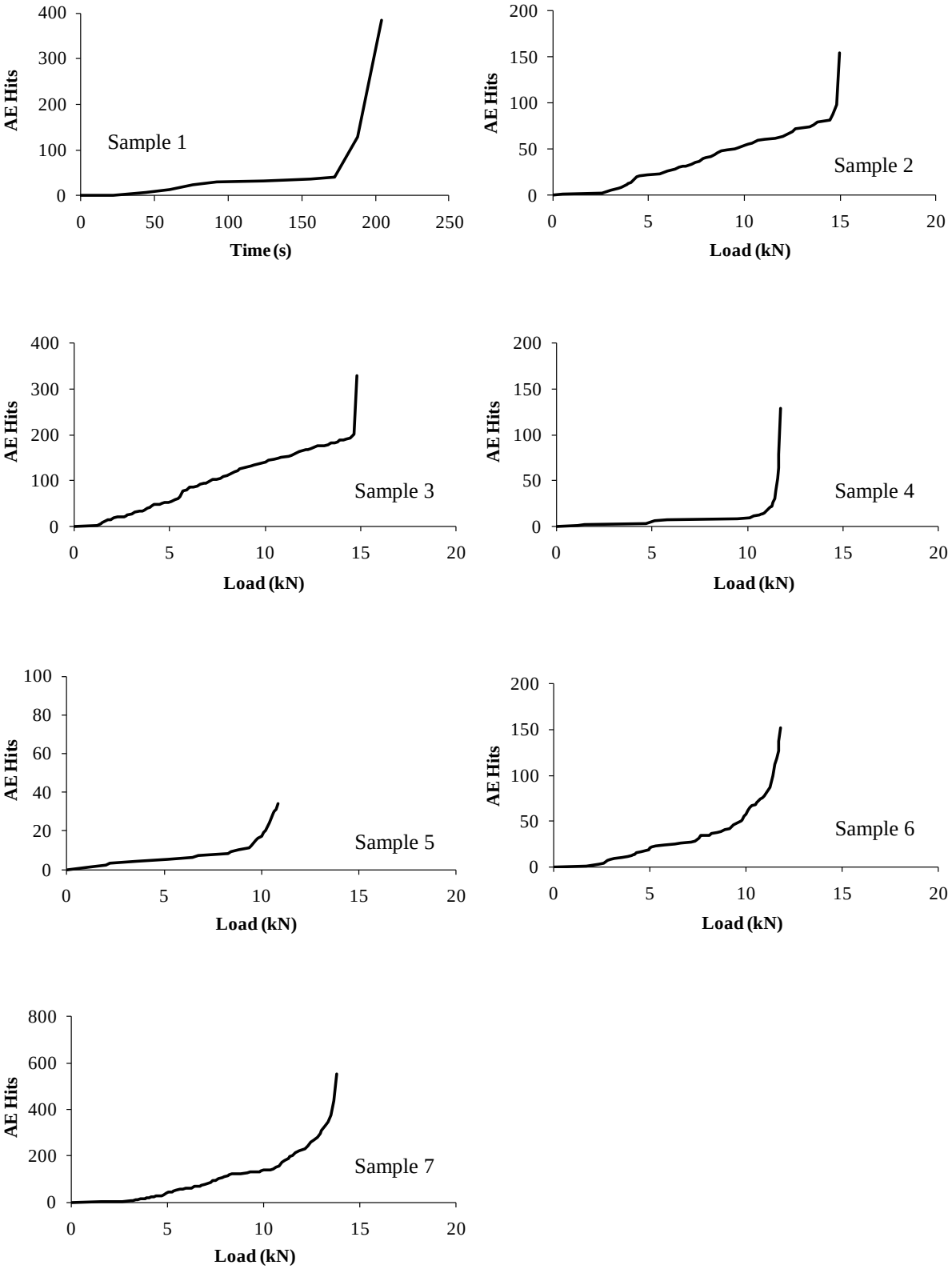

Figure A.4. Variation in cumulative AE hits as a function of applied load for the four samples of sandstone sub-types 4. Threshold level for all the graphs is fixed on 30.6 dB, except for sample 4 which is 35.5 dB. For sample 1 variation in cumulative AE hits is presented as a function of applied load duration.

Appendix B:
Diagrams of Load Displacement

Variation in applied load as a function of displacement for all 31 samples of sandstone sub-type 1 in nine different groups of inclination angle (0°, 15°, 30°, 45°, 60°, 65°, 70°, 80° and 90°) is presented in this Appendix. Also the total energy to which the samples are subjected to is presented for every sample.

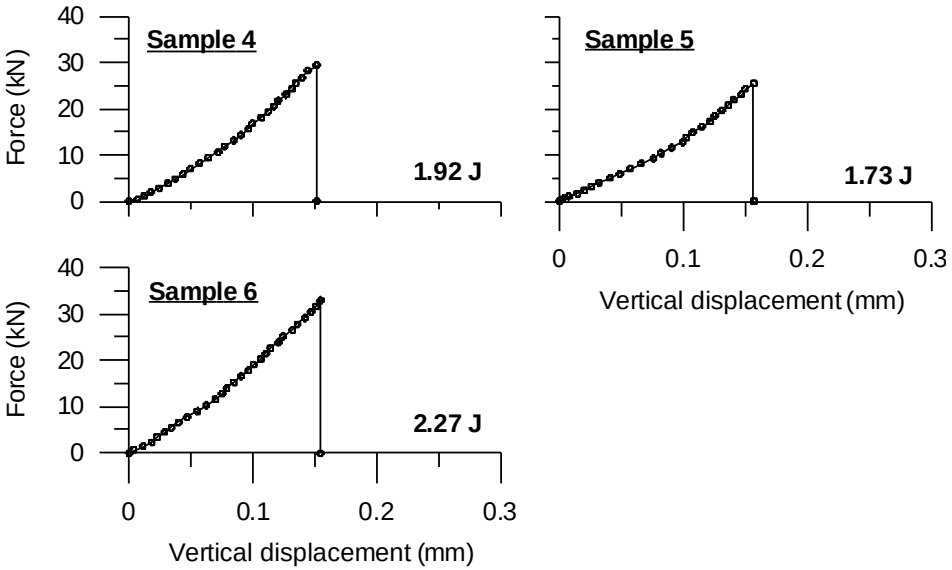

Figure B.1. Variation in applied load as a function of displacement for group I (θ = 0°). Applied energy is put on the graph.

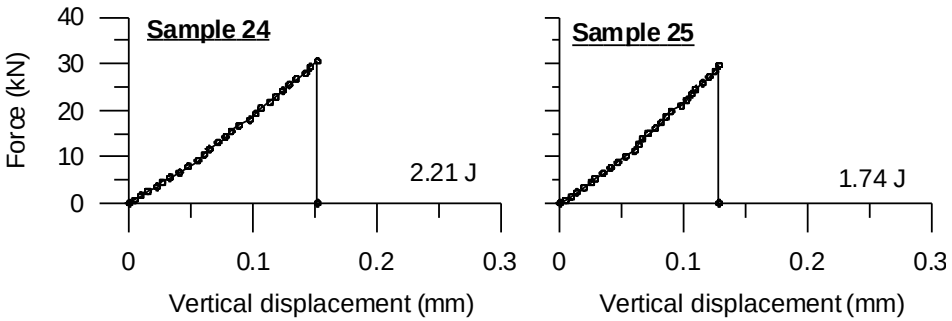

Figure B.2. Variation in applied load as a function of displacement for group II (θ = 15°). Applied energy is put on the graph.

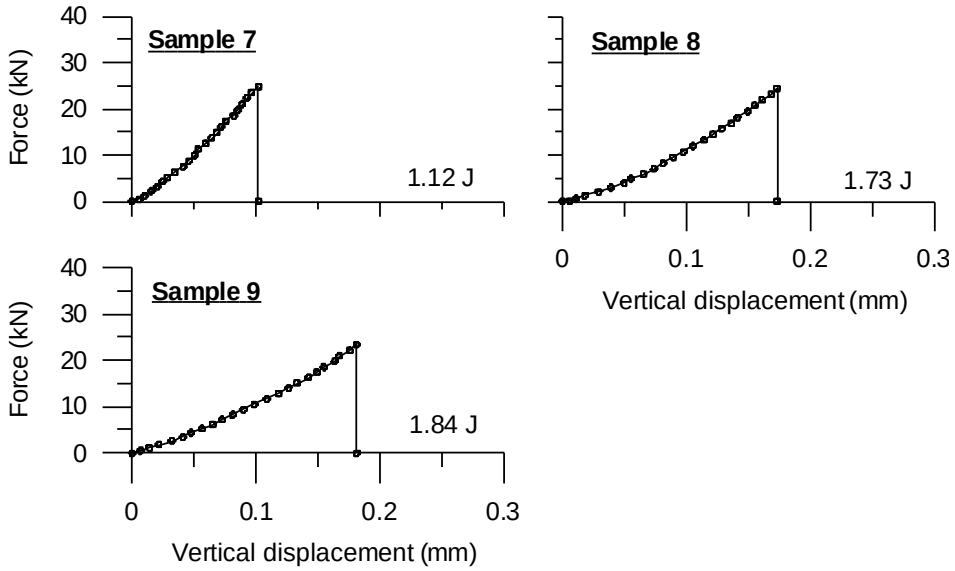

Figure B.3. Variation in applied load as a function of displacement for group III (θ = 30°). Applied energy is put on the graph.

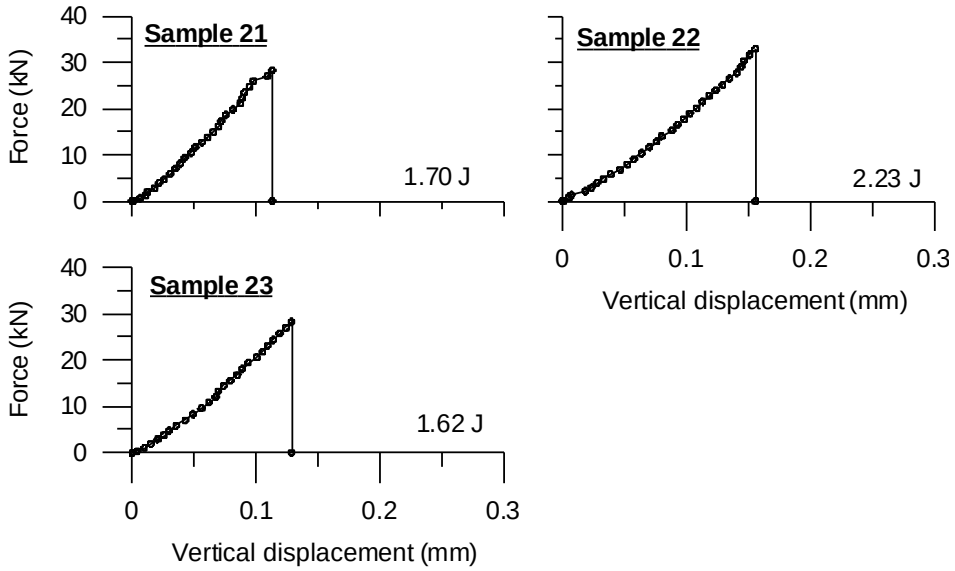

Figure B.4. Variation in applied load as a function of displacement for group IV (θ = 45°). Applied energy is put on the graph.

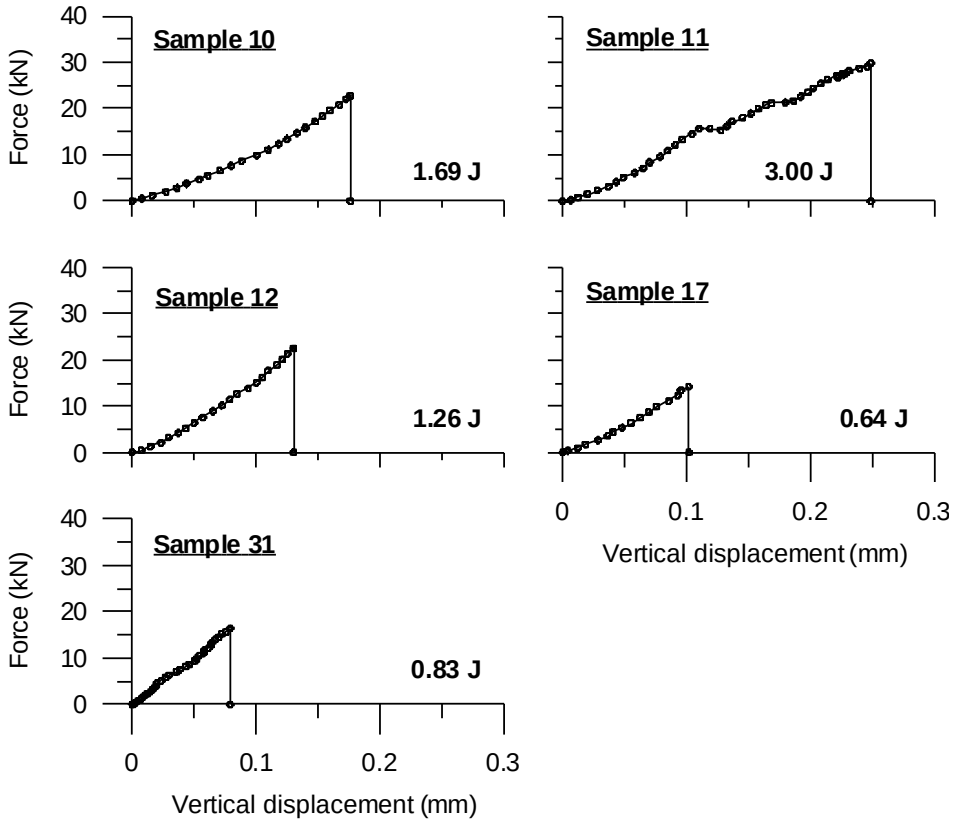

Figure B.5. Variation in applied load as a function of displacement for group V (θ = 60°). Applied energy is put on the graph.

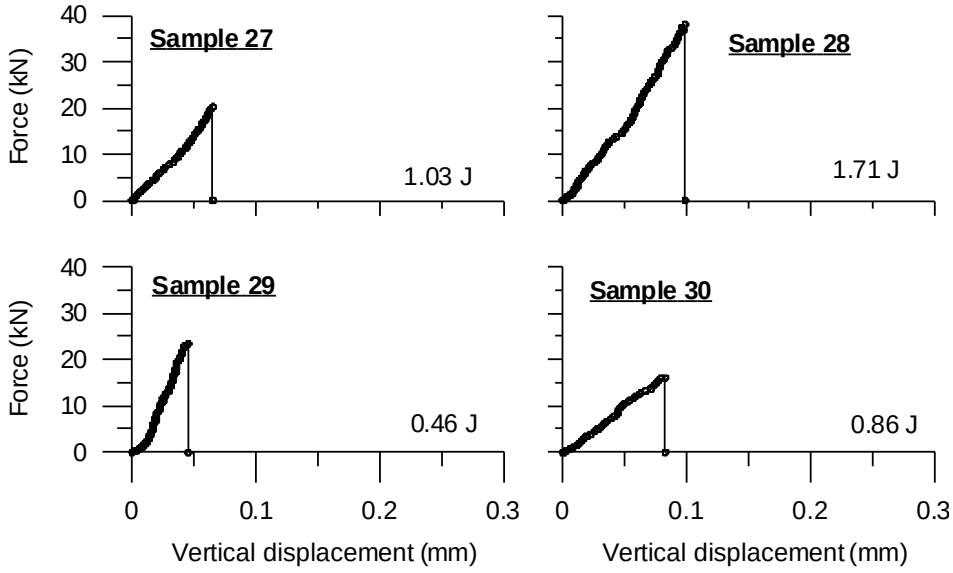

Figure B.6. Variation in applied load as a function of displacement for group VI (θ = 65°). Applied energy is put on the graph.

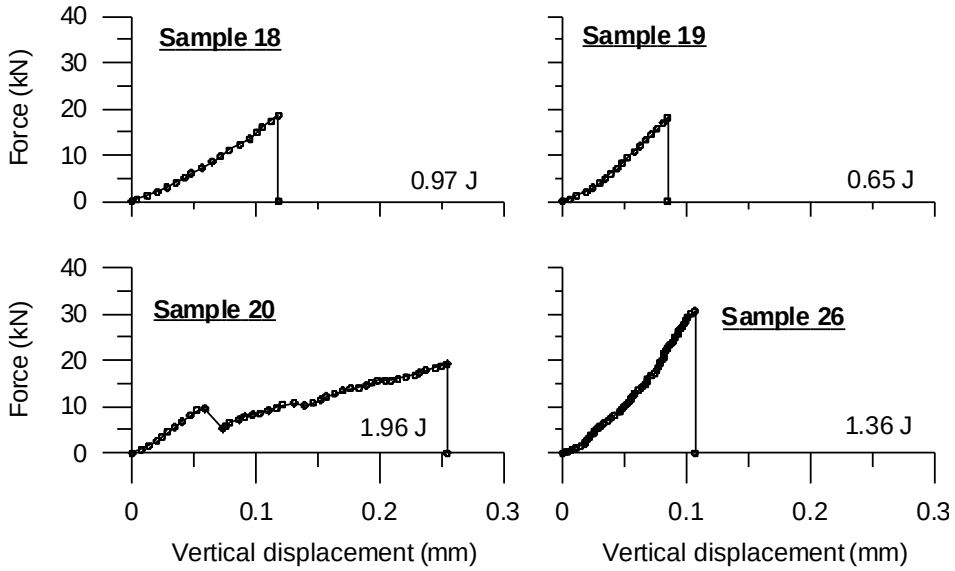

Figure B.7. Variation in applied load as a function of displacement for group VII (θ = 70°). Applied energy is put on the graph.

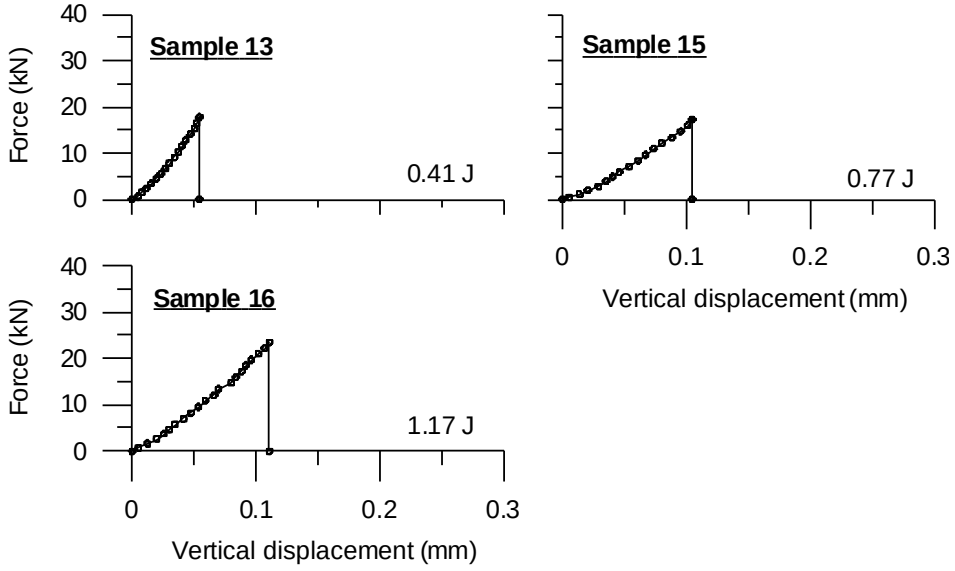

Figure B.8. Variation in applied load as a function of displacement for group VIII (θ = 80°). Applied energy is put on the graph.

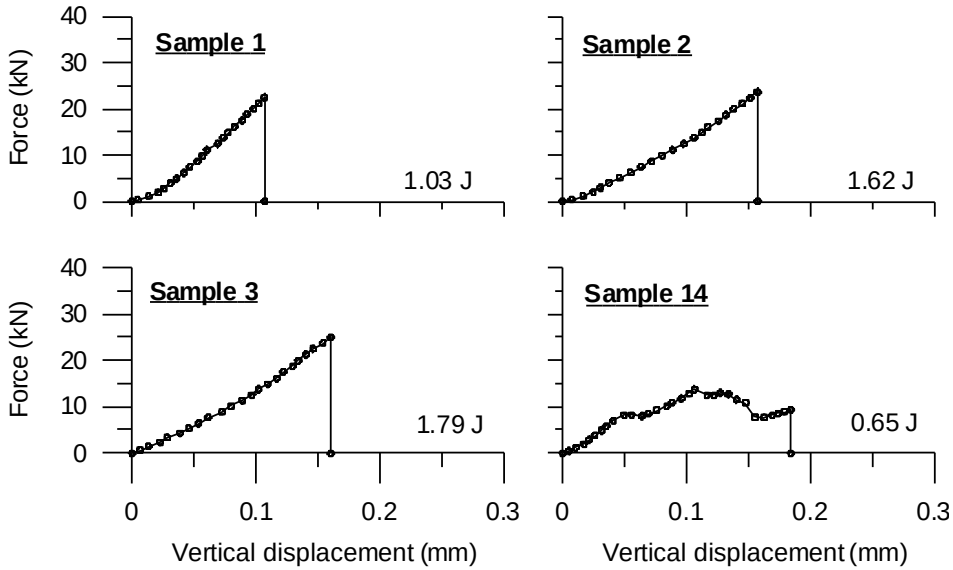

Figure B.9. Variation in applied load as a function of displacement for group IX ($\theta = 90°$). Applied energy is put on the graph.

Appendix C:
Information of Tested Samples

In this appendix the information about all samples of sandstone sub-types 2, 3, 4 and 5 after conducting Brazilian tests is presented. The number of tested samples for sandstone sub-types 2, 3, 4 and 5 are 29, 30, 22 and 30, respectively.

Tables C.1 to C.4 gives the inclination angle θ, the diameter D, the thickness t, the failure load F and some other information about the tested samples.
The failure patterns (one side) of all the samples after failure are digitalised and shown in Figures C.1 to C.4 in different groups of the inclination angle.
Tables C.5 to C.8 presents the fracture length of all samples in the seven groups. In these tables fracture lengths corresponding to layer activation, central fracture(s) and non-central fracture(s) are presented.

Table C.1 Brazilian test results for Modave sandstone sub-type 2

Group	θ (°)	Sample N°	D (mm)	t (mm)	ρ (t/m³)	t/D	F (kN)	BTS (MPa)
I 	0	1	49.3	25.3	2.6	0.51	31.2	15.9
	0	2	49.3	25.5	2.6	0.52	25.9	13.1
	0	3	50.1	24.4	2.6	0.49	19.5	10.2
	0	4	50.2	25.2	2.6	0.50	29.5	14.8
II	20	5	50.2	25.3	2.6	0.50	28.2	14.1
	20	6	50.1	25.1	2.6	0.50	23.9	12.1
	20	7	50.1	25.2	2.6	0.50	29.3	14.8
	20	8	50.1	27.4	2.6	0.55	33.7	15.6
II	45	9	50.2	23.6	2.6	0.47	23.7	12.7
	45	10	50.1	25.5	2.6	0.51	20.6	10.3
	45	11	50.1	25.3	2.6	0.50	16.3	8.2
	45	12	50.1	25.2	2.6	0.50	13.9	7.0
IV	60	13	50.1	27.5	2.6	0.55	15.8	7.3
	60	14	50.3	25.3	2.6	0.50	21.6	10.8
	60	15	50.1	25.4	2.6	0.51	16.5	8.3
	60	16	50.3	25.5	2.6	0.51	17.2	8.6
V	70	25	50.1	24.9	2.6	0.50	18.6	9.5
	70	26	50.0	24.8	2.6	0.50	9.9	5.1
	70	27	50.1	24.9	2.6	0.50	14.5	7.4
	70	28	50.1	25.0	2.6	0.50	19.2	9.8
VII	80	17	50.1	24.1	2.6	0.48	1.7	0.9
	80	18	50.1	25.6	2.6	0.51	13.4	6.6
	80	19	50.1	25.2	2.6	0.50	10.2	5.1
	80	20	50.1	24.5	2.6	0.49	6.3	3.3
	80	29	49.4	25.4	2.6	0.51	21.1	10.7
VIII 	90	21	50.1	27.2	2.6	0.54	15.7	7.3
	90	22	49.4	25.3	2.6	0.51	16.5	8.4
	90	23	49.4	25.6	2.6	0.52	19.3	9.7
	90	24	50.1	27.5	2.6	0.55	14.2	6.6

θ is the angle of layer direction from horizontal. D = Diameter, t = Thickness and F = Failure load of the samples. Presented density is measured in laboratory conditions.

Table C.2 Brazilian test results for Modave sandstone sub-type 3

Group	θ (°)	Sample N°	D (mm)	t (mm)	ρ (t/m³)	t/D	F (kN)	BTS (MPa)
I	0	1	50.0	24.8	2.5	0.50	34.7	17.9
	0	2	50.0	25.8	2.5	0.52	27.5	13.6
	0	3	50.1	24.8	2.6	0.49	26.9	13.8
	0	4	50.1	23.8	2.6	0.48	28.3	15.1
II	20	5	50.1	24.8	2.6	0.50	28.6	14.6
	20	6	50.1	24.9	2.6	0.50	24.5	12.5
	20	7	50.1	24.7	2.6	0.49	32.3	16.6
	20	8	50.1	25.5	2.5	0.51	25.5	12.7
II	45	9	50.1	24.8	2.6	0.49	26.2	13.4
	45	10	50.0	25.1	2.5	0.50	29.3	14.9
	45	11	50.0	24.9	2.5	0.50	26.0	13.3
	45	12	50.1	24.8	2.6	0.49	29.3	15.0
IV	60	13	50.0	24.5	2.5	0.49	19.1	9.9
	60	14	50.2	24.8	2.5	0.49	30.5	15.6
	60	15	50.0	25.0	2.5	0.50	22.7	11.5
	60	16	50.0	24.3	2.6	0.49	26.2	13.8
	60	29	49.9	24.9	2.5	0.50	28.4	14.6
V	70	25	50.1	25.0	2.5	0.50	28.9	14.7
	70	26	50.2	24.8	2.6	0.49	26.2	13.4
	70	27	50.2	24.6	2.6	0.49	32.3	16.7
	70	28	50.1	24.5	2.6	0.49	25.4	13.1
VII	80	17	49.9	24.6	2.5	0.49	14.3	7.4
	80	18	50.0	25.3	2.6	0.51	27.3	13.7
	80	19	50.0	25.7	2.6	0.51	18.7	9.3
	80	20	50.2	24.0	2.6	0.48	24.8	13.1
	80	30	50.0	25.5	2.6	0.51	25.8	12.9
VIII	90	21	50.0	24.0	2.6	0.48	18.9	10.0
	90	22	50.0	25.1	2.6	0.50	31.7	16.0
	90	23	49.9	23.9	2.5	0.48	17.1	9.1
	90	24	50.2	24.7	2.5	0.49	28.5	14.6

θ is the angle of layer direction from horizontal. D = Diameter, t = Thickness and F = Failure load of the samples. Presented density is measured in laboratory conditions.

Table C.3 Brazilian test results for Modave sandstone sub-type 4

Group	θ (°)	Sample N°	D (mm)	t (mm)	ρ (t/m³)	L/D	F (kN)	BTS (MPa)
I 	0	1	50.0	25.8	2.6	0.52	21.7	10.7
	0	2	50.1	25.2	2.6	0.50	31.1	15.7
	0	21	50.1	17.3	2.6	0.35	21.0	15.5
II	20	3	50.0	25.7	2.6	0.51	29.4	14.5
	20	4	50.1	25.5	2.6	0.51	31.9	15.9
	20	22	50.1	17.5	2.6	0.35	15.5	11.3
II	45	5	50.1	25.5	2.5	0.51	27.3	13.6
	45	6	50.1	25.3	2.6	0.51	23.6	11.9
	45	7	50.0	25.1	2.6	0.50	24.0	12.2
IV	60	8	50.0	25.9	2.6	0.52	24.3	11.9
	60	9	50.1	25.9	2.6	0.52	21.0	10.3
	60	10	50.1	25.9	2.6	0.52	21.2	10.4
V	70	17	50.1	25.1	2.6	0.50	23.2	11.8
	70	18	50.1	24.7	2.6	0.49	21.4	11.0
	70	19	50.1	25.2	2.6	0.50	23.0	11.6
	70	20	50.1	25.2	2.6	0.50	22.1	11.1
VI	80	11	50.0	25.9	2.6	0.52	17.5	8.6
	80	12	50.1	25.4	2.6	0.51	22.2	11.1
	80	13	50.1	25.3	2.6	0.51	20.6	10.3
	80	15	50.0	25.9	2.6	0.52	17.0	8.4
VII 	90	14	50.1	26.0	2.6	0.52	16.3	8.0
	90	16	50.1	26.8	2.6	0.54	17.7	8.4

θ is the angle of layer direction from horizontal. D = Diameter, t = Thickness and F = Failure load of the samples. Presented density is measured in laboratory conditions.

Table C.4 Brazilian test results for Modave sandstone sub-type 5

Group	θ (°)	Sample N°	D (mm)	t (mm)	ρ (t/m³)	t/D	F (kN)	BTS (MPa)
I	0	1	50.0	26.0	2.6	0.52	26.9	13.2
	0	2	49.9	25.6	2.6	0.51	19.2	9.6
	0	3	50.0	25.8	2.6	0.52	17.5	8.6
	0	4	50.0	25.2	2.6	0.50	29.4	14.8
II	20	5	49.8	25.0	2.6	0.50	31.6	16.2
	20	6	50.1	25.7	2.6	0.51	32.9	16.3
	20	7	50.0	26.2	2.6	0.52	27.9	13.6
	20	8	50.1	25.7	2.6	0.51	29.8	14.7
II	45	9	50.1	25.7	2.6	0.51	28.1	13.9
	45	10	50.0	25.5	2.6	0.51	28.0	13.9
	45	11	50.0	25.7	2.6	0.51	29.5	14.6
	45	12	50.0	25.4	2.6	0.51	26.0	13.0
IV	60	13	50.0	25.7	2.6	0.51	23.3	11.5
	60	14	50.0	25.8	2.6	0.52	7.2	3.5
	60	15	50.1	25.8	2.6	0.52	20.8	10.2
	60	16	50.1	25.9	2.6	0.52	22.6	11.1
	60	29	50.0	25.2	2.6	0.50	23.7	12.0
	60	30	49.8	25.4	2.6	0.51	21.2	10.7
V	70	25	50.1	25.3	2.6	0.50	25.3	12.7
	70	26	50.1	25.6	2.6	0.51	23.4	11.6
	70	27	50.1	25.4	2.6	0.51	27.3	13.7
	70	28	50.1	25.2	2.6	0.50	25.8	13.0
VII	80	17	50.0	25.6	2.6	0.51	17.9	8.9
	80	18	49.8	25.2	2.6	0.51	18.7	9.4
	80	19	49.8	24.8	2.6	0.50	17.3	8.9
	80	20	50.1	25.8	2.6	0.51	21.3	10.5
VIII	90	21	50.0	25.7	2.6	0.51	19.0	9.4
	90	22	50.0	25.7	2.6	0.51	18.9	9.3
	90	23	50.0	25.8	2.6	0.52	18.2	9.0
	90	24	50.0	25.8	2.6	0.52	17.1	8.5

θ is the angle of layer direction from horizontal. D = Diameter, t = Thickness and F = Failure load of the samples. Presented density is measured in laboratory conditions.

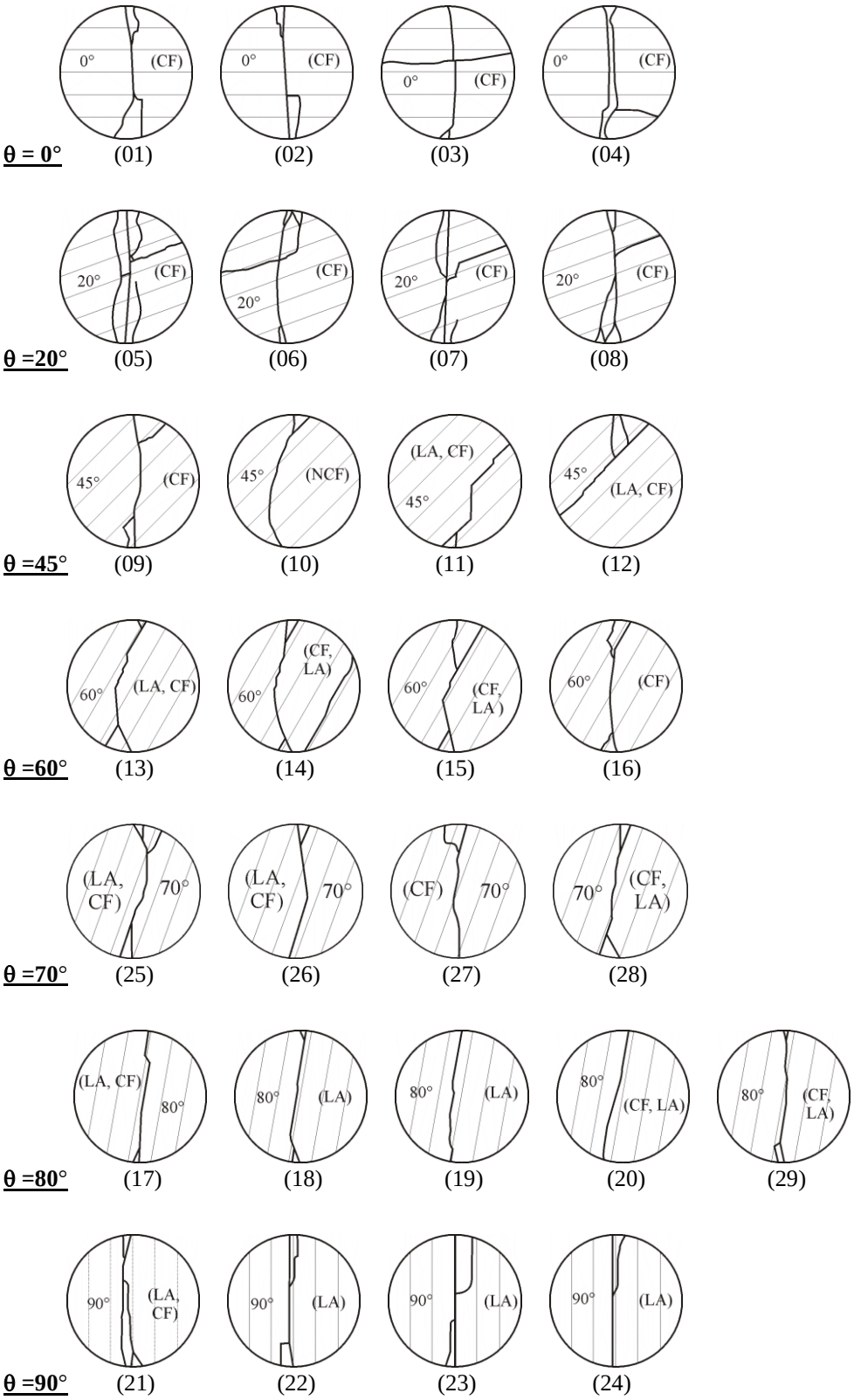

Figure C.1 Observed failure patterns (one side) of samples for different values of the inclination angle θ for Modave sandstone sub-type 2 after conducting Brazilian tests. Sample number and the predominant mode are put in parentheses, CF = Central fracture, NCF = Non-central fracture, LA = Layer activation. Quantification of predominant and secondary failure modes is presented further (Table C.5).

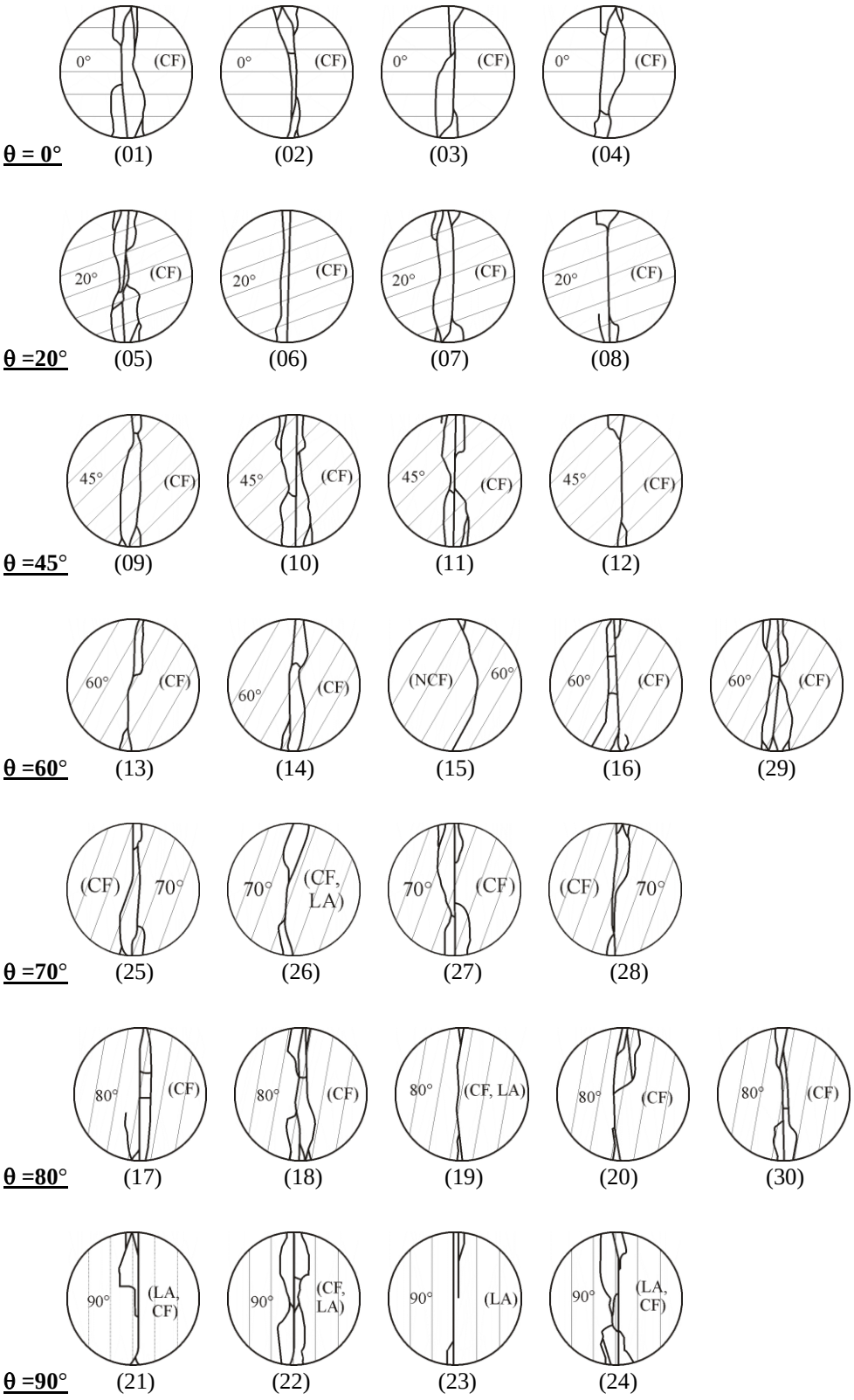

Figure C.2 Observed failure patterns (one side) of samples for different values of the inclination angle θ for Modave sandstone sub-type 3 after conducting Brazilian tests. Sample number and the predominant mode are put in parentheses, CF = Central fracture, NCF = Non-central fracture, LA = Layer activation. Quantification of predominant and secondary failure modes is presented further (Table C.6).

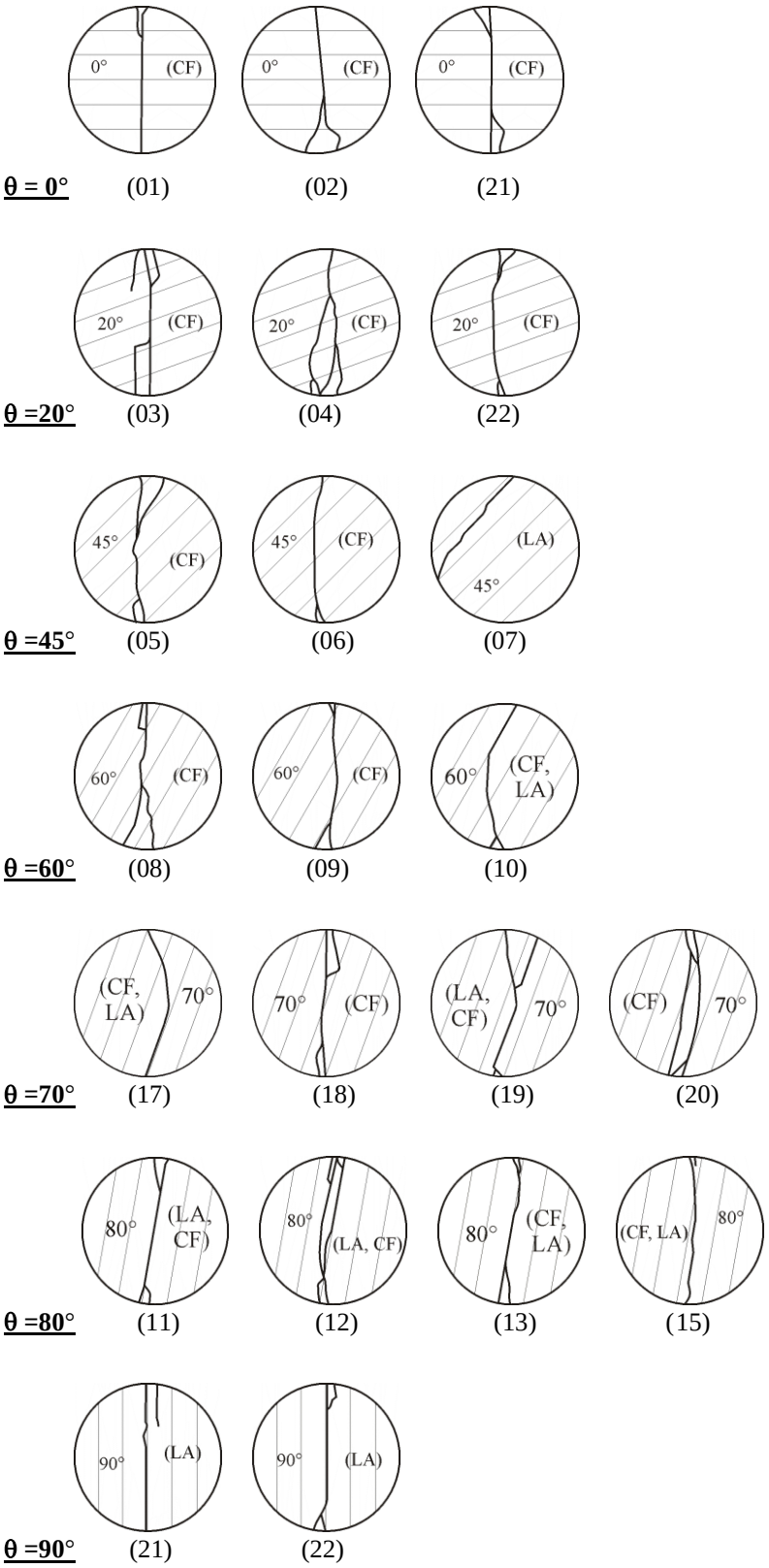

Figure C.3 Observed failure patterns (one side) of samples for different values of the inclination angle θ for Modave sandstone sub-type 4 after conducting Brazilian tests. Sample number and the predominant mode are put in parentheses, CF = Central fracture, NCF = Non-central fracture, LA = Layer activation. Quantification of predominant and secondary failure modes is presented further (Table C.7).

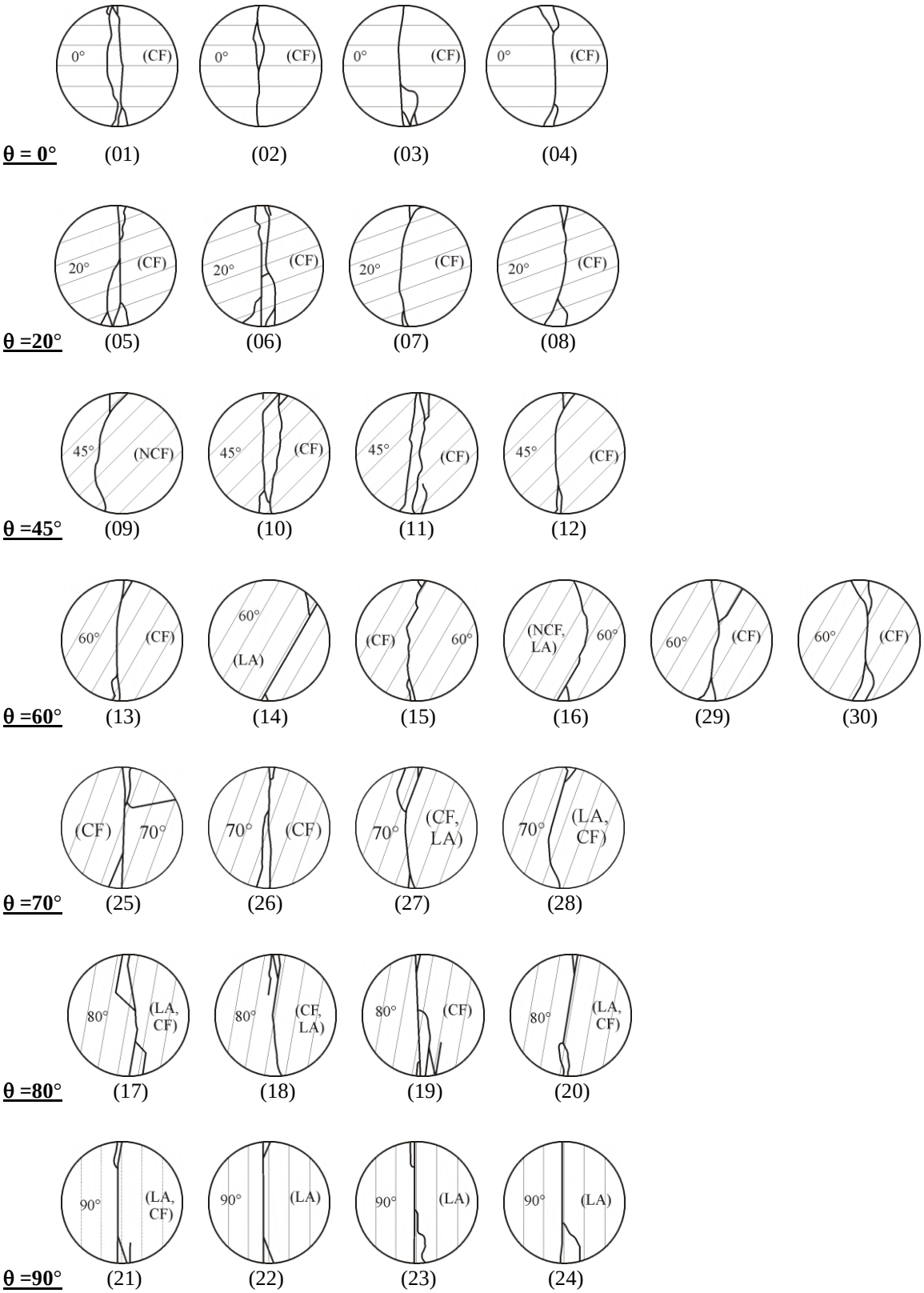

Figure C.4 Observed failure patterns (one side) of samples for different values of the inclination angle θ for Modave sandstone sub-type 5 after conducting Brazilian tests. Sample number and the predominant mode are put in parentheses, CF = Central fracture, NCF = Non-central fracture, LA = Layer activation. Quantification of predominant and secondary failure modes is presented further (Table C.8).

Table C.5 Fracture length of samples of Modave sandstone sub-type 2 (Brazilian tests)

Group	θ (°)*	Sample	Fracture length (sandstone sub-type 2)						
			Layer activation		Central fracture		Non-central fracture		Total
			(mm)	(%)	(mm)	(%)	(mm)	(%)	(mm)
I	0	1	0	0	65	78	19	22	84
		2	5	6	79	94	0	0	84
		3	21	20	56	54	26	25	104
		4	9	7	103	86	8	6	119
		Average	9	8	76	78	13	14	98
III	20	5	8	5	145	91	8	5	160
		6	16	14	85	74	14	12	115
		7	21	16	110	84	0	0	131
		8	14	12	100	88	0	0	114
		Average	15	12	110	84	5	4	130
IV	45	9	13	15	69	85	0	0	81
		10	10	17	8	13	43	71	60
		11	35	55	21	33	8	12	64
		12	39	52	28	37	9	12	75
		Average	24	35	31	42	15	24	70
V	60	13	33	50	33	50	0	0	65
		14	44	41	46	44	16	15	106
		15	38	47	43	53	0	0	80
		16	19	24	59	76	0	0	78
		Average	33	41	45	56	4	4	82
VII	70	25	40	51	39	49	0	0	79
		26	31	53	28	47	0	0	59
		27	14	21	51	79	0	0	65
		28	28	39	43	61	0	0	70
		Average	28	41	40	59	0	0	68
VIII	80	17	29	52	26	48	0	0	55
		18	41	70	18	30	0	0	59
		19	38	75	13	25	0	0	50
		20	19	43	25	57	0	0	44
		29	24	39	38	61	0	0	61
		Average	30	56	24	44	0	0	54
IX	90	21	50	51	48	49	0	0	98
		22	60	79	16	21	0	0	76
		23	78	82	18	18	0	0	95
		24	60	83	13	17	0	0	73
		Average	62	74	23	26	0	0	85

* Inclination angles θ is the angle of layer direction from horizontal. In all the samples, the length of fractures is measured from one side, except samples 11 which is the average from both sides.

Dark gray indicates the predominant failure mode and light gray indicates the secondary failure mode. The second percentage of either fracture is arbitrarily called the secondary failure mode only if it is equal or more than half of the largest percentage.

Table C.6 Fracture length of samples of Modave sandstone sub-type 3 (Brazilian tests)

Group	θ (°)*	Sample	Fracture length (sandstone sub-type 3)						
			Layer activation		Central fracture		Non-central fracture		Total
			(mm)	(%)	(mm)	(%)	(mm)	(%)	(mm)
I	0	1	3	2	133	82	26	16	161
		2	3	2	130	98	0	0	133
		3	0	0	114	100	0	0	114
		4	0	0	124	100	0	0	124
		Average	1	1	125	95	7	4	133
III	20	5	0	0	176	100	0	0	176
		6	0	0	101	100	0	0	101
		7	0	0	130	96	5	4	135
		8	0	0	83	100	0	0	83
		Average	0	0	123	99	1	1	124
IV	45	9	0	0	115	100	0	0	115
		10	9	5	154	87	14	8	176
		11	0	0	158	100	0	0	158
		12	0	0	71	100	0	0	71
		Average	2	1	124	97	3	2	130
V	60	13	8	9	76	91	0	0	84
		14	15	13	103	87	0	0	118
		15	16	28	4	7	38	65	58
		16	21	16	109	84	0	0	130
		29	0	0	175	100	0	0	175
		Average	12	13	93	74	8	13	113
VII	70	25	16	14	101	86	0	0	118
		26	35	41	38	43	14	16	86
		27	21	14	98	66	30	20	149
		28	8	7	101	93	0	0	109
		Average	20	19	84	72	11	9	115
VIII	80	17	15	11	118	89	0	0	133
		18	46	30	109	70	0	0	155
		19	25	38	41	62	0	0	66
		20	26	21	99	79	0	0	125
		30	25	20	101	80	0	0	126
		Average	28	24	94	76	0	0	121
IX	90	21	65	62	40	38	0	0	105
		22	75	47	86	53	0	0	161
		23	84	88	11	12	0	0	95
		24	73	49	61	41	15	10	149
		Average	74	61	50	36	4	3	128

* Inclination angles θ is the angle of layer direction from horizontal. In all the samples, the length of fractures is measured from one side.

Dark gray indicates the predominant failure mode and light gray indicates the secondary failure mode. The second percentage of either fracture is arbitrarily called the secondary failure mode only if it is equal or more than half of the largest percentage.

Table C.7 Fracture length of samples of Modave sandstone sub-type 4 (Brazilian tests)

Group	θ (°)*	Sample	Fracture length (sandstone sub-type 4)						
			Layer activation		Central fracture		Non-central fracture		Total
			(mm)	(%)	(mm)	(%)	(mm)	(%)	(mm)
I 	0	1	0	0	61	100	0	0	61
		2	0	0	69	100	0	0	69
		21	0	0	76	100	0	0	76
		Average	0	0	69	100	0	0	69
III	20	3	0	0	98	100	0	0	98
		4	0	0	106	100	0	0	106
		22	0	0	65	100	0	0	65
		Average	0	0	90	100	0	0	90
IV	45	5	0	0	74	100	0	0	74
		6	0	0	55	100	0	0	55
		7	30	71	0	0	13	29	43
		Average	10	24	43	67	4	10	57
V	60	8	9	10	76	90	0	0	85
		9	10	15	56	85	0	0	66
		10	24	42	33	58	0	0	56
		Average	14	23	55	77	0	0	69
VII	70	17	24	46	28	54	0	0	51
		18	0	0	80	100	0	0	80
		19	38	52	35	48	0	0	73
		20	26	23	86	77	0	0	113
		Average	22	30	57	70	0	0	79
VIII	80	11	44	64	25	36	0	0	69
		12	56	51	55	49	0	0	111
		13	33	47	36	53	0	0	69
		15	23	40	34	60	0	0	56
		Average	39	50	38	50	0	0	76
IX 	90	14	48	72	19	28	0	0	66
		16	44	67	21	33	0	0	65
		Average	46	70	20	30	0	0	66

* Inclination angles θ is the angle of layer direction from horizontal. In all the samples, the length of fractures is measured from one side.

Dark gray indicates the predominant failure mode and light gray indicates the secondary failure mode. The second percentage of either fracture is arbitrarily called the secondary failure mode only if it is equal or more than half of the largest percentage.

Table C.8 Fracture length of samples of Modave sandstone sub-type 5 (Brazilian tests)

Group	θ (°)*	Sample	Fracture length (sandstone sub-type 5)						
			Layer activation		Central fracture		Non-central fracture		Total
			(mm)	(%)	(mm)	(%)	(mm)	(%)	(mm)
I	0	1	0	0	119	100	0	0	119
		2	0	0	71	100	0	0	71
		3	0	0	83	100	0	0	83
		4	0	0	76	100	0	0	76
		Average	0	0	87	100	0	0	87
III	20	5	0	0	106	94	6	6	113
		6	6	5	129	95	0	0	135
		7	3	4	63	96	0	0	65
		8	0	0	74	100	0	0	74
		Average	2	2	93	96	2	1	97
IV	45	9	8	12	8	12	48	76	63
		10	16	14	99	86	0	0	115
		11	5	4	123	96	0	0	128
		12	13	19	55	81	0	0	68
		Average	10	12	71	69	12	19	93
V	60	13	11	16	59	84	0	0	70
		14	46	77	3	4	11	19	60
		15	18	27	48	73	0	0	65
		16	24	38	6	10	33	52	63
		29	16	21	61	79	0	0	78
		30	15	17	71	83	0	0	86
		Average	22	33	41	55	7	12	70
VII	70	25	14	14	66	65	21	21	101
		26	8	9	80	91	0	0	88
		27	28	33	45	55	10	12	83
		28	29	50	29	50	0	0	58
		Average	19	26	55	65	8	8	82
VIII	80	17	48	51	45	49	0	0	93
		18	31	41	45	59	0	0	76
		19	39	33	80	67	0	0	119
		20	39	53	34	47	0	0	73
		Average	39	45	51	55	0	0	90
IX	90	21	44	54	38	46	0	0	81
		22	50	74	18	26	0	0	68
		23	73	81	18	19	0	0	90
		24	49	72	19	28	0	0	68
		Average	54	70	23	30	0	0	77

* Inclination angles θ is the angle of layer direction from horizontal. In all the samples, the length of fractures is measured from one side.

Dark gray indicates the predominant failure mode and light gray indicates the secondary failure mode. The second percentage of either fracture is arbitrarily called the secondary failure mode only if it is equal or more than half of the largest percentage.

Curriculum Vitae

Abbass Tavallali
Geotechnical and civil engineer
September 18th 1973
Married, 1 child

Rue de Namur 177-1
Wavre 1300, Belgium
Tel.: +32 (0) 496 37 62 97
E-mail: abtavallali@yahoo.com

Education :

2006-2010	Ph.D. student of geotechnical engineering, department of civil engineering, KULeuven, Belgium.
2005-2006	Pre-doc in geotechnical engineering, department of civil engineering, KULeuven, Belgium.
2004-2005	D.E.A. (research master) in mechanics of soils, rocks and structures in their environment, Ecole Nationale des Ponts et Chaussées, France, (13.39/20).
1995-1997	M.Sc. in geotechnique, Tehran University, Iran, (16.94/20).
1991-1995	B.Sc. in civil engineering, Shiraz (Pahlavi) University, Iran, (15.63/20).

Work experience:

1995-2004	Pars Garma development and industrial company, Iran. Most of the activities: contractor of dam construction and tunnelling. Last title: technical manager.
1997-2000	Shahroud Azad University, Iran. Lecturer (part-time)

List of Publications

Book chapter

1. **Tavallali A.**, Vervoort A. Detection of induced micro-cracks in quartz grains. Optical measurements techniques for structure and systems, Shaker publishing, ISBN 978-90-423-0366-9, 339-348, 2009.

2- **Tavallali A.**, Tang A.M., Cui Y.J. Thermo-hydro-mechanical behaviour of compacted bentonite. Experimental unsaturated soil mechanics, Springer proceedings in physics, ISBN 978-3-540-69872-2, 112: 259-265, 2007.

International journals

1. **Tavallali A.**, Vervoort A. Effect of layer orientation on the failure of layered sandstone under Brazilian test conditions. Int. J. Rock Mech. Min. Sci., 47: 313-322, 2010.

2. **Tavallali A.**, Vervoort A. Failure of layered sandstone under Brazilian test conditions: effect of micro-scale parameters on macro-scale behaviour. Rock Mech. Rock Eng. DOI 10.1007/s00603-010-0084-7, 2010.

International conferences proceedings: full paper (with review)

1. **Tavallali A.**, Vervoort A. Acoustic emission monitoring of layered sandstone under Brazilian test conditions. In: Proceedings of European rock mechanics symposium (EUROCK 2010), Lausanne, June 2010, 91-94, 2010.

2. **Tavallali A.**, Vervoort A. Failure of transversely isotropic rock material: effect of layer orientation and material properties. In: Proceedings of the 6th international symposium on ground support in mining and civil engineering construction, Southern African Institute of Mining and Metallurgy, Cape Town, April 2008, 317-328, 2008.

3. Debecker B., **Tavallali A.**, Vervoort A. Probability distribution of rock properties: effect on the rock behaviour. In: Proceedings of the 6th international symposium on ground support in mining and civil engineering construction, Southern African Institute of Mining and Metallurgy, Cape Town, April 2008, 357-368, 2008.

4. **Tavallali A.**, Debecker B., Vervoort A. Evaluation of Brazilian tensile strength in transversely isotropic sandstone. In: Proceeding of the 11th congress of the international society for rock mechanics (ISRM 2007), Taylor and Francis/Balkema, Lisbon, July 2007, 269-272, 2007.

National conference proceedings: full paper (with review)

1. Mirghasemy A.A., **Tavallali A.** Three-dimensional analysis of stress transfer in clay core of embankment dams located in narrow valleys (in Persian). In: Proceedings of the 4th conference of dam construction IRCOLD (Iranian National Committee of Large Dams), Tehran, Dec 2000, paper 84, 954-960, 2000.

Published abstract at international conference

1. **Tavallali A.**, Vervoort A. Detection of induced micro-cracks in quartz grains. In the 4th international conference on optical measurements techniques, Antwerp, May 2009, Abstract 29, 2009.

Non published or only available as abstract

1. **Tavallali A.**, Debecker B., Vervoort A. Evaluation of failure pattern in transversely isotropic sandstone. Grasmech poster day, Louvain-la-Neuve, May 2007.

Master thesis

1. **Tavallali A.** Study on thermo-hydro-mechanical behaviour of compacted unsaturated bentonite (in French). Ecole Nationale des Ponts et Chaussées, France, 2005.

2. **Tavallali A.** Investigation of stress transfer in clay core of embankment dams located in narrow valleys (in Persian). Tehran University, Tehran, 1997.